School of Engineering

Newcastle University

Reinforcement Learning based Adaptive Model Predictive Power Pinch Analysis Systems Level Energy Management Approach to Uncertainty in Isolated Hybrid Energy Storage Systems

Nyong-Bassey Bassey Etim

A thesis submitted for the degree of

Doctor of Philosophy

March 2020

I am sincerely grateful and thankful to my lovely and wonderful parents Prof. Etim Nyong Bassey and Mrs Mfon E. Bassey for their kind words of encouragement and support during the actualisation of this Thesis.

Declaration

I hereby declare that this thesis is a record of work undertaken by myself, that it has not been the subject of any previous application for a degree, and that all sources of information have been duly acknowledged.

Nyong-Bassey Bassey Etim

March 2020

Abstract

Hybrid energy storage systems (HESS) involves the integration of multiple energy storage technologies with different complementary characteristics which are significantly advantageous compared to a single energy storage system, and can greatly improve the reliability of intermittent renewable energy sources (RES). Aside from the advantages HESS offer, the control and coordination of the multiple energy storages and the vital elements of the system via an optimised energy management strategy (EMS) involves increased computational time. Nevertheless, a systems-level graphical EMS based on Power Pinch Analysis (PoPA) which is a low burden computational tool was recently proposed for HESS. In this respect, the EMS which effectively resolved deficit and excess energy objectives was effected via the graphical PoPA tool, the power grand composite curve (PGCC). PGCC is basically a plot of integrated energy demands and sources in the system as a function of time. Although of proven success, accounting for uncertainty with PoPA is a cogent research question due to the assumption of an ideal day ahead (DA) generation and load profiles forecast. Therefore, the proposition of several graphical and reinforcement learning based 'adaptive' PoPA EMSs in order to address the issue of uncertainty with PoPA, has been the major contribution of this thesis. Firstly, to counteract the combined effect of uncertainty with PoPA, an Adaptive PoPA EMS for a standalone HESS has been proposed. In the Adaptive PoPA, the PGCC was implemented within a receding horizon model predictive framework with the current output state of the energy storage (in this case the battery) used as control feedback to derive an updated sequence of EMS, inferred via PGCC shaping. Additionally, during the control and

operation of the HESS, re-computation of the PGCC only occurs if a forecast uncertainty occurs such that the error between the real and estimated battery's state of charge becomes greater than an arbitrarily chosen threshold value of 5%. Secondly a Kalman filter for the optimal estimation of uncertainty distributed as a normal Gaussian is integrated into the Adaptive PoPA in order to recursively predict the State of Charge of the battery based on the likelihood of uncertainty. Thus, the Kalman filter Adaptive PoPA by anticipating the effect of uncertainty offers an improved approach to the Adaptive PoPA particularly when the uncertainty is of a Gaussian distribution. The algorithm is therefore more sophisticated than the Adaptive PoPA but nevertheless computationally efficient and offers a preventive measure as an improvement. Furthermore, Tabular Dyna Q-learning algorithm, a subset of reinforcement learning which employs a learning agent to solve a discrete Markov Decision Process by maximising an expected reward in accordance with the Bellman optimality, is integrated within the Power Pinch Analysis. Thereafter, a deep neural network is used to approximate the Q-Learning Table. These aforementioned methods which have been highlighted in order of computational time can be deployed with only a minimal level of historical data requirements such as the average load profile or base load data and solar irradiance forecast to produce a deterministic solution. Nevertheless, this thesis proposed a probabilistic adaptive PoPA strategy based on a (recursive least square) Monte Carlo simulation chance constrained framework, in the event where there is sufficient amount of historical data such as the probability distribution of the uncertain model parameters. The probabilistic approach is no doubt more computationally intensive than the deterministic methods presented though it proffers a much more realistic solution to the problem of uncertainty. In order to enhance the probabilistic adaptive PoPA, an actor-critic deep neural network reinforcement learning agent is incorporated. The six methods are evaluated against the DA PoPA on an actual isolated HESS microgrid built in Greece with respect to the violation of the energy storage operating constraints and plummeting carbon emission footprint.

Acknowledgements

First, I wish to appreciate the Federal Government of Nigeria, whom through the Petroleum Technology Development Funds (PTDF), sponsored this research and notably the Federal University of Petroleum Resources (FUPRE) for the study leave approval.

Second, I wish to acknowledge and appreciate my Project Supervisors Dr Damian Giaouris, Dr Charalampos Patsios and Prof. Simira Papadopoulou, for their immense contributions towards the tremendous wealth of knowledge and experience I have gained in the course of carrying out this research.

Third, I wish to acknowledge, appreciate and thank my Father, Prof. Etim Nyong Bassey, who proofread the entire thesis and painstakingly followed through the progression of the research study, from the inception up to the conclusion.

Finally, I wish to acknowledge my colleagues; Engr Najib Dankadai, Engr. Fado Unom and friends; Dr John Nwobu and Dr Benafa Oyinkuro, for their encouragement, moral support and the quality time which they availed toward technical discussions. And special thanks to Dr Benafa Oyinkuro who has meticulously assisted in ensuring the thesis presentation is in pristine form.

Table of contents

List of figures

List of tables

Nomenclature

Roman Symbols

η_{CV}	DC converter systems efficiency
η_{PV}	PV efficiency
$\mathcal{R}$	Zero mean Gaussian noise
At	Autonomy of Battery
h	Hour
I_T	Total solar radiation (KWh/m^2)
P_f	Packing factor of the Photo-voltaic panels
P_{PV}	Output power (KW)
U_c	Control decision variable for Power Pinch
W_1, W_2	Penalty weights which control the propagation of the negative reward exerted

Greek Symbols

Δ k	Hourly time interval
σ	Standard deviation

ε_i Binary decision variable for the state of the i^{th} dispatchable unit

Superscripts

m, n Model and the plant respectively

j Indicates the j_{th} Resources $\in POW, H2, H2O$

L Number of iterative loops

Subscripts

$\rightarrow$ The arrow head indicates the direction of flow of energy/material from source to sink

Avl Availability of Resources

c Controllable element used to effect Power Pinch Analysis targeting

i Index of converter

l Accumulator

max Maximum

min Minimum

PV Photo-voltaic

k Time step

M,N M^{th} row and N^{th} column of a Matrix

Acronyms / Abbreviations

A2C Actor-Critic neural network

A_{PV} Surface area of PV (m^2)

$AEEND$ Available excess energy for the next day

AI Artificial intelligence

$ANFIS$ Adaptive neuro-fuzzy inference system

ANN Artificial neural network

BAT Battery

C_l The capacity of accumulator l (KWh)

C_{BAT} Capacity of battery(KWh)

$CAES$ Compressed air energy storage

CHP Combined heat and power

$CO2$ Carbon dioxide

DA Day ahead

DER Distributed energy resources

DG Distributed generators

DOD Depth of discharge

DQN Deep Q-network

DRL Deep reinforcement learning

DSL Diesel generator

EL Electrolyser

EMS Energy management strategy

$EPoPA$ Extended power pinch analysis

ES energy storage

EV Electric vehicle

F Faraday constant, (C/mol)

FC Fuel cell

FES Flywheel energy storage

FF Fire fly optimisation

G A fixed Reward

GA Genetic algorithm

GHG Greenhouse gases

GWO Grey wolf optimisation

$H2$ Hydrogen $(mols/h)$

$H2O$ Water $(mols/h)$

$HESS$ Hybrid energy storage systems

HEV Hybrid electric vehicle

$HOMER$ Hybrid optimisation model for electric renewable

HPS Hybrid power system

HT Hydrogen Tank (m^3)

I_E Electrolyser current (Ah)

I_FC Fuel cell current (Ah)

I_T Total solar radiation KW/m^2

LD Load demand (KWh)

$Li-on$ Lithium ion battery

$LOLP$ Loss of load probability

MAE Minimum absorbed energy (KWh)

MCS Monte Carlo simulation

MDP Markov decision process

$MEES$ Minimum excess energy for storage

MG Microgrid

$MOES$ Minimum amount of outsourced electricity supply

$MOES$ Minimum outsourced energy supply (KWh)

MPC Model predictive control

N 24h Terminal horizon

n_E Electrolyser efficiency

n_F Fuel cell efficiency

nc_{EL} Number of cells in the electrolyser

nc_{FC} Number of cells in the fuel cell

ne	Number of electrons
P_{PV}	Output power of PV (KW)
$PGCC$	Power grand composite curve
PHS	Pumped hydro storage
$PoPA$	Power Pinch Analysis
POW	Power (KW)
PSO	Particle swarm optimisation
RES	Renewable energy systems
RL	Reinforcement learning
RLS	Recursive least square
Rs	Resources
s^{-}	Previous state before a transition by the agent
S_{Lo}^{l}	Lower
$SAPV$	Standalone photo-voltaic system
SC	Super capacitor
$SMES$	Super-conducting magnetic energy storage
$SOAcc_{l}$	State of Accumulator l (%)
SVR	Support vector regression
TD	Temporal difference

$TLBO$	Teacher learner based optimisation
UC	Ultra capacitor
VRB	Vanadium battery
WT	Water Tank (m^3)
WTS	Wind turbine systems
$ZnBr$	Zinc bromide battery
n	Number of Monte Carlo simulation samples

Chapter 1

Introduction

1.1 Background of the Study

In rural villages, remote communities, and particularly developing countries, electrification via a traditional grid distribution network can either be non-existent (as in the case of a conventional standalone microgrid) or too expensive to connect, erratic and unreliable [1–3]. Therefore, the reliance on non-renewable fossil fuel-based technologies such as diesel generators (DSLs) as primary energy generation source for microgrid has not only been extensive but also an age-old traditional solution [4]. Besides, these fossil fuel based technologies such as the DSLs, retain certain unique features such as reliability, power density, ease of usage, and portability which has continued to encourage widespread patronage [5]. Nevertheless, high operational and maintenance cost, noise pollution, fossil fuel depletion and the ensuing detrimental impacts of greenhouse gases (GHGs) (Such as CO2) pollutants released into the environment, are some genuine concerns inhibiting the continued usage of DSLs as a primary energy source. [2, 5]. Alternatively, energy generation via renewable energy systems (RESs) such as Photovoltaic (PV) and Wind turbine systems (WTS), which derive energy from replenish-able naturally occurring processes (e.g. solar, wind respectively; geothermal, wave and biomass energy etc.) has become increasingly attractive and an

effective solution in recent times for curbing the unfavourable ecological impact of fossil fuel-based energy generation [6]. More so, with the integration of RES which is a source of clean energy, any existing fossil-based solution such as DSL which has a high carbon emission footprint, can be consigned to operate mainly as backup supply [7, 8].

In addition, global trends to decarbonise, decentralise and democratise the world's energy supply since 2005, have led to the creation of energy policies which in turn have significantly stimulated the penetration and cost reduction of RES assets [9, 10]. In the year 2017, the installed global capacity of PV and WTS were 401 GW and 539 GW respectively [11, 12] as shown in 1.1. Despite this trend, in developing and under-developing countries, about

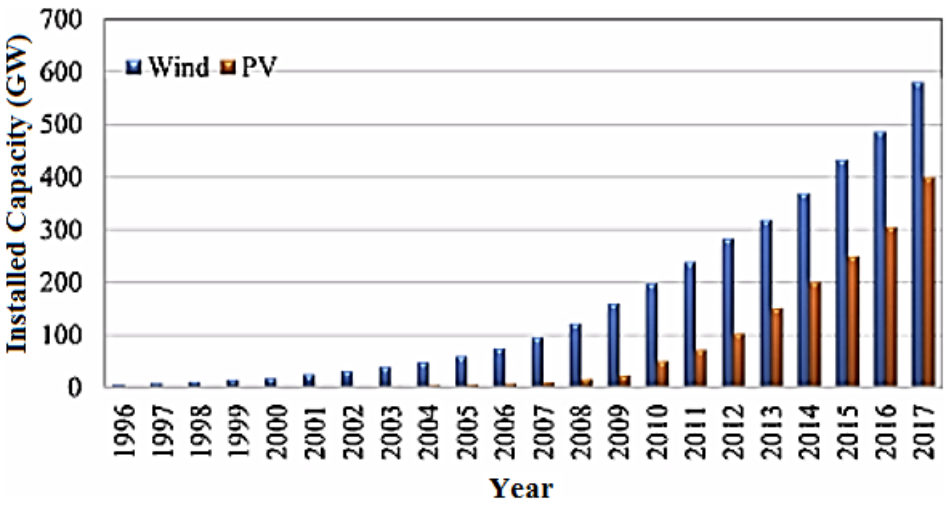

Fig. 1.1 Installed capacity of PV and WTS Worldwide from 1996 - 2017 [11]

1 billion people, still lack access to stable and reliable electricity or none at all, however, microgrid (MG) concept has been envisaged to address this problem [10].

The MG as an assemblage of interconnected loads and distributed energy resources (DERs) (such as fuel cells, Solar PV and Batteries (BAT), proposes maximum RES penetration, and has emerged as a flexible design particularly enabled to operate in grid-connected and islanded modes [11, 13]

The MG is fit for purpose and can be scaled to match the needs of different communities, from developed metropolitan cities to underdeveloped or remote settlements. MG perhaps seems to be the most suitable strategy in delivering electricity, which is an essential resource for satisfying human needs and stimulating development. More so, MG is taking advantage and deployment of cutting edge state of the art expansions in areas such as power electronics, information and communication technologies and DER are transforming the conventional grid in industrialised nations, while potentially advancing developing countries into the realm of smart MG [10].

1.2 Hybrid Energy Storage Systems Uncertainty

Although, RES integration is suitable for islanded MG applications mainly due to their low carbon emission impact, the energy produced by RES is intermittent. Therefore, neither photo-voltaic (PV) systems alone which relies on intermittent solar irradiation nor the WTS which produces usable energy only when cut-in wind speed is in the range of 2.5 to 4.5m/s, can sufficiently satisfy a 24h load demand requirement[2, 14, 15].

Alternatively, RES MG are often integrated with energy storage (ES) or accumulators in order to mitigate and flatten energy fluctuations or uncertainties, improve power quality and achieve energy practicability, especially in islanded MG [11].

Therefore, multiple ES technologies (e.g. battery (BAT) and hydrogen (H2)) with complementary properties (such as life cycle, seasonality, power and energy density etc.) are often combined to realize the concept of the hybrid energy storage systems (HESS), in order to enhance reliability and mitigate RES uncertainty [16, 17]. Several configurations of HESS architectures exist, however, some common implementations RES off grid MG applications are super-capacitor (SC)/BAT [18, 19], fuel cell (FC)/BAT [20, 21], FC/SC [22] and BAT/FC/SC [23, 24] HESS. Other HESS combinations, are compressed air energy storage (CAES)/SC [25] and superconducting magnetic energy storage (SMES)/BAT [26].

Nevertheless, a HESS shown in Figure 1.2 which was designed and built-in Xanthi, Greece with mathematical model of the assets previously validated in [17, 27] has specifically been considered as a case study in this thesis due to the regenerative use of H2 and availability of extensive. However, the dynamics of the converters, the efficiency of some of the devices and degradation are not included as a high-level systems theory approach is adopted.

In principle, the operation of this HESS [17] is such that during the period when supply from the PV exceeds demand and the battery is fully charged, the excess energy from the PV is converted to H2 by the electrolyser (EL) for long term storage (as opposed to the BAT which is a short-term storage). Thereafter, the H2 via a FC is used to satisfy energy demand which exceeds supply thus, this makes the HESS attractive and quite interesting to understudy due to the regenerative use of H2 energy carrier. [17, 28]. Therefore, in times of excess supply the HESS can reduce the dumped load, and as well reduce the necessity of a backup DSL in times of excess demand [29].

Though, electricity generated from most HESS, come at a higher price per KWh in contrast with the national grid tariff. Nevertheless, HESS are still regarded as a more economically cost-effective electrification solution for MG in remote and isolated areas without access to an electrical grid [30]. This is primarily due to the technical encumbrance in deploying high voltage transmission lines (including the resulting power losses) and other necessary infrastructures associated with the extension of the national grid [4, 6, 31–33].

1.3 Energy management Strategies for Hybrid Microgrid

In contrast to grid-connected MG which is much simpler and flexible to manage since additional power can easily be sourced from the grid whenever it is needed, islanded MG requires local control and energy management of the MG assets [34].

Furthermore, HESS, which involves the mixing of heterogeneous components/devices, consequently introduces systems complexity [35–37]. Hence, state of the art energy manage-

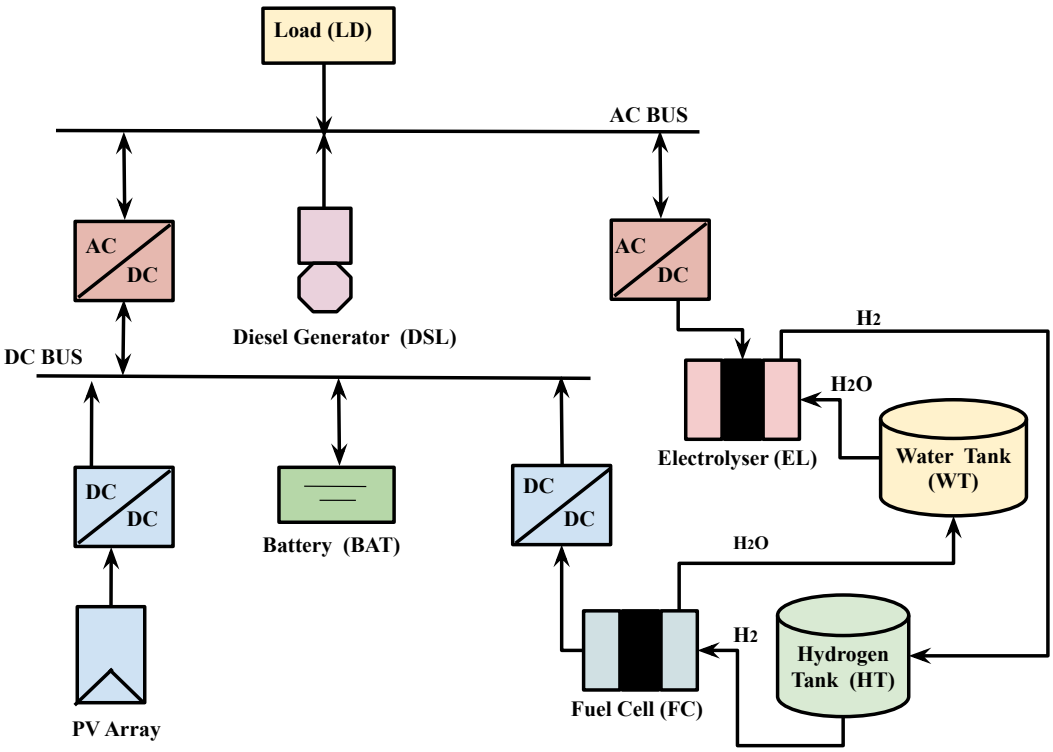

Fig. 1.2 Schematics of the Islanded HESS [17] used as a case study

ment strategies (EMSs) are often employed in order to coordinate the different forms/characteristics of energy/material (e.g. power and H2) flows between the multiple assets. Nevertheless, HESS are not easily controlled by optimised energy management strategies (EMS's) which are essential for the optimal use of the assets, consistent energy supply and energy savings. In order to address such complexity, several studies have considered a varied range of EMS's for HESS which are based on artificial intelligence (AI) (e.g. fuzzy logic controllers, machine learning; neural network, and genetic algorithm), if-then-if-else rules, linear and dynamic programming and advanced control techniques [38–40]. On the one hand, AI or mathematical programming methods are able to investigate a vast number of decisions and solutions which are optimal. However, due to combinatorial complexity or non-linear models, these methods are known to suffer from increased computational time, which can result

in unsuitability for on-line decision-making [40, 41]. Furthermore, these methods provide only on one final solution, which hinders the opportunity to obtain insights, exploit and analyse intermediate solutions for the HESS operation. On the other hand, Power Pinch Analysis (PoPA) a process integration technique [42, 43] which considers the aforementioned inadequacies has often been used for MG sizing and design but was only recently used, as an EM tool, as first reported in [8]. Specifically, in [44], the power grand composite, a graphical-based PoPA tool which is simply the integrated energy supply and demand in the HESS, was realised within a model predictive control (MPC) framework using a day ahead DA forecast strategy. Thereafter, a series of optimal control decisions for the activation and duration of the standalone HESS operation are inferred by shaping the PGCC. Therefore, the EMS was contingent on the identification of the energy recovery targets within the prediction horizon. Nevertheless, the assumption of a perfect DA weather and load forecast limits the effectiveness and success of PoPA approach in a realistic scenario with uncertain parameters.

However, the pinch analysis despite being a well-known process integration recovery and conservation technique for assets such as waste management, water, heat, and carbon emission, requires adequate consideration and expansion for power systems application [42]. Also, most literature on PoPA have not addressed the issues of uncertainty, as these studies have mostly relied on the assumption of a perfect (or ideal) weather forecast and load profile with the exception of [45] where uncertainty was considered in sizing a MG asset. Consequently, the significant impact of uncertainty in a realistic scenario imposes the need to integrate PoPA tools with a complementary technique, particularly when consistency is so desired. Therefore accounting for uncertainty in HESS with EMS derived from PoPA strategies has been the main focus of this thesis.

1.4 Contributions-Novelty

PoPA has hardly addressed the problem of uncertainty in HESS, even so, as highlighted, only a few publications have considered uncertainty in the design and sizing of HESS. Nevertheless, despite the advantages of the DA-PoPA for HESS EM, counteracting the effects of forecast error deters PGCC due to uncertainty in RES/Load demand, which has never been considered. Therefore, the focus of this thesis has been to address the problem of RES/load forecast error, which is bound to occur in a realistic scenario, in the context of the PoPA. Therefore, the main contributions of the thesis are the proposal of six new adaptive PoPA EMS algorithms which are presented in order of increasing computational burden for an islanded HESS aimed at negating the effects of forecast error while shaping the PGCC as follows:

1. The DA PoPA in [44] for EM of HESS was adapted to realise an 'Adaptive PoPA' [46], by shaping the PGCC in a multi-step, look ahead, receding horizon MPC framework as shown in 1.3. This method, which is the most computationally efficient amongst others proposed here, offers a simple closed-loop feedback. Thus, the scheme which employs an error correction mechanism to limit the effects of forecast error due to uncertainty did not consider projected uncertainty.

2. A Kalman filter has been used in conjunction with the aforementioned Adaptive PoPA [65] (KL+Adaptive), to predict the state of charge of the battery based on the likelihood estimation of uncertainty. This algorithm though more sophisticated but with increased computational time than the Adaptive PoPA offers a more preventive measure as an improvement. Furthermore, unlike case (1), the corrective action which may improve the algorithmic performance seeks to minimise the effects of projected uncertainty and re-occurrence of the forecast error. However, the performance of a Kalman filter

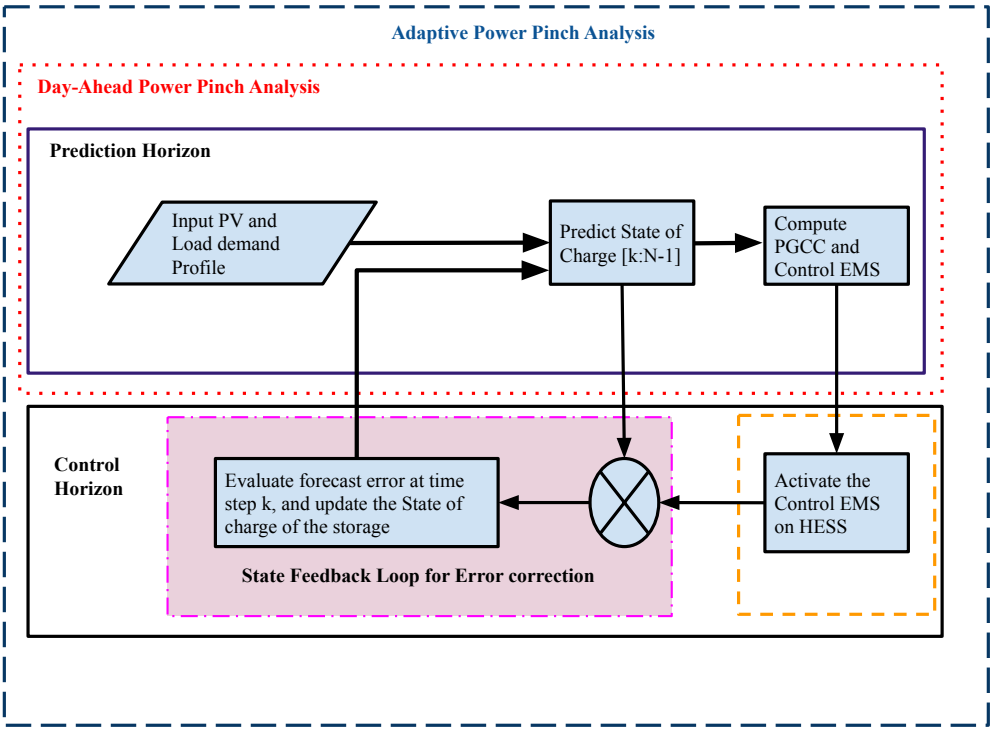

Fig. 1.3 Schematics of the Adaptive Power Pinch Analysis EMS for HESS [46]

is optimal only when uncertainty is normally distributed; hence, it can be limiting in practice.

3. A reinforcement learning-based adaptive PoPA (RL+Adaptive) method has been proposed, in the context of the Dyna Q-learning algorithm. The Dyna Q-learning algorithm entails direct learning and indirect learning a policy via experience replay, by means of rewarding an agent based on the next state of the system after inferring a control action given the current state of the system. Therefore, the agent learns an EMS by solving for the optimal action policy. Additionally, with the action policy, the agent decides the de/activation of the dispatchable units in accordance with a corrected PGCC shaped with the Adaptive PoPA. This approach does not assume that the underlying uncertainty is normally distributed in the procedure that minimises the mean squared error in the

estimated state-of-charge, as in case (2). The algorithm has further been modified to incorporate online learning regardless of the status of the energy carriers.

4. Deep RL based Adaptive PoPA (DQN+Adaptive) approach has proposed fully connected deep neural networks trained by an L2 regularised minimum squared error loss functions to extend the generalisation capabilities of approximate information learned by the intelligent computer agent in case (3).

5. A Probabilistic adaptive PoPA (P+Adaptive) method [47] realised by a recast of the deterministic model, case (1) in a probabilistic framework has been proposed. The probabilistic approach employs a Monte Carlo simulation in order to investigate n-stochastic scenarios in a predictive receding horizon. Thereafter, a robust EMS which satisfies a chance constraint probability factor corresponding to the operating constraints of the HESS is derived from a 'bounded' probabilistic PGCC and inferred in the control horizon.

6. Similarly, the probabilistic Adaptive PoPA (P+Adaptive) has been integrated into an actor-critic (A2C) reinforcement learning algorithm framework. So far, the aforementioned RL methods are with regards to discrete state and action space; nevertheless the actor-critic which naturally enabled a continuous action and state-space without the need for handcrafted discretisation has been implemented. The actor-critic neural network which combines a policy and a value-based RL approach is realised using a recurrent neural network and trained using an L2 regularised cross-entropy and minimum squared error loss functions respectively.

These six methods have been analysed in the thesis. Table 1.1 briefly summarises the computational intensity of the proposed PoPA methods. Furthermore, a sensitivity analysis with hydrogen availability is used to evaluate the proposed methods against the DA PoPA under both Gaussian and non-Gaussian uncertainty.

Table 1.1 Representation of the proposed PoPA techniques with computational intensity

EMS PoPA Algorithms		Simulation time for 72h	Computational intensity	Complexity Big $\mathcal{O}$
Deterministic EMS	Adaptive PoPA	0.67s	Very low	$Log(N.L)$
	Kalman+ Adaptive	1.33s	Low	$Log(N.L)$
	RL + Adaptive	1.35s	Moderate	$Log(N.L)$
	DRL + Adaptive	7.70s	High	$Log(N.L)$
Probabilistic EMS	P - Adaptive	137.44s	Very high	$Log(N.L.n)$
	A2C + P-Adaptive	631.55s	Extremely high	$Log(N.L.n)$

1.5 Scope and limitations of the thesis

A high-level systems theory modelling approach [17, 27] which considers only the steady-state response at an hourly interval and neglects transient characteristics response of the sub-components of the HESS, has sufficiently been used throughout the research study. Hence, the thesis did not strictly consider modelling most of the devices to include a micro time-scale resolution (such FC or EL star-time transient responses) as well as multi-objective economic cost factors. Although, not a trivial undertaking, the highlighted aspects can be included in the proposed adaptive PoPA framework in future work by improving the modelled devices and optimising constraints within the minimum and maximum energy recovery targets. The thesis has only considered the EM of the energy storages with respect to hierarchy with the BAT's state of charge being the most important parameter since in a standalone system especially in the case study, the most important objective is energy reliability with a minimum usage of the hydrogen carrier resources. In the event, the BAT is fully charged, and the HT is filled up, the PV is consequently turned off for the next simulation interval. Therefore, considering the above case inclusive of the WTS, where the

WTS is empty, the Electrolyser device will cease to operate as it requires electrolysis of water for its operational function. Throughout the thesis, it is assumed that the PEM FC and EL operate solely on an independent power supply separately from the BAT being considered or controlled by the EMS. The thesis assumed a case study of DC hybrid energy storage systems microgrid considering real power only. Therefore, there is no necessity for frequency, phase and reactive power control and synchronisation of the BAT to a bus network.

1.6 List of Publications

The work of this thesis is based on the following publications:

- Journal publications

    1. Nyong-Bassey Bassey Etim, Damian Giaouris, Haris Patsios, Simira Papadopoulou, Athanasios I. Papadopoulos, Sara Walker, Spyros Voutetakis, Panos Seferlis, and Shady Gadoue 'Reinforcement learning based adaptive power pinch analysis for energy management of stand-alone hybrid energy storage systems considering uncertainty', Energy, 2019, Dec 2:116622.
    2. 'Deep Reinforcement learning based probabilistic Adaptive PoPA Energy management for Smart Microgrids' for submission to Journal of Energy Storage, Elsevier.

- Conference Papers

    1. Nyong-Bassey Bassey Etim, Damian Giaouris, Athanasios I. Papadopoulos, Haris Patsios, Simira Papadopoulou, Spyros Voutetakis, Panos Seferlis, Sara Walker, Philip Taylor, "Sensitivity Analysis of Hybrid Energy Storage Systems Utilising Adaptive Power Pinch Analysis", UKES Conference, Newcastle 2018.

2. Nyong-Bassey Bassey Etim, Damian Giaouris, Athanasios I. Papadopoulos, Haris Patsios, Simira Papadopoulou, Spyros Voutetakis, Panos Seferlis, Sara Walker, Philip Taylor, and Shady Gadoue. "Adaptive Power Pinch Analysis for Energy management of Hybrid Energy Storage Systems." In 2018 IEEE International Symposium on Circuits and Systems (ISCAS), pp. 1-5. IEEE, 2018.
3. Nyong-Bassey Bassey Etim, Damian Giaouris, Haris Patios, Shady Gadoue, Athanasios I. Papadopoulos, Panos Seferlis, Spyros Voutetakis, Simira Papadopoulou, "A Probabilistic Adaptive Model Predictive Power Pinch Analysis (PoPA) Energy Management Approach To Uncertainty", In 2018 PEMD, IET, 2018.

1.7 Thesis Structure

The rest of the thesis is structured as follows: Chapter 2 briefly describes sizing methods, energy management strategies and HESS asset modelling. In Chapter 3 the background of the Graph theory HESS modelling and Power Pinch concept for HESS are presented. In Chapter 4 the formalisation of the receding adaptive MPC-PoPA concept and the Kalman filter state estimator approach with Adaptive PoPA are both presented. Chapter 5 presents the probabilistic adaptive PoPA in a receding horizon which was realised using Monte Carlo simulation with chance constraint and a recursive least square residual error correction. In Chapter 6, RL (Dyna-QLearning), deep RL (DQN) based Adaptive PoPA algorithms and Actor-critic RL based probabilistic Adaptive PoPA algorithms are presented. The results and discussions are presented in Chapter 7, and Chapter 8 provides a conclusion of the study.

Chapter 2

Literature Review

OUTLINE

First, this chapter reviews relevant literature with regards to sizing and design hybrid energy storage systems which are mainly categorised as intuitive, numerical, artificial intelligence and hybrid methods. Second, a preliminary investigation utilising three simple sizing methods [48] via simulation as case study, justified the validity for the inclusion of active EMS to enhance reliability and limit the use of DSL. Thus, sizing of HESS assets alone is inadequate to carter for uncertainty and intermittency of renewable energy sources, an underpinning element in the design of a reliable HESS. Third, literature review on EMSs, which are very vital are presented in the research study. These EMSs methods are grouped into categories; forecast/historical, heuristic logic, ANN-fuzzy logic and reinforcement learning. Fourth, the specific mathematical models for the HESS assets [17, 27]; such as the BAT, EL and FC are presented.

2.1 Methods for Microgrid Sizing and Design

Several research studies [14, 15] have underscored the importance of hybrid energy systems in contrast to conventional standalone power systems as they are more cost-effective and

reliable due to the use of multiple sources of electricity generation. Nevertheless, adequate sizing of the hybrid energy systems components and devices has often been a challenge largely due to the influence of capital and operating costs. Therefore, various empirical models have been proposed in literature which aims at sizing components of the standalone RES-MG with respect to a minimum cost and environmental impact, full utilisation of the assets as well as guaranteed reliability. These methods can be classed as intuitive, numerical, artificial intelligence and hybrid methods [49, 50].

2.1.1 Intuitive Method

In the intuitive processes, the required number of PV panels and energy storage capacity are determined by simple mathematical calculation. The net energy balance calculation (which is based on the net summation of the power demand, load demand and power generation) is used iteratively at every sampling instance over a 24h period. More specifically, the data profile of the residential annual average power demand, and typical meteorological wind velocity, and solar insolation to deduce the capacity of the battery storage. Thereafter, the energy storage capacity in the RE microgrid is based on the load and RE instantaneous power, which is scaled up by an autonomy factor. In addition, a DSL is used as a redundant energy source, in the event of an emergency, were the energy generated by the wind/solar is insufficient as is usually the case in a real life situation. This method was used for sizing a standalone hybrid with configuration WTS/PV/BAT micro-grid in [7]. In [30], the WTS-DSL hybrid configurations are sized using a similar approach.

[51] presented a generalized methodology for sizing RE systems. The solar radiation on the inclined surface of the PV is used to derive the global diffused and direct radiation indices according to the model presented by Collare-Pereira and Rabl in [52] while the total irradiance is based on a Hay's anisotropic model [53]. Thereafter a daily energy balance

derived from the PV and the daily load demand profile is used to determine the PV array capacity based on multivariate linear regression via optimization using radiation information.

The mathematical equation for the energy balance of a typical wind/PV battery standalone topology sampled hourly for a year is given as follows in (2.1):

$$\text{Net Energy, } E(t) = \sum_{k=1}^{8760} ((n_{PV}P_{PV}(k) + n_{WTS}P_{WTS}(k)) - P_L(k))\Delta K \tag{2.1}$$

Where,

n_{PV} and n_{WTS} are the numbers of PV panels and wind turbine systems respectively.

ΔK and k are the hourly sampling interval and hour in a year, respectively.

$P_L(k)$ is the instantaneous load demand.

$P_{PV}(k)$ and $P_{WTS}(k)$) are the generated instantaneous power for PV and WTS with respect to available wind and solar insolation at a given time (k).

Positive and negative values of E(k) denote availability and deficiency of energy generation. The total energy deficiency of the system is thereafter used to determine the size of the BAT as follows;

$$C_{BAT} = DE/(DOD * \eta_{BAT}) * At \tag{2.2}$$

Where,

DOD is the depth of discharge of Battery (BAT) at 80%

DE is deficit energy (KWh) battery

η_{BAT} is the efficiency of the battery

At is the autonomy factor of the battery storage asset

C_{BAT} is the required capacity of the battery (KWh)

$$N_{BAT} \geq C_{BAT}/E_{BAT} * DOD \tag{2.3}$$

Where,

N_{BAT} is the number of battery units required

E_{BAT} is the rated capacity of each battery

Additionally, in [48] three simple methods for determining the minimum surface area of a stand-alone photo-voltaic (SAPV) system to cater for the annual consumer load demand and any associated losses. The mathematical equations for the three methods; A_1, A_2 and A_3 are as follows:

$$A_1 = (\sum_{1}^{12}(L_{dm} + L_{nm}/\eta_b)(\eta_w \eta_T \eta_{vr} \eta_c))(\sum_{1}^{12} H_{k,m} \eta_i \eta_d)^{-1} \tag{2.4}$$

$$A_2 = ((L_{dp} + L_{np}/\eta_b)(\eta_w \eta_T \eta_{vr} \eta_c)) * (1/12 \sum_{1}^{12} H_{k,m} \eta_i \eta_d)^{-1} \tag{2.5}$$

$$A_3 = ((L_{dm} + L_{nm}/\eta_b)(\eta_w \eta_T \eta_{vr} \eta_c)) * (H_{k,mw} \eta_i \eta_d)^{-1} \tag{2.6}$$

Where,

L_{dm} and L_{nm} are the day and night time monthly average load respectively.

L_{dp} and L_{np} are the day and night time annual peak load respectively.

η_b, η_w,η_T, η_{vr} and η_c are efficiencies for BAT, PV wiring, maximum powerpoint tracking, voltage regulator, battery and cabling, respectively.

η_i and η_d are the average hourly PV efficiency and factor of degradation respectively

$H_{k,m}$ is the monthly average of the daily insolation.

$H_{k,mw}$ is the monthly average of the daily insolation pertaining to the worst month.

The PV surface area derived from A_1 is as a function of the ratio between L_{dm}, L_{nm} and $H_{k,m}$. Furthermore, in A_2 the average night and day time monthly average load are replaced with L_{dp} and L_{np}, thus, A_2 results in a smaller area than A_1. While, A_3 is similar to A_2, $H_{k,m}$ is replaced with $H_{k,mw}$. Thus, it is obvious that using method A_2 will result in the PV having a smaller surface area than A_3. However, A_3 will have a smaller surface area compared to A_1 since A_3 makes use of L_{dp} and L_{np} which will be ideally smaller than L_{dm} and L_{nm}.

The methods; A_1, A_2 and A_3 are evaluated as a function of the unserved energy and the loss of load probability (LOLP) expressed mathematically as:

$$LOLP = \sum_{k=1}^{8760} DE(k) / \sum_{k=1}^{8760} LD(k) \tag{2.7}$$

Where,

$LD(k)$ is the hourly load demand

This sizing method suffers certain shortcomings peculiar to a deterministic approach, which does not account for intermittent solar radiation. Therefore, decreased reliability associated with under sizing or increased operational and maintenance cost as a consequence of over sizing is bound to occur.

2.1.2 Numerical Method

This method employs the use of linear or quadratic optimisation techniques to minimise an objective function which may comprise the total annual cost of the system and environmental impact factor. The most suitable combination of the system components such as how large the size of the PV/WTS or BAT ES capacity should be determined and solved by an optimisation algorithm aimed at minimising objective cost function [31, 7]. Typically, the sizing problem

is with respect to finding the optimum combination with minimum cost which satisfies the net energy balance constraint is formalised using an optimisation objective function.

The objective cost function is usually composed of the summation of the annualised cost of owing the PV/WTS/Battery and the balance of system cost as well as the environmental impact factor.

In [54] hybrid optimisation model for electric renewables (HOMER) was used as a pre-feasibility study optimisation and sizing tool for HESS assets with hydrogen energy carrier, for an application in Newfoundland, Canada. The study revealed that the most feasible hybrid energy systems configuration, which resulted in the least cost at the time was the WTS-BAT-DSL hybrid systems which comprised a WTS, battery and DSL. Nevertheless, with future reduction in FC cost, a superior configuration would be the WTS-FC architecture. In [55] a simple algorithm was developed to size the components of a standalone hybrid microgrid. The optimal size of the hybrid MG components; number of PV, WTS and BAT were determined such that the load demand is satisfied with a zero load rejection criterion while maximising the life cycle cost of the assets. However, the work assumed that the state of charge of the BAT will periodically remain invariant without due consideration for daily or seasonal variation, which is far-fetched from reality.

In [3] chance-constrained optimisation probabilistic approach is adopted in contrast to a deterministic approach to size a PV-DSL hybrid energy systems under resources uncertainty. And similarly, in [45], the chance constrained approach was realized within the Power Pinch Analysis (PoPA) framework for sizing the area of a PV, after that validated via a Monte Carlo simulation.

2.1.3 Artificial intelligence optimisation method

Artificial intelligence optimisation techniques such as an artificial neural network (ANN), genetic algorithm (GA), particle swarm optimisation (PSO) have been proposed by several

authors [45, 49, 56, 57] in order to determine the PV asset sizing ratio in a standalone grid. These methods have the advantage of finding the global optimal value with respect to a multi-objective cost function while considering the intermittency of the meteorological data. The PSO is therefore used to minimise cost, Carbon IV Oxide emission, life cycle cost, and loss of power probability while predicting the size and number of PV, Battery, and Diesel generator.

In addition, [58] PSO, was compared to the result from HOMER software with respect to the concurrent sizing of a standalone HESS which included water desalination by reverse osmosis. The optimisation objective was to minimize a multi-objective function such as the total net present cost NPC, which comprised the capital, maintenance and replacement cost; and the overall CO2 emission cost, estimated over a period of 25 years while meeting water and electrical load demands. The PSO was found to have a lower NPC compared to solution rendered by HOMER software [59–61]

In [62] AI based on adaptive neural fuzzy inference system (ANFIS) and artificial neural network (ANN) were compared with respect to the optimal PV system component sizing and tilt angle prediction of a PV/BAT/DSL hybrid system. The AI sizing approach which did not require meteorological data and employed different load demands in 34 different remote locations in India, was validated to have a LOLP less than 0.01. The approach utilised 80 percent of the entire data set for training, while 20 percent was used for validation. The prediction performance indices based on mean square error showed that the ANFIS performed better than the ANN for the standalone grid component sizing.

The significance of BAT capacity with respect to the operational cost of the microgrid is emphasized in [63]. Thus, the grey wolf optimisation (GWO), is formulated to determine the BAT size that best minimises the operational cost while satisfying operational constrains such as power capacity of distributed generators (DGs), power and energy capacity of BAT, charge/discharge efficiency of BAT, in service reserves and consumer load demand.

Interestingly, the GWO out performed other popular algorithms such as the GA, PSO, Bat, Differential Evaluation, Tabu search, teaching-learning based optimisation with regards to computational efficiency and quality of the solution in the sizing of the MG asset.

2.1.4 Hybrid evolutionary Optimisation techniques

Hybrid configuration of several evolutionary, Swarm Intelligence Teaching Learning based optimisation methods have also been explored to harness the advantages inherent in these metaheuristic methods. In [64], six metaheuristic AI algorithms; FireFly, PSO, Teaching Learning-based Optimization TLBO, the Whale optimisation WO, Differential Evaluation and GA, are comprehensively reviewed, in a bid to aid engineers and researchers better solve smart microgrid optimisation problems with respect to the economic cost and operational constraint. The TLBO was found to have a better performance in comparison to the aforementioned methods. Also, TLBO had a faster convergence with the capability to explore a much wider search space with the GA and PSO having better performance compared to the WO and FF.

Nineteen hybrid metaheuristic methods comprising several combination of PSO, modified PSO, improved PSO, PSO with constriction, inertia weight and repulsion factor, bee swarm optimization, harmony search, simulated annealing, chaotic search, and Tabu search algorithm were investigated in [65]. The objective was to minimise the total life cycle cost and a loss of power supply reliability index with respect to sizing the components of a hybrid renewable energy system which comprised a WTS-PV-BAT architecture, reverse osmosis desalination asset. The hybrid configuration of the evolutionary algorithms which yielded the best and worst performance index were the improved harmony search-based chaotic simulated annealing and the artificial bee swarm optimisation respectively. The metaheuristic methods were found to have the advantage of searching for both global and local optima, better accuracy with a faster convergence rate.

Furthermore, in [66], hybridization of analytical and numerical method is presented. The hourly intermittency of the RES and Load profile are studied with respect to loss of load probability. Afterwards, the life cycle cost of the system is minimized by an adaptive feedback iterative numerical optimisation in order to obtain the optimally sized components of the SAPV microgrid. In [67] incorporated the use of mathematical optimisation in parallel with ANN and thereafter with the GA technique. More specifically, ANN with longitude, latitude and altitude information was used to predict thirty possible PV sizing values which are further optimised using the GA technique for faster convergence while minimising the capital cost of the systems. In [68] the design and sizing of hybrid Power system HPS is based on a mathematical superstructure model which incorporates chance-constrained programming which considers uncertainty introduced by intermittent RES and consumer load. Thus, the optimal generation and storage capacities of the assets are determined such that a specified level of minimum systems reliability is achieved. Thereafter, fuzzy optimisation is incorporated to resolve a multi-objective trade-off concerning economic, environmental and parametric uncertainties in the HPS design. The approach was validated using a Monte Carlo simulation and is similar to ref. [45].

2.1.5 Power Pinch Analysis Sizing, design and planning methods for Microgrids

The PoPA is a process integration technique, inspired from the original Pinch Analysis for heat exchange networks [69] and evolved to sophisticated tools [42] [44] that allow the analysis of complex energy systems based on the identification of insights pointing toward promising design and operating decisions [70]. Several researchers have considered PoPA for electric power systems sizing and design. In [43, 45] the grand composite curve was realised by integrating the energy demand and supply over time, and then it was used to size an isolated power generation system optimally. Additionally, in [71] the PoPA was

utilised as a combination of both the graphical analysis and numerical approach with the aid of the power cascade analysis and storage cascade table for optimal sizing of the hybrid power system. The extended Power Pinch analysis (EPoPA) in [72] was proposed as an enhancement to the PoPA to optimally design renewable energy systems integrated with battery-hydrogen assets as well as a DSL. The EPoPA was used graphically and algebraically to determine the required external electricity to be outsourced, the wasted energy which could not be stored in the BAT, but can perhaps be stored in the form of hydrogen in a normal operational year. Thereafter, the sizes of the HT and DSL were determined by minimising the total annualised cost. These studies on PoPA for sizing MG assets with the exclusion of [45] in which chance-constrained programming was used to achieve technical and economic feasibility, were realised without recourse to uncertainty.

2.1.6 Simulation Results of PV Sizing Methods for Advanced based EMS Justification

The simulation results utilising the Net Energy modelling concept for hierarchical energy management strategy in a renewable MG comprising a PV, BAT, consumer load and a backup diesel generator are presented in this section. The for all time instances, the BAT is charged with excess energy in the event the PV power exceeds the load power. In order to avoid overcharging, the fully charged battery ($SOAcc_{BAT}$>90%) is disconnected from the MG, while the load is sustained by the energy from the PV. During periods of unavailability of power from the PV, the load demand is satisfied by discharging the BAT as long as the SOAcc of the BAT is not less than 30% (i.e. $SOAcc_{BAT}$<30%). The diesel generator is activated if the $SOAcc_{BAT}$ is below 30% and the power from the PV is less than the load (i.e. $P_{Pv} < P_L$). The BATis sized with respect to the average consumer load energy per day, autonomy of 2 days for safety factor as well as the allowable depth of discharge. While the PV surface area is sized using the three methods presented in [48].

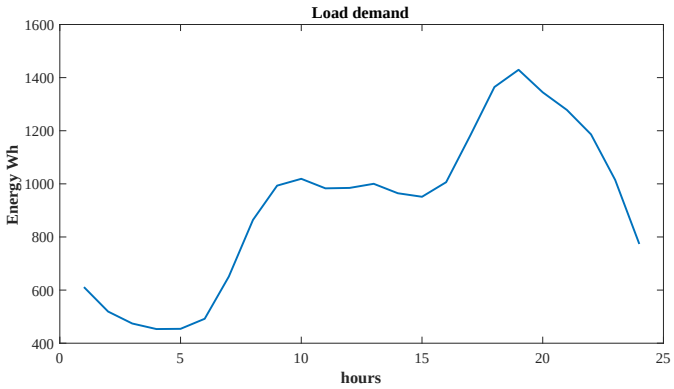

Fig. 2.1 Typical residential load demand profile

A typical deterministic residential consumer load profile, characterised by dual peaks in the morning (1.2KW) and evening (1.5KW) is shown in Figure 2.1. Figures 2.2, 2.3 and 2.4 shows the response of the MG with subplots (a) explicitly showing the PV power response, the battery's *SOAcc* and Net Energy for 8760 h, (b) 1st of January, (c) 1st of April, (d) 1st of July, and (e) 1st of December with respect to PV sizing methods 1,2 and 3.

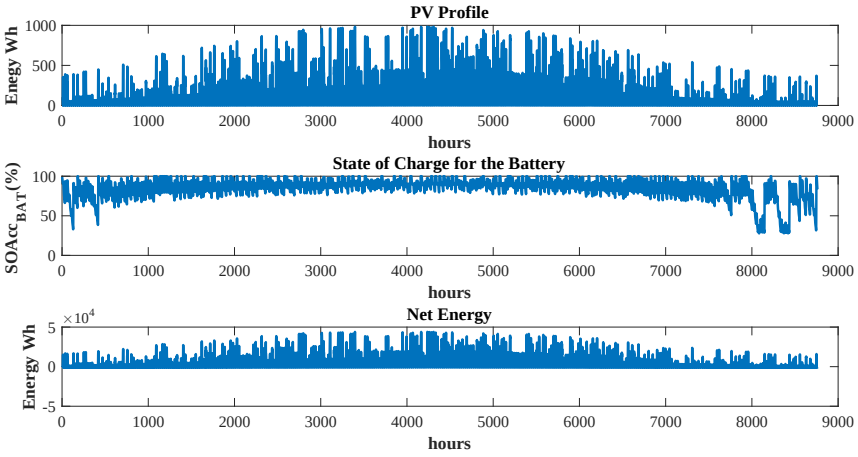

(a) 8760 h MG response

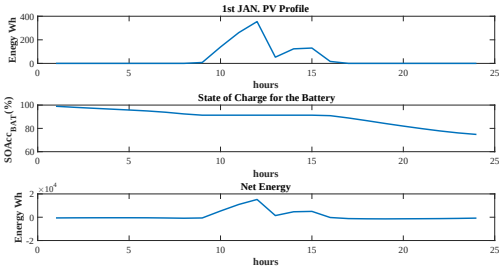

(b) 1st January

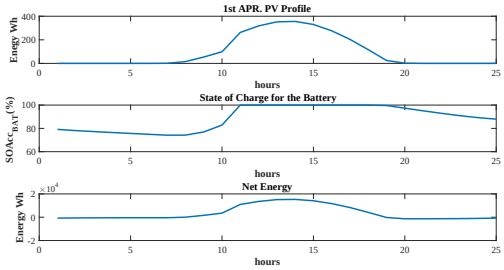

(c) 1st April

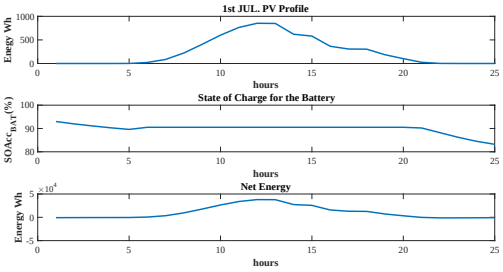

(d) 1st July

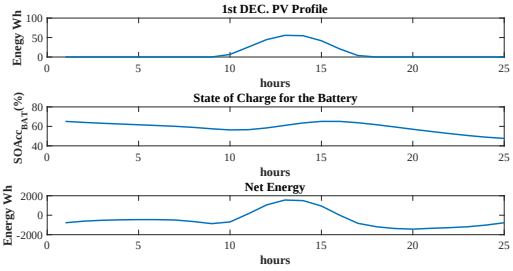

(e) 1st December

Fig. 2.2 PV power profile, Battery's *SOAcc* response and Net energy with sizing method 1

Table 2.1 Performance indices for the PV sizing methods.

Reliability Indices	**Method 1**	**Method 2**	**Method 3**
Battery Failure with DSL	57	4238	2098
Battery Failure NO DSL	212	8717	5488
Battery Overcharged with DSL	3817	8	471
Battery Overcharged No DSL	3804	8	437
Battery Deactivated	1058	0	1836
LOLP with DSL	0.5006	0.3286	0.4312
LOLP no Diesel	0.5055	0.8305	0.6421
Level of Autonomy with diesel	0.9935	0.5162	0.7904
Level of Autonomy NO diesel	0.9758	0.0049	0.3735

Table 2.1 shows the performance indices of the methods employed when a diesel generator serving as backup is absent and present. Method 1, is easily seen to be more reliable as it has a level of autonomy of 0.9758 and 0.9935 and LOLP of 0.5006 and 0.5055 when the backup generator is absent and present respectively. With the LOLP a 0 means the load demand will always be satisfied while a one connotes it will never be satisfied. However, the level of Autonomy increases as it approaches 1. The Diesel generator does not improve the LOLP significantly of the Microgrid sized by method 1. The battery is also overcharged despite having the least failure due to lack of advance control incorporated. The second sizing method has the least level of autonomy as it does not proffer any form of reliability; this improves drastically with the integration of a diesel generator. The third method has a better performance than the second method; however, it is not reliable as the diesel generator is needed to improve it. Also, method 1 has the most excess energy occurrence, which indicates oversizing, while method 2 has the least excess energy, which also shows under-sizing. This underscores the problem of correctly sizing the MG assets, as the PV intermittent introduces offsets in the energy targets. Therefore, active control utilising advanced EMS technique such as those based on MPC as opposed to a logic-based EMS is indeed justified and required to absorb excess energy and supply deficit energy in advance adequately.

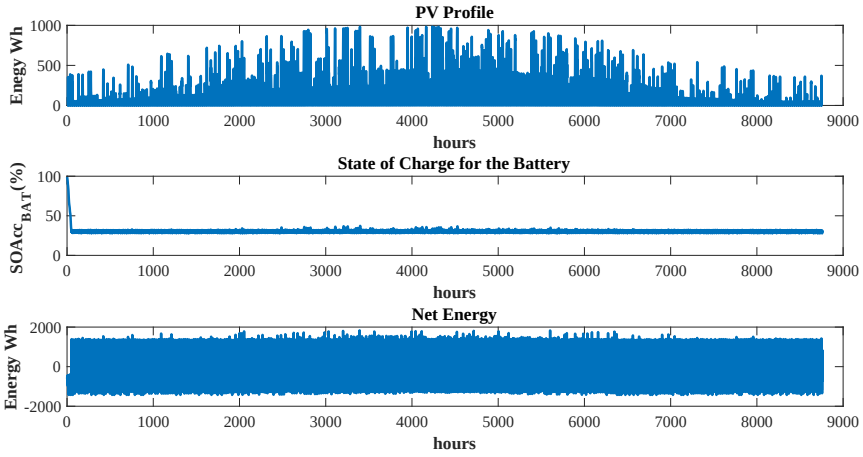

(a) 8760 h MG response

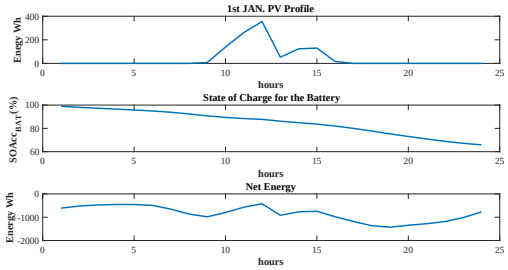

(b) 1st January

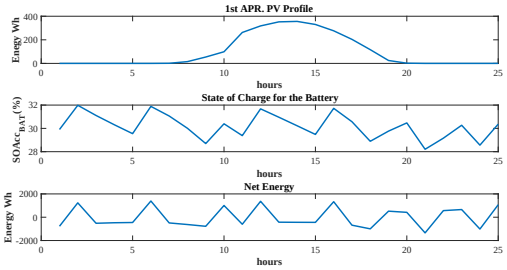

(c) 1st April

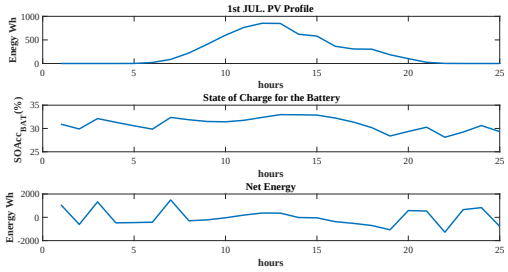

(d) 1st July

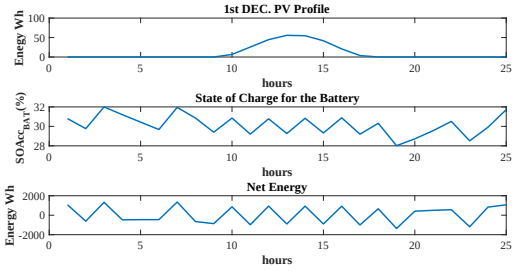

(e) 1st December

Fig. 2.3 PV power profile, Battery's *SOAcc* response and Net energy with sizing method 2

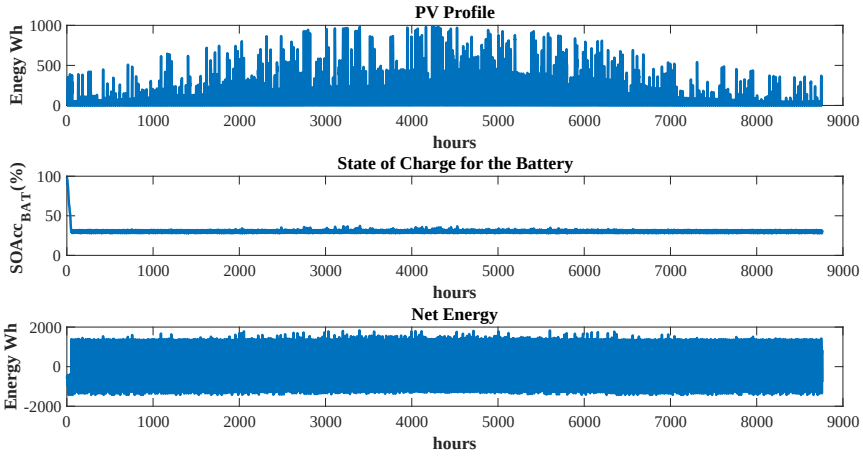

(a) 8760 h MG response

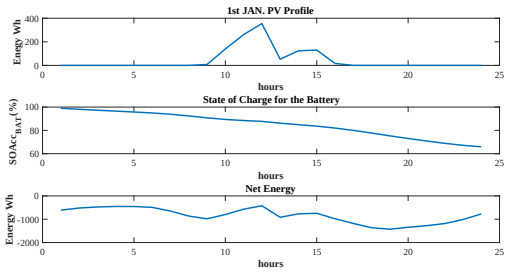

(b) 1st January

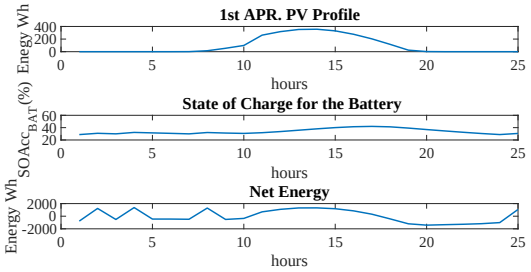

(c) 1st April

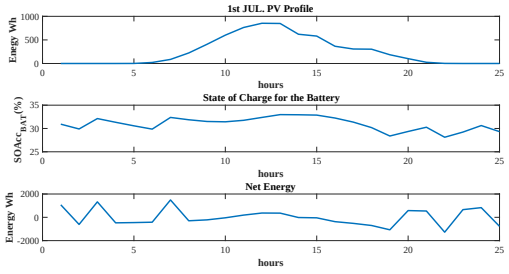

(d) 1st July

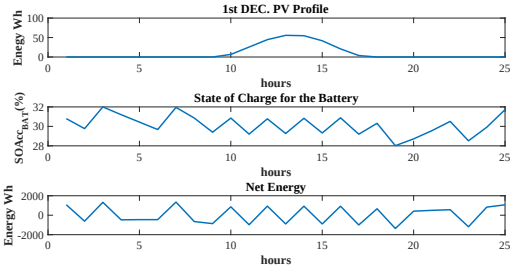

(e) 1st December

Fig. 2.4 PV power profile, Battery's *SOAcc* response and Net energy with sizing method 3

2.2 Energy Management Strategies for hybrid Microgrid

The most vital decision making required for optimal operation of HESS is the systematic distribution of energy amongst the heterogeneous energy storages with regards to dis/charging schedules while serving the load demand [36].

In spite of the benefits, HESS can offer, such as enhanced reliability, if the system's design (including inter-dependencies) is not adequately considered an improvement in performance can not be guaranteed compared to a homogeneous ESs.

In addition, the heterogeneity of the ESs technology, which portends certain benefits (such as enhanced life cycle and energy efficiency of the assets) when exploited, imposes the need for a sophisticated EMS at the system level in contrast to a conventional EMS suitable for a homogeneous ESs [36].

In literature, several EMS for optimal control and decision making have been investigated, especially to negate the effects of energy resources uncertainty in HESS. These approaches range from the use of historical data to better improve the forecast of RE energy to dynamic expert rule-based intervention strategies.

2.2.1 Forecast/Historical based Energy Management Strategies

The work presented in [73] employed game theory for the first time in an adaptive model predictive framework for demand-side response management in a grid-connected RE network and shows superiority over the day ahead scheme when forecasting error is significantly large (>10%). In [74] to achieve accurate DA forecast, learning tools; self-organising map (SOM) and Learning vector quantisation (LVQ) are combined and used to classify historical PV power, and weather data patterns for training by Support vector regression (SVR), a Bayesian machine learning method. During the classification, the historical data is loaded as an input vector, representing the pattern of the hourly PV power generation. A minimisation of the Euclidean norm is used to adjust the weight of the selected neuron during the classification

with a learning rate. The SVR consists of 5 SVR models and 6 sub-models each having 5 inputs and 3 outputs. The input data correspond to weather elements such as precipitation, temperature and solar irradiance. The SVR machine learning is a technique that is selected based on its proven forecasting accuracy and learning competency. After that, a fuzzy logic inference system was utilised as an intermediary switch for mapping any given input to output via the learned models for forecasting.

In [75], an adaptive model predictive control (MPC) is used to negate the effects caused by forecast uncertainties for optimal operation in a smart residential microgrid. The Microgrid comprised both Renewable / non Renewable energy resources such as PV solar panels and WTS, as well as combined heat and Power (CHP) as well as energy storages such as batteries and water tanks. A mixed integer programming optimisation technique is used to iteratively at each sampling time to minimise a cost function, formulated using a day's short term forecast of solar radiation wind, load demands, and electricity price. The optimal solution is derived using feasible power balance constraints on the MG for the thermal, electricity supply and demand-side energy capacity. The adaptive MPC which combined a receding horizon and forecast error compensation showed superiority with a lower cost of operation, compared to the Day-ahead programming technique. This is chiefly due to lack of state feedback and correction while using the rolling horizon optimisation method. Additionally, the erroneous forecast is modelled as a deviation from the actual forecast trajectory by summing the actual forecast and a Gaussian noise distribution for all-time. Furthermore, work done in [76] concerning sensitivity analysis reinforced the superiority of the recursive MPC over the Day-ahead strategy implemented in residential MG home energy management system. In [77] a review work on optimal control techniques, mixed-integer linear programming (MILP) an optimisation technique which makes use of both binary or integer values, as well as non-integer values for selected variables, is utilised. A centralised controller integrating load and generation forecasting via two days ahead neural network is used to proffer online

trajectory for the systems sub-components, users and water flow while guaranteeing minimal operating cost and power balance over time [78].

In [79] a nonlinear model predictive control (NMPC) algorithm is used on a standalone Microgrid for load shedding and optimal control of voltage stability within the acceptable +/- 5 percent deviation recommended by the ANSI C8.1-1989 standard while balancing the energy in the Microgrid. The NMPC algorithm performs a binary type continuous optimisation (mixed-integer nonlinear programming) for optimal decision with respect to load dispatch based on predicted power imbalance. A typical case study here is the decision to switch off the load when the power demanded by the load is higher than the power generated. Two approaches for the system model are exploited within the NMPC; (a) Comprises the use of Artificial Neural Network (ANN) is used for the load prediction and Newton – Raphson (NR) algorithm for Power flow. (b) Systems Identification for modelling based on ARX artificial neural fuzzy inference system (ANFIS) is used. The ANN predictor is trained using historical load data profile and time interval in hours, t = 1, 2, 3, . . . , N - 1 as input to predict the subsequent load demand as output. The literature did not include economic consideration as well as charge and discharge rate of the battery in the cost function as it targeted only load dispatch. However, the effect of model accuracy on the controller's performance, the benefit of this method over the open-loop approach as well as the superiority of the ARX-ANFIS were noted.

In [80], the thermal overload limits of a transmission line is considered and incorporated into a linearised AC loss transmission network model for more realistic handling of voltage magnitude and reactive power in an adaptive MPC framework. The constraints for the optimisation problem are selectively made minimal to improve the incurred unacceptable polynomial-time caused by the high dimension of the problem.

In [81] an adaptive intelligence technique (AIT) for EMS a battery (BAT) – ultra-capacitor (UC) based HESS was proposed in order to maximise self-consumption while minimising

the effects of forecast error which consequently impact on the deviation of load shaving and the corresponding threshold for dispatchable power. The AIT method, after computing techno-economic feasible fixed power and energy thresholds, incorporates robustness to forecast error by updating these fixed thresholds at every iteration with information derived from the previous day's optimal trend. Thus, AIT which did not require an accurate RES and Load data was shown to have superior performance over the PSO algorithm. However, a limitation is that the AIT algorithm depends on the averaging method which requires a fixed number of samples to determine the energy state of charge in the battery and only the UC will function as energy storage if this condition is not met. The AIT method guaranteed high self-consumption and mitigated potential reverse power dynamics amongst RES, load and ESs assets.

In [82], a ANN architecture is used for prediction and to realise a feed-forward control and a conventional state of charge energy management strategy which uses feed-forward control were compared. Furthermore, the authors, through a cost function sensitivity analysis showed that in HESS, the key contributors to the total asset's cost are the battery and hydrogen assets. Also, the fractional cost of combining hydrogen–battery technologies, was 48% percent and 9% percent compared with a hydrogen or battery only system respectively.

In [83], to control the deviation in dc-link voltage arising from the variable load and RES uncertainty in a grid-connected HESS MG which comprised a BAT and ultra-capacitor, a dynamic EMS was proposed. In [84] a multivariate quadratic optimisation was formulated to solve a real-time optimal control energy management operational task relating to a dual-mode split HEV. An offline approach is used to solve the multivariate quadratic optimisation problem in order to obtain the control decision, which is thereafter, imposed on the HEV in real-time as in a traditional MPC fashion. The method which was compared to a traditional MPC approach achieved 97.46% computational efficiency and 23.3% in fuel savings.

In HESS the concept of hybridisation is even so very often harnessed especially in electrical vehicles (EV), where a super-capacitor (SC) with high efficiency and power density properties is combined with a conventional battery which lacks such properties but has a relatively lower cost and a high energy density which the SC lacks. Hence, the exploitation of the SC and Battery in a complementary mode enhances the life cycle of the battery at a lower design cost. In a HESS was designed based on the analogy of a computer memory architecture [36].

2.2.2 Heuristic Logic-based method with forecast prediction

An energy management power regulation system was proposed in [5] for a standalone HESS comprising WTS, PV FC, EL, BAT and Load. The proposed logic-based EMS employed three stages to guarantee the continuous operation of the HESS. The first stage involved predicting the wind speed and load demand profile. In the second stage, the predicted variables and the available energy in the ES are used to estimate and schedule the maximum load demand, which can be supplied. After that, in the third stage, each subsystem was coordinated with eight dynamic operation modes generated based on the predicted variables and parameters associated with the net power flow and the intrinsic limitations of the subsystem. The allowable range for the SOC of the ES during an emergency and normal operation was 40% - 95% and 75% - 95% respectively. ESs are generically categorised based on specific characteristics of interest such as high energy and power density, life cycle ramp rate. Regrettably, no one ES has all these characteristics of interest. Thus, while ESs are generally suited for mitigating generation and consumption mismatches in a DC MG, their practicality and performance, will perhaps largely depends on their characteristics and the dynamics of the mismatch [85].

2.2.3 ANN-Fuzzy Optimisation

In [86] an expert energy management system based on artificial neural network was proposed for grid connected hybrid energy storage systems, specifically integrating WTS, ES and several DERS. The framework presented consisted of three stages; the first trained an ANN with historical data to forecast wind speed within a probabilistic error confidence interval in order to incorporate robustness in the prediction. Hence, negating the difficulty imposed by wind speed uncertainty in energy scheduling and optimal operation of the assets. Secondly, a modified bacteria Foraging Optimisation (MBFO) technique was used to minimise cost and emission objectives. Thirdly, an interactive Fuzzy satisfying approach, was simulated to resolve the trade-off between the multi-objectives.

In [87], Artificial intelligence AI (ANN and FLC) based energy management techniques were used to optimise the efficiency and operation of hybrid power systems, HPS. The HPS consisted of both primary RESs such as PV and WTS, and backup sources such as FC and Gas micro Turbine. Furthermore, the study underscored the role and importance of Hydrogen as a long-term ES employed to buffer RESs intermittency. In addition, hydrogen is considered as a clean renewable energy carrier which may perhaps be transformed into various forms such as liquid, gaseous or metal hydride for convenient storage or use.

2.2.4 Generic methods for uncertainty

Consequently, the significant impact of uncertainty in a realistic scenario imposes the need to integrate EM tools with a complementary technique, particularly when consistency is so desired. Several techniques which account for uncertainty in EM can fundamentally be classed as either a predictive or reactive approach [43]. These techniques may perhaps be considered in PoPA application, whereby, the scheduling of dispatchable units are realised with (predictive) or without (reactive) before consideration of the impact of an impending uncertainty. The responsive approach uses the latest state feedback for re-computation, upon

model mismatch due to uncertainty, which may be expensive when seeking an optimum solution in the event of frequent perturbation. The predictive technique may employ Monte Carlo simulation (MCS), stochastic programming, fuzzy programming, robust optimisation, machine learning techniques, in order to infer the optimal control action that negates the effect of uncertainty [44-46].

Furthermore, the linear Kalman filter (KF), first presented by Kalman in 1960 for solving the Wiener problem has since been applied extensively in areas of control system, navigation tracking, for short-term prediction, and for systems state estimation associated with uncertainty [47]. In [48] the ensemble KF was combined with a multiple regression model to enhance forecasting accuracy of electricity load. Similarly, in [49] the Kalman filter was used recursively to estimate short-term hourly load demand forecast parameters based on the historical load and weather data and the current measurements of the time-varying parameters.

2.2.5 Reinforcement learning-based Energy Management Strategy

In [88] a work on temporal difference (TD) learning, a model-free reinforcement learning (RL) algorithm, introduced a prediction method which relies on the experience of successive predictions to infer the behaviour of an unknown system. This was a paradigm shift to the conventional approach, which depended only on the difference between the actual and predicted outcome. Hence, RL is a machine learning technique, suitable for solving a Markov decision process (MDP) which involves optimal sequential decision making under uncertainty. Thus, many researchers have sought to deploy several machine learning algorithms in an MDP.

In [89], machine learning algorithms such as policy iteration and value iteration Dynamic programming, and RL techniques such as the least-squares policy iteration, Q-Learning, and SARSA were reviewed for MDPs.

Specifically of interest, is the Q-learning, a class of model-free RL, a similar algorithm to Sutton's (1988) TD learning [90], first introduced by Watkins in 1989, which proffers an intelligent agent with the learning ability to act optimally in a MDP based on experience [91].

In Q-learning, an agent seeks to maximise the sum of expected reward by acting optimally concerning any given circumstance (referred to as a state). Typically, an agent will evaluate a state, and will then undertake an action either in an exploitative or exploratory manner thereafter and finally will receive an instant reward, while transitioning to a new state. Q-learning has tremendous success in robotics, especially in mobile robot navigation and obstacle avoidance [92, 93].

In [94], the Dyna AI architecture was proposed to integrate both learning and experience, based on online planning, as well as reactive execution in a stochastic environment.

Furthermore, in [95], a comparative study of MPC and Monte Carlo RL on a nonlinear deterministic system with known uncertainty dynamics was undertaken.

More recently, [96] harnessed the merits of the MPC and RL control strategies to form an adaptive controller for a heat pump thermostat. The adaptive controller maximised energy savings while tracking a varying temperature set-point for thermal comfort.

In [86] a novel Markov decision process algorithm simulated in SIMULINK with a MATLAB MDP toolbox is presented to solve prioritised dis/charging problem in a HESS with two energy storages (ESs); a 22Kwh Lead Acid (LA) and 20Kwh Vanadium (VR) battery system coupled with a PV. The HESS installed in a residential home in Wolfenbüttel, Germany, serves the electrical load demand of four occupants with one 16KWh fast charging (Lithium-ion battery) Peugeot electric vehicle. The domestic load demand model for North-Westt Germany is used in the absence of a test case Load demand profile with the assumption that the EV's LI BAT is charged at home and resulting demand aggregated to the annual load demand. The states of charge of the ESs and net power flow were discretised and

normalised within a range of 0 - 1 accordingly. Thereafter, combined to form a tuple which defines the model state space in the MDP for which only one discrete action space (defined overcharge/discharge or null of the ESs) can be selected at any time interval. Then, a reward is awarded based on the next transitioned state where-in LA depth of discharge is 50%, and the VR is maintained between 33% - 74% of the nominal capacity.

In [97], the authors proposed a real-time energy management algorithm to optimise performance and energy efficiency with power split control for a hybrid (battery and ultra-capacitor) tracked vehicle for various road driving conditions. A speedy Q-Learning algorithm is used to accelerate the convergence of a multiple transition probability matrix, which is also updated whenever the error norm exceeds a set criterion. The proposed method, which was compared to a stochastic dynamic programming approach and a conventional RL using two driving cycles, had an improved fuel economy. More recently, in [98], a Dyna-H RL was proposed for real-time optimisation of fuel consumption in a PHEV. The agent was used to optimally control four traction configuration modes enabled using two clutch state and a braking state. Furthermore, energy management methods for hybrid electric vehicles are largely optimisation based; hence, requiring explicit knowledge of the system.

Furthermore, the authors in [99] proposed a real-time based RL power management for plug-in hybrid electric vehicle aimed at optimally distributing power between a battery and an ultra-capacitor. The results validated using different driving conditions and vehicle parameters showed the RL based approach reduced total energy loss by 16.8% compared to a rule-based strategy. The authors in [100] proposed for the first time applied reinforcement learning technique to minimise the fuel consumption of a hybrid electric vehicle. The formulation required only a partial model of the system without the need for an explicit model or TPM.

The application of RL based energy management for HESS has mostly been considered in literature with respect to hybrid Electric vehicle while only a few have considered hybrid MG.

In [101] deep RL EMS which uses a convolution neural net to extract relevant time-series information, from a large continuous non-handcrafted feature space, is proposed to address stochastic electricity production in residential microgrids. The neural net is validated periodically during training on historical features of observation to reduce overfitting and positive bias. The levelized energy cost economic criterion concerning maximising operation revenue is used to evaluate the performance of the algorithm.

In [102] an EMS based on a cooperative multi-agent strategy, where the different learning agents ranged from simple to complex learning agents cooperatively monitor and optimally control the assets (such as RES, ES) pertaining to integrated homes/buildings and MGs. In [103] the authors propose an EMS which applies a decentralised cooperative multi-agents enabled Fuzzy Q-learning to a standalone microgrid. The formulation of the continuous input states entails the use of five membership functions and the action space comprising a fuzzy set pertaining to each microgrid asset, with two fuzzy sets which in conjunction with a reward formulation which shapes the agent's continuous action policy.

In [104], a 2 steps-ahead RL EM strategy was proposed for a grid-connected RES microgrid with ES and consumer load. The RL utilising a 2 steps-ahead prediction of available wind power via a MCM, enables the learning agent to optimally utilise the WTS, independent of the grid to charge ES and on the other hand, maximise the use of the ES the during peak demands, thus solving a multi-criteria decision process. Therefore, stochastic scenarios which are learnt are used by an intelligent consumer to facilitate experience-based optimal control actions.

In [105] multi-agent based RL was applied for optimal control of a micro-grid associated with randomness while minimising the average electricity cost outsourced from an external

grid. In [106], a comprehensive review undertaken by the authors, underscores the importance of RL as a viable solution for many decision and control problems spanning across electric power systems. Furthermore, control system techniques for power systems application which are largely developed based on advances in certain fields; applied mathematics, control theory, telecommunication, computer science and operational research, have continued to evolve to meet dynamical challenges and requirements especially with the availability of more powerful computationally efficient resources. Therefore, learning algorithms such as RL which enables controllers to learn a goal-oriented task should be embedded in the control architecture to ensure controllers can learn and update their decision making based on experience[106].

2.2.6 Conclusion

Although, optimally sizing a MG is crucial to reliability, the importance of decision making with regards to optimal distribution and control of energy and elements of HESS can not be over emphasised. While there are a lot of studies on sizing of MG, there is equally an active interest in the area of EM by researchers. Recent studies on EMS have focused mostly on forecast/ historical and heuristic logic based EMS using A.I and optimisation. These approaches are not only computationally intensive but also largely heuristic thus they can limit potential options as well as omit satisfactory yet intermediate solutions which may improve the HESS performance, as illustrated in [17]. Power Pinch analysis [43, 42] which can can reduce the computational burden of optimisation strategies has been proposed as a graphical EM tool and was recently been used for EM of HESS. However, the PoPA was realised using a DA approach which did not consider the effect of uncertainty. Furthermore,

However, the use of robust optimisation method which considers uncertainty is considered as a pessimistic approach. Therefore, the consequence of over budgeting resources can result in wastage and become an issue in real world application [107]. Furthermore, stochastic

and chance constrained based optimisation which were applied in [38, 39] and [108, 109] [33e35] respectively for EM of MGs were found to be computationally cumbersome and also intractable. Hence, an alternative has been the use of approximate solutions which extensively depend on the accuracy of probabilistic distribution or explicit modelling of the underlying uncertainty in parameters, can be practically limiting in real-world applications as the distribution might be unavailable [110, 111].

Interestingly, an intelligent agent based algorithm, RL which has the capability to learn a MDP has been exploited mostly in literature with respect to hybrid Electric vehicle while only a few have considered MGs. Nevertheless, the RL has often been used in conjunction with computationally cumbersome optimisation strategies. Therefore, this thesis proposes a reinforcement learning based adaptive power pinch analysis energy management strategy in order to integrate the advantages of the methods while limiting their short comings. The RL approach in this thesis excludes the use/build-up and as well as update of a markov chain to model a stochastic transition matrix (TPM) in contrast with [97, 112, 99].

Typically, the application of the RL to optimise fuel consumption in hybrid electric vehicle (HEV) has been with the use of prior drive sequence and a partial HEV model. However, this thesis proposes a RL formulation which requires only the (corrected) adaptive Pinch analysis target, in order to strictly appraise the environment state and scalar reward which the RL agent should obtain only after an action has been successfully undertaken in a given state.

Furthermore, step wise non-linear optimisation often used to derive the optimal control strategy in[97] and a backward-looking optimisation in [100] will be replaced with a heuristic graphical based adaptive power pinch analysis MPC framework, which will be proposed in this work. Thus, the computational cost associated ensuring from building a TPM offline as well as solving a complex non-convex optimisation EMS for HESS (particularly with

heterogeneous energy and flow mix as in our case, where we have to deal with the intrinsic interaction of power, hydrogen, and water flow between sub-systems) will be avoided.

Most importantly, the evaluation and formulation of a scalar reward for the performance of the RL agent in the aforementioned RL papers excluding [99] have been based on a backward-looking optimisation, which has been implemented subjectively and without recourse to a systematic approach which determines the ideal optimal action strategy as in the use of a corrected adaptive PoPA. Hence, these rewards are based on a local maximisation which increases the operational cost and incurred excess energy losses in contrast with a global maximum insight which the corrected adaptive PoPA offers

2.3 Modelling of Hybrid Energy Storage Systems as a Graph

The configuration of the hybrid energy storage microgrid (MG) system typically comprises a BAT as the primary ES, PV, FC, EL, water tank (WT), HT, DSL and LD [8, 17, 44]. The mathematical modelling of each sub-component is as follows:

2.3.1 PV modelling

In [9] the model of the instantaneous PV output power (P_{PV}), is expressed mathematically as a product of the sum of diffused and direct solar radiation incident on the surface area of PV solar panel (m^2)(A_{PV}), packing (P_f), total solar radiation (I_T) and converter systems efficiency (η_{CV}) and PV efficiency (η_{PV}) factor as follows:

$$P_{PV}(\mathrm{k}) = I_T \times A_{PV} \times P_f \times \eta_{CV} \times \eta_{PV} \tag{2.8}$$

2.3.2 Battery modelling

Currently, BATs such as the lead-acid, Ni-MH, Ni-Cd, and Li-ion [113] are being utilised in MG. In [114, 115] BAT is modelled using the state of charge concept, which depicts the remaining capacity or available energy in the battery at any point in time. The state of charge is expressed mathematically as follows with consideration for both charging and discharging dynamics;

$$SOAcc_{BAT}(k+1) = SOAcc_{BAT}(k) \pm (I_{BAT}(k) * \Delta k * \eta_{ch})/C_{BAT}) \tag{2.9}$$

Where,

η_{ch} is battery's efficiency (discharging and charging)

$I_{BAT}(k)$ is the battery's current

$SOAcc_{BAT}$ is the battery's state of charge

According to [114] modelling the SOAcc of a battery is a fundamental issue, as the SOAcc is used as an essential parameter for both battery life elongation and control in an optimal EMS framework. Typically in practice, the minimum SOAcc is limited to 30% for Li-ion battery. Several existing battery models, including the Sheppard, Unnewehr universal, Nernst, Linear and Resistor-capacitor models were also compared using the 1A pulse discharge test in order to predict voltage and $SOAcc_{BAT}$. The RC model had the best prediction error. Also, [116] combined the coulomb counting and unscented Kalman filter KL techniques, which had prediction error of less than 10% for online $SOAcc_{BAT}$ estimation to serve as input to the battery management system targeting increased battery lifetime. It is important to note that an accurate battery model is nonexistent due to the difficulty and complexity in modelling the chemical reaction dynamics of a battery. Hence, in practice, an inaccurate $SOAcc_{BAT}$ estimation still abounds. Commonly used ES technologies are briefly reviewed in A.

2.3.3 PEM Electrolyser and Fuel cell modelling

By applying electrical direct current (DC) between the anode and cathode electrodes of a PEM EL which are separated by an aqueous electrolyte, the splitting water into hydrogen and oxygen molecules occurs, and consequently hydrogen is produced.

The modelling of the PEM EL such that the H2 production which corresponds to the transformation of excess energy resulting from a generating source (like a PV) is calculated based on faraday's Law in 2.10 as follows [27]:

$$H2 = nc_{EL} * 3600 * n_F * I_{EL}/(ne * F) \text{ in mols/hr} \tag{2.10}$$

Where, I_{EL} has been derived from experimental data shown in Figure 2.5, which has been validated in previous study [27]. The experimental data is expressed as a quadratic polynomial function as shown in equation 2.11, wherein the power (W) equivalent, which is to be converted to H2 by the EL is the dependent variable.

$$I_{EL} = -1.4e-06x^2 + 0.028x + 2.5 \tag{2.11}$$

Similarly, hydrogen consumption is simply determined as a function of the equivalent power transformed by a FC required to charge the BAT.

$$I_{FC} = 9e-07x^2 + 0.033x - 0.28 \tag{2.12}$$

2.4 Diesel Generator for Back-up

To ensure sustained reliability of the PV-Battery Microgrid due to intermittent insolation, a diesel generator plant usually utilised as a backup power supply to satisfy unmet load demand

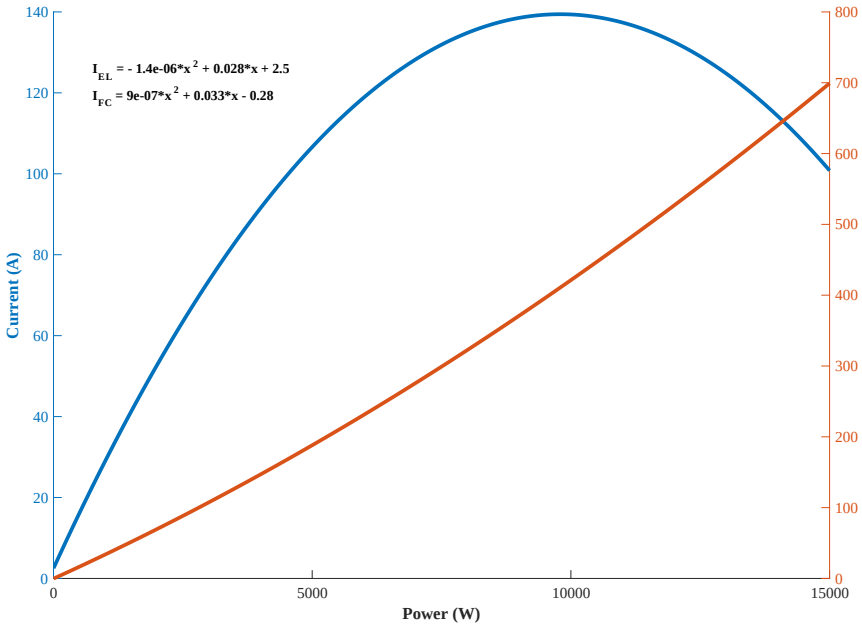

Fig. 2.5 PEM EL and FC response

in the event of failure [3, 7, 117] with a recommended power capacity to sustain the load demand for at least an hour.

Chapter 3

Background of Study

3.1 Graph based Interconnection of HESS

The interconnection of the components in the HESS is such that the flow of energy is modelled based on the state of the energy storages employed using the net energy and graph theory concept [80].

The energy storage elements l and the energy transformation assets which form the 'nodes' and are categorised as resources Rs, grouped into a subset of energy storages $l \in$ {BAT, WT, HT} and energy transformation assets $E_{tr} \in$ {PV, DSL, EL, FC, LD} respectively. The connection between the two nodes either results in the flow of electrical energy (such as BAT $\rightarrow$ [EL, LD] or BAT$\leftarrow$ FC, BAT $\leftarrow$ [PV, DSL]) or material (HT$\leftarrow$EL or HT$\rightarrow$FC). Where the arrow pointing towards the right denotes energy transferred from the BAT to the LD and/or transformed into H_2 by an EL. Consequently, an arrow pointing towards the left likewise indicates energy transferred into the BAT from the PV, FC or DSL.

Furthermore the flow of energy or material $F_{l \leftrightarrow E_{tr}}$ into and or out of an energy storage or node, as indicated by the bi-directional arrow $\leftrightarrow$ termed an 'edge', to an adjacent node(s) is a set of $j \in \{POW, H2, H2O\}$, where POW is electrical power, hydrogen is H2 and water is H2O.

The state of energy or energy carrier $SOAcc_l(k)$ in a storage unit l of capacity C_l at time step k, depends concurrently, on both the previous state of the storage unit $SOAcc_l(k-1)$ i.e at time step k-1 and the net-flow of energy $\mathcal{F}^j_{l\leftrightarrow E_{tr}}(k)$. Furthermore, we shall define two subsets X_l ,Y_l of the energy transformation assets E_{tr} with respect to a storage unit l. Where, X_l comprises nodes requesting or consuming energy from l and Y_l consists of nodes supplying energy or material to l. For instance, if the flow of energy in and out of the Battery is considered, then the subsets are defined as follows: X_{BAT} $\{PV, DSL, FC\}$ and $Y_{BAT}\{EL, LD\}$.

The state of energy in the energy storage, at any instance in time is a function of the net energy flow across the energy storage as consequence of the energy producing and consuming assets and the initial energy state of the storage as follows:

$$SOAcc_l^{m,n}(k) = SOAcc_l(k-1) + (\sum_{X_{l\in E_{tr}}} \mathcal{F}^j_{l\leftarrow E_{tr}}(k) - \sum_{Y_{l\in E_{tr}}} \mathcal{F}^j_{l\rightarrow E_{tr}}(k))\Delta k * C_l^{-1} \tag{3.1}$$

$$\Delta k = 1 \tag{3.2}$$

Where,

Δk is the hourly time interval

$$\mathcal{F}^j_{l\leftrightarrow i} = \varepsilon_i(k) * \delta\mathcal{Q}^j_i(k),\ i \in \{X_l, Y_l\} \tag{3.3}$$

Where,

$\varepsilon_i(k)$ is a binary state of the adjacent node is used for varying the magnitude of energy or material $\delta\mathcal{Q}^j_i(k)$ converted by the i^{th} dispatchable unit. In addition, the existence of an edge, represented by the binary variable $\varepsilon_i(k)$ $i \in \{0-1\}$ is

inferred from the state of the storages $SOAcc_l \in \{0, 100\%\}$ and subscript l refers to storage system. And m, n superscripts refer to the actual and estimated value of the $SOAcc_l$.

In [17, 44] the logic state ε_i of the converter attaining a binary variable [0, 1] depends simultaneously on a combination of three sub-logic operations; availability of resources by a node $\varepsilon_i^{Req}(k)$, request or demand for resources by a node $\varepsilon_i^{Avl}(k)$ and an override logic $\varepsilon_i^{Gen}(k)$. The HESS propositions are shown in Appendix B and the logic state of the converter is expressed as follows:

$$\varepsilon_i(k) = \mathcal{L}(\varepsilon_i^{Avl}(k), \varepsilon_i^{Req}(k), \varepsilon_i^{Gen}(k)) \tag{3.4}$$

Where,

$\mathcal{L}$ is logic function and the sub-conditional variables for satisfying the conditional logic state $\varepsilon_i(k)$ of the dispatchable i_{th} unit are expressed mathematically as follows:

$$\varepsilon_i^{Avl}(k) = \mathcal{L}_{l \in E_{tr}}^{Avl}(\mathcal{V}_i^{SOAcc_l}) \tag{3.5}$$

$$\varepsilon_i^{Avl}(k) = \mathcal{L}_{l \in E_{tr}}^{Req}(q_i^{SOAcc_l}) \tag{3.6}$$

$$\varepsilon_i^{Avl}(k) = \mathcal{L}_{l \in E_{tr}}^{Gen}(\rho_{U_c}^{SOAcc_l}) \tag{3.7}$$

Where,

$\mathcal{V}_i$ and q_i represents energy availability and request respectively determined based on some operational limits conditioned on the $SOAcc_l$. While ρ_{U_c} denotes

an override action imposed on equations 3.5 and 3.6 and the subscript $U_c \subseteq i \in \{FC, EL\}$ denotes the dispatch-able assets used to realize the EMS obtained from PoPA.

3.2 Power Pinch Analysis Energy Management Strategy

3.2.1 Generic illustration

The fundamentals of the PoPA concept, as applied to the HESS shown in Figure 1.2 for energy management PoPA via a graphical tool called the 'Power grand composite curve' (PGCC) are illustrated in Figures 3.1, 3.2, 3.3, 3.4 and 3.5 . The PGCC is simply an integration of the energy demand and supply dynamics pertaining to a particular storage, with respect to time as shown in Figure 3.1 (black dotted line).

The PoPA, implemented via a graphical tool called the PGCC for energy management is illustrated for the islanded HESS shown in Figure 1.2 which was presented in Chapter 1. The PGCC as shown in Figure 3.1 (black dotted line), is basically an integration of the energy generation and uncontrolled energy demands in the system as a function of time The PGCC is analogous to the grand composite curve (GCC) in heat exchanger networks (HEN) which is a plot of the integrated heat transferred between hot streams (sources) and cold streams (demand) as a function of temperature (quality) [43]. In general, the principles of pinch analysis are known to be well suited for source-sink problems with generalised flow parameters and quality attributes.

Therefore, in considering the operation of the HESS for a year (8760h), the energy management strategy realised with the PGCC is derived in prediction horizon using a DA strategy, after that, it is effected on the HESS in a control horizon.

The predictive and control horizon both consist of hourly intervals with an equal duration which spans $24h \in [k : N]$

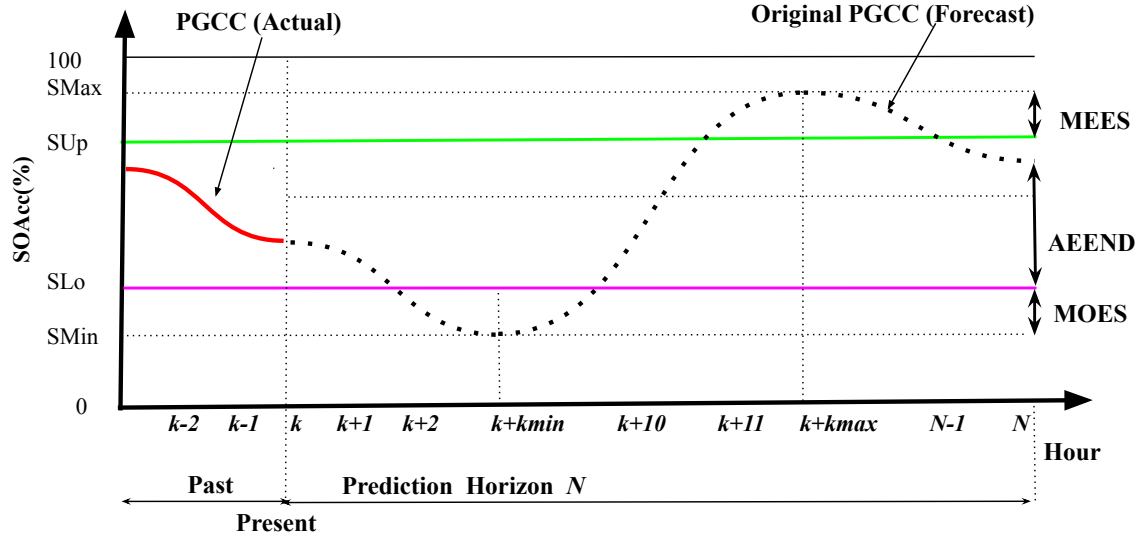

Fig. 3.1 Original PGCC

Where k is the ith hour in a day and N denotes the end of the day (or 24^{th} h). The hourly interval Δk, is defined as the time difference between two successive periods; $\Delta k = [(k+1)-k]$ where, k and $k+1$ indicates the present and next time step respectively. The interval between the present time step k and the terminal horizon N is given as $[N-k]/\Delta k$, hence the full length of horizon would span for 23 intervals, if k is counted from the first hour, 01:00h and $N = (k+23)$ is the 24:00h of the day.

In the prediction horizon, when the HESS is at a specific instant k, the PGCC is predicted as presented in Figure 3.1 with the assumption that the controllable assets are deactivated. Where the PGCC violates operational limit(s), at least a time instance before the instance of violation, an appropriate controlled asset is be activated in a control horizon of interval 24h $\in [k:N]$ in order to supply/consume the required energy/material and consequently prevent the violation from occurring.

3.2.2 Case Study

In the HESS [17] shown in Figure 1.2, the stored electrical energy (i.e. state of charge, SOAcc) is considered as the specific parameter requiring control within predefined operational limits by the EMS. Therefore, in the prediction horizon using a DA strategy, an EMS is derived and consequently implemented on the HESS in a control horizon. The SOAcc is plotted (dotted black line in Figure 3.1) at an hourly time step k for a 24h duration in a prediction horizon, as defined previously in section 3.2.1.

The PoPA enables the identification of deficit and excess energy targets, which must be successively met, in order to prevent the SOAcc in the control horizon from falling below the lower pinch utility (or limit) S_{Lo} (say 30%) and/or rising above the upper pinch utility S_{Up} (say 90%). The PoPA via the PGCC graphical tool, enables the identification of deficit and excess energy targets which must be sequentially matched in order to avoid the SOAcc from falling below the lower utility or limit, S_{Lo} (30%) and/or rising above the upper utility or limit S_{Up} (90%).

Firstly, the PoPA EMS identifies the energy deficit target from the minimum *SOAcc*, indicated as *Smin*. In this case study, the energy deficit results from insufficient energy supply from generation assets like PV. The energy deficit target is, therefore, the exact amount of energy supply necessary to ensure that SOAcc avoids the violation of the S_{Lo} at time $k+kmin$. Thus, the PGCC designates the minimum amount of outsourced electricity supply (MOES) by which to shift the PGCC in order to avoid the use of a non-renewables (such as DSL) which may perhaps be activated after the S_{Lo} has occurred. Hence, a dispatchable asset (such as FC) indicted by a red arrow pointing upward at time k, shown in Figure 3.2 supplies the MOES needed to shift the PGCC above S_{Lo}.

Secondly, the PoPA EMS identifies the amount of energy denoted as the minimum excess energy for storage (MEES) that needs to be dumped in order to avoid the violation of the S_{UP} (90%) limit at the time, $k+kmax$ is indicated by the PGCC. Thus, the MEES is recovered

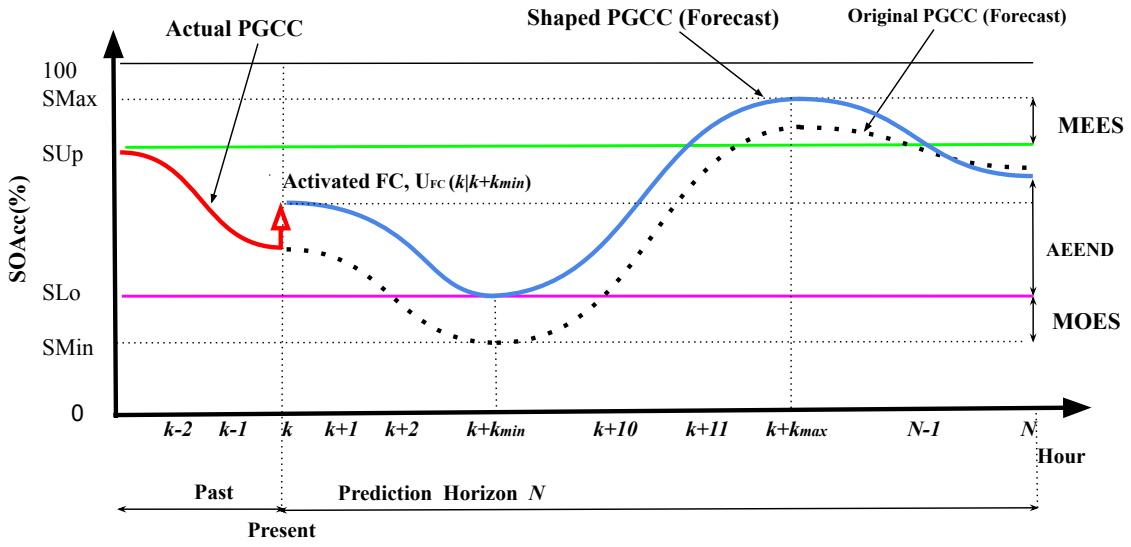

Fig. 3.2 Shaped PGCC with respect to Lower Pinch

for storage at a time step earlier than $K + Kmax$ i.e at time step $K + 10$ when a dispatchable asset (such as an EL) denoted by the red arrow pointing downwards is activated in order to perform reshaping of the PGCC, shown in Figure 3.3.

Thirdly, to adequately preserve duty cycle of the energy storage, the available energy for the next day (AEEND) has to be matched to the SOAcc at start of the shifted PGCC by activating an EL.

Consequently, by shifting PGCC (black dot-dashed line in Figure 3.4) up or down such that at the instance where the PGCC touches the S_{Lo} or S_{Up} horizontal lines at times, $k + kmin$ and $k + kmax$ is termed the Pinch point. Therefore, the complete process of shifting or shaping PGCC as shown in Figure 3.5 resolves to a graphical PoPA EMS which determines the instant and duration, at which the energy targeting resources are activated/deactivated in the control horizon [8, 17, 46, 47].

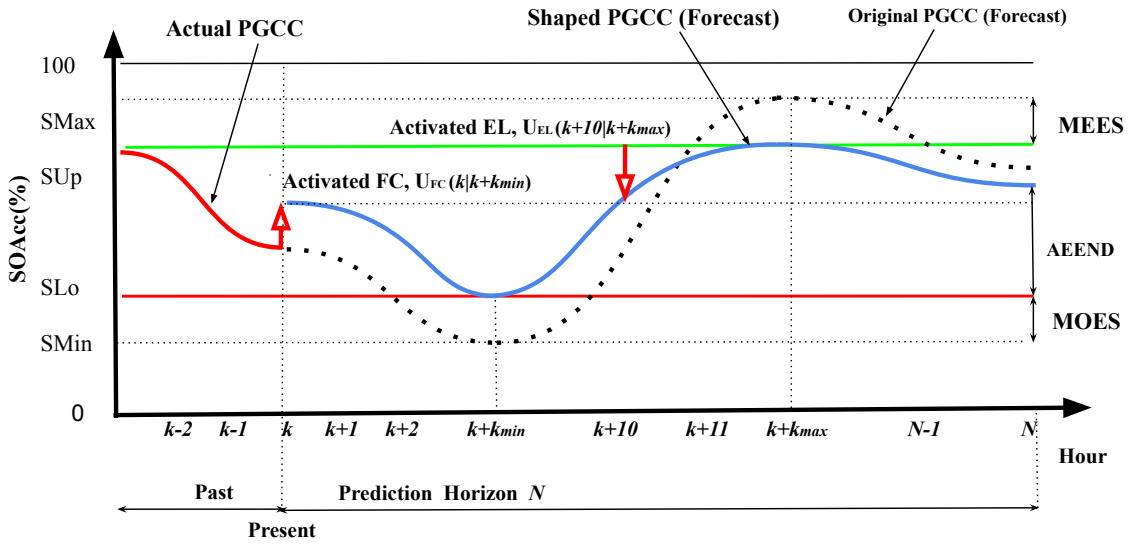

Fig. 3.3 Shaped PGCC with respect to Upper Pinch

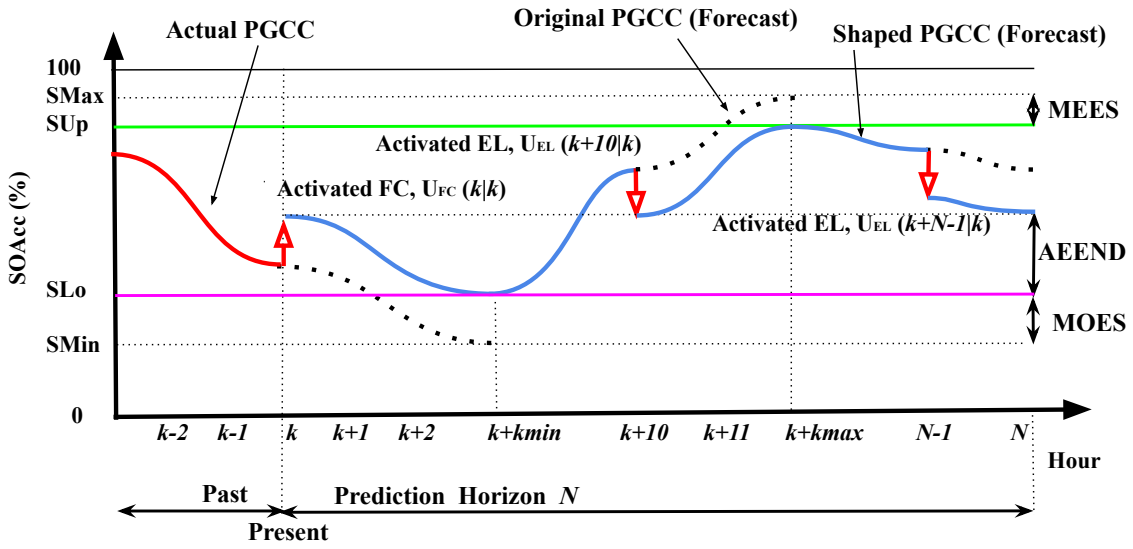

Fig. 3.4 Shaping of PGCC with respect to AEEND

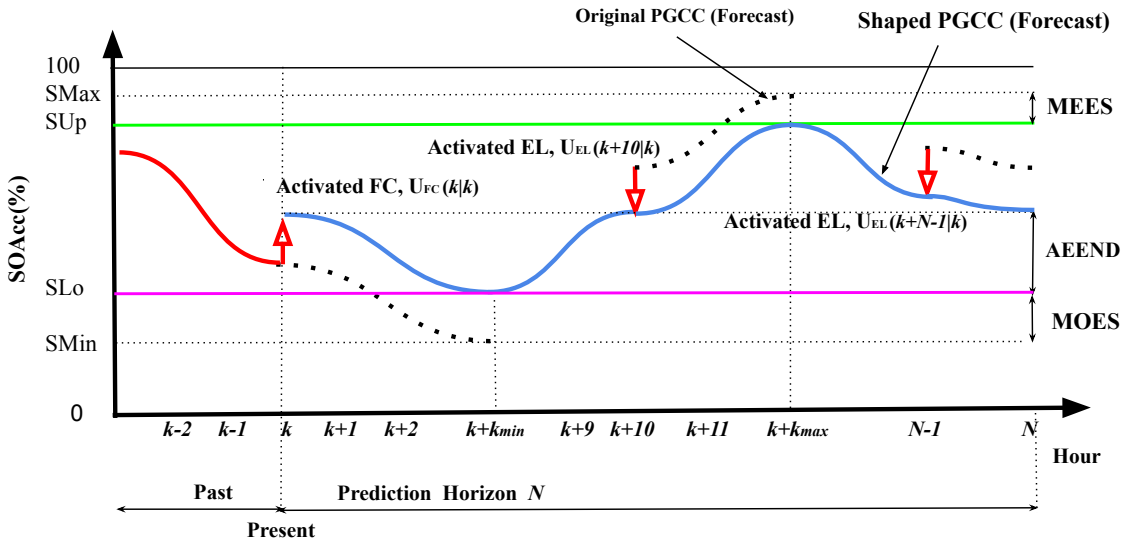

Fig. 3.5 Completely Shaped PGCC in the Predictive Horizon

However, effectively realising the optimal PoPA EMS via Day-ahead operation requires an accurate load and weather forecast model for an ideal PGCC plot, which is impractical due to uncertainty. Thus, the consequence of uncertainty, ΔH due to RES variability and electricity demand stochasticity, caused a mismatch between the actual (red line) and predicted (blue line) $SOAcc$ as illustrated in Figure 3.6 and consequent violation of both S_{Up} and the duty cycle constraint. Therefore, the utilisation of a feedback loop is arguably not only crucial to improve the excess energy recovery and reliability indices but also to plummet fossil emission footprint.

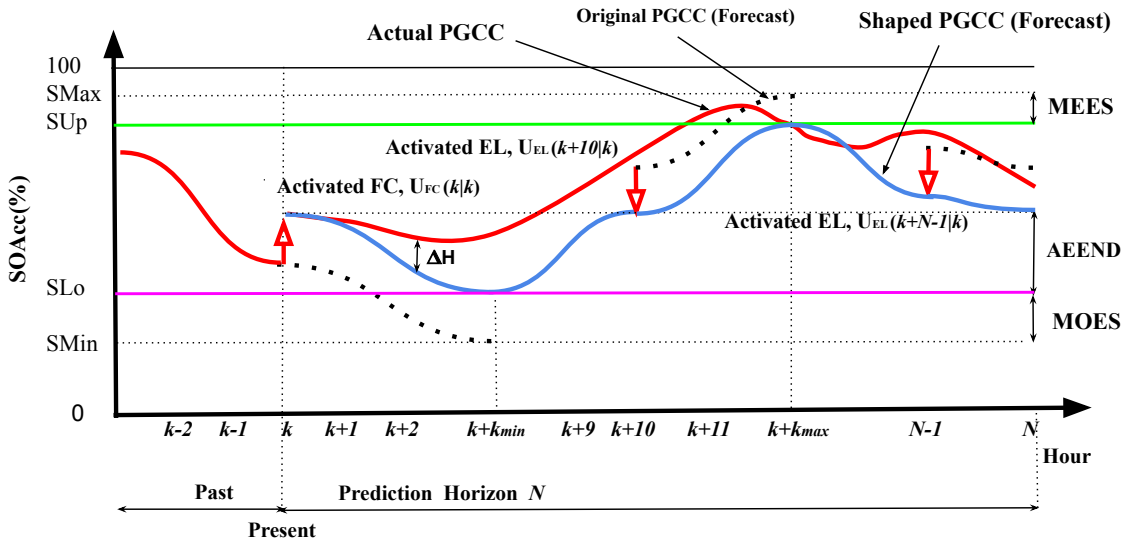

Fig. 3.6 The Effects of Uncertainty respectively with the DA-PoPA

3.3 Probabilistic Forecast for Energy Uncertainty

As illustrated in 3.6, the EMS, ensures a balance between energy demand and supply, as excess supply and undersupply of energy result in wastage and degradation of the storage assets, respectively. Unfortunately, due to the uncertainty associated with RES and load demand, which is often probabilistic and may exhibit daily, seasonal, and geographical variability, forecast error may be introduced. Thus, in reality, satisfying the energy systems constraints can become challenging to achieve using a deterministic model. Furthermore, deterministic models are often considered with a set of deterministic input variables and upon the occurrence of each variation, it becomes imperative to repeat the simulation process in order to obtain a new solution [118]. Therefore, if adequate historical and statistical evidence regarding the uncertain parameter is available, it can be leveraged using a probabilistic approach. The probabilistic techniques have been proposed in several studies for robustness to uncertainty in power systems. According to [119, 120] the probabilistic methods for dealing with power flow uncertainty can be classed under the following; Monte Carlo

simulation, analytical (such as Fourier transform and Cumulant) and approximate (such as point estimation, first and second-order moments) techniques.

More specifically, the Monte Carlo simulation uses repetitive sampling of random input parameters to statistically parameterise the uncertainty associated with a dependent variable via a probability distribution. The Monte Carlo integration is expressed mathematically in equation 3.8 as follows [121, 122];

$$I = \int_a^b f(x)\,\mathrm{d}x. \tag{3.8}$$

Where, I is the integral of a function with input random variable x.

Furthermore, a good approximate estimation of I can be obtained such that by repeating the simulation in consonance with the theory of large numbers, the expectation $E\{f(X)\}$ of the random variable $f(x)$ in equation 3.9 as follows;

$$E\{g(X)\} = 1/n \sum_{j=1}^{n} g(x) f(x_j) \tag{3.9}$$

Where X is the value of a stochastic variable drawn from a normal distribution $f(x_j)$ such that $X \in \mathbb{R}$ are independent and identically uniformly distributed i.i.d and $g(x)$ is a function.

The Monte Carlo simulation (MCS) provided probabilistic insight and was used to negate uncertainty in RES sizing [45] , energy reserve planning [123] and peak load shaving [124]. It has also been used for economic risk analysis in power systems in [125]. Furthermore, Monte Carlo simulation is favourable for low capacity planning in low voltage grid to which the simultaneity factor often employed in high-medium reserve planning becomes less accurate. In [126] a stochastic optimisation incorporated the joint chance constraint and Monte Carlo simulation in order to assess several levels of risk aversion on energy procurement from an energy market with fluctuating prices at a minimum cost while meeting the energy demand at a high probability level. In [127], a probabilistic economic dispatch tool in an energy

management framework was proposed for support sizing, planning, analyses, and dynamic operation of dispatchable resources. This focused particularly on battery storage, generators and interlinking Converters in an AC/DC standalone hybrid MG, in order to cope with fluctuating energy demands at minimum cost. In [128], an NP-hard robust optimisation was recast as a randomised algorithm for probabilistic energy management strategy of a commercial electrical vehicle (EV) charging station was proposed. The objective was to ensure safety and sustainable operation of the power grid by means of combining a real-time randomised EV occupancy scenarios and an upper bound day–ahead forecast of the EV's power consumption profile while assuring the quality of service is within a predefined probability index.

Furthermore, in [120] a probabilistic power flow model based on an extended point estimation method with an equivalent performance of a Monte Carlo simulation but with reduced computational cost was presented The proposed method which considered the spatial correlation dependencies between consumer load and intermittent energy sources was validated on the IEEE 24 and 118 bus systems and shown to offer significant improvement to generic point estimation method. A probabilistic framework based on the two-points estimation (2-PEM) method was modified to consider [129] uncertain correlated parameters in hybrid renewable energy systems. The authors' findings highlighted the importance of considering the correlation of uncertain input variables in a probabilistic model framework most notably when such variables are concerted and influence the power flow in the system. In [130] a probabilistic optimisation problem was presented for home energy management of a renewable-based residential energy hub. This included; plug-in hybrid electric vehicle, combined heat and power and a heat storage unit, involving two-point estimation, 2-PEM method to model the uncertainty of a RES. The 2-PEM was acclaimed to have a favourable performance which can match the Monte Carlo simulation, yet, without the burden of computational complexity. In [131], a probabilistic approach to uncertainty using a quantile

long and short term memory Q-LSTM deep learning neural network (NN) was proposed for an interval estimation based on short term residential load forecasting. In the forecast approach, the singular loads were considered as an aggregate rather than separately in order to avoid the problem of non-stationarity. Furthermore, the method was shown to outperform the quantile fully connected Q-FCNN and an FCNN trained on an historical-error distribution in terms of an average quantile performance index.

Chapter 4

Adaptive Power Pinch Analysis

OUTLINE

This chapter is based on published work in ISCAS, IEEE and an unpublished manuscript currently under review in Energy, Elsevier. A graphical energy management strategy based on an adaptive shaping of the power grand composite curve (PGCC) is exploited within a receding horizon model predictive framework, for robustness to forecast uncertainty in islanded HESS. Although, the Adaptive PoPA utilised a close-loop feedback error mechanism, the effects of impending un-modelled uncertainty are not adequately considered due to a reactive approach to uncertainty. Therefore, the Kalman filter which is the optimal estimator for normally distributed uncertainty, has been combined with the adaptive PoPA in order to incorporate the effect of uncertainty when predicting the state of charge of the energy storage.

4.1 Adaptive Power Pinch for Energy Management

The effects of uncertainty in renewable energy sources and electricity demand, which consequently introduces forecast error resulting in a sequence of inadequate EMS derived from a DA-PoPA operation have been highlighted in 3. Therefore, in this Chapter, the DA-PoPA

is modified to create an Adaptive PoPA which is implemented in a receding horizon MPC framework. In a prediction horizon which spans 24 h with an hourly interval Δk beginning at time step k, as defined in Chapter 2, the dispatchable control variable U_c (k) is derived contingent on the PoPA targets. Consequently, U_c(k) derived in the prediction horizon is activated in the control horizon at each time interval k. In addition, the EMS which controls the SOAcc as a consequence of the minimum energy recovery targeting J_{Pinch}, is realised in accordance with the Adaptive PoPA as follows:

$$S_{Lo}^{l} \leq SOAcc_{l}^{m}(k) \leq S_{Up}^{l} \tag{4.1}$$

$$SOAcc_{l}^{n}(k_1) \cong SOAcc_{l}^{m}(N) \tag{4.2}$$

$$\varepsilon_{FC}(k) + \varepsilon_{EL}(k) \leq 1 \tag{4.3}$$

where, k_1 is the first hour , ε_{i}^{Gen} (k) is an overide binary variable of the dispatchable asset's state, $i \in [FC,\ EL]$, $U_c(k)$ represents the PoPA EMS control variable and subscript $c \in \{FC, EL\}$ indicates the dispatchable asset. While, superscripts m,n in $SOAcc_{l}^{m,n}$ refer to the predicted and real SOAcc respectively and subscript $l \in \{BAT, HT, WT\}$ indicates the energy storage of note.

The constraints imposed by equation 4.1 ensures the pinch operating limits are not violated. The duty cycle of the energy storage is preserved by the terminal constraint 4.2 to infer the available energy at the end of the prediction horizon N (AEEND). The binary variable constraint 4.3 prevents the simultaneous dispatch of assets that concurrently consume and produce the same energy carrier (e.g. FC and EL).

The following explanation is for one asset, the BAT, but is relevant to all asset types. At every time step k, the proposed algorithm compares the forecast and real $SOAcc_{BAT}^{n}$ (k) for

inconsistency or forecast deviation via a state feedback close-loop [46]. As illustrated in Figure 4.1a, ΔH exceeds $\pm 5\%$ at time $k+2$. Therefore, state correction is effected at the next time , $k+kmin$, to decrease the forecast deviation between the predicted $SOAcc^{m}_{BAT}$ and actual $SOAcc^{n}_{BAT}$. The re-computation of the PGCC (dotted black line in Figure 4.1a) which follows reveals an anticipated violation of the S_{UP} such that $SOAcc^{m}_{BAT}$ is a maximum at time $k+11$, and the AEEND. Thus, the predicted PGCC is re-shaped as shown in Figure 4.1b (blue line) with the EL dispatched at time $k+10$ and $N-1$. The Adaptive PoPA schematics, pseudo and MATLAB .m codes, are shown in Figure 4.2, Appendix C and Appendix D respectively. The error e(k) and magnitude of uncertainty ΔH between the forecast and real state of charge of the Battery are expressed in 4.4 and 4.5 respectively as follows:

$$e(k) = SOAcc^{n}_{BAT}(k) - SOAcc^{m}_{BAT}(k|k-1) \tag{4.4}$$

$$\Delta \mathrm{H}(k) = |e(k)| \tag{4.5}$$

where, $SOAcc^{m}_{BAT}(k|k-1)$ is the predicted battery state of charge at time k based on a prior time step k-1 and $SOAcc^{n}_{BAT}(k)$ is the actual battery state of charge at time step k.

Furthermore, if $\Delta \mathrm{H}$ is greater than the deviation error threshold (ζ) at any sampling instance, the PoPA is repeated in the predictive horizon in order to determine the optimal dispatch and schedule sequence from that instant up until time N. ζ (which may be varied or decreased for a tighter bound) is set at $\pm 5\%$, to ensure minimal forecast deviations as well as to reduce any computational cost. Re-computation of the PGCC uses equations 4.6 and 4.7 as follows:

$$SOAcc^{m}_{BAT}(k) = \left\{ \begin{array}{cc} f(\Delta \mathrm{H}(k)) & if \Delta \mathrm{H}(k) > \zeta \\ SOAcc^{m}_{BAT}(k|k-1) & Otherwise \end{array} \right\} \forall_{k \in [1:N]} \tag{4.6}$$

Where, the function, $f(\Delta \mathrm{H(k)})$ corrects $SOAcc^{m}_{BAT}(\mathrm{k})$ as follows:

$$SOAcc^{m}_{BAT}(k) = \left\{ \begin{array}{ll} SOAcc^{m}_{BAT}(k|k-1) + \Delta \mathrm{H}(k) & e(k) > 0 \\ SOAcc^{m}_{BAT}(k|k-1) - \Delta \mathrm{H}(k) & e(k) < 0 \end{array} \right\} \tag{4.7}$$

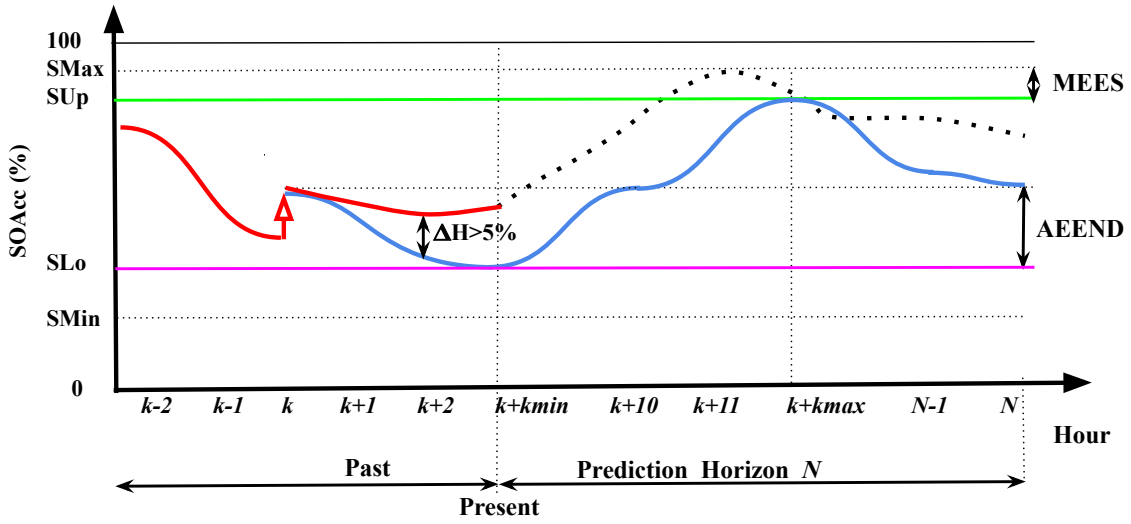

(a) State error correction

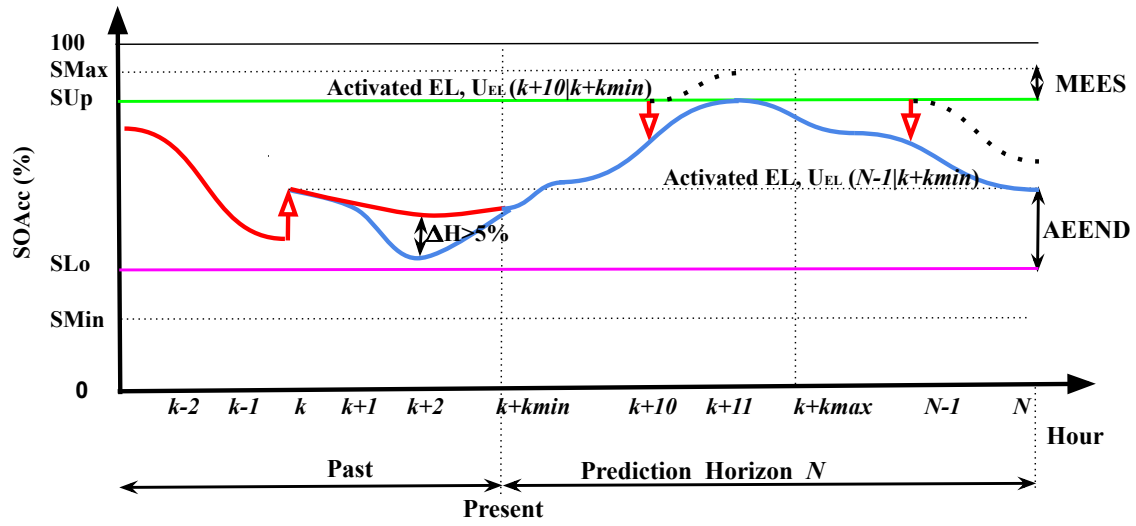

(b) Re-shaped PGCC with Adaptive PoPA

Fig. 4.1 PGCC shaping with Adaptive PoPA

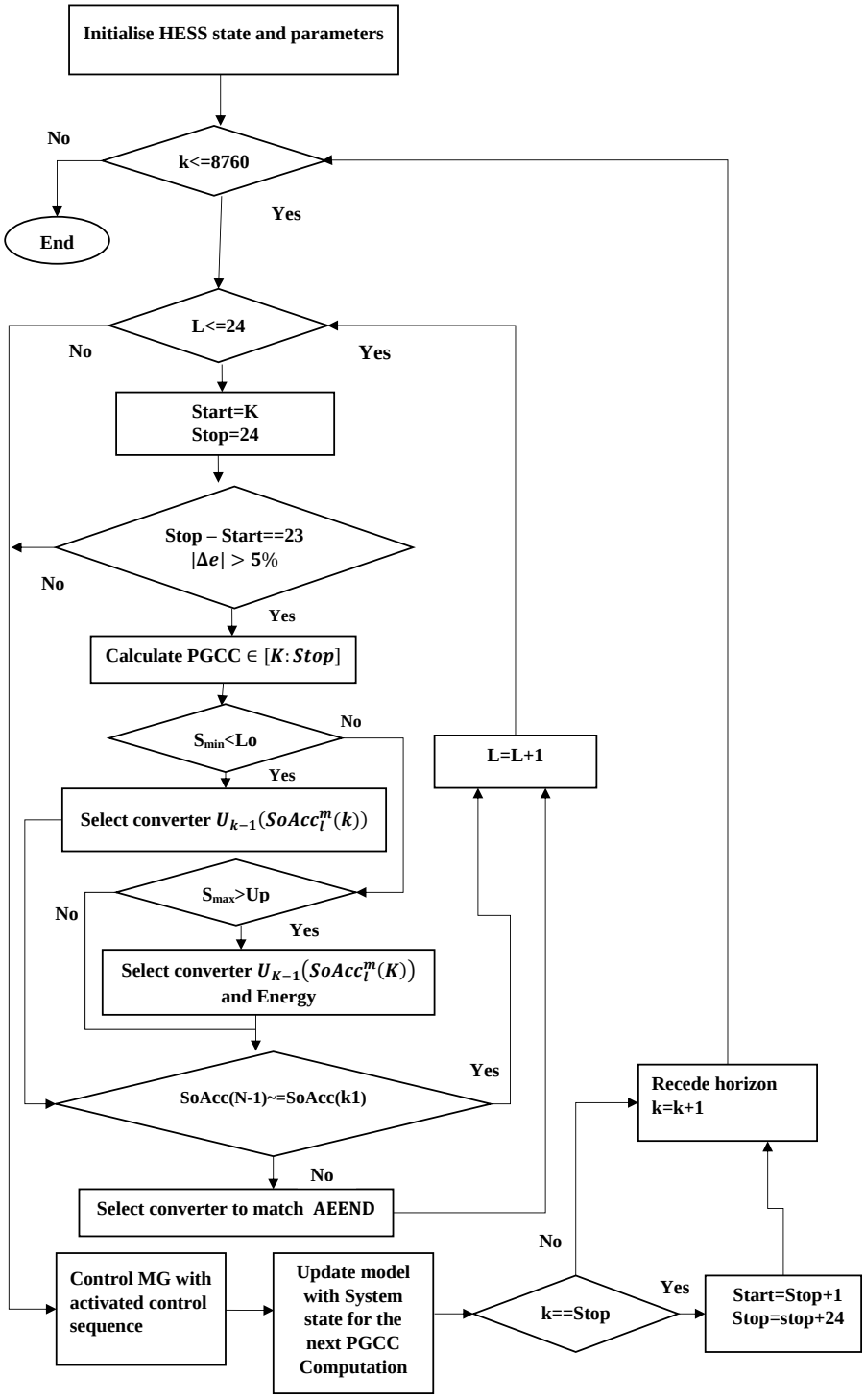

Fig. 4.2 Adaptive PoPA Algorithm

4.2 Kalman Filter-Adaptive PoPA

In section 4.1, the adaptive PoPA which serves as a measure to counteract uncertainty only offers a reactive error correction strategy and does not adequately account for the effect of un-modelled impending uncertainty. Therefore, as a consequence, the violation of the operating limits may eventually occur, as shown in 4.1b. Therefore, to address this issue, a one-step-ahead prediction is achieved using a Kalman filter (KF) estimator. Thus, the Kalman filter is integrated into the Adaptive PoPA framework (Kalman+Adaptive PoPA) for robustness. Hence, the ES's future state $SOAcc_l^m(k+1|k)$ is predicted while incorporating the effect of uncertainty at each time interval upon the availability of the most recent state $SOAcc_l^n(k)$ measurement of the ES. However, a KF estimator aims to minimise the variance between the real and the estimated ES's state of charge at each time instance (k). Nevertheless, KF is only an optimal estimator, contingent on the condition that the uncertainty is of a normal Gaussian distribution. Hence, it is included for comparison.

Firstly, in order to integrate the Kalman filter into the Adaptive PoPA framework, the standalone HESS is defined using a multiple-input-multiple-output discrete time state space representation as follows;

$$\mathcal{Z}: \begin{cases} \mathcal{X}(k+1) = \mathcal{A}\mathcal{X}(k) + \mathcal{B}\mathcal{U}(k) \ + \mathcal{W} \\ \mathcal{Y}(k) = \mathcal{C}\mathcal{X}(k) \end{cases} \tag{4.8}$$

Where,

$\mathcal{X}$: the systems state $\in R^n$

$\mathcal{A}$: state transition matrix $\in R^{nXn}$

$\mathcal{B}$: input transition Matrix is based on state activation $\in R^{nXm}$

$\mathcal{U}$: Input $\in R^m$

$\mathcal{C}$: is the observable matrix$\in R^{pXn}$

$\mathcal{Y}$: is the output state $\in R^k$

$\mathcal{W}$: is the Gaussian noise $\in R^n$

$\mathcal{Z}$: is the HESS model dynamics

Therefore, the expansion of the MIMO HESS state space is as follows:

$$\mathcal{X}(k) = \begin{bmatrix} 1 & 0 & 0 \\ 0 & 1 & 0 \\ 0 & 0 & 1 \end{bmatrix} \begin{bmatrix} SOAcc^n_{BAT}(k-1) \\ SOAcc^n_{HT}(k-1) \\ SOAcc^n_{WT}(k-1) \end{bmatrix} +$$

$$\begin{bmatrix} \varepsilon_{PV\to BAT} & \varepsilon_{BAT\to EL} & \varepsilon_{FC\to BAT} & \varepsilon_{BAT\to LD} & \varepsilon_{DSL\to BAT} & 0 & 0 \\ 0 & 0 & 0 & 0 & 0 & \varepsilon_{BAT\to EL} & 0 \\ 0 & 0 & 0 & 0 & 0 & 0 & \varepsilon_{FC\to BAT} \end{bmatrix} *$$

$$\begin{bmatrix} \mathcal{F}^{POW}_{PV\to BAT}(k) \\ -\mathcal{F}^{POW}_{BAT\to EL}(k) \\ \mathcal{F}^{POW}_{FC\to BAT}(k) \\ -\mathcal{F}^{POW}_{BAT\to LD}(k) \\ \mathcal{F}^{POW}_{DSL\to BAT}(k) \\ \sum(\mathcal{F}^{H2}_{EL\to HT}(k) - \mathcal{F}^{H2}_{HT\to FC}(k)) * \frac{C_{BAT}}{C_{HT}} \\ \sum(\mathcal{F}^{H2O}_{FC\to WT}(k) - \mathcal{F}^{H2O}_{WT\to EL}(k)) * \frac{C_{BAT}}{C_{WT}} \end{bmatrix} * \frac{100}{C_{BAT}} + W(k), : W(k) \in \mathcal{N}(\mu, \sigma \mid k) \quad (4.9)$$

$$\mathcal{Y}(k) = \begin{bmatrix} 1 & 0 & 0 \\ 0 & 1 & 0 \\ 0 & 0 & 1 \end{bmatrix} \begin{bmatrix} SOAcc^n_{BAT}(k) \\ SOAcc^n_{HT}(k) \\ SOAcc^n_{WT}(k) \end{bmatrix} \quad (4.10)$$

Hence, in order to predict the battery's state, a priori error covariance $\mathcal{P}_{k-1}$ matrix with respect to $SOAcc_l$, updates the Kalman gain K_G(k) as follows:

$$K_G(k) = \mathcal{P}_{k-1}\mathcal{I}^T[\mathcal{I}\mathcal{P}_{k-1}\mathcal{I}^T + \mathcal{R}_k]^{-1} \tag{4.11}$$

The updated Kalman gain is used to update the a priori co-variance matrix:

$$\mathcal{P}_k = \mathcal{P}_{k-1}[\mathcal{I} - K_{G(k)}\mathcal{I}] \tag{4.12}$$

Furthermore, the most recent output state measurement $SOAcc_l^n(k)$ is used to update the estimated state as follows:

$$SOAcc_l^m(k) = SOAcc_l^m(k|k-1) + K_{G(k)}[SOAcc_l^n(k) - \mathcal{I}SOAcc_l^m(k|k-1)] \tag{4.13}$$

$$\mathcal{P}_{k+1} = \mathcal{A}\mathcal{P}_k\mathcal{A}^T + \mathcal{Q}_k \tag{4.14}$$

Where, $\mathcal{A} \in l$ x l is an identity state transition matrix of the energy storages l, $\mathcal{I} \in l$xl is an identity matrix, Q_k is the process noise and R_k is the co-variance noise matrix related to the uncertainty in $SOAcc_l^m$.

The formulation presented has been generalised to consider a multi-vector case of uncertainty in the energy storages. Nevertheless, in this thesis, since the *SOAcc* of the BAT is the only element significantly affected by uncertainty, any uncertainty in both the *SOAcc* of HT and WT can be ignored.

In 4.13, the $SOAcc_{BAT}^m$(k) $\in [SOAcc_l^m$ (k)] is determined in order to identify the uncertainty over successive k- steps ahead until N, by the re-computation of the PGCC. Thereafter, the PGCC is re-shaped via PoPA minimum energy targeting as before. Thus, a sequence of dynamic EMSs which satisfies both the PoPA S_{LO} and S_{UP} constraints with uncertainty projection is realised in the prediction horizon for the optimal dispatch and scheduling of energy resources (FC and EL) in the control horizon. The concept is illustrated in Figure

5b, where the cyan plot indicates the PGCC re-shaped via the Kalman+Adaptive PoPA.The violation of the S_{UP} at time $k+11$, which occurred with the Adaptive PoPA EMS in Figure 4.1b, is avoided by dispatching the EL for recovery of the correct the MEES earlier than $k+10$. Similarly, the procedure is repeated for the AEEND constraint. Figure 4.4 shows the Kalman+Adaptive PoPA algorithm while the pseudo code is presented in Appendix C.

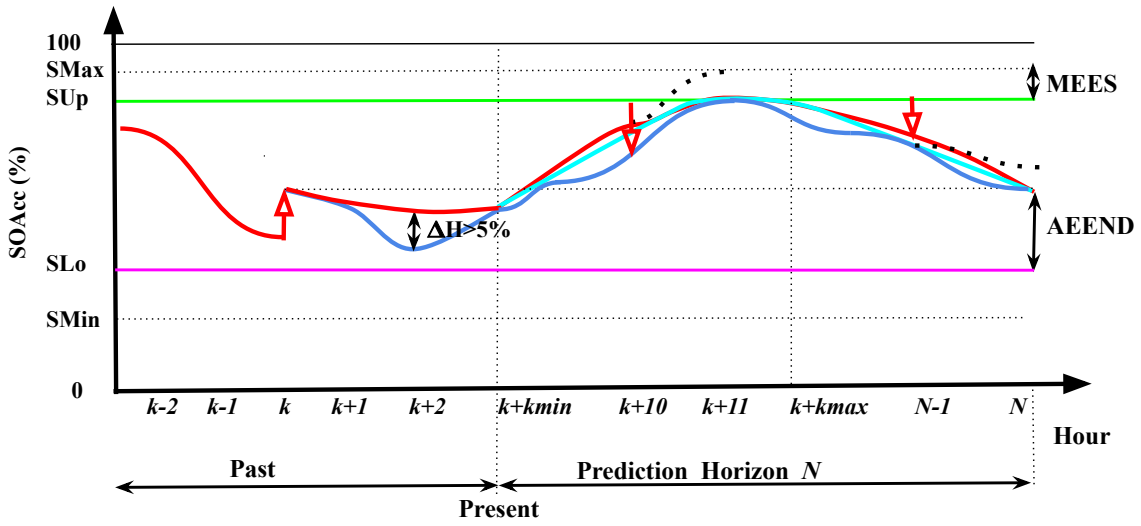

Fig. 4.3 PGCC shaped with Kalman+Adaptive PoPA

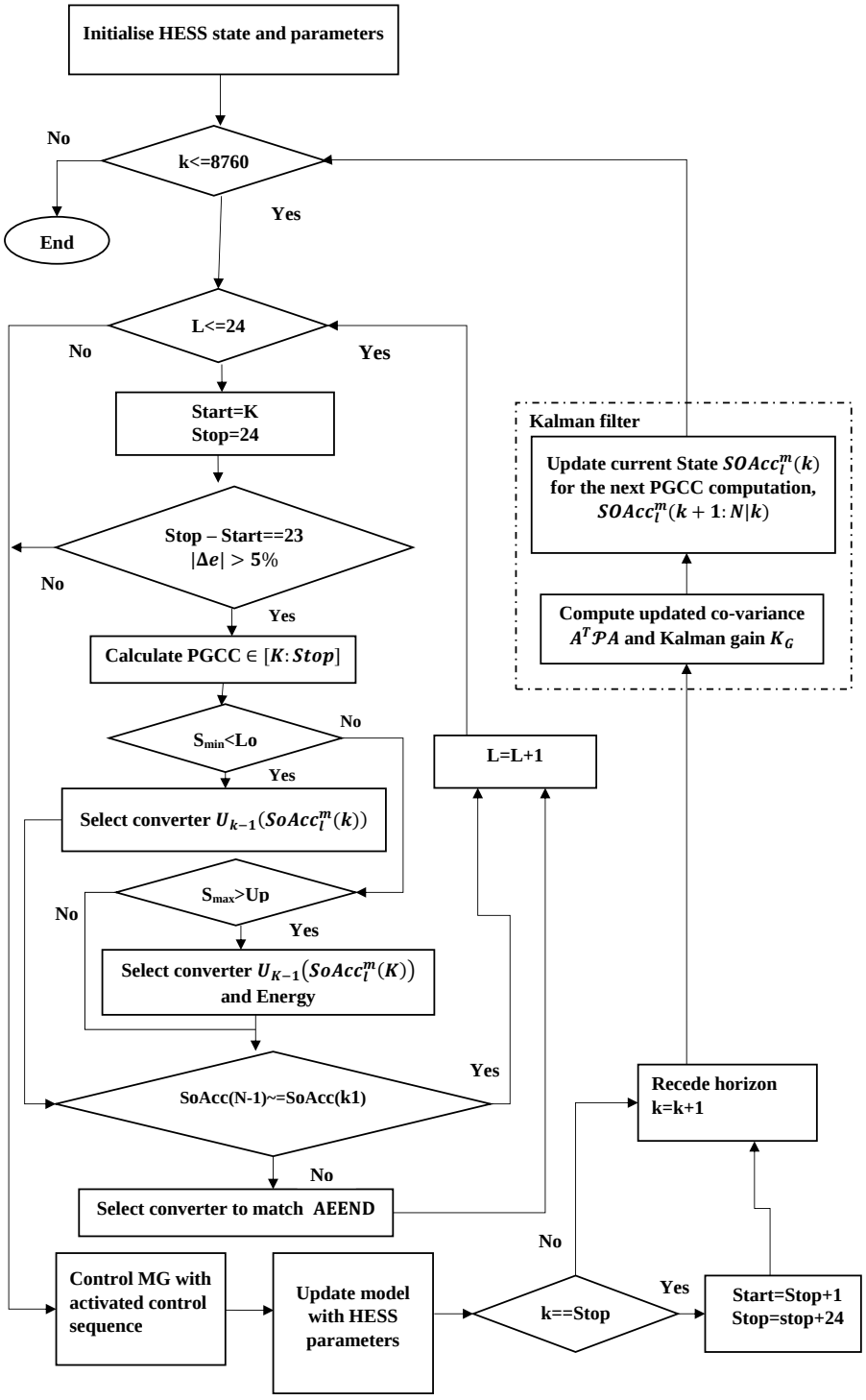

Fig. 4.4 Kalman+Adaptive PoPA Algorithm

4.3 Results and Discussion

The performance of the graphical EMS derived based on the Adaptive, and Kalman-Adaptive PoPA are evaluated against the DA PoPA with regards the HESS over three days (72h). The $SOAcc_l^m$ of storage elements $l \in \{BAT, HT, WT\}$ are initialised to 70%, 80% and 30% respectively. Prior to the investigation, the uncertainty dynamics in solar irradiance is modelled such that, a zero-mean μ and standard deviation σ^2 Gaussian noise $\mathcal{N}(0, \sigma^2 = 20)$ is added to the solar irradiance available to the HESS model. The solar irradiance which pertains to a location in Newcastle, United Kingdom with corresponding coordinates 54.9783° N, 1.6178° W, is obtained from National Renewable Energy Laboratory (NREL), Department of Energy, United States of America [132]. Also, real load demand profiles for a typical residential home pertaining to Newcastle, United Kingdom, are sourced from ELEXON [133]. Furthermore, a stochastic hourly LD is obtained by randomly sampling the quarterly hourly LD profiles pertaining to a typical residential home in the United Kingdom. In addition, two sets of LD uncertainty have been considered; a non-Gaussian and Gaussian. The non-Gaussian and Gaussian uncertainty both have the same first and second-order moments (μ=0 and σ=280 respectively), but different higher-order moments, skewness and kurtosis. Furthermore, the average LD, which is an unbiased estimate is used as the forecast LD parameter in the HESS model. The performance indices in equations 4.15-4.17 used for evaluating the EMSs, are mainly with respect to the total number of times the $S_{Lo}(30\%)$ and $S_{Up}(90\%)$ are violated and the DSL activated [44] as follows;

$$\text{Sum of deficit} = \sum_{k=1}^{N=8760} \left\{ \begin{array}{cc} 1 & S_{Lo} > SOAcc_{BAT}^n(k) \\ 0 & Otherwise \end{array} \right\} \tag{4.15}$$

$$\text{Sum of surplus} = \sum_{k=1}^{N=8760} \left\{ \begin{array}{cc} 1 & S_{Up}^l < SOAcc_{BAT}^n(k) \\ 0 & Otherwise \end{array} \right\} \tag{4.16}$$

$$\text{Sum of DSL activation} = \sum_{k=1}^{N=8760} \left\{ \begin{array}{ll} 1 & 20\% > SOAcc^{n}_{BAT}(k) \\ 0 & Otherwise \end{array} \right\} \tag{4.17}$$

4.3.1 DA-PoPA

As illustrated in Figures 4.5, the originally predicted PGCC reveals the $SOAcc^{m}_{BAT}$ would dip successively below S_{LO} due to impending energy deficit within the first 72 h if electricity is not outsourced in advance. Thus the PGCC is shaped accordingly by activating the FC four times, as shown in Figure 4.6. The activation of the FC consequently causes a 0.1% decrease of H2 in the HT and 0.07% increase of H2O in the WT, as indicated in Figure 4.7. Nevertheless, the PGCC continuously violates S_{Lo} 14 times which consequently led to the activation of the DSL twice successively due to uncertainty as indicated by the error plot as shown in Figure 4.5, regardless of hydrogen availability as shown in Figure 4.7.

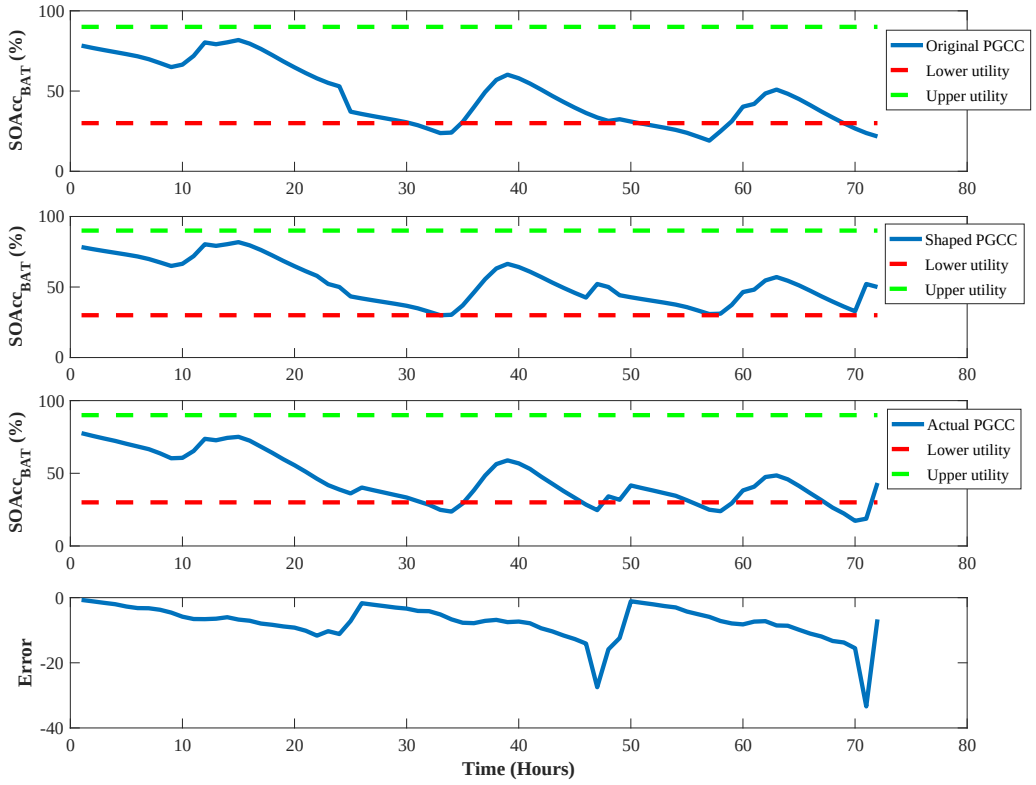

Fig. 4.5 DA-PoPA PGCC shaping and BAT response

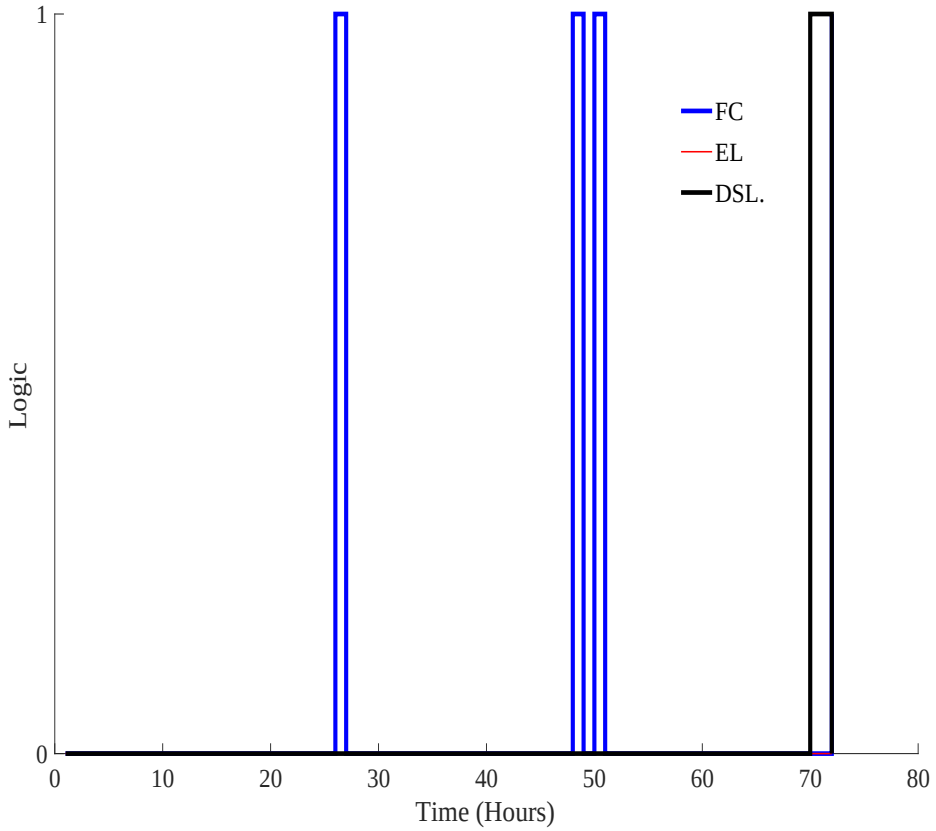

Fig. 4.6 Converter Logic for 72h with DA-PoPA

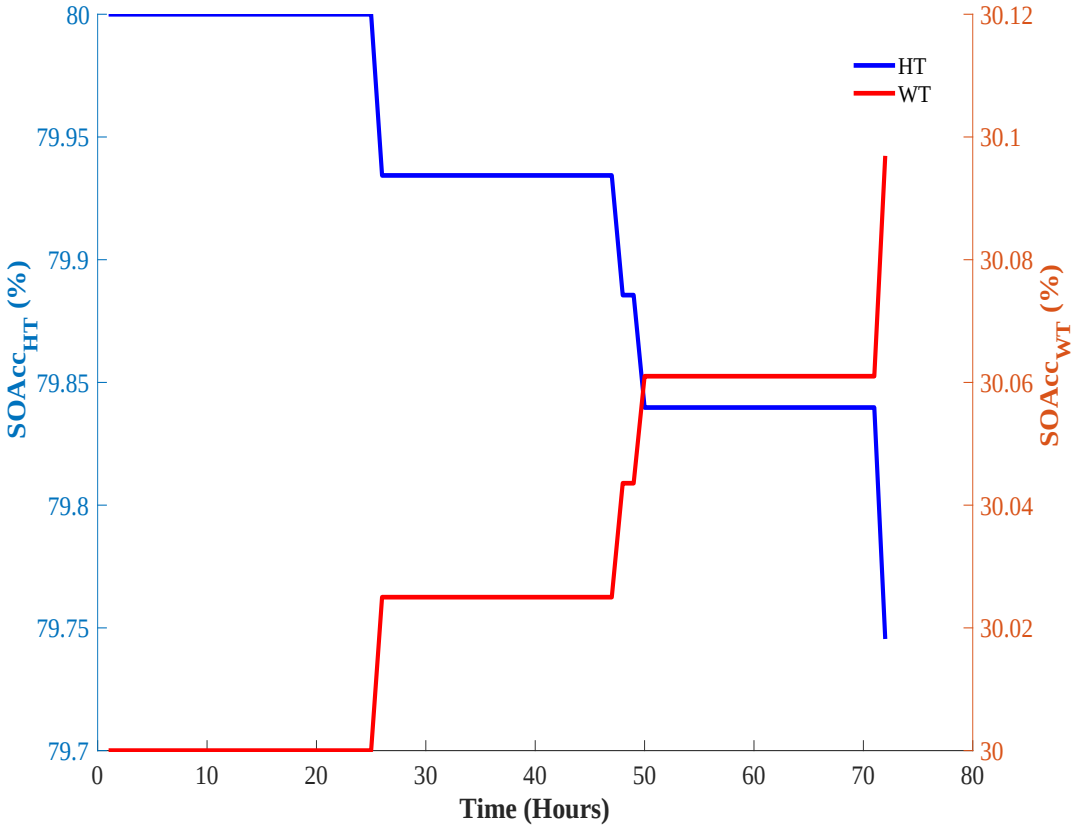

Fig. 4.7 HT and WT response for 72h with DA-PoPA

4.3.2 Adaptive PoPA

The incurred energy deficit, which was contingent on the forecast error deviation exhibited by the DA-PoPA, is reduced by the dynamic shaping of the PGCC within a receding control horizon, as shown in Figure 4.8a. Figure 4.8b illustrates the state error correction at the inception of the 11:00 h after ΔH became greater than 5% at 10:00 h. However, the $SOAcc^{n}_{BAT}$ dipped at the 33^{rd}, 34^{th}, 47^{th}, 57^{th}, 58^{th}, 70^{th}, and 71^{st} h, without activating the DSL. Furthermore, despite the activation of the FC six times, as shown in Figure 4.9 after the occurrence of the unexpected dip, a further violation of S_{Lo} re-occurred. This was because the MOES delivered by the FC was less than required, due to deficit energy target variability.

The successive dips underscore the need for a preventive approach since the reactive approach responds only after a forecast error has occurred.

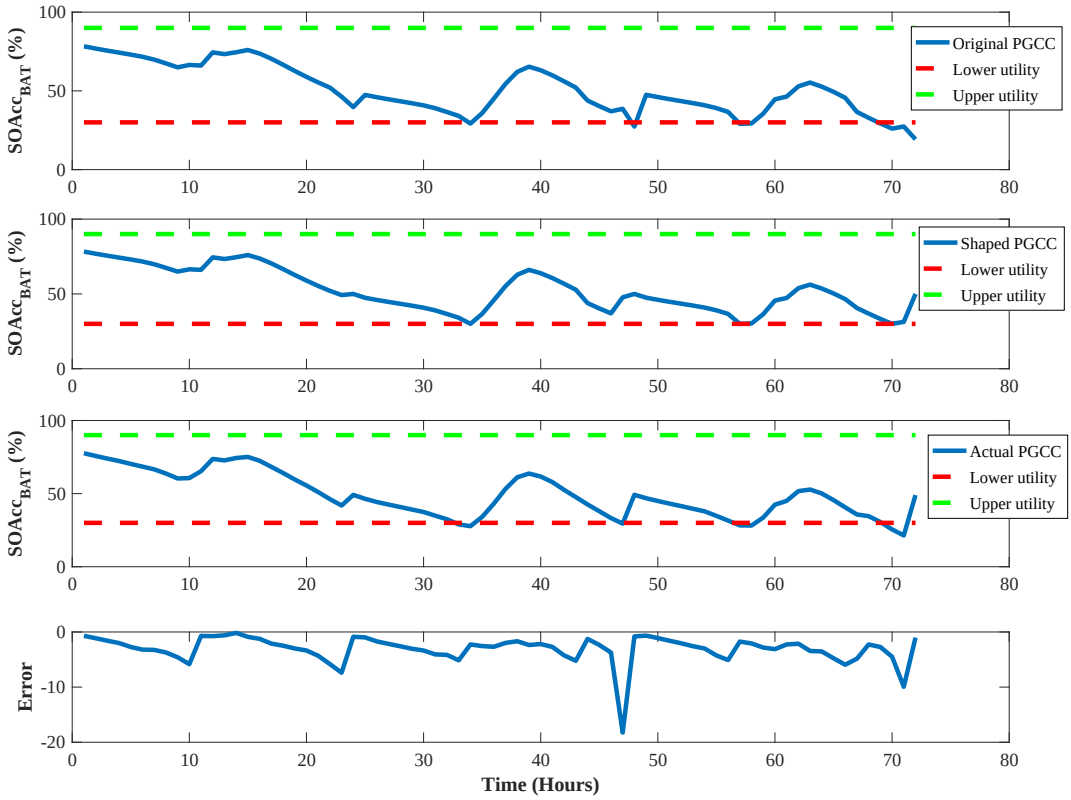

(a) PGCC shaping and BAT response under Gaussian uncertainty

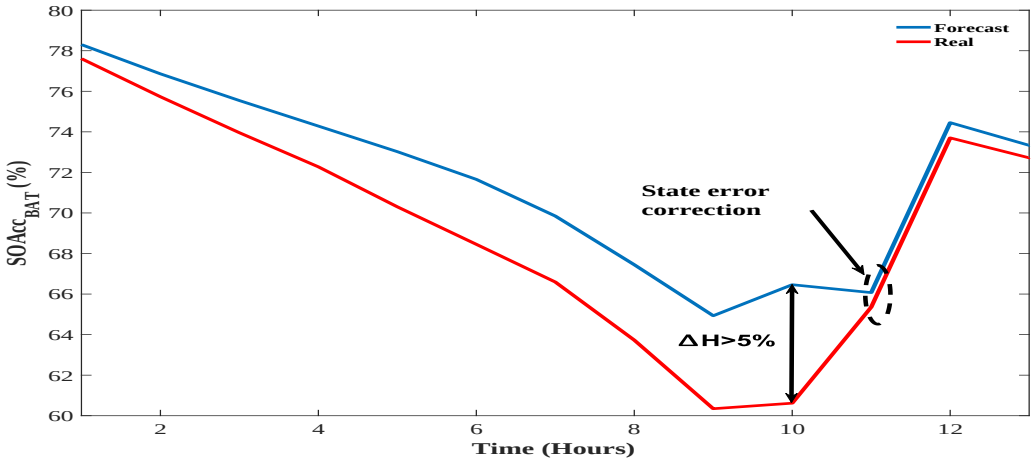

(b) Zoomed plot of State error correction

Fig. 4.8 PGCC shaping and BAT response with Adaptive PoPA

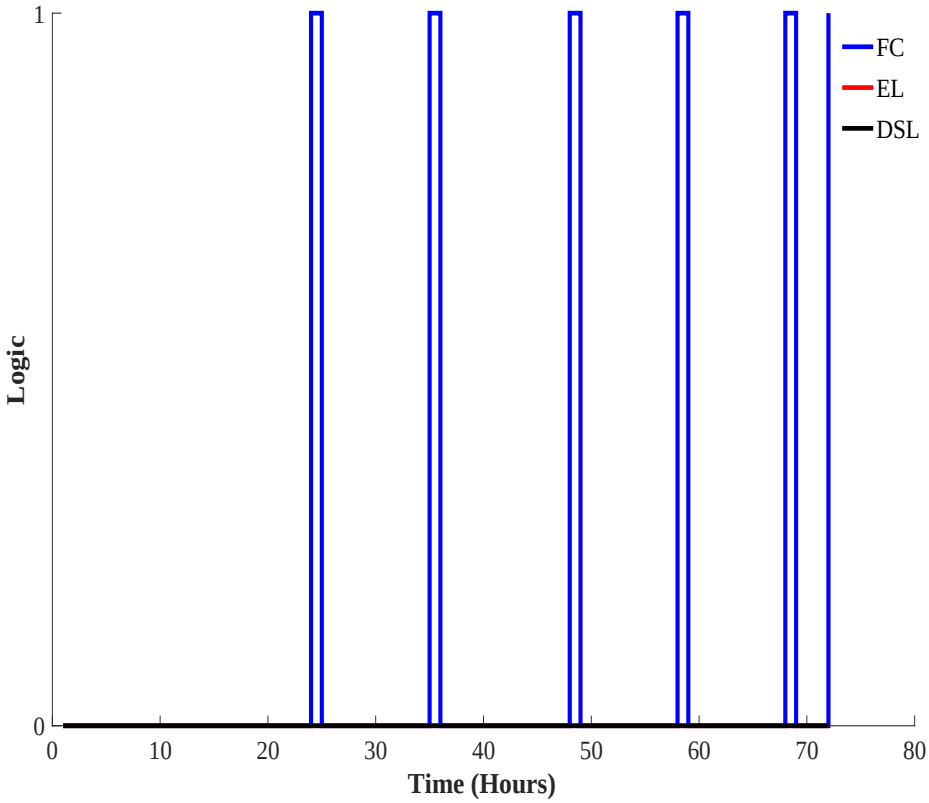

Fig. 4.9 Adaptive PoPA Converter Logic for 72h

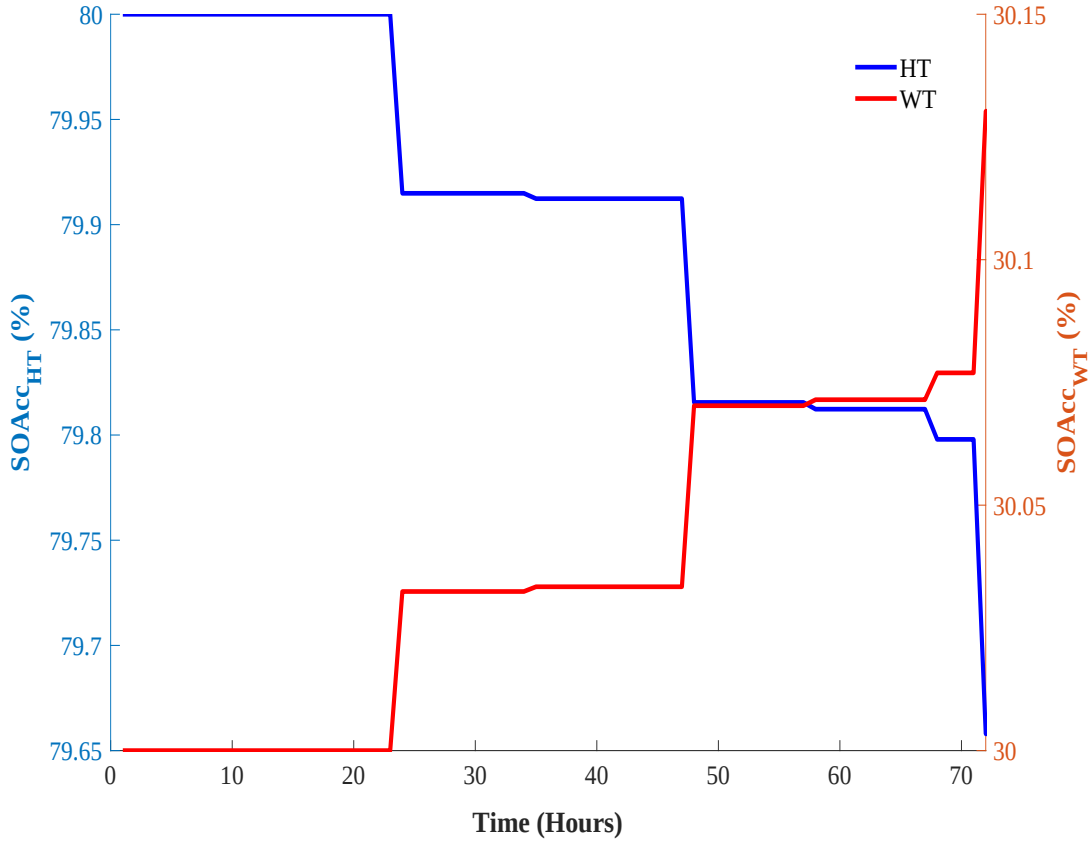

Fig. 4.10 HT and WT response for 72h with Adaptive PoPA

4.3.3 Kalman-Adaptive PoPA

The Kalman + Adaptive approach under a non-Gaussian uncertainty case study, resulted in the PGCC violating S_{LO} 7 times at time 49:00 - 56:00 h and at time 64:00 - 70:00 h, as shown in Figure 4.11. Consequently, the FC was activated 20 times in response to uncertainty with the DSL never activated, as shown in Figure 4.12. The Kalman+Adaptive PGCC closely matched the actual state of the plant as shown in Figure 4.11, with the uncertainty adequately propagated within the first 72h, hence, the performance was better than using the Adaptive PoPA alone. However, the uncertainty (previously unknown until now, but expected to be a normal Gaussian distribution) was essentially non-Gaussian (bimodal). Thus, further

investigation, as illustrated in Figures 4.14a and 4.14b shows that the Kalman+Adaptive PoPA performs better as the forecast error is reduced when the uncertainty is normally distributed. Hence, a more sophisticated approach when the uncertainty is unknown should suffice. Furthermore, Figure 4.12 shows the converter logic, while Figure 4.13 shows the corresponding effect on the $SOAcc_{HT}$ and $SOAcc_{WT}$ as a result of the FC being activated. At the end of the 72^{nd}h, the $SOAcc_{HT}$ decreased by 0.7% with a corresponding increase of 0.25% recorded in the WT.

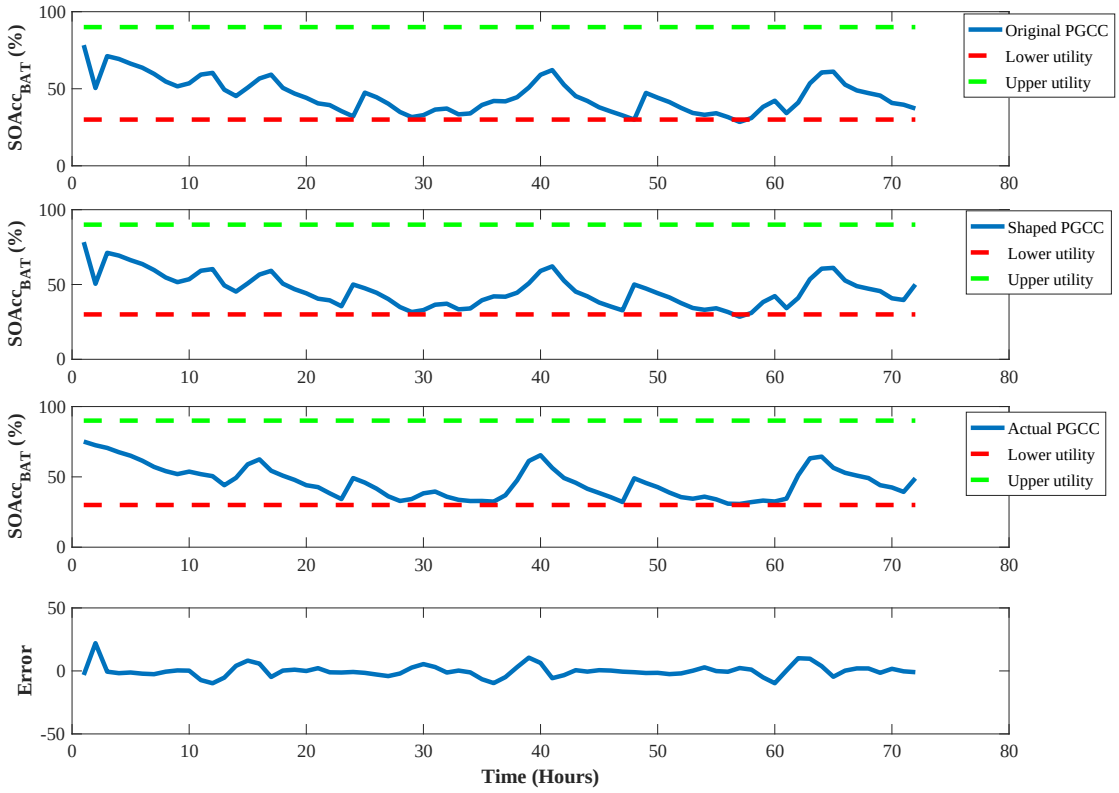

Fig. 4.11 PGCC shaping and BAT response for 72h under non-Gaussian uncertainty

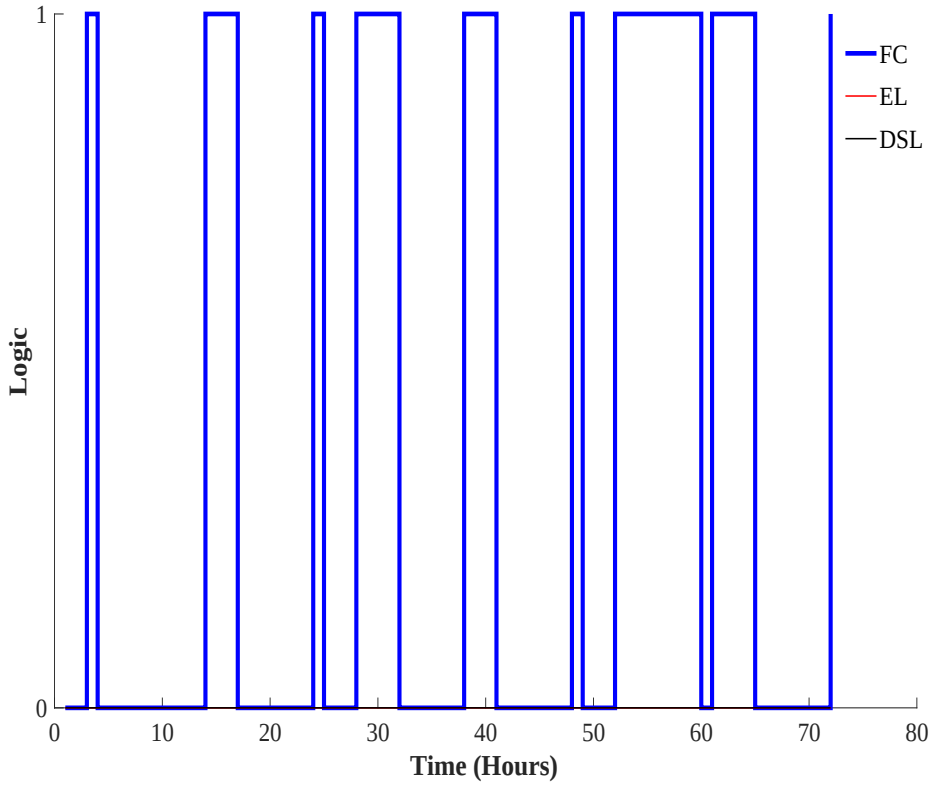

Fig. 4.12 Kalman-Adaptive PoPA Converter Logic for 72h under non-Gaussian uncertainty

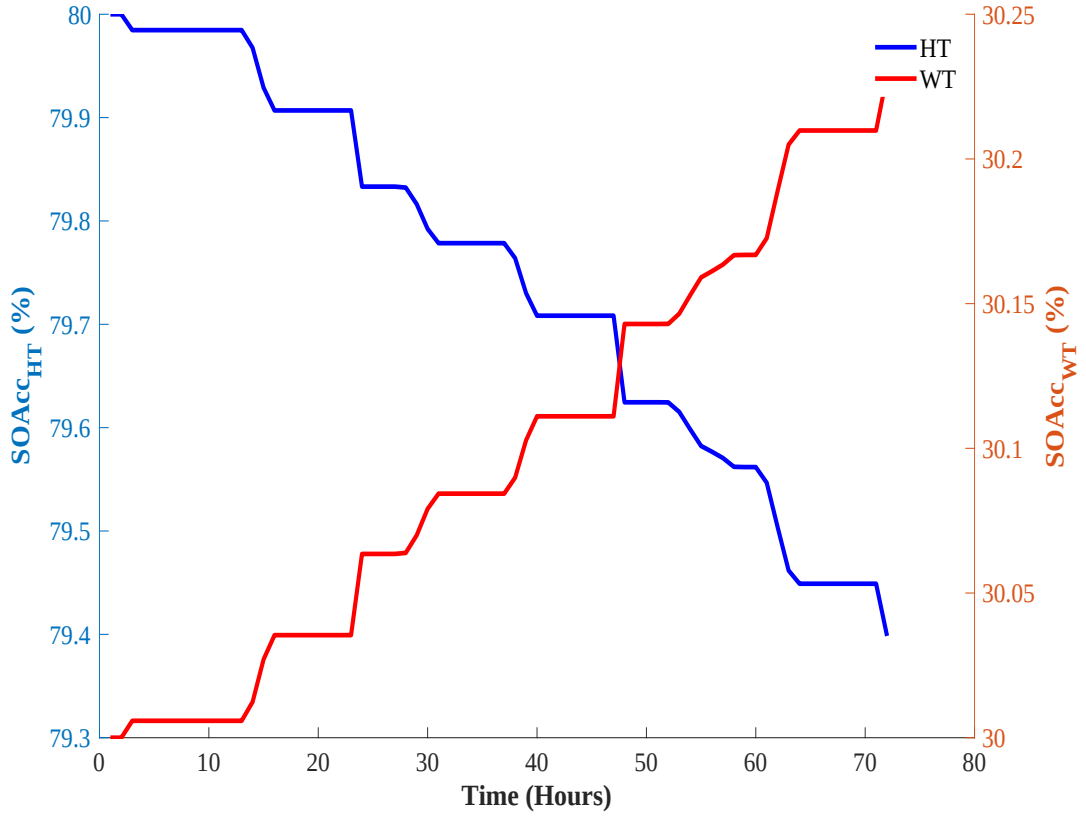

Fig. 4.13 HT and WT response for 72h with Kalman-Adaptive PoPA under non-Gaussian uncertainty

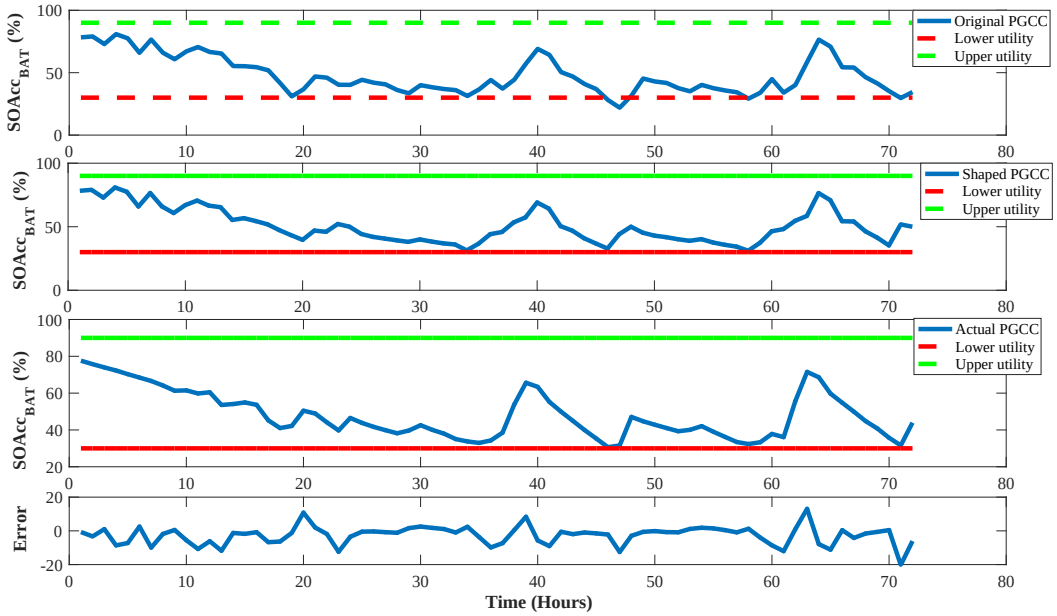

(a) PGCC shaping and BAT response under Gaussian uncertainty

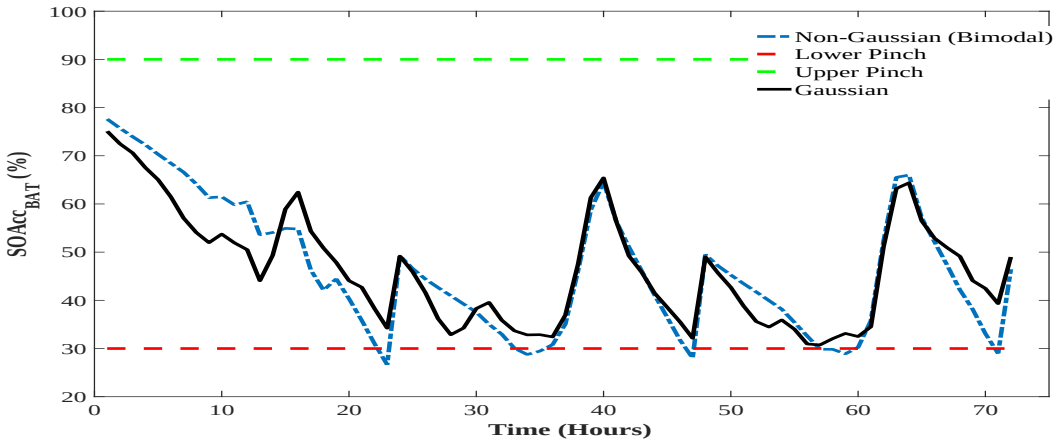

(b) Comparison of the real SOAcc response under both Gaussian and Non-Gaussian uncertainty

Fig. 4.14 PGCC shaping and BAT response with Kalman Adaptive PoPA under Gaussian uncertainty

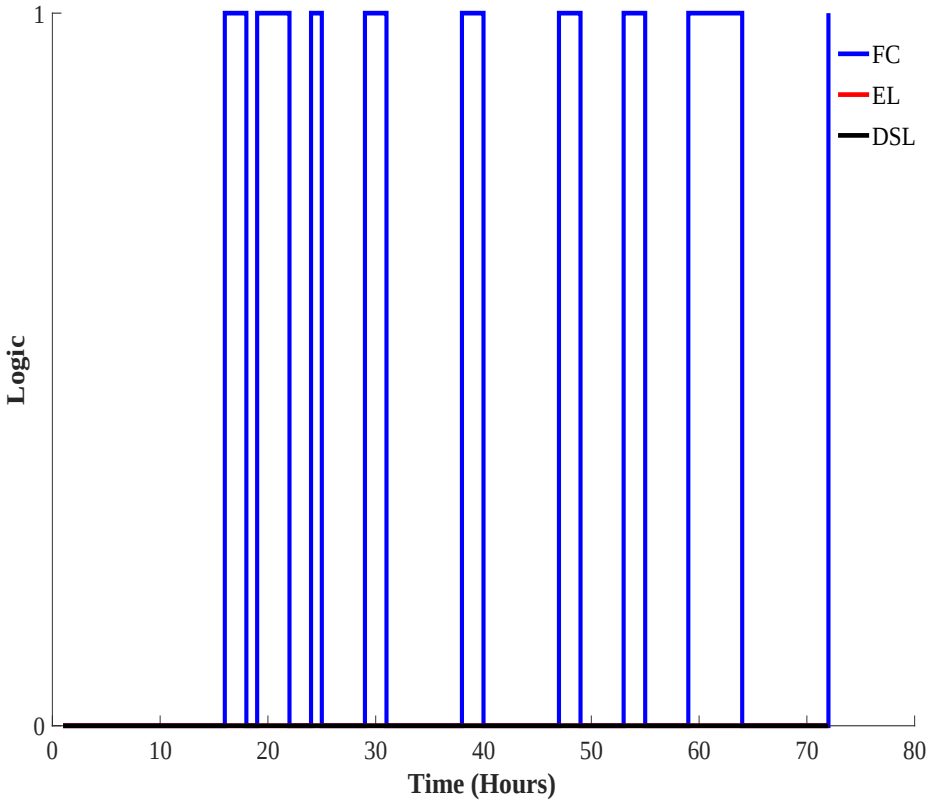

Fig. 4.15 Kalman-Adaptive PoPA Converter Logic for 72h

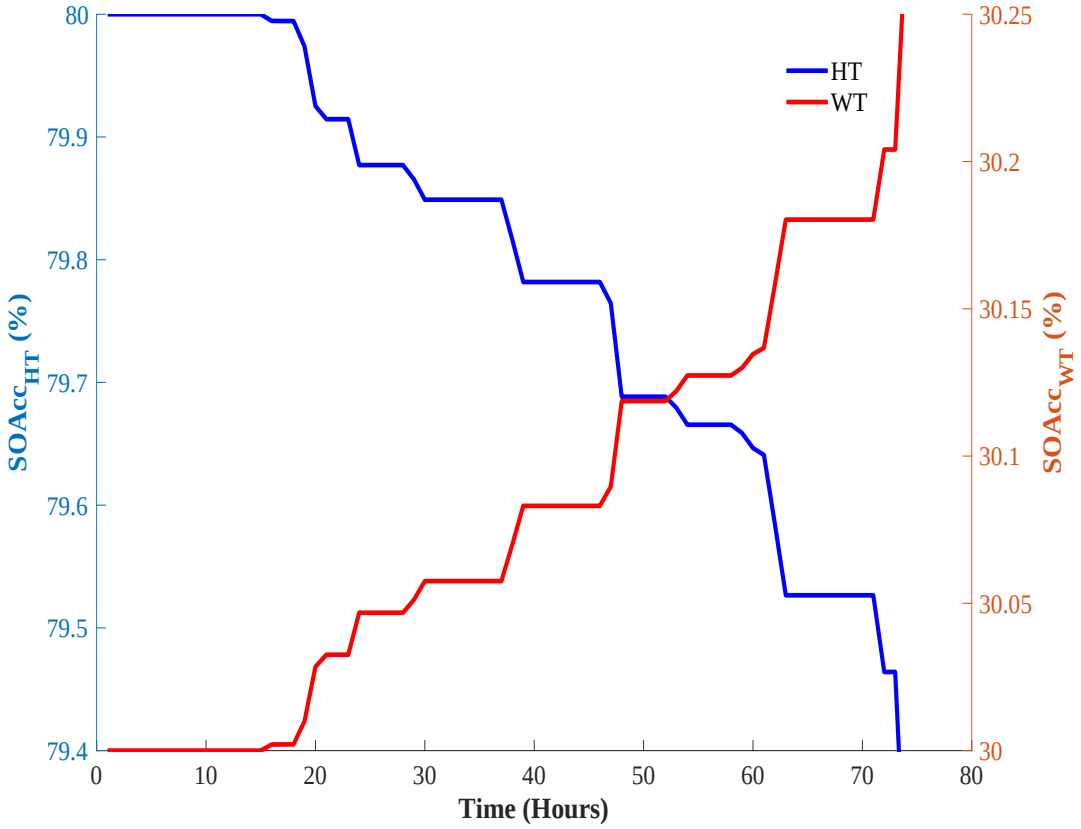

Fig. 4.16 HT and WT response for 72h with Kalman-Adaptive PoPA under non-Gaussian uncertainty

The DA had a negligible better computational time of 0.59s and 0.58s for both non-Gaussian and Gaussian uncertainty than the Adaptive which had 0.67s and 0.65s respectively. The Kalman+Adaptive computational time was the highest with the performance at 0.67s and 0.65s under non-Gaussian and Gaussian uncertainty as shown in Tables 4.1-4.2. The computational time for the DA, Adaptive and Kalman+Adaptive PoPA had a negligible increase under non-Gaussian uncertainty. The violation of *SLo* as indicated in Table 4.1-4.2 showed Kalman Adaptive PoPA had the most significant improvement from 7 to 0 *SLo* violations, though none for the S_{Up} under Gaussian uncertainty and non-Gaussian case

respectively. The Adaptive PoPA had an improvement when the uncertainty was Gaussian, with only a negligible change of 1, in the DA-PoPA's performance.

Table 4.1 Summary of the performance indices of the DA, Adaptive, Kalman+Adaptive PoPA for 72h under non-Gaussian uncertainty

Performance index	**Non-Gaussian uncertainty**		
	DA-PoPA	**Adaptive PoPA**	**Kalman+Adaptive PoPA**
Lower Pinch violation	14	7	7
Upper Pinch Violation	0	0	0
DSL Activation	2	0	0
Computation Time (s)	0.59	0.67	1.33

Table 4.2 Summary of the performance indices of the DA, Adaptive, Kalman+Adaptive PoPA for 72h under Gaussian uncertainty

Performance index	**Gaussian uncertainty**		
	DA-PoPA	**Adaptive PoPA**	**Kalman+Adaptive PoPA**
Lower Pinch violation	13	3	PoPA
Upper Pinch Violation	0	0	0
DSL Activation	0	0	0
Computation Time (s)	0.58	0.65	1.26

4.4 Summary

The Adaptive PoPA and Kalman-Adaptive PoPA have been in evaluation against the DA-PoPA, with the violation of the S_{Lo}, S_{Up} and DSL activation used as the main performance indices. In the 72h investigation, the DA-PoPA which utilised a DA forecast without consideration for uncertainty had the worst overall performance. The investigation entailed two cases of non-Gaussian (Bi-modal) and Gaussian uncertainty. The DA-PoPA was shown

to have the highest number of the S_{Lo} violations due to reliance on a DA strategy, which lacks a feedback error mechanism necessary to counteract the impacts of uncertainty. Nevertheless, the Adaptive PoPA which was proposed showed robustness to uncertainty. However, the Adaptive PoPA was shown to suffer from the effects of un-anticipated uncertainty, which led to 7 S_{Lo} violations. The Kalman-Adaptive PoPA, which used a Kalman filter to project the uncertainty, given the likelihood of deviation, enhanced the performance of the Adaptive PoPA. However, this enhanced performance was only evident under a Gaussian uncertainty case study.

Chapter 5

Probabilistic Adaptive Power Pinch Analysis

OUTLINE

This chapter is based on a published work, "Probabilistic adaptive power Pinch Analysis for energy management" [47] in The Journal of Engineering, IET. The approach is facilitated by harnessing stochastic information such as the joint probability density function of the historical consumer load demand profile and renewable sources variability. In contrast to the previous deterministic approach presented in Chapter 4, the probabilistic adaptive Power Pinch Analysis is formulated within a least-square recursive Monte Carlo chance-constraint model predictive framework. However, the approach necessitates a trade-off between computational complexity and robustness with regards to leveraging uncertainty information from historical data.

5.1 Introduction

As illustrated in Chapter 4, the EMS based on an Adaptive PoPA identified and matched energy demand, and excessive energy supply is conservatively based on a deterministic

model approach. Unfortunately, due to the uncertainty associated with RES and load demand, which is often probabilistic and may exhibit daily, seasonal, and geographical variability, forecast error may be introduced. Thus, in reality, satisfying the energy systems constraints using a deterministic model may not easily be achieved. Furthermore, deterministic models are often considered with a set of deterministic input variables and upon the occurrence of each variation, and more often than necessary, it becomes imperative to repeat the simulation process in order to obtain a new solution or analysis [118]. Therefore, from a practical perspective, where adequate historical and statistical evidence regarding the uncertain parameters is available, it can be leveraged using a probabilistic approach. Hence, the adaptive PoPA [46] presented in Chapter 4, is recast in a probabilistic framework [47] in the present Chapter. Two PGCC's which represents a probabilistic chance-constrained bound on the certainty of the SOAcc are simultaneously obtained from Monte Carlo simulation (MCS) by analysis of stochastic or random scenarios in order to proffer enhanced robustness to uncertainty. Furthermore, in order to enhance the EMS, a recursive correction factor which is determined based on least-squares error approach via the residual error between the actual and predicted SOAcc is used to update the prediction SOAcc. The chance constraint sizing approach presented in [45], in order to determine the minimum solar panel array area in the PoPA framework, primarily targeted reliability of the deterministic load demand being met as well as the battery being charged. Furthermore, energy management of BAT in the event that the battery becomes fully charged and the utilisation of the excess energy were not discussed. Thus, inspired by the of the works of [44, 45] an adaptation is presented by defining the adaptive energy management algorithm in a recursive least square probabilistic MCS chance-constrained framework. Furthermore, the excess energy in the system, represented by overcharging the BAT ($SOAcc^n_{BAT}$>90%) and energy recovered as well as over-discharging the BAT ($SOAcc^n_{BAT}$<30%) is considered in the chance constraints evaluated with the MCS. The MCS sampling is performed iteratively in the prediction horizon to determine the chance

of the PGCC, violating the HESS operational constraints. The pinch set limits, as well as the AEEND constraints, are expressed probabilistically using the chance constraint. Therefore, two PGCCs forms an upper and a lower closed bound within which the uncertainty is defined. Consequently, the EMS which infers the optimal control sequence to keep the system within the desired operating limits is effected in advance at the beginning of the receding control horizon, while incorporating robustness to uncertainty [46].

5.2 Probabilistic Adaptive PoPA Formalization

Firstly, the deterministic PGCC computed in the predictive horizon [46] as described in Chapter 4, is expressed in an adaptive receding horizon model predictive framework, with state error correction as follows;

$$SOAcc_l^m(k) = \min_{U_c} \sum_{k=1}^{N} \left[SOAcc_l^m(k-1) + \left(\sum_{X_l \in E_{tr}} \mathcal{F}^j_{l \leftarrow X_l}(k) - \sum_{Y_l \in E_{tr}} \mathcal{F}^j_{l \rightarrow Y_l}(k) \right) * \frac{\Delta k}{C_l} \right] \quad (5.1)$$

Let the vector $mSOAcc_l^m$ contain elements of corresponding time series state of charge of the storages $SOAcc_l^m(k)$ as follows:

$$mSOAcc_l^m := \langle SOAcc_l^m(k), SOAcc_l^m(k+1), SOAcc_l^m(k+2) \ldots SOAcc_l^m(N) \rangle \quad (5.2)$$

Secondly, by decoupling the energy consuming assets $Y_l \in \{LD, EL\}$ with emphasis on $l \in \{\text{BAT}\}$ and corresponding energy flow $\mathcal{F}^j_{l \rightarrow Y_l}$, the $SOAcc^m_{BAT}$ is defined as a function of the flow of energy from the Battery to an i.i.d random load $LD^i \in (LD^1, \ldots, LD^M)$.

$$SOAcc_l^m(k) = \sum_{i=1}^{M}\sum_{k=1}^{N} \left[SOAcc_l(k-1) + \left(\sum_{X_l \in E_{tr}} \mathcal{F}^j_{l \leftarrow X_l}(k) - \left[\mathcal{F}^j_{l \rightarrow EL_l}(k) + \mathcal{F}^j_{l \rightarrow LD_l}(k) * f_X(LD^i(k)) \right] \right) * \frac{\Delta k}{C_l} \right] \tag{5.3}$$

Where, $f_X\left(LD^i\right)$ is the probability density of the random variable LD, estimated using a non-parametric kernel density estimator, KDE [134] in MATLAB and subscript indicates the i^{th} sample of the random variable drawn from a prior distribution.

Furthermore, a matrix which contains mn-elements of $SOAcc_l^m$, is defined as follows:

$$MSOAcc_l^m = \begin{bmatrix} SOAcc_{1,1} & SOAcc_{1,2} & \cdots & SOAcc_{1,N} \\ SOAcc_{2,1} & SOAcc_{2,2} & \cdots & SOAcc_{2,N} \\ \vdots & \vdots & \ddots & \vdots \\ SOAcc_{M,1} & SOAcc_{M,2} & \cdots & SOAcc_{M,N} \end{bmatrix} = SOAcc(i,j) \in R^{M,N} \tag{5.4}$$

$*$*Subscript l in $SOAcc_{MN}$ has been omitted in equation* (5.4) *for conciseness and* $m,n \neq M,N$.

Therefore, the matrix comprises the posterior distribution of the $SOAcc_l$ for each consumer load, sampled randomly from the priori distribution.

Furthermore, the probabilistic PoPA performed with $z \in [1:L]$ iterations until the lower and upper limits expressed using the chance constraints are matched and do not violate any of the operating limits as follows:

$$SOAcc_l^m(i,j)^z = \sum_{z=1}^{L}\sum_{i=1}^{M}\sum_{k=1}^{N-1} \left[SOAcc_l(k-1) + \left(\sum_{X_l \in E_{tr}} \mathcal{F}^{j(i)}_{l \leftarrow X_l}(k) - \sum_{Y_l \in E_{tr}} \mathcal{F}^{j(i)}_{l \rightarrow Y_l}(k) \right) * \frac{\Delta k}{C_l} \right] \tag{5.5}$$

Thus, analytically by plotting the cumulative density function (CDF) at each time step k, the probability, Pr of violating the lower limit is constrained by the chance factor α_1:

$$SOAcc_l^m(i,j)^z = \sum_{z=1}^{L}\sum_{i=1}^{M}\sum_{k=1}^{N-1}$$
$$Pr\left[\left[SOAcc_l(k-1) + \left(\sum_{X_l\in E_{tr}} \mathcal{F}_{l\leftarrow X_l}^{j(i)}(k) - \sum_{Y_l\in E_{tr}} \mathcal{F}_{l\rightarrow Y_l}^{j(i)}(k)\right) * \frac{\Delta k}{C_l}\right] \geq S_{min}\right] \geq \alpha_1 \quad (5.6)$$

Where $\alpha_1 \in [0,\ 1]$ is the chance constraint factor as regards the lower pinch limit.

Similarly, the chance of violating the upper pinch limit is expressed as follows:

$$SOAcc_l^m(i,j)^z = \sum_{z=1}^{L}\sum_{i=1}^{M}\sum_{k=1}^{N-1}$$
$$Pr\left[\left[SOAcc_l(k-1) + \left(\sum_{X_l\in E_{tr}} \mathcal{F}_{l\leftarrow X_l}^{j(i)}(k) - \sum_{Y_l\in E_{tr}} \mathcal{F}_{l\rightarrow Y_l}^{j(i)}(k)\right) * \frac{\Delta k}{C_l}\right] \geq S_{max}\right] \leq 1-\alpha_2 \quad (5.7)$$

Where $\alpha_2 \in [0,\ 1]$ is the chance-constraint factor pertaining to the upper pinch limit.

Thus, the probability density function (PDF) of $SOAcc_l^m$ can be analytically computed from the j^{th} column of the matrix, $MSOAcc_l^m$ and represented as follows;

$$f_X(SOACC_l^m) = [f_{X_{11}}(SOAcc_l^m),\ f_{X_{12}}(SOAcc_l^m)\cdots,\ f_{X_{1N}}(SOAcc_l^m)] \quad (5.8)$$

Where, f_X denotes the PDF and subscript X indicates the dependent variable $SOAcc_l^m$.

Therefore, the desired operating range for $SOAcc_l^m$ (k) with respect to the chance constraint is determined analytically with the CDF as follows:

$$\int_{S_{min}}^{S_{max}} f_{SOAcc_l^m}(SOAcc_l^m)d(SOAcc_l^m) = F_{SOAcc_l^m}(S_{max}) - F_{SOAcc_l^m}(S_{min}) \quad (5.9)$$

Where, $F_{SOAcc_l^m}$ denotes the CDF of $SOAcc_l^m$ and the right-hand side of equation 5.9 is an equivalent PDF.

Therefore, the desired operating range for $SoAcc_{BAT}^m(k)$ with respect to the chance constraint can be expressed as follows:

$$F^{-1}_{SOAcc^m_{BAT}}(\alpha_1) \leq F(SOAcc^m_{BAT}) \leq F^{-1}_{SOAcc^m_{BAT}}(1-\alpha_2) \tag{5.10}$$

Furthermore, in order to evaluate the probability of the $SOAcc_l^m$ violating the lower limit, we utilise the inverse CDF as follows:

$$LSOAcc_l^m(k) = \sum_{k=1}^{N-2} inf\left\{F_{X_k}^{-1}(\alpha_1) < S_{min}\right\} \tag{5.11}$$

Where, $LSOAcc_l^m$ is a vector of n-elements, which represent point estimates of $SOAcc_l^m(k)$ that are less than the lower pinch chance constraint factor α_1 evaluated using the inverse CDF F_X^{-1}.

In addition, the MOES based on the probabilistic approach is determined as follows:

$$If\ \exists\ LSOAcc_l^m < S_{min}$$

$$\mathcal{F}^{POW}_{BAT\leftarrow FC} = (S_{min} - \arg\min[LSOAcc_l^m]) * C_l \tag{5.12}$$

Thus, by activating the dispatchable resources (in this case the FC), the energy storage (such as BAT) is supplied with the MOES with an equivalent magnitude of flow $\mathcal{F}^{POW}_{BAT\leftarrow FC}$ as determined in (5.12) at the present time step k

Similarly, after satisfying the lower pinch constraint, the PGCC is recomputed as in (5.1) and the violation of the upper pinch limit is determined as follows:

$$If\ \exists\ USOAcc_l^m(.) > S_{max}$$

$$USOAcc_l^m(k) = \sum_{k=1}^{N-2} Sup\left\{F_{X_k}^{-1}(1-\alpha_2) > S_{max}\right\} \tag{5.13}$$

Where, $USOAcc_l^m$ is a vector of n-point estimates of $SOAcc_l^m\ (k)$ which are greater than the upper pinch chance constraint factor α_2 evaluated with the inverse CDF F_X^{-1}.

Consequently, the MEES is estimated from equation (5.14) in order to match any existing upper pinch violation in 5.13 as follows:

$$\mathcal{F}_{BAT\rightarrow EL}^{POW} = (\arg\max[\ USOAcc_l^m] - S_{max}) * C_l \tag{5.14}$$

Thereafter, the available electricity for the next day (AEEND) for life cycle preservation is determined using the upper bound chance constraint as follows:

Thus,

$$AEEND:\ U_c(k) = \left\{ \begin{array}{cc} \mathcal{F}_{BAT\leftarrow FC} & F_{X_k}^{-1}(1-\alpha_2) < SOAcc_{BAT}^n(k_1) \\ \mathcal{F}_{BAT\rightarrow EL} & F_{X_k}^{-1}(1-\alpha_2) < SOAcc_{BAT}^n(k_1) \\ 0 & Otherwise \end{array} \right\} \forall_{k\in[N-1]} \tag{5.15}$$

The PoPA EMS decision making variable $U_c(k)$ with the corresponding magnitude of energy flow determined in equations 5.12, 5.14 and 5.15 will satisfy both the lower and upper pinch points and AEEND, with regards to the chance constraint equations which have been formulated in an adaptive receding horizon model predictive framework. Furthermore, the EMS sequence obtained with the probabilistic model is, therefore effected in the control horizon while taking into account the overall risk of violating the utility pinch constraints. Figure 5.1 graphically summarises the stages in the realisation of the Probabilistic Adaptive PoPA EMS and Figure 5.2 shows the P+Adaptive PoPA algorithm.

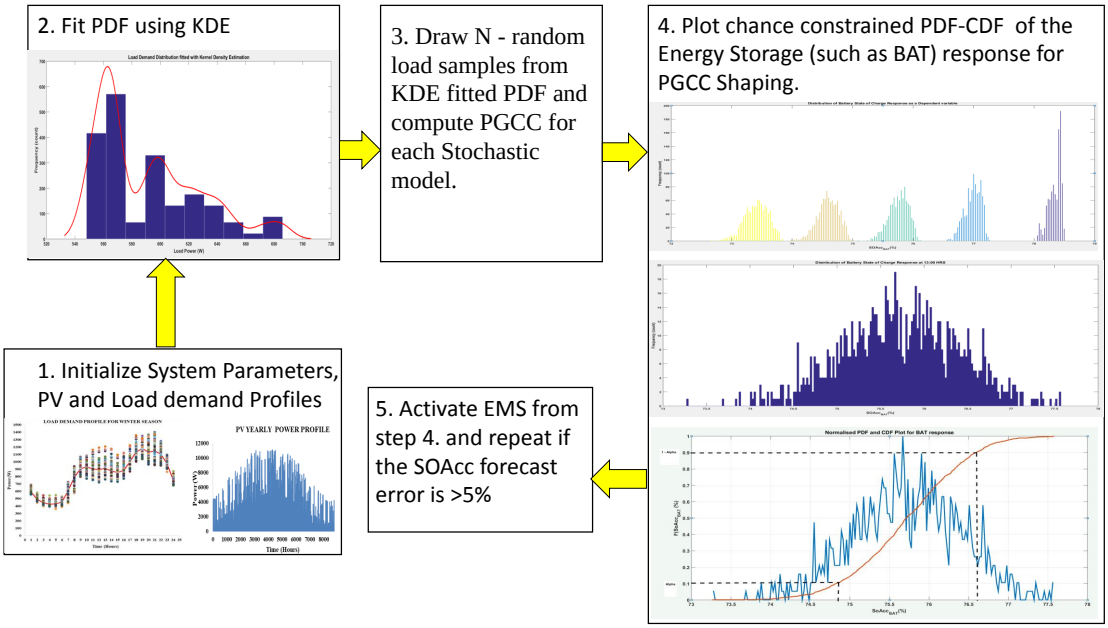

Fig. 5.1 Illustration of the Probabilistic+Adaptive PoPA EMS

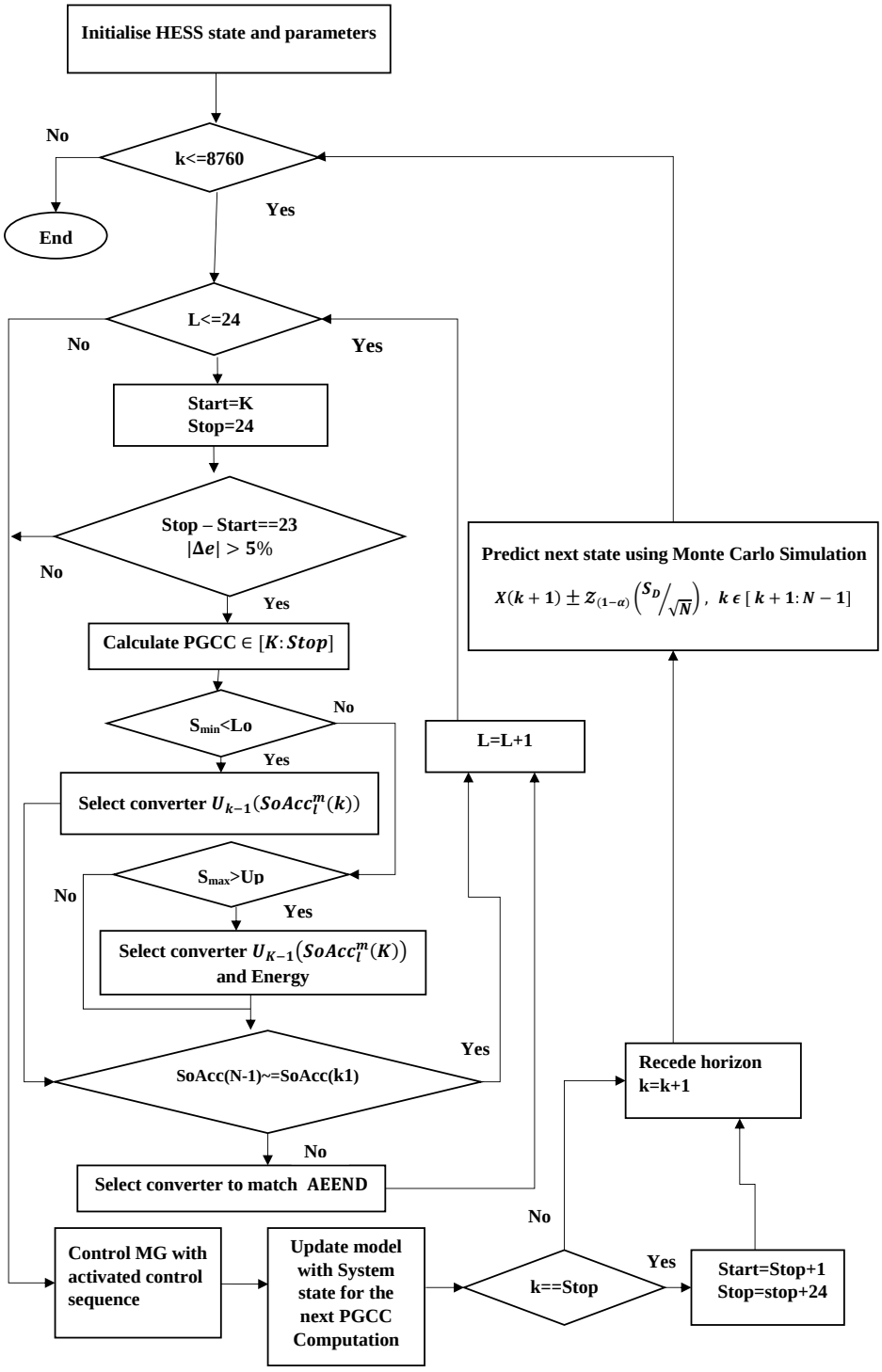

Fig. 5.2 Probabilistic+Adaptive PoPA Schematic Flow Chart

5.3 Recursive Least Square Probabilistic Adaptive PoPA

To improve the estimation of actual $SOAcc^n$ via the probabilistic PoPA, a simple correction factor which minimises the residual error loss function between the actual $SOAcc^n$ and estimated $SOAcc^m$ can be incorporated recursively into the process.

Let the equilibrium relationship between the actual $SOAcc^n$, the estimated $SOAcc^m$ and an unbiased multiplicative correction factor be:

$$SOAcc^n(k) = SOAcc^m(k) * x \tag{5.16}$$

Where,

$$SOAcc^m(k) = (LSOAcc^m(k) + USOAcc^m(k))/2 \tag{5.17}$$

Where,

$SOAcc^m$ is the expectation of the dependent variable $SOAcc^m$, and $LSOAcc^m$ and $USOAcc^m$ respectively are the lower and upper bound confidence intervals (of say 98%) on the expected value, and x is the multiplicative correction factor.

Thus, by ordinary least square error method [135, 136], the unbiased residual error correction factor is determined via a mean squared error (MSE) loss function in equations 5.18-5.21 as follows:

$$MSE = \frac{1}{2N}\sum_{k=1}^{N}(SOAcc^n(k) - SOAcc^m(k) * x)^2 \Delta k \tag{5.18}$$

Taking derivative of MSE Error denoted as E, w.r.t x,:

$$\frac{dE}{dx} = -\frac{1}{N}\sum_{k=1}^{N}(SOAcc^{n}(k) - SOAcc^{m}(k) * x)SOAcc^{m}(k) \tag{5.19}$$

Decomposing the right hand side of the equation:

$$\frac{1}{N}\sum_{k=1}^{N} SOAcc^{n}(k) * SOAcc^{m}(k) - \frac{x}{N}\sum_{k=1}^{N} SOAcc^{m}(k)^{2} = 0 \tag{5.20}$$

Therefore, the correction factor x, is expressed:

$$x = \frac{\sum_{k=1}^{N} SOAcc^{n}(k) * SOAcc^{m}(k)}{\sum_{k=1}^{N} SOAcc^{m}(k)^{2}} \tag{5.21}$$

Thus, x is a least-square solution that minimises the residual error function in equation 5.18.

Furthermore, equation 5.21 is decomposed into a recursive formulation to form an online correction factor with x in equation 5.22-5.26 as follows:

$$x_{k} = \frac{\sum_{k=1}^{N} SOAcc^{n}(k) * SOAcc^{m}(k)}{\sum_{k=1}^{N} SOAcc^{m}(k)^{2}} \tag{5.22}$$

$$x_{k-1} = \frac{\sum_{k=1}^{N-1} SOAcc^{n}(k) * SOAcc^{m}(k)}{\sum_{k=1}^{N-1} SOAcc^{m}(k)^{2}} \tag{5.23}$$

$$x = \frac{SOAcc^{n}(k) * SOAcc^{m}(k)}{SOAcc^{m}(k)^{2}} \tag{5.24}$$

$$x_{k} = \frac{(N-1)x_{k-1} + x}{N} \tag{5.25}$$

$$x_{k} = x_{k-1} + \frac{x - x_{k-1}}{N} \tag{5.26}$$

Therefore, for all real values of $SOAcc^n$ greater than zero, the optimal value of the error correction term is 1, if the prediction of $SOAcc^m$ is accurate (error is 0), and less than or greater than 1, if the error between the actual and predicted *SOAcc* is positive or negative respectively. Consequently, x is 1 at initialisation. The MATLAB code for the RLS-P PoPA (y=Ax) is shown in Appendix F. Furthermore, in the MATLAB environment, the regression fitting toolbox is used to fit a simple linear model y=Ax+B in the same manner as presented in this section for the sake of comparison. Thus, the probabilistic adaptive PoPA fitted with the least-squares are denoted as RLS+P PoPA (y=Ax), and RLS+P PoPA (y=Ax+B), where B in the later model is the bias and A is the multiplicative factor.

5.4 Results and discussion

5.4.1 Load demand and Photo-voltaic Data

The historical household load demand profile with a peak load of 2.08 KWh and a 10KWh peak solar irradiance data shown in Figure 5.4 corresponding to 54.9783° N, 1.6178° W, is obtained from [133] and [132] respectively. The load profile data set consists of the aggregated power demand of uncontrollable appliances at each hourly time interval representing consumer's usage pattern. The historical load profile data set, $A(i,k)$ obtained over 365 days, at each hourly time step k, is such that i=1, 2, 3...365 and partitioned into disjointed groups of $A(i,k) = \{A_1, A_2, A_3, A_4\}$ which forms the LD distribution $F_X(LD^i(k))$ [133]. Each group of load demand data set distinctly corresponds to the consumer's power usage pattern concerning the four seasons in a year[123]. Therefore, from the consumer's historical energy consumption profile (with average load plotted in red) as shown in Figure 5.3, a probability distribution $F_X(LD^i(k))$ is easily realised.

Similarly, the uncertainty in the solar irradiance can be realised as a Gaussian distribution $\mathcal{N}(0, \sigma = 20)$ or consequently as any type of distribution within the presented procedure.

Typically, as shown in Figure 5.3, the historical load profile for Q1, has a dual peak characteristic, which mostly peaks at noonday and during the late evening. Specifically, as shown in Figure 5.3, the historical load profile for Q1, has a dual peak characteristic, which mostly peaks at noonday and during the late evening period.

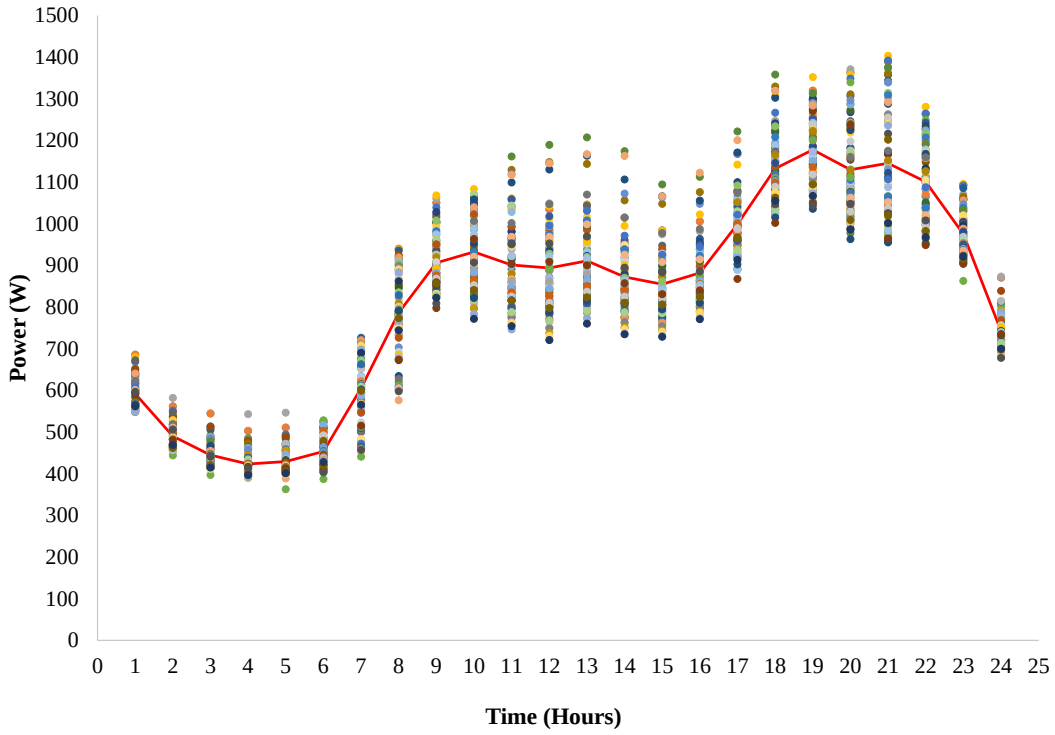

Fig. 5.3 Load demand profile showing energy consumption pattern variability during Q1.

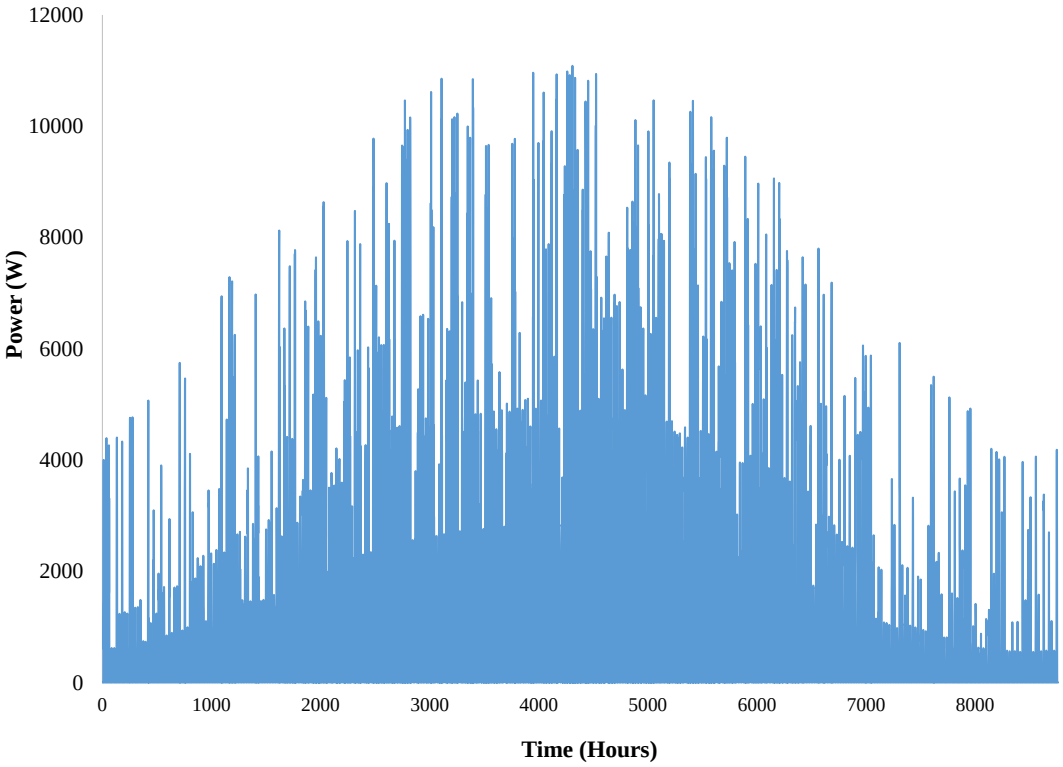

Fig. 5.4 PV energy profile for 8760h

The histograms of the quarterly load consumption variability from historical data are shown in Figures 5.5-5.8 for each hour, k in the four seasons as follows; winter (Q1), summer (Q2), spring (Q3) and autumn (Q4) respectively. The histograms significantly depicts a Weibull, bimodal and normally distributed load demand profile. Furthermore, Tables 5.1-5.4 convey the statistical information of the quarterly Load profiles with Q1 exhibiting the most significant uncertainty in contrast to the other seasons. Specifically, as seen in Table 5.1 during Q1, the uncertainty peaked at 12 noon with a magnitude of 30.2% and thereafter, at 20:00h with a magnitude of 27.9%. Similarly, as shown in Table 5.2, the largest uncertainty occurred at 20:00h, with a magnitude of 28% in Q2. Furthermore, as depicted in Tables 5.3-5.4, the highest uncertainty was recorded during the periods of 14:00h with 18% and 13:00h with 14% during Q3 and Q4, respectively. As shown in Tables 5.1-5.4, the load demand uncertainty

mainly depicts both daily and seasonal variation patterns. The proposed method utilising the chance-constrained power pinch for energy management is simulated in MATLAB based on N-samples randomly generated from a uniform distribution A(i,k). In the Monte Carlo simulation, the resulting load demands sampled randomly from the KDE distribution in each cluster (for each i at time step k) are assumed to be normally distributed, since the samples are sufficiently or approximately large (i=1000) enough to support convergence in accordance with the central limit theorem [124, 137, 138]. The chance constraints factors were both set to 1% during the simulation. Therefore, the state of charge of the battery has a 98% probability of operating within the optimal region $(30\% \leq SOAcc^{n}_{BAT} \leq 90\%)$ as illustrated by point 4 in Figure 5.1. The red line is the CDF, and the blue is an equivalent PDF plot, while the dotted black lines represent quantiles corresponding to the chance constraints.

In order to validate the proposed probabilistic approach, the actual load is randomly selected with uniform probability from the load demand distribution cluster corresponding to the time instance (k) and season. Furthermore, the Day-Ahead PoPA and Adaptive strategies which used the average load for each season as forecast have both been compared against the proposed probabilistic PoPA methods.

Table 5.1 Statistical central tendencies in First Quarter (Winter) Load demand profiles

Hour	Min	Mean	Max	Std. Dev	Uncertainty (%)
1	337.54	506.53	685.89	99.45	20
2	219.05	392.51	582.01	101.90	26
3	182.02	355.55	544.39	101.99	29
4	137.43	323.00	543.02	109.08	34
5	161.62	338.27	546.75	103.84	30
6	388.38	453.44	528.14	38.75	9
7	561.52	633.66	726.40	40.22	6
8	668.35	792.64	940.07	76.56	10
9	517.91	788.05	1068.01	158.81	20
10	637.11	849.31	1083.32	124.98	15
11	456.76	749.44	1129.45	173.06	23
12	334.49	686.32	1148.28	207.92	30
13	436.26	738.48	1143.96	178.95	24
14	470.46	724.31	1056.30	150.62	20
15	304.11	642.92	1047.95	199.80	30
16	395.35	698.36	1076.06	178.93	26
17	809.37	949.34	1168.15	83.75	9
18	825.33	1043.20	1329.60	129.13	12
19	980.98	1147.90	1352.21	98.56	9
20	489.23	932.63	1370.90	260.43	28
21	980.74	1177.57	1403.60	116.79	10
22	878.18	1070.26	1280.90	113.14	11
23	727.39	910.22	1096.18	107.54	12
24	332.51	593.02	873.32	153.22	26

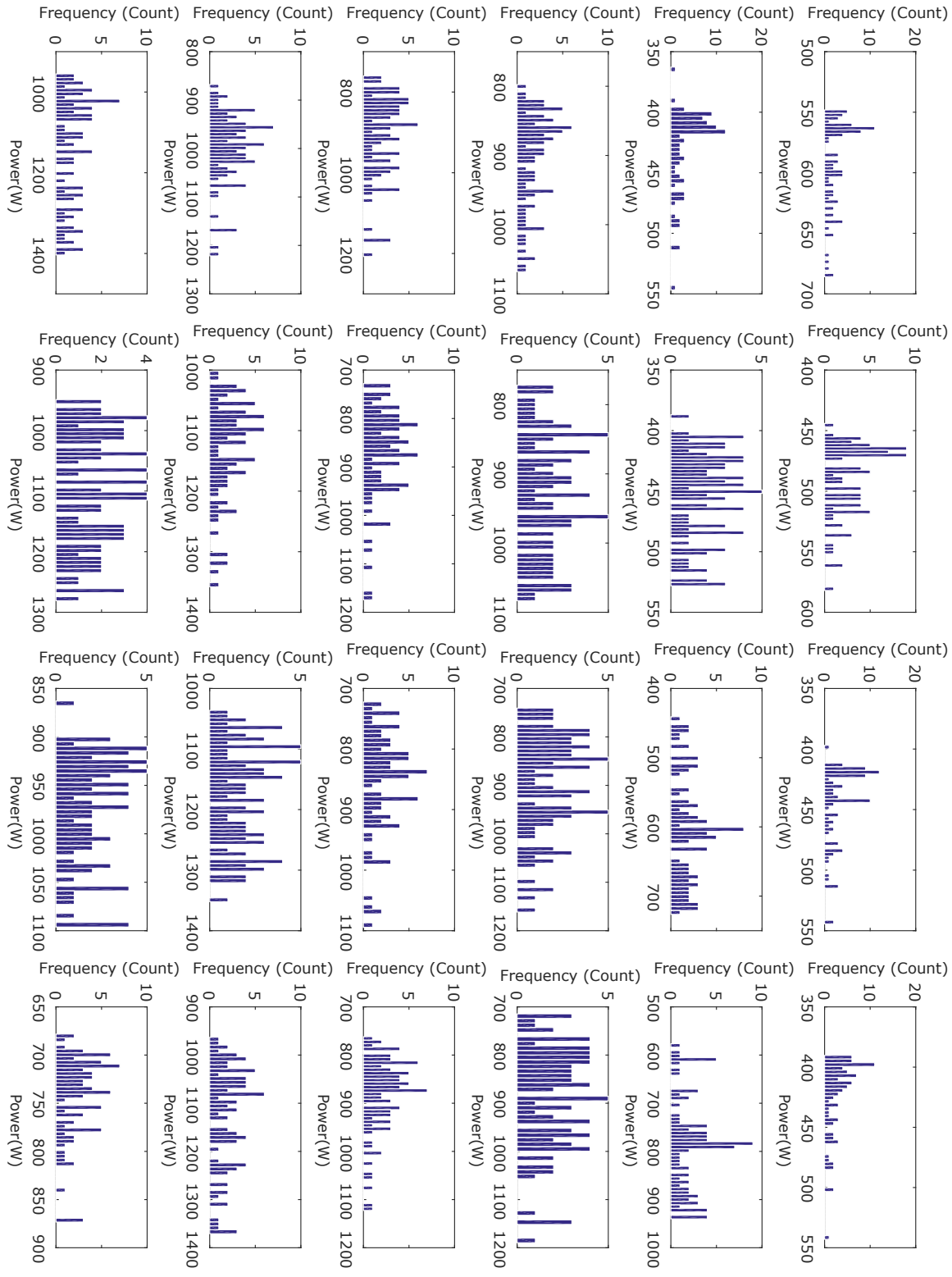

Fig. 5.5 Histogram plot of the hourly daily load distribution in Q1

Table 5.2 Statistical central tendencies in Second Quarter (Spring) Load demand profiles

Hour	Min	Mean	Max	Std. Dev.	Uncertainty(%)
1	510.14	556.25	596.76	18.59	3
2	438.27	467.62	502.22	16.52	3
3	389.54	423.93	443.35	12.44	2
4	380.33	407.36	432.72	12.38	3
5	378.42	406.05	430.42	11.46	2
6	387.67	433.27	453.65	13.80	3
7	435.13	550.96	647.90	57.34	10
8	560.24	718.43	848.45	74.42	10
9	749.35	848.41	926.63	33.98	4
10	776.69	882.41	1037.53	52.99	6
11	745.21	843.51	1027.90	64.87	8
12	724.00	841.08	1043.65	69.79	8
13	745.65	851.30	1074.91	72.62	8
14	716.19	814.69	990.98	61.93	8
15	687.54	794.92	972.88	66.54	8
16	704.96	812.59	992.43	57.27	7
17	751.18	928.16	1117.74	58.89	6
18	960.89	1057.50	1260.05	61.62	6
19	897.11	1115.82	1336.29	84.86	8
20	921.14	1082.27	1377.33	107.21	10
21	916.80	1073.18	1267.34	95.69	9
22	924.98	1041.46	1145.29	54.20	5
23	858.78	914.67	969.19	19.90	2
24	669.39	699.22	752.65	18.53	3

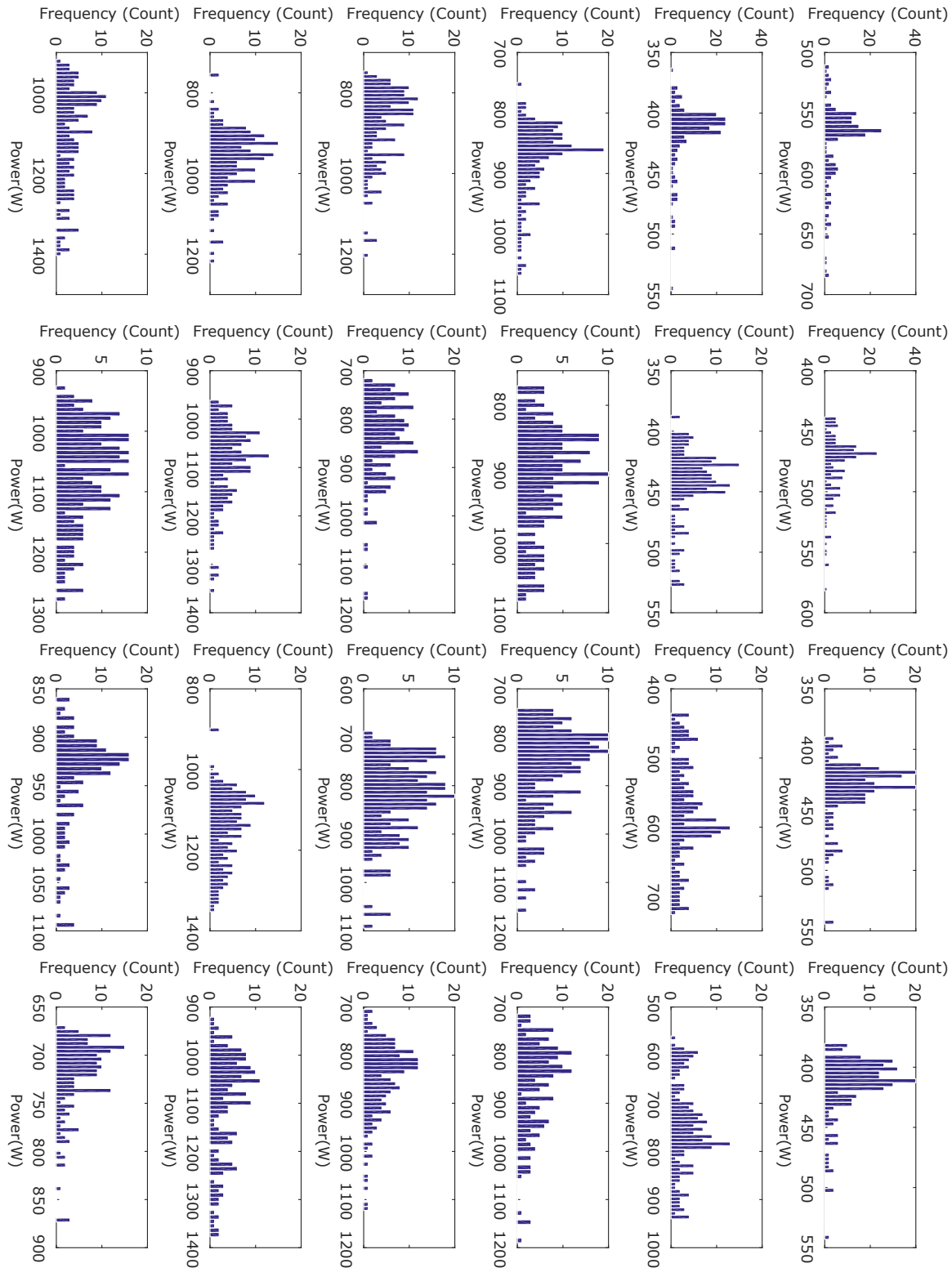

Fig. 5.6 Histogram plot of the hourly daily load distribution in Q2

Table 5.3 Statistical central tendencies in Third Quarter (Summer) Load demand profiles

Hour	Min	Mean	Max	Std. Dev.	Uncertainty(%)
1	529.15	626.54	849.61	61.99	10
2	446.92	537.40	719.74	57.79	11
3	410.59	493.52	680.25	47.61	10
4	396.35	470.89	609.29	43.37	9
5	400.36	469.63	580.05	44.63	10
6	401.45	516.60	601.53	50.70	10
7	475.17	692.40	833.33	94.53	14
8	584.95	942.58	1145.93	137.34	15
9	768.61	1080.10	1324.77	100.23	9
10	881.20	1105.27	1721.76	126.24	11
11	799.63	1065.51	1684.74	162.93	15
12	771.15	1071.81	1830.50	178.84	17
13	802.39	1093.08	2080.63	192.05	17
14	748.07	1057.64	1950.51	189.47	18
15	748.64	1050.68	1859.37	180.39	17
16	805.96	1145.92	1695.94	191.88	17
17	964.02	1396.11	1772.11	239.06	17
18	1124.19	1599.69	1926.59	229.42	14
19	1284.69	1665.88	1875.90	168.05	10
20	1279.21	1551.36	1726.05	114.96	7
21	1198.14	1417.81	1576.08	98.29	7
22	1116.13	1279.11	1428.12	88.27	7
23	919.36	1067.80	1219.20	77.17	7
24	685.44	807.32	1008.23	68.66	9

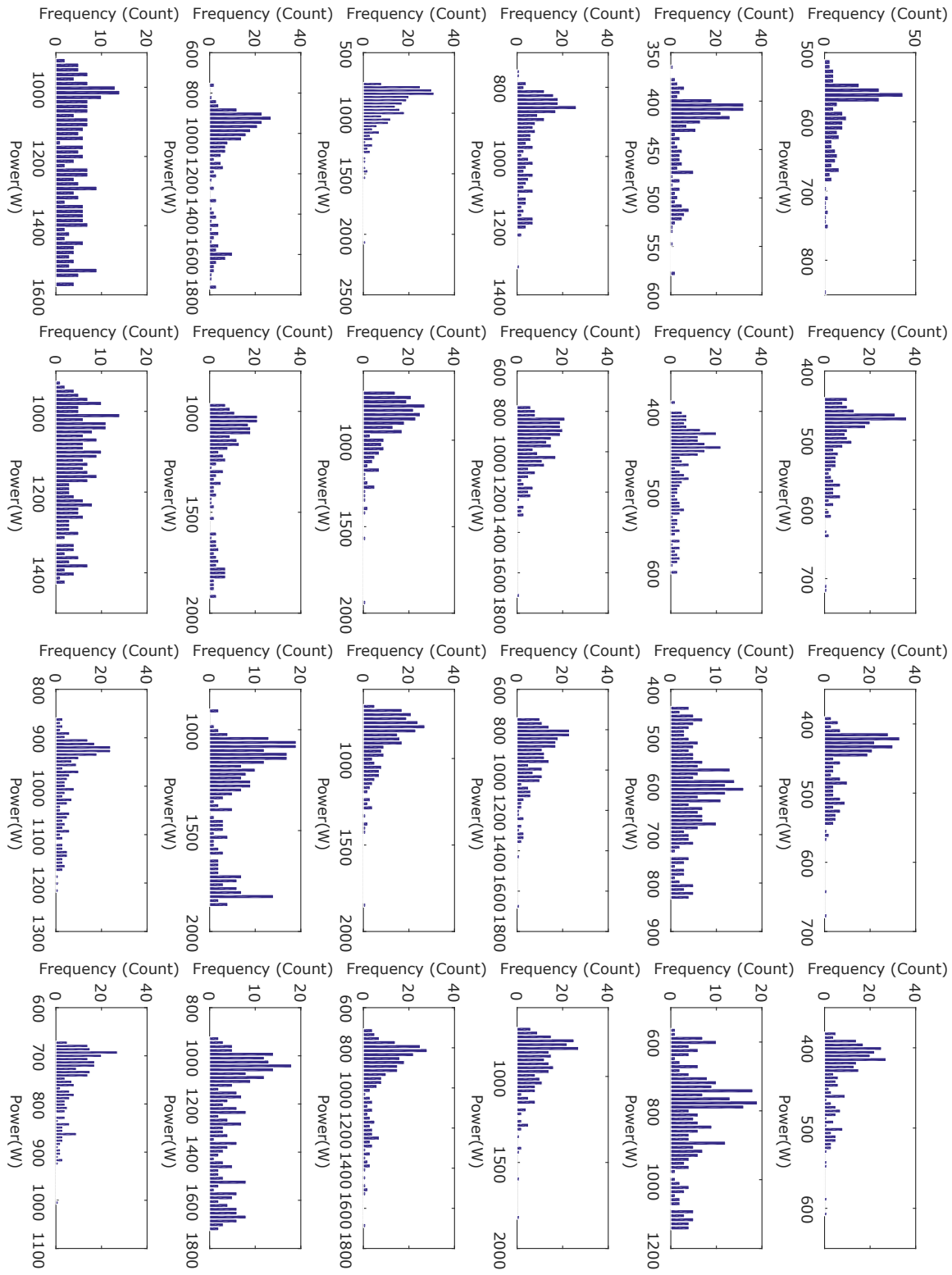

Fig. 5.7 Histogram plot of the hourly daily load distribution in Q3

Table 5.4 Statistical of central tendencies in Fourth Quarter (Autumn) Load demand profiles

Hour	Min	Mean	Max	Std. Dev.	Uncertainty(%)
1	590.50	667.63	868.28	46.71	7
2	490.68	578.61	733.56	36.00	6
3	467.73	531.37	693.20	33.10	6
4	449.77	508.93	619.65	29.48	6
5	463.54	508.91	569.21	22.15	4
6	486.03	560.76	752.66	32.84	6
7	596.28	749.87	989.58	80.00	11
8	712.81	1002.34	1157.68	116.34	12
9	908.92	1131.98	1223.91	62.60	6
10	933.61	1150.35	1349.69	100.19	9
11	858.53	1116.62	1369.72	138.17	12
12	860.48	1126.17	1467.43	154.29	14
13	692.17	1139.31	1491.61	160.38	14
14	851.28	1107.45	1442.08	150.62	14
15	844.05	1098.29	1427.08	141.98	13
16	914.37	1176.29	1514.24	152.02	13
17	1065.92	1394.59	1753.03	181.45	13
18	1204.22	1653.73	1936.02	185.91	11
19	1322.72	1742.30	1889.59	133.87	8
20	1175.20	1602.12	1703.42	87.39	5
21	1224.47	1467.94	1562.38	61.83	4
22	1079.99	1317.84	1416.04	59.18	4
23	936.24	1097.91	1202.61	52.00	5
24	758.83	841.72	947.73	43.51	5

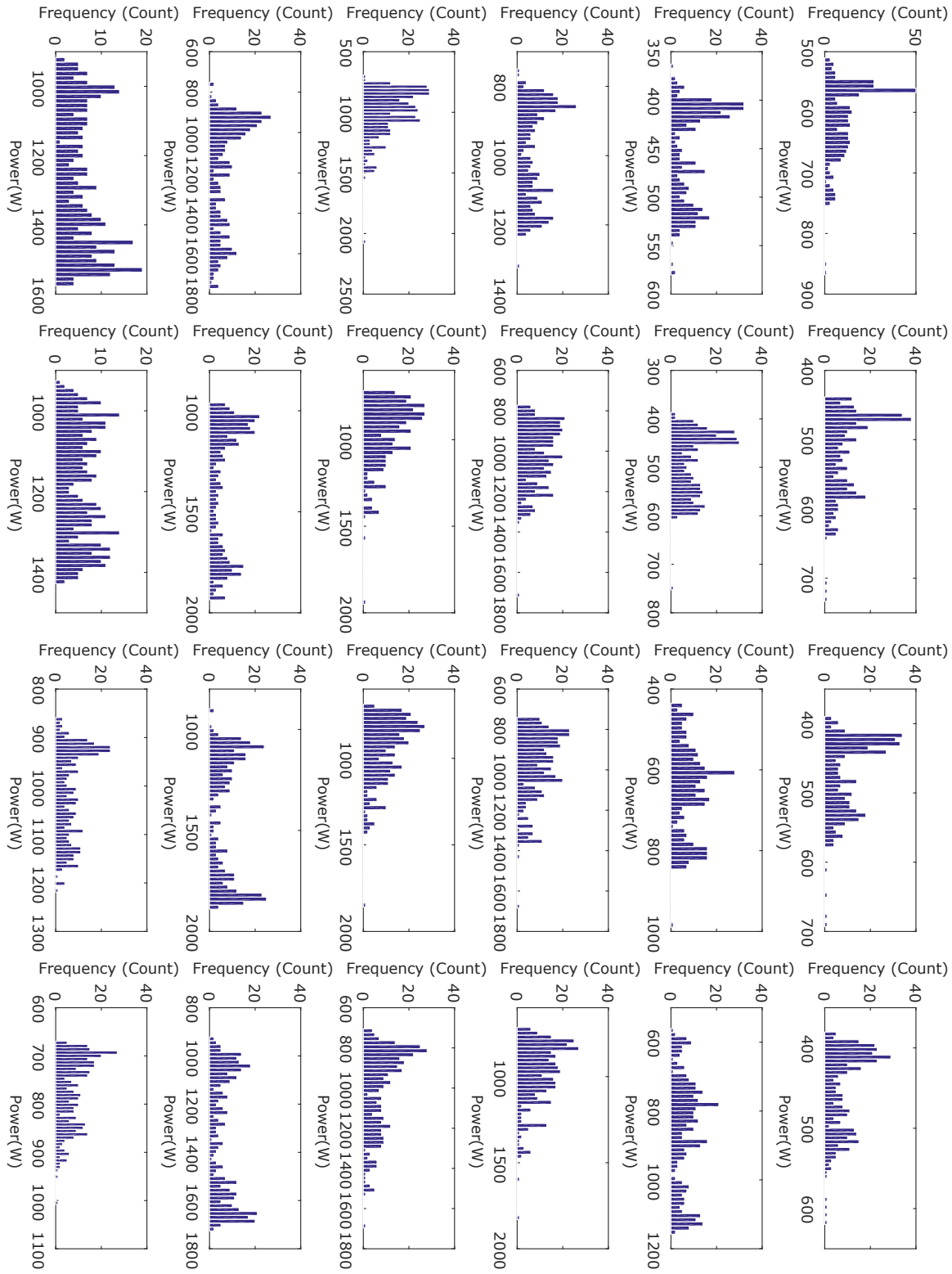

Fig. 5.8 Histogram plot for the hourly daily load distribution in Q4

5.4.2 Uncertainty Analysis of the Probabilistic Adaptive Algorithms

The performance of the proposed probabilistic methods; P+Adaptive PoPA, RLS+P PoPA with/without bias are compared over a period of 72h to the Day-ahead, Adaptive and Kalman+Adaptive PoPA EMSs presented in Chapter 4. The same properties of the non-Gaussian and Gaussian uncertainty used in Chapter 4, have also been has been used in this present Chapter and throughout the thesis for uniformity.

5.4.2.1 Non-Gaussian uncertainty

As shown in Figure 5.9, the actual PGCC is bounded by both the probabilistic lower and upper PGCC based on a 98% chance of violating the S_{Lo} and S_{Up} pinch utility under non-Gaussian uncertainty. The upper and lower predicted PGCC bounds are shown as the red and blue plots in Figure 5.9, while, the actual PGCC is indicated by the yellow dashed line. The operational constraints were never violated by the P+Adaptive PoPA. Nevertheless, as seen in Figure 5.10, the FC and EL were activated 6 and 3 times, respectively. Similarly, the RLS+P PoPA with and without the bias also recorded no violations concerning the S_{Lo} and S_{Up} pinch utility as shown in Figures 5.15 and 5.12 respectively. Nevertheless, while RLS+P PoPA without bias activated the FC 7 times and the EL 3 times as shown in Figure 5.13, with the RLS-P PoPA with the bias, the activation of the FC and EL increased to 8 and 5 times respectively as shown in Figure 5.16. Hence, an increase in operational cost or resources with probabilistic PoPA approach, particularly with an increase in the complexity of the residual error regression model is a trade-off for robustness. The HT and WT response pertaining to the P+Adaptive, the RLS-P without bias and with bias are shown in Figures 5.11, 5.14 and 5.17 respectively.

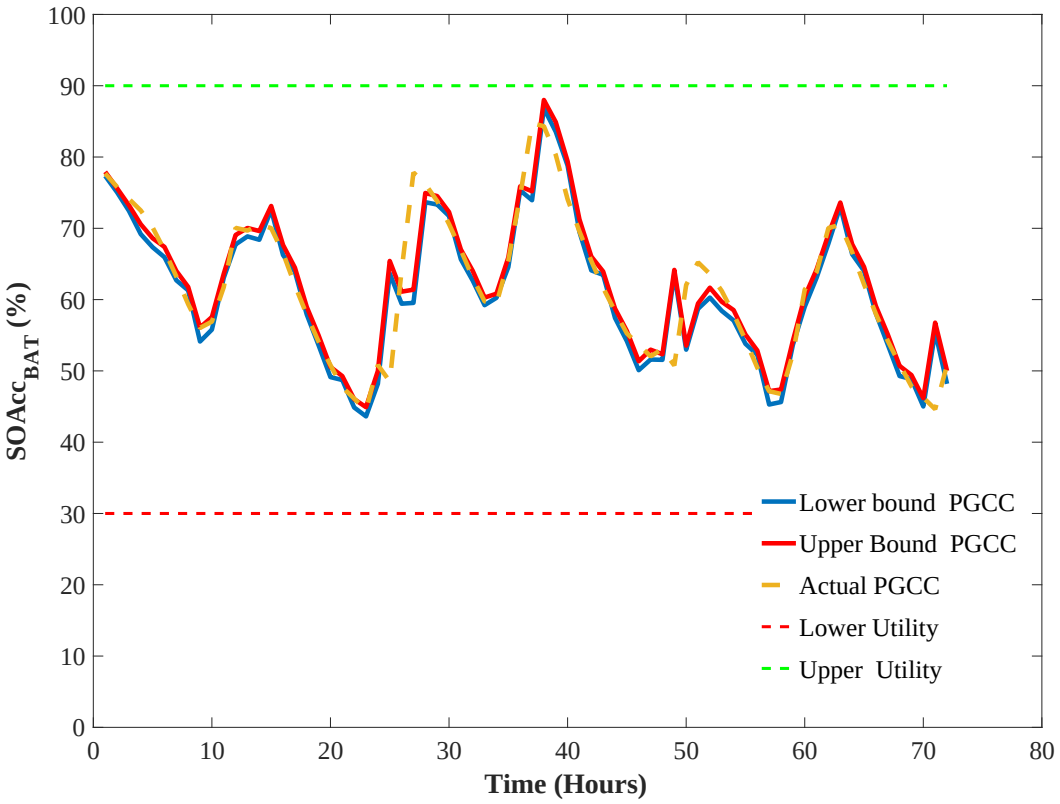

Fig. 5.9 Performance of the P+Adaptive PoPA strategy over 72h

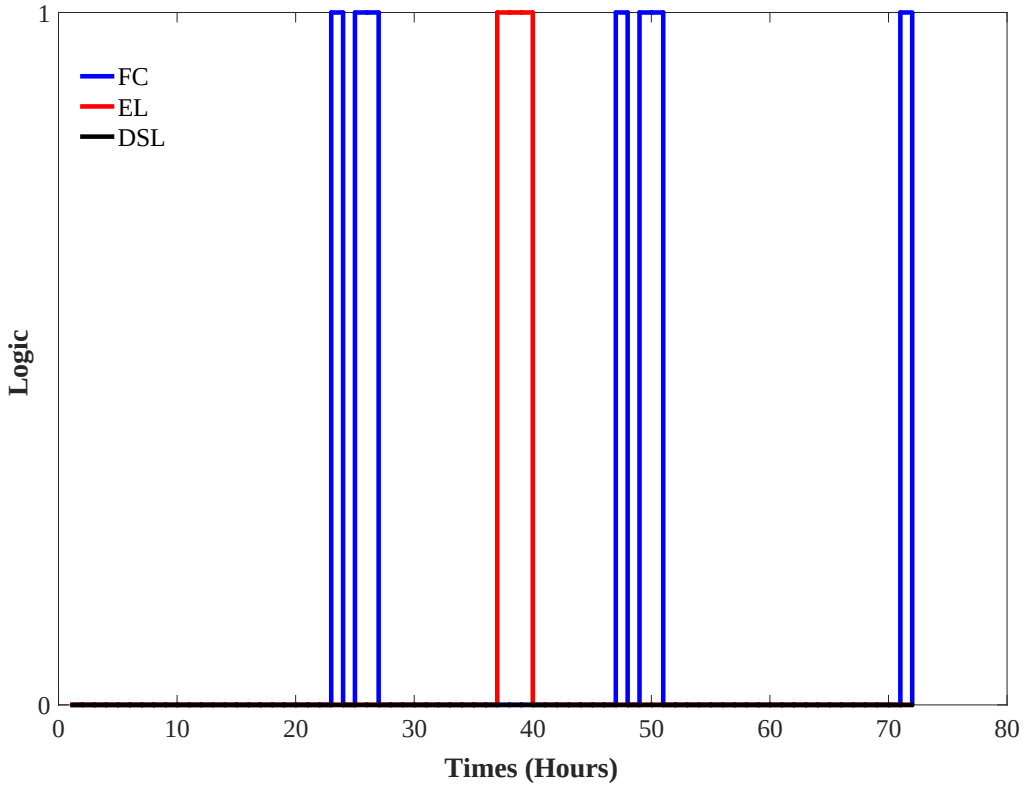

Fig. 5.10 P+Adaptive PoPA converter logic over 72h

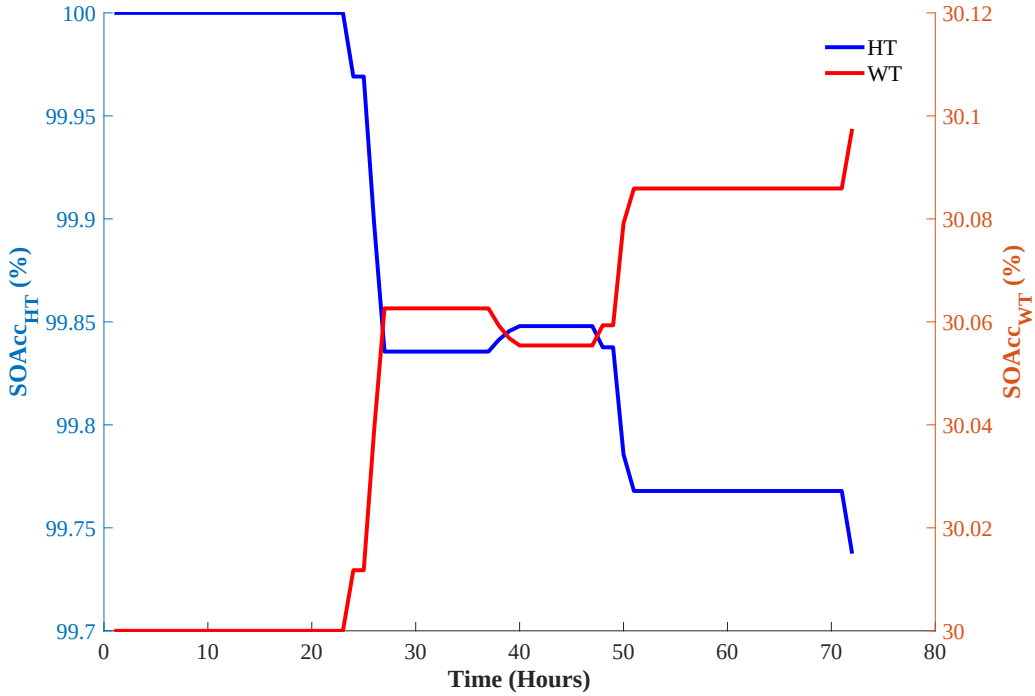

Fig. 5.11 P+Adaptive PoPA HT and WT response over 72h

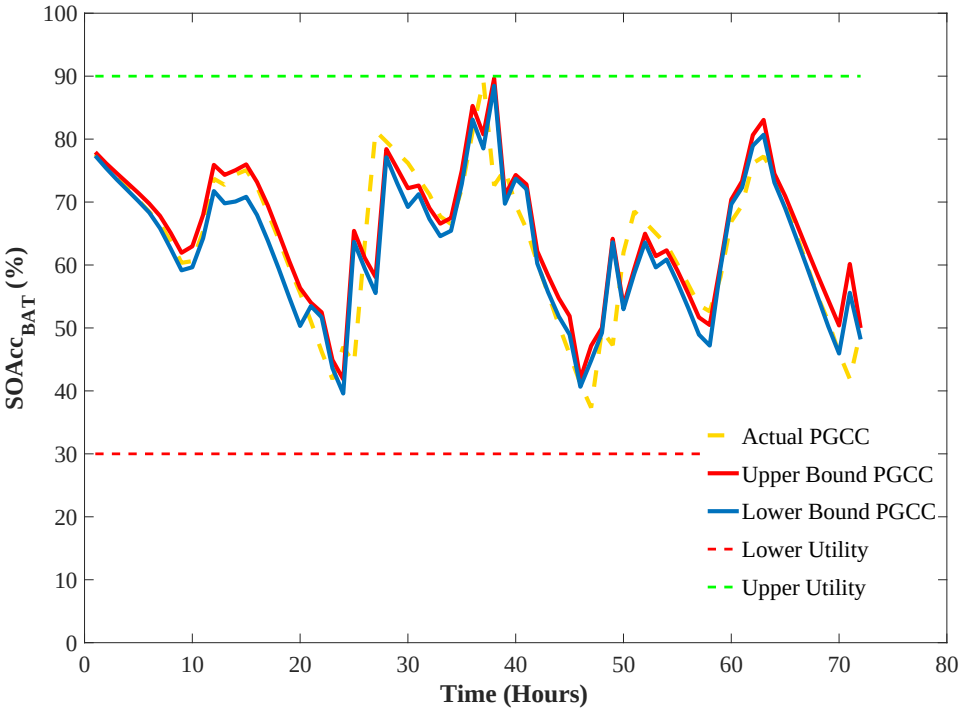

Fig. 5.12 Performance of the RLS-P PoPA (y=Ax) strategy over 72h

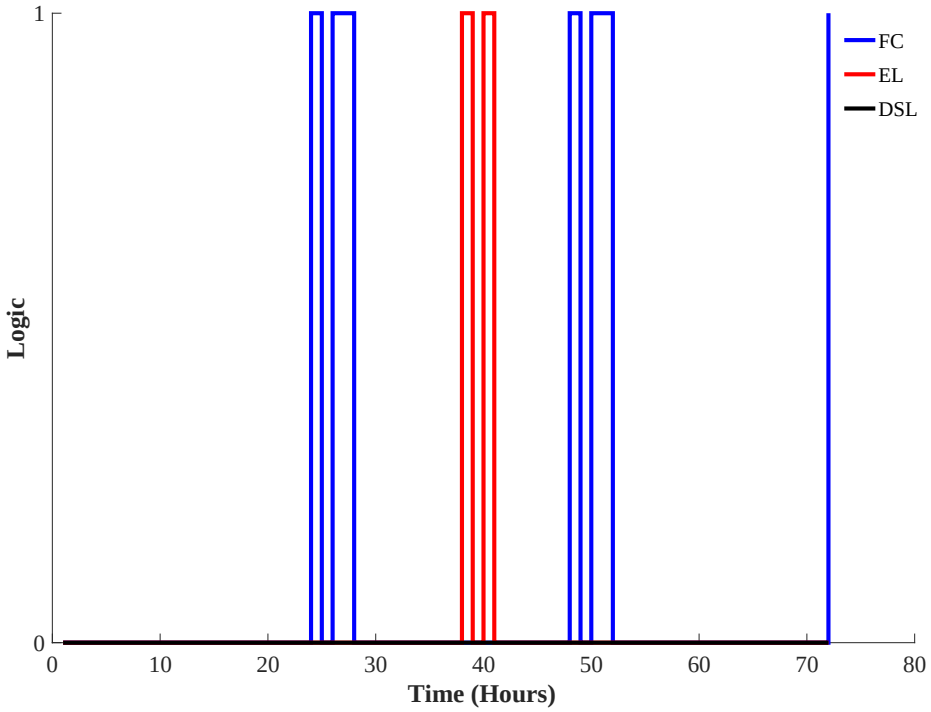

Fig. 5.13 RLS-P PoPA (y=Ax) converter logic over 72h

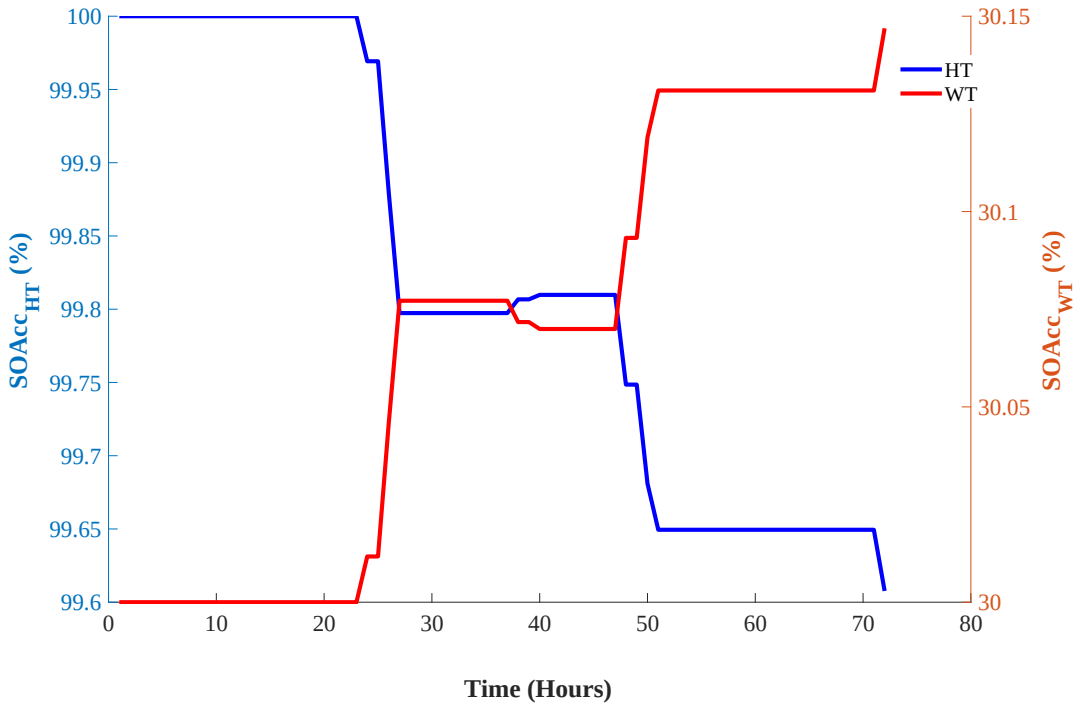

Fig. 5.14 RLS-P PoPA (y=Ax) HT and WT response over 72h

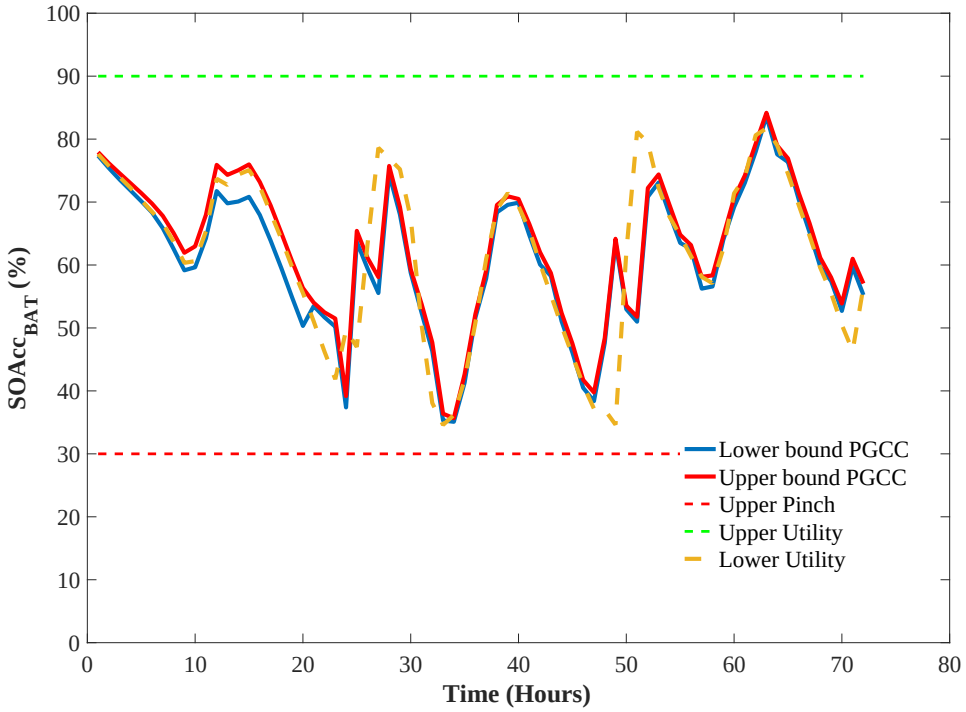

Fig. 5.15 Performance of the RLS-P PoPA (y=Ax+B) strategy over 72h

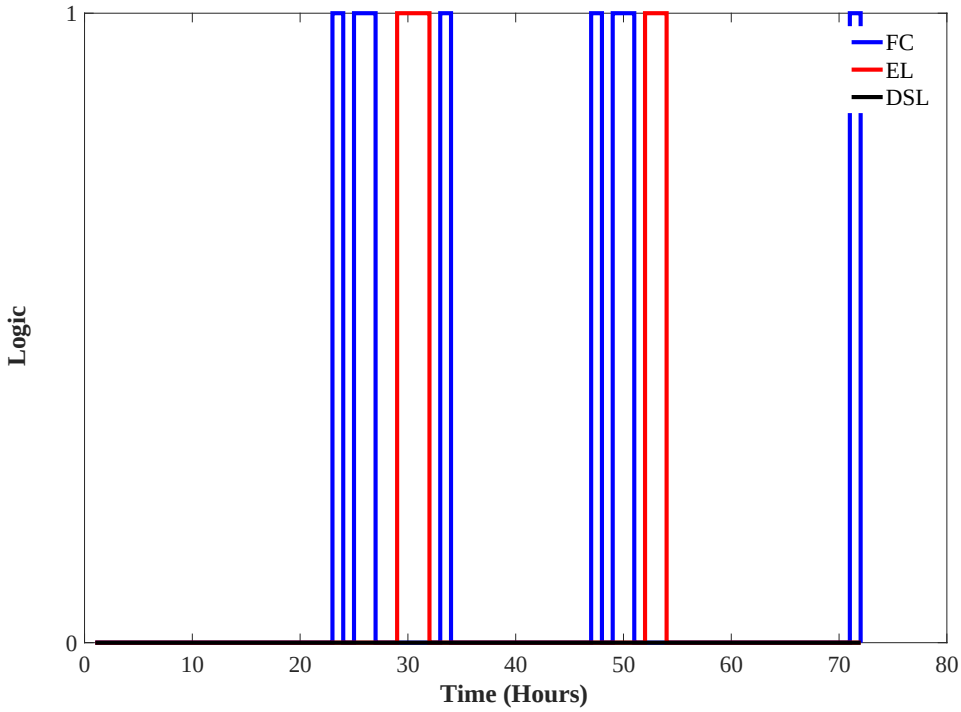

Fig. 5.16 RLS-P PoPA (y=Ax) converter logic over 72h

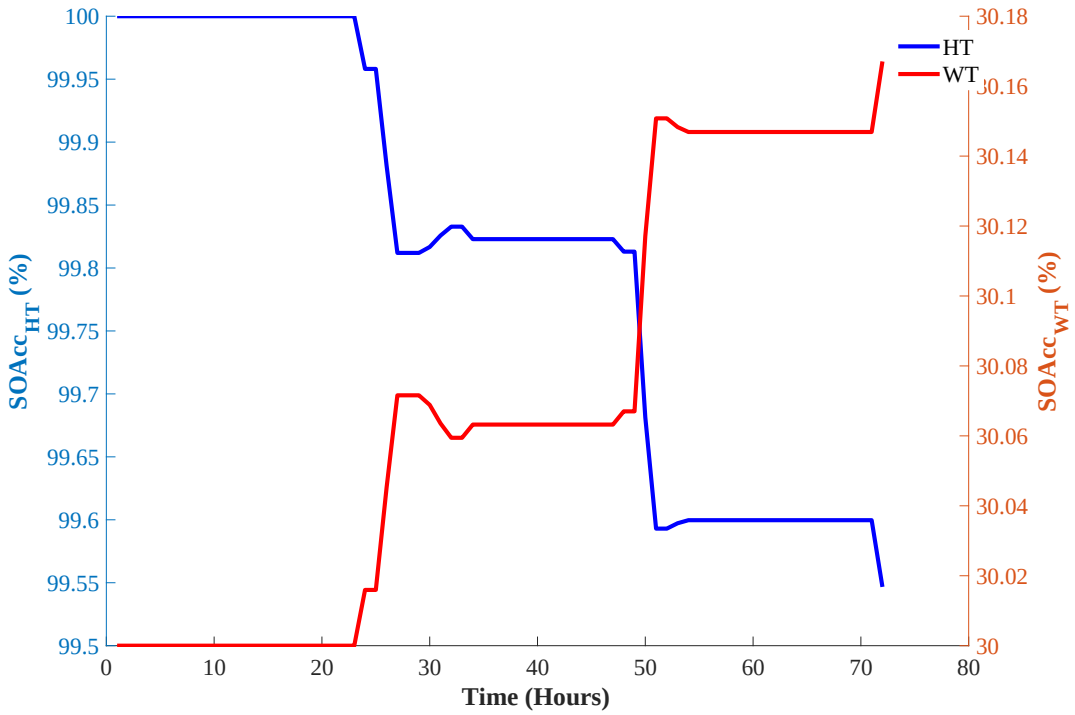

Fig. 5.17 RLS-P PoPA (y=Ax) HT and WT response over 72h

5.4.3 Gaussian

Similarly, under the Gaussian uncertainty case study, the RLS+PoPA with the simple correction factor (i.e. without the bias), violated the S_{Up} once, while the P+Adaptive, RLS+Adaptive with bias as shown in Table 5.5. Nevertheless, in contrast to the DA and Adaptive PoPA which had 13 and 3 violations of the S_{Lo}, the P+Adaptive, RLS+PoPA without bias, Kalman+Adaptive PoPA had none. Apparently, accounting for robustness and accuracy can result in an increased frequency of FC and EL activation cycles which can incur losses and further increase the operating cost with the simple least-squares mechanism aimed at minimising the mean squared error between the actual $SOAcc^{n}_{BAT}$ and estimated $SOAcc^{m}_{BAT}$

from the MC process. Nevertheless, further investigation using a long term (8760h) scenario case study will be presented in Chapter 6.

5.5 Summary

Three Probabilistic+Adaptive PoPA which uses a stochastic process based on Monte Carlo simulation, enabled by historical data and high computer processing speed have been proposed for energy management of HESS uncertainty. A short term (72h) stochastic analysis evidently showed the proposed method performed better in clipping the PGCC from violating the S_{Lo} in contrast to the DA, Adaptive and Kalman +Adaptive PoPA methods previously presented in Chapter 4. The proposed methods were compared to the Day-ahead and Adaptive PoPA, which utilised the average load.

In contrast to the DA - PoPA which had the most S_{Lo} and S_{Up} violations and DSL usage. The adaptive PoPA had a marginally, better lower pinch violation compared to the proposed approach.

The three algorithms; P+Adaptive PoPA, RLS+P PoPA with and without bias, have all shown superior performance with regards avoiding the violation of the S_{Lo} and S_{Up} pinch limits. This superior performance is in contrast to the DA approach, which had the worst S_{Lo} violation and rivals the Kalman+Adaptive, which had the best performance so far in this thesis. Nevertheless, the RLS+PoPA without bias has shown sensitivity to violating the S_{Lo} constraint. Furthermore, these probabilistic algorithms, adequately considered the effects of impending uncertainty with the same forecast error correction mechanism in the Adaptive PoPA, which is absent in the DA PoPA. Moreover, robust planning against uncertainty within the context of the historical data rather than with the average load demand profile yielded promising result in terms of better performance. A summary of the performance indices for the P+Adaptive, RLS+P PoPA with and without bias are shown in Table 5.5.

Table 5.5 Summary of performance of the P+Adaptive, RLS-P PoPA (y=Ax) and RLS-P PoPA (y=Ax+B) algorithms over 72h.

Indices		P+Adaptive PoPA	RLS - P PoPA (y=Ax)	RLS-P PoPA (y=Ax+B)
Non-Gaussian Uncertainty	Lower Pinch Violation	0	0	0
	Upper Pinch Violation	0	0	0
	DSL Activation	0	0	0
Gaussian Uncertainty	Lower Pinch Violation	0	0	0
	Upper Pinch Violation	0	1	0
	DSL Activation	0	0	0

Chapter 6

Reinforcement learning based Adaptive Power Pinch

OUTLINE

This chapter is based on an unpublished manuscript currently under review in Energy, Elsevier. This chapter focuses on integrating the adaptive and probabilistic PoPA developed in Chapters 3 and 4, with a reinforcement learning technique, a type of machine learning algorithm in order to achieve enhanced performance to uncertainty. Specifically, the RL used, are variants of the Q-Learning techniques such as Tabular Dyna Q-Learning and deep Q-learning (DQN) which are modified and exploited in an Adaptive PoPA context, as well as a deep Actor-critic RL network which is implemented within the Probabilistic adaptive PoPA framework.

6.1 Introduction

Generally, machine learning refers to the capability of computers to explicitly learn predefined examples directly or indirectly by interacting and exploiting the real world or environment. These machine learning algorithms are basically classed into three categories; supervised,

unsupervised and RL. On the one hand, supervised learning entails the classifying or inferring regression parameters of an underlining function for structured or well-labelled training examples or data. On the other hand, unsupervised learning entails drawing inference from an unlabelled data set. Whereas, RL is basically a software agent tasked with inferring an action which maximises the cumulative reward [101].

The RL algorithms have evolved dramatically due to recent methodological insights in deep neural networks (DNN) for function approximation of hyper-dimensional space. The hybrid combination of the RL algorithm and DNN is generically known as deep RL (DRL), and has been used in several EM applications as in [139] for complex decisions making to optimally manage and balance uncertainty in electricity supply and consumption while purchasing more energy during off-peak periods. The remarkable successes of DRL are seen in playing Atari game [140], where a deep Q-network (DQN) model for the first time, successfully learnt control policies directly from high-dimensional sensory via the perception of features, observed and extracted via a convolutional (deep) neural net and a variant of Q-learning. In evaluating the proposed deep Q network on seven Atari 2600 games, the learning algorithm had a performance which was indeed comparable to that of a human expert player. Another tremendous contribution to the field of RL is the successful integration of deep RL and a Monte Carlo tree search to play AlphaGo, which is regarded as one with the most challenging classical games for A.I due to its vast dimensional search space. Monte Carlo simulation is combined with two networks; value and policy, which are used to determine the board position and perform moves respectively. Specifically, the approach entailed combining supervised learning and RL from expert games and self-play, respectively, where the self-played game is generated based on a Monte Carlo simulation of thousands of random games without any look-ahead search. The algorithm defeated an 18-time world champion Lee Sedol by 5 games to 0 whilst achieving a 99.8% winning rate in contrast to other Go algorithms [141].

Furthermore, in [142] AlphaGo zero, which is solely based on deep RL and the game's rules without the guidance of a human expert data is proposed to improve on the effectiveness of the tree search in [141]. During the evaluation, the AlphaGo zero algorithm won 100 games to 0 against a human champion in AlphaGo.

Recent advancements in deep learning, especially Q-network, have attained significant success and have become an interesting subject of interest in the RL research community in tasks involving complex decision making with uncertainty. Therefore, this chapter aims to leverage the advantages of the Tabula Q-Learning and DRL with the Adaptive and Probabilistic adaptive PoPA frameworks proposed in chapters 3 and 4.

6.2 Q-Learning Adaptive Power Pinch Analysis

The, Q learning algorithm approach in this work involves formulating the problem of the uncertainty, as a Markov Decision Process (MDP), considered in a discretised time step k. Thus, a learning agent acts optimally by anticipating the best action given any HESS state as determined by the adaptive MPC PoPA trajectory from trial and error.

6.2.1 Q-learning State and action formalisation

The approach presented in this work involves formulating the uncertainty problem as a Markov Decision Process (MDP) considered in the discrete-time step k, where an agent has to act optimally by inferring an action in each state as determined by the adaptive MPC PoPA trajectory.

The finite MDP is a tuple$(S, A, R, S',\ A')$ such that;

$\mathcal{S}$: is a set of discrete n-states $\mathcal{S} = \{s_1,\ s_2,\ \ldots, s_n\ \}$ and s_k denotes the state of the environment at time step k.

In this work,

$$s_k := f\left\langle SOAcc^{m}_{BAT}(k),\ SOAcc^{n}_{BAT}(k),\ e(k)\right\rangle \tag{6.1}$$

This is such that the states are finely discretised to form 270 states with the use of '$if\ else$, $then\ do$' logic statements. Furthermore, the state space which consists of 270 discretised states, are classed into three groups each with 90 discrete state space, where each group pertains to the sign (+,-, or 0) of $e(k)$ and the 90 discrete states are extracted using if-else statement from the magnitude of error between $SOAcc^{m}_{BAT}$ (k) and $SOAcc^{n}_{BAT}$ (k) normalised by 100.

$\mathcal{A}$: is a discrete set of n-actions, where only one is available for selection at any given state by the agent $\mathcal{A} = \{a_1\ , a_2, \ldots, a_7\ \}$ and a_k indicates the action undertaken or selected by an agent at time k.

Furthermore, the set of dispatchable assets for the PGCC shaping is expressed as follows:

$$U_c(t) \subseteq \mathcal{A}_k\ := \{a_1,\ \delta_1 FC, \delta_2 FC, \delta_3 FC, \delta_4 EL,\ \delta_5 EL,\ \delta_6 EL\ \}$$

where,

$\delta_x,\ \ x = [1,2,3]$, characterises the proportional percentages {10, 50, 90} and {10, 50, 100} of corresponding energy or material flow such as between the assets such as FC and BAT; $F^{Pow}_{FC\rightarrow BAT}(k)$ in order to forestall an impending energy deficit or between the BAT and EL; $F^{Pow}_{BAT\rightarrow EL}(k)$ in response to anticipated occurrence of excess energy from RES. a_1 denotes null action.

$\mathcal{T}(s,a,s')$: is the probability of transitioning to a next state s' from state s over a given set of transitions when an action a is chosen.It is important to note that a transition probability matrix (TPM) which has been used in [97, 100] is however not mandatory [112] and can be omitted. The reason behind this is the Q-learning values eventually accumulate a transition probability mapping, with respect to the actions taken and the state visited. Hence, the agent

learns the optimal action in a state with each visit, and so the use of a transition probability matrix is however not required.

$\mathcal{S}$ x $\mathcal{A} \rightarrow R$: An immediate reward r_t is received as a result of the system state transition $\mathcal{T}(s,a)$ to the next state s' by mapping state and action pair (s, a) due to a decision making policy π.

Therefore, both the transition and reward probability distributions are implicitly Markov properties where the future state s' only depends on the present state s. The current action a is independent of the past state(s) s^- that lead to the present state [143, 144].

$$\mathcal{T}(s'|s^-,s,a) = \mathcal{T}(s'|s,a) \tag{6.2}$$

The model of the system which is required for initial training of the agent is simulated twice for a duration of 8760 h, in order to infer the control action on the actual system from the Adaptive PoPA. The agent adapts to the real system over time and retrains on newer samples. The MDP learning agent learns the optimal policy $\pi^*(a|s)$ from accumulated experience, which maps an optimal action to a given state. Hence, this maximises the cumulative reward return, as shown in (6.3).

$$\mathcal{V}^{\pi} = E\left[\sum_{k=1}^{\infty} \gamma^{k-1} r_k(s_1, a_1|\pi)\right] \tag{6.3}$$

The Q-function Q^{π} (s, a) for a given MDP represents the optimal value function $\mathcal{V}^{\pi *}$.

The agent learns the optimal action to take in the environment through experience by taking actions in the environment while learning the optimal policy.

The Q-learning agent is updated after taking an action a in a state s, obtaining a reward r and transitioning to s' as follows:

$$Q_k(s,\ a) = \left\{ \begin{array}{cc} Q_k(s,\ a) + \alpha[r_k + \gamma_{a'}^{max} \Omega_{k+1}(s',a') - \Omega_k(s,a)] & \forall\ k = [1,2,\ldots N-2] \\ Q_k(s,\ a) + \alpha[r_k - Q_k(s,\ a)] & \forall\ k = N-1 \\ Q_k(s,\ a) & \forall\ k = N \end{array} \right\} \tag{6.4}$$

Where $\alpha, \gamma \in [0, < 1]$ are learning rate and future reward discount factor with the future discounted reward omitted during the update of the agent at a terminal state at time step $N-1$.

6.2.2 Planning stage for Q-learning Agent

The MPC-PoPA model is used to bootstrap the Q-learning agent to ensure that the agent acts considerably optimally concerning tracking the PoPA trajectory computed offline before online deployment to minimise and avoid exploiting costly mistakes on the real system. The advantage of the Q-algorithm is that the agent garners experience from the real environment and retrains offline by replaying the experience after each episode at time N to further reinforce the learning agent's Q - value to guaranty optimality. The model-free learning takes course using the Q-learning algorithm and switches to a Monte Carlo algorithm at $N-1$, which denotes the terminal state (horizon) for the agent, as shown in (6.4). Therefore, the learning involves two steps; direct and indirect learning, from the model and the actual system (environment) respectively.

6.2.3 Action Selection

The action selection approach in (6.5) – (6.6) which has been modified to include safety precautions in critical states (near the Pinch limits), is based on the probability (1 - θ) of selecting a *greedy* policy π(s) over a random action with probability of θ [145, 146]. This approach exploits the best action as indicated by the maximum value function $Q^{\pi *}(s,a)$ for a given state while performing exploration with the inverse probability (θ) of acting greedily.

This strategy strikes a balance between exploration and exploitation while satisfying the famous Bellman's principle of optimality [147], minimizing the deviation of the system controlled by the learning agent from the Adaptive PoPA target, while exploring the state space. Therefore, if the $SOAcc^{n}_{BAT}$(k) is less than *Lo* or greater than *Up*, the FC and EL are dispatched by the agent respectively. Furthermore, the AEEND constraint imposed at the end of the day is achieved by overriding the agent's action with the Adaptive PoPA's EMS. The action policy π(s) is expressed as follows:

$$\pi(s) = \begin{Bmatrix} a_k(s) & U < greedy\ action\ probability(1-\theta) \\ \delta_3 FC & U > greedy\ action\ probability(1-\theta) \wedge SOAcc^{n}_{BAT}(k) \leq 30\% \\ \delta_6 EL & U > greedy\ action\ probability(1-\theta) \wedge SOAcc^{n}_{BAT}(k) \geq 90\% \\ select\ random\ action & otherwise \end{Bmatrix} \tag{6.5}$$

Where, U is a randomly generated value between 0 and 1 given each k time step.

$$a_k(s) := \begin{Bmatrix} \delta_3 FC & SOAcc^{n}_{BAT}(k) \leq 30\% \\ \delta_6 EL & SOAcc^{n}_{BAT}(k) \geq 90\% \\ \underset{a_k(s) \subseteq \{a_1, \delta_n FC\},\ n \in [1:3]}{argmax} Q(s_k, a_k) & SOAcc^{n}_{BAT}(k) \geq 30\% \wedge SOAcc^{n}_{BAT}(k) \leq 40\% \\ \underset{a_k(s) \subseteq \{a_1, \delta_n EL\},\ n \in [4:6]}{argmax} Q(s_k, a_k) & SOAcc^{n}_{BAT}(k) \geq 80\% \wedge SOAcc^{n}_{BAT}(k) \leq 90\% \\ \underset{a_k(s) \subseteq A_t}{argmax} & otherwise \end{Bmatrix} \tag{6.6}$$

6.2.4 Reward Function Formalisation

In order to train the Q-learning agent, a suitable reward function is expressed mathematically. This is such that the agent follows the optimal policy $\pi^*(s)$ which minimises the cost function

between the agent's off-policy and the adaptive MPC PoPA trajectory, and expressed as follows:

$$J_\pi\left(SOAcc^n_{BAT}\right) = \lim_{N-2 \to \infty} E\left[\sum_{k=1}^{N-2} |SOAcc^m_{BAT} - SOAcc^n_{BAT}|^2 + \left(\gamma^k J_\pi(s_{k+1})\right)\right] \quad (6.7)$$

Thus, it follows that:

$$\min_{U_c} J_\pi\left(SOAcc^n_{BAT}\right) \triangleq \lim_{k \to \infty} \operatorname*{argmax}_{a_k \in A_k} E \sum_{k=N-2}^{\infty} \left[\left(\gamma^{k-1}\mathcal{R}(s_{k+1}, a_{k+1})\right)^{-1}\right] \quad (6.8)$$

The reward function in equations (6.10) comprising a fixed reward G, with penalty factors W_1 and W_2, represents a squared error penalty cost function, and constant penalty factor respectively is aimed at accelerating learning. The magnitude of the W_1 penalty factor is such that it increases proportionally to the absolute squared error deviation from the pinch target at that instant and the systems state if the agent takes a sub-optimal action as shown in equation (6.11). Furthermore, the rewarded function in equations (6.12) - (6.14) derived abstractly is able to update the agent $Q(s,\ a)$ regardless of if the availability proposition $\varepsilon_i^{Avl}(k)$ for both the FC and EL assets are met while exploiting an action which minimises the error.

A typical illustration; if the operating point dictated by adaptive PoPA anticipates future energy deficit and requests activation of the Fuel cell, while the agent activates the PEM Electrolyser, a penalty should suffice. The penalty function, therefore, serves as a closed-loop negative feedback to the agent.

The reward function proposition for $\mathcal{S}\ x\ \mathcal{A}\ : \mathcal{R}(\mathcal{S}, \mathcal{A})$ is implemented as follows;

$$\mathcal{R}(s_k, a_k) = \tag{6.9}$$

$$\begin{cases} G & \begin{array}{c} SOAcc^n_{BAT}(k+1) \geq SOAcc^m_{BAT}(k+1) \wedge a_k == Uc_{min} \wedge \\ [SOAcc^n_{BAT}(k+1) > S^l_{Lo} \wedge SOAcc^n_{BAT}(k+1) < (S^l_{Up} - 10\%)] \end{array} \\ -W_1 & \begin{array}{c} [SOAcc^n_{BAT}(k+1) \leq SOAcc^m_{BAT}(k+1)] \wedge a_k \neg = Uc_{min} \wedge \\ [SOAcc^n_{BAT}(k+1) > S^l_{Lo} \wedge SOAcc^n_{BAT}(k+1) < (S^l_{Up} - 10\%)] \end{array} \\ G - W_1 & \begin{array}{c} [SOAcc^n_{BAT}(k+1) \geq SOAcc^m_{BAT}(k+1)] \wedge a_k \neg = Uc_{min} \wedge \\ [SOAcc^n_{BAT}(k+1) > S^l_{Lo} \wedge SOAcc^n_{BAT}(k+1) < (S^l_{Up} - 10\%)] \end{array} \\ -(W_1 + W_2) & \begin{array}{c} \left(\begin{array}{c} [SOAcc^n_{BAT}(k) \leq SOAcc^n_{BAT}(k+1) \wedge \\ [SOAcc^n_{BAT}(k) \geq S^l_{Up} \wedge SOAcc^n_{BAT}(k+1) \geq S^l_{Up}] \wedge \\ a_k \neg = Uc_{min} \vee SOAcc^n_{BAT}(k+1) \geq S^l_{Up} \wedge a_k \neg = Uc_{min} \end{array} \right) \vee \\ \left(\begin{array}{c} [SOAcc^n_{BAT}(k) \leq SOAcc^n_{BAT}(k+1) \wedge \\ [SOAcc^n_{BAT}(k) \geq S^l_{Up} \wedge SOAcc^n_{BAT}(k+1) \geq S^l_{Up}] \wedge \\ a_k \neg = Uc_{min} \vee SOAcc^n_{BAT}(k+1) \leq S^l_{Up} \wedge a_k \neg = Uc_{min} \end{array} \right) \end{array} \end{cases} \tag{6.10}$$

Where, W_1 *and* W_2 is a penalty factors.

$$W_1 = [(SOAcc^n_l(k+1) - SOAcc^m_{BAT}(k+1))/SOAcc^m_{BAT}(k+1)]^2 \tag{6.11}$$

The action which results in the minimum optimal control action is derived abstractly as follows:

$$Uc_{min} := \left\{ \begin{array}{ll} D & SOAcc^{m}_{BAT}(k+1) > S^{l}_{Lo} \wedge\ SOAcc^{m}_{BAT}(k+1) \leq (S^{l}_{Up} - 10\%) \\ E & SOAcc^{m}_{BAT}(k+1) > (S^{l}_{Lo} + 50\%) \wedge\ SOAcc^{m}_{BAT}(k+1) < (S^{l}_{Up}) \end{array} \right\} \tag{6.12}$$

Where,

$$D := \inf\{(SOAcc^{m}_{BAT}(k+1) \,|\, \sum_{i=1}^{7} Q(a_i, s_{k+1})) \geq SOAcc^{n}_{BAT}(k+1)\} \tag{6.13}$$

$$E := \sup\{(SOAcc^{m}_{BAT}(k+1) \,|\, \sum_{i=1}^{7} Q(a_i, s_{k+1})) \leq SOAcc^{n}_{BAT}(k+1)\} \tag{6.14}$$

During the real-time deployment, the PoPA target is modified respectively with the MOES or MAE so as to capture the effect of uncertainty after S_{Lo} or S_{Up} violation occurs at any instant as follows;

$$SOAcc^{m}_{BAT}(k \mid k) := \left\{ \begin{array}{ll} S^{l}_{Up} & SOAcc^{n}_{BAT}(k) > S^{l}_{Up} \\ S^{l}_{Lo} & SOAcc^{n}_{BAT}(k) < S^{l}_{Lo} \end{array} \right. \quad , \quad \forall_t \ if \ \exists\, \Delta\mathfrak{H}(k) \neq 0 \tag{6.15}$$

The reward function is modified to incorporate the MOES or MEES thus guaranteeing the model-free agent will act optimally in the event of uncertainty to maximise the expected reward is as follows:

$$J_{Pinch}\ (SOAcc^{n}_{BAT}) + J_e\ (\Delta H) = min_U\ \ J_\pi\ (SOAcc^{n}_{BAT}) \tag{6.16}$$

Furthermore, by performing the optimal policy π^* the corresponding cost is as follows:

$$J^{*}_{\pi}(SOAcc^{n}_{BAT}) \rightarrow \lim_{k\rightarrow\infty} E\ \left[\sum \gamma\ (\ J_{Pinch}\ (SOAcc^{n}_{BAT}) + J_e\ (\Delta H))\right] \tag{6.17}$$

Since the cost of the error due to uncertainty tends to zero by following the optimal policy, J^*_π(s) agent incorporates the uncertainty estimation into the PoPA, therefore:

$$\lim_{k\to\infty} \quad J^*_\pi\left(SOAcc^n_{BAT}\right) \leq \gamma J_{Pinch}\ \left(SOAcc^n_{BAT}\right) \tag{6.18}$$

The expected cost following the pinch analysis and uncertainty propagation is less than following only the PoPA model. Hence, the experience of the agent integrated into the Adaptive PoPA framework guarantees optimal operation, as long as the conditions of optimal action selection and learning rate decay are satisfied. Figures 6.1 and 6.2, illustrates the reinforcement learning adaptive PoPA architecture and algorithm, respectively. Furthermore, the pseudo and MATLAB .m codes have been presented in Appendix C and Appendix E respectively.

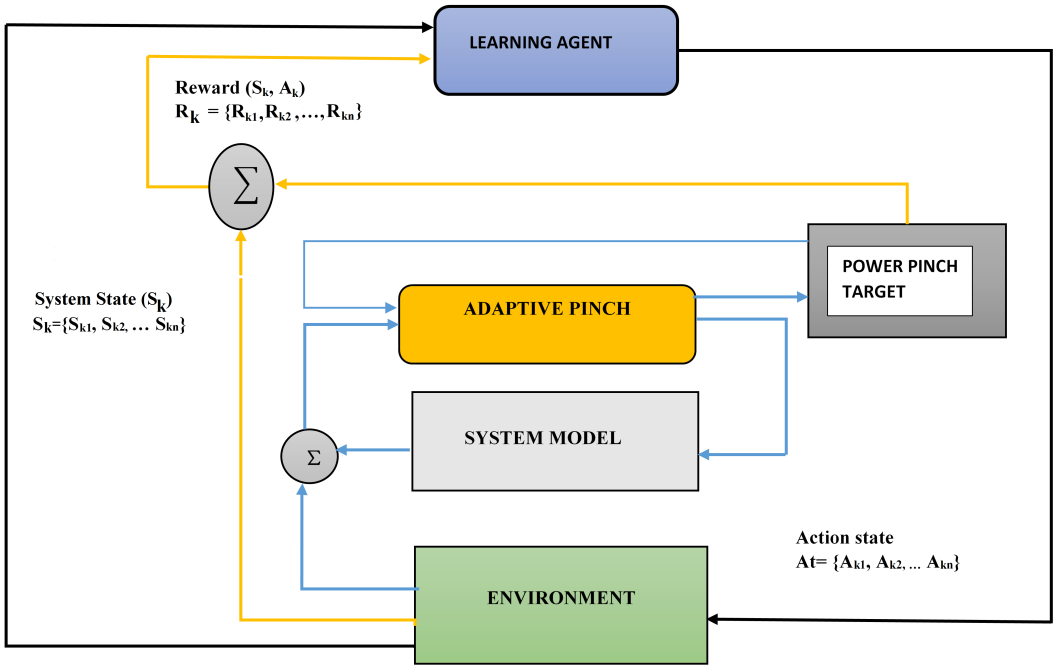

Fig. 6.1 Reinforcement Learning Adaptive Power Pinch Schematic

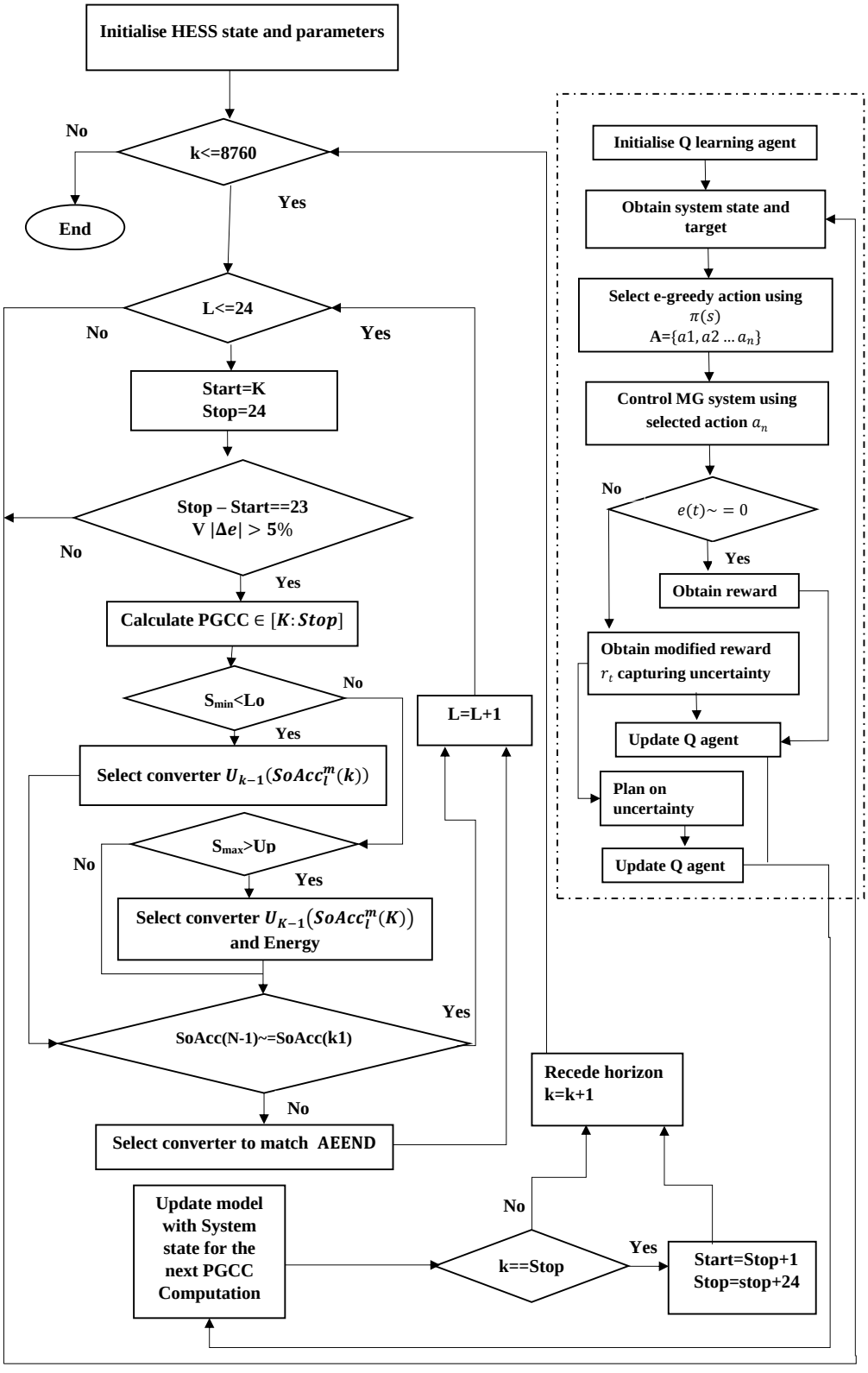

Fig. 6.2 RL+Adaptive Power Pinch Algorithm

6.2.5 Deep Reinforcement Learning Adaptive PoPA

The discretisation of the state and action space in RL introduces the curse of dimensionality [148]. Hence, in the machine learning community, function approximators such as fuzzy logic [149], approximate nearest neighbour [150] and deep neural network [151] are often used. Nevertheless, Fuzzy logic approximation is based on predefined rules, while deep neural network in order to perform proper and effective generalisation requires a lot of training and validation from enormous data sets. However, these function approximators do not guarantee better performance over tabular Q-Learning counterpart, especially concerning fewer dimensional state and action space.

In this work, for the purpose of investigating the generalisation ability of the deep RL with the adaptive PoPA, a fully connected deep neural net, comprising one (1) input, fifteen (15) hidden layers and seven (7) actions, is trained to approximate the 270 x7 dimensional Q –Table, previously derived in section 6.2.1. The DNN is trained in MATLAB with the neural net toolbox, using a mean squared error minimisation loss function as in [140, 152] but with the inclusion of an L2 regularisation [153] to prevent overfitting, since the 270 x7 dimensional Q –Table represents a shallow data set. Hence, the cost function J(w) of the DNN is expressed as follows;

$$J(w) = [r_k + \gamma_{a'}^{max} Q_{k+1}(s', a', w') - Q_k(s, a, w)]^2 + \lambda \sum_{i=1}^{T} w_i^2 \tag{6.19}$$

Where, the reward r_k in addition to the discounted next state-action value $Q_{k+1}(s', a', w')$ obtained from the DNN's target, while $Q_k(s, a, w)$ is the output of the DNN. Also, w is the weight of the neural network, i is the i_{th} weight, $i \in [1 : T]$ and λ is a weighting factor, $\lambda \in [0 : 1]$. Therefore, by taking the derivative of the loss function $\nabla_w J(w)$ in equation 6.20 the weights of the deep neural net are updated via back-propagation as follows;

$$w \leftarrow w + \psi \nabla_w J(w) \tag{6.20}$$

Where, ψ represents the learning rate.

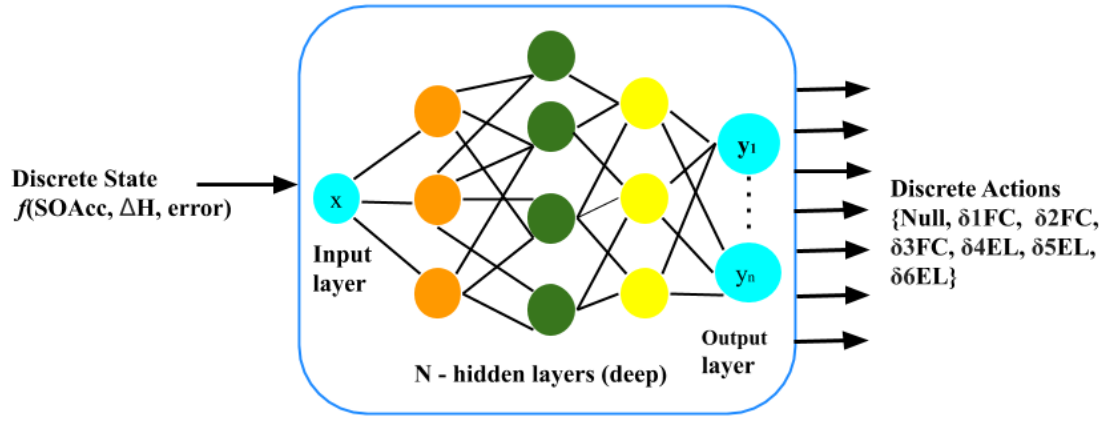

Fig. 6.3 DRL+Adaptive Power Pinch Algorithm

6.2.6 Actor Critic Reinforcement learning with Probabilistic PoPA

This section combines the concept of the probabilistic adaptive PoPA within an actor-critic deep reinforcement learning algorithm (A2C+P). The actor-critic network RL algorithm naturally enables the support for continuous state and action space is realised based on the deep policy gradient approach [154]. While a value based critic network evaluates the quality of the policy based actor network's performance, the resulting TD error is back propagated to correct the critic as well as combined with the log likelihood [155] or mean squared error [154] of the action taken to correct the actor network. Furthermore, recent successes with the actor-critic approach are discussed in [156].

6.2.6.1 Actor-Critic neural net Architecture with P+Adaptive PoPA

The proposed deep RL architecture used with the probabilistic adaptive PoPA, consists of two neural networks, as shown in Figure 6.4. In this work, the Actor neural network is a NARX recurrent deep neural network [157, 158] which is suitable for processing time-series data. Whereas the Critic is a deeply layered fully connected neural net, both neural networks have ten (10) hidden layers (with sigmoidal activation function).

Specifically, the continuous input state space fed into the Actor and critic neural networks consists of six (6) tuples: $\{USOAcc_l^m(k), LSOAcc_l^m(k), SoAc_{BAT}^m(k-1), \phi_S, \phi_H, a_(k-1)\}$.

Where, $USOAcc_l^m(k)$ and $LSOAcc_l^m(k)$ are the upper and lower confidence interval bounds respectively expressed as point estimates of the predicted SOAcc of BAT. $SoAc_{BAT}^m(k-1)$ is the predicted SOAcc of BAT at the previous time step k ϕ_S: represents seasonal period and subscript $S \in [1:4]$ indicates the specific season. ϕ_H : represents the hour of the day and subscript $H \in [1:24]$, indicates the k^{th} hour. a_{k-1} :represents the past output information (action) generated by the Actor critic network.

The continuous action space is such that $U_c(k)$ can operate within the maximum range of $\mathcal{F}_{BAT\rightarrow EL}^{POW}$ and $\mathcal{F}_{FC\rightarrow BAT}^{POW}$ as expressed in equation 6.21 as follows:

$$U_c(k) = \left\{ \begin{array}{cc} \mathcal{F}_{BAT\leftarrow FC}^{POW} & if\ U_c > 0 \\ \mathcal{F}_{BAT\rightarrow EL}^{POW} & if\ U_c < 0 \\ 0 & Otherwise \end{array} \right\} \forall_{k\in[1:N]} \tag{6.21}$$

The variance derived from past N-optimal $U_c(k)$ is determined by the probabilistic PoPA and thus used to enhance exploration.

Typically, at every time step for a given input state derived by extracting feature parameters from the HESS and probabilistic model, the Actor neural network generates an optimal predictive action a_k, based on an action policy π_w which results in the de/activation of the EL or FC or null.

The Critic which is a deep recurrent neural network is pre-trained using an action policy π_θ generated from the Probabilistic adaptive PoPA with a cross-entropy method loss function. Thus, given the continuous state information, the Critic acts as a feed-forward model, thereby predicting an action which might either activate the FC or the EL or null.

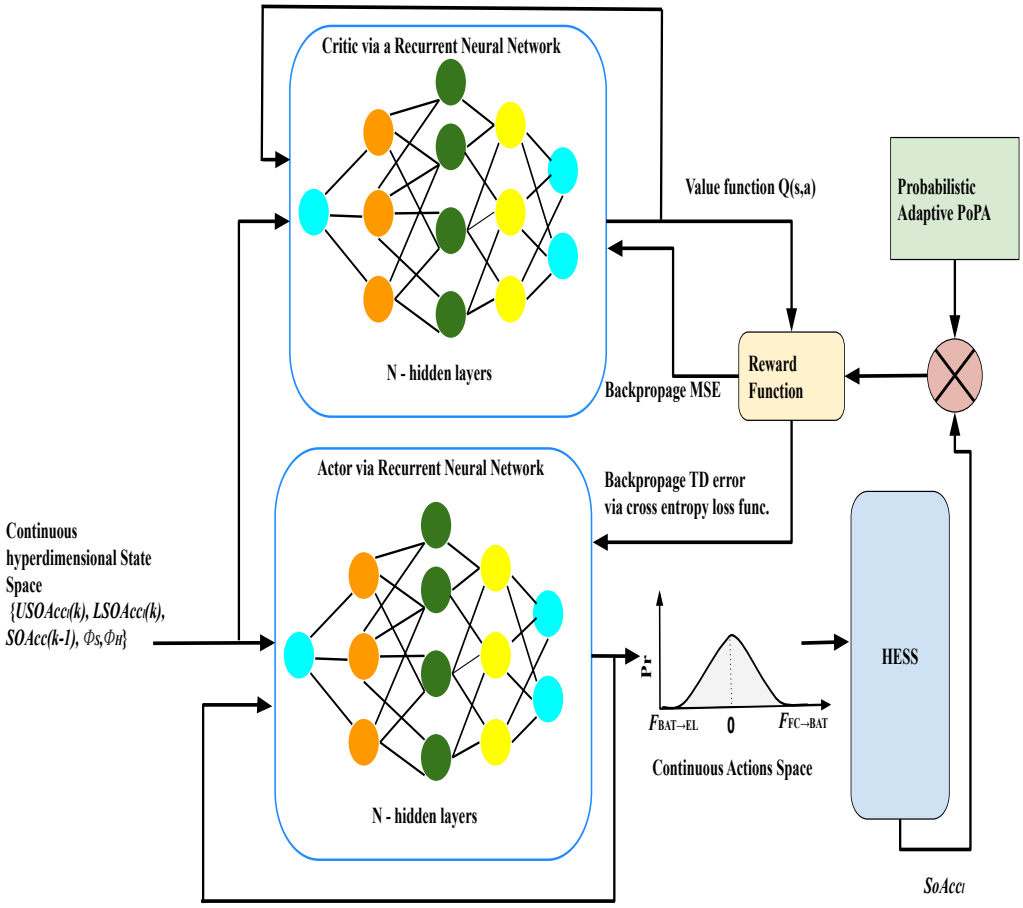

Fig. 6.4 Actor-Critic Probabilistic Adaptive PoPA Schematic

6.3 Results and Discussion

6.3.1 RL+Adaptive PoPA

6.3.1.1 Training of the RL Intelligent Agent

In order to deploy the RL agent, the agent has to be trained using the Adaptive PoPA. The Q table which holds the value function of the state -action pairs and used by the RL agent is initialized randomly between 0 and 1. Nevertheless, how the Q table is initialized during the training can affect the total training time. The agent which starts out with the random value estimate for each state action pair, eventually accumulate the needed experience to

operate the HESS model during the training session. The 3D surface plot at initialization is shown in Figure 6.5. The scalar reward which was found to have worked well is 0.01 unit, as larger rewards quickly diverged exponentially. After the initialization the RL agent is trained using the Adaptive PoPA offline in order to garner some appreciable experience of the actual HESS. The training was done in 2 epochs, each with a duration of 8760h. In the first epoch the exploration parameter ep, is set to 0.9 which implies that 90% of the time the agent will explore random actions while exploiting optimal actions 10% of the time. Furthermore, since the agent is to leverage from experience the in the 2nd epoch the exploitation is increased from the initial 0.1 to 0.7. Figures 6.6 and 6.7 show the 1st and 2nd training epochs respectively. The cumulative reward which has an exponential response, converges in the 1st and 2nd epoch as shown indicated by the red line in Figure 6.7. Ideally, the RL agent has to be trained infinite number of times on every state-action pair in order to guarantee convergence. With respect to convergence, rather than over-fit the agent on the Adaptive PoPA model, a practical approach was employed, hence, saving computational time to only 2 epochs. Therefore, the training was stopped when the violation S_{Lo} and S_{Up} were both less than 10 violations and the DSL never activated. The 3D surface plot at the end of the 3rd training epoch is shown in Figure 6.8 and the maximum cumulative reward at the end of the the training session was 24 units, as shown in Figure 6.8.

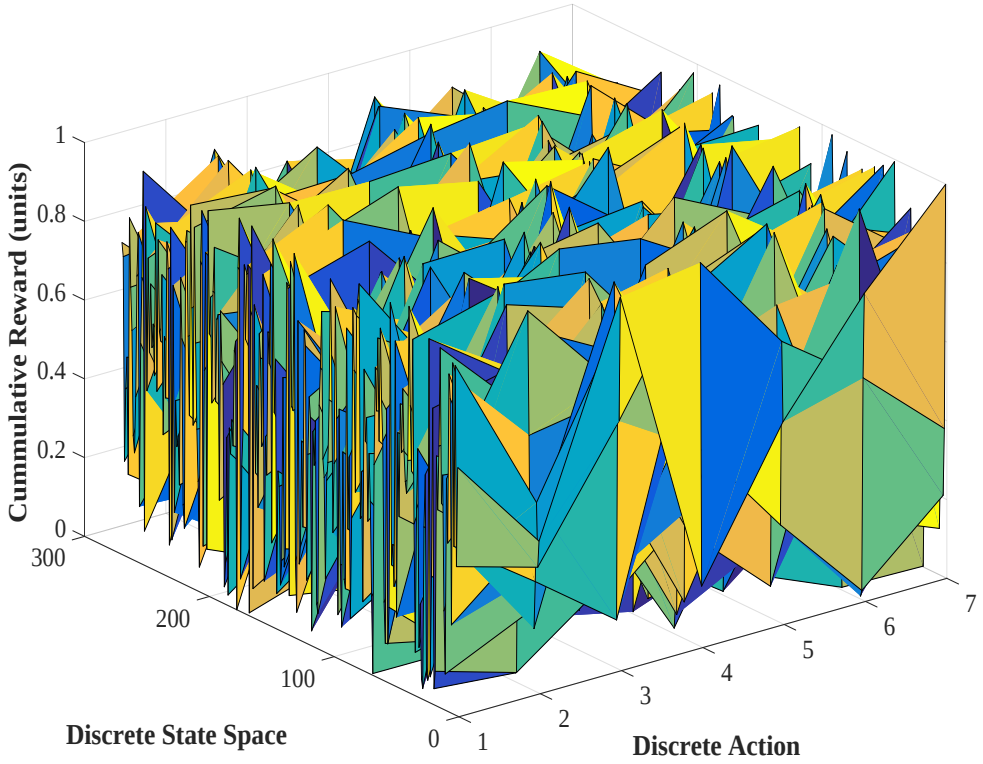

Fig. 6.5 3D surface plot of the RL cumulative Reward at initialisation

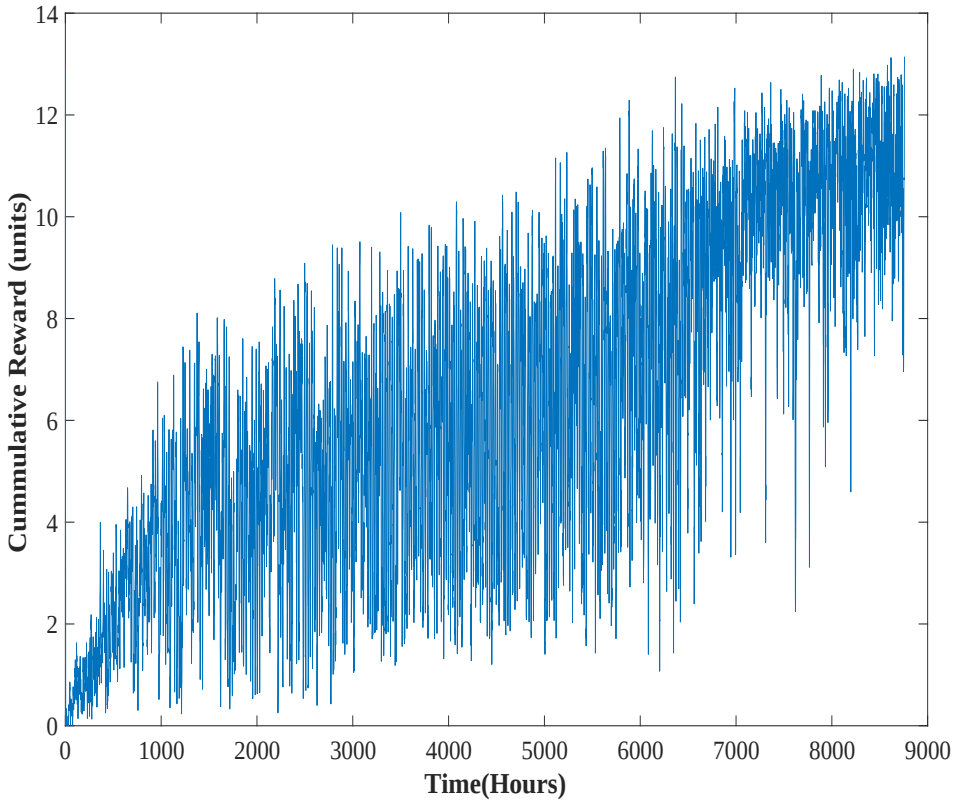

Fig. 6.6 Cumulative Reward at Epoch 1

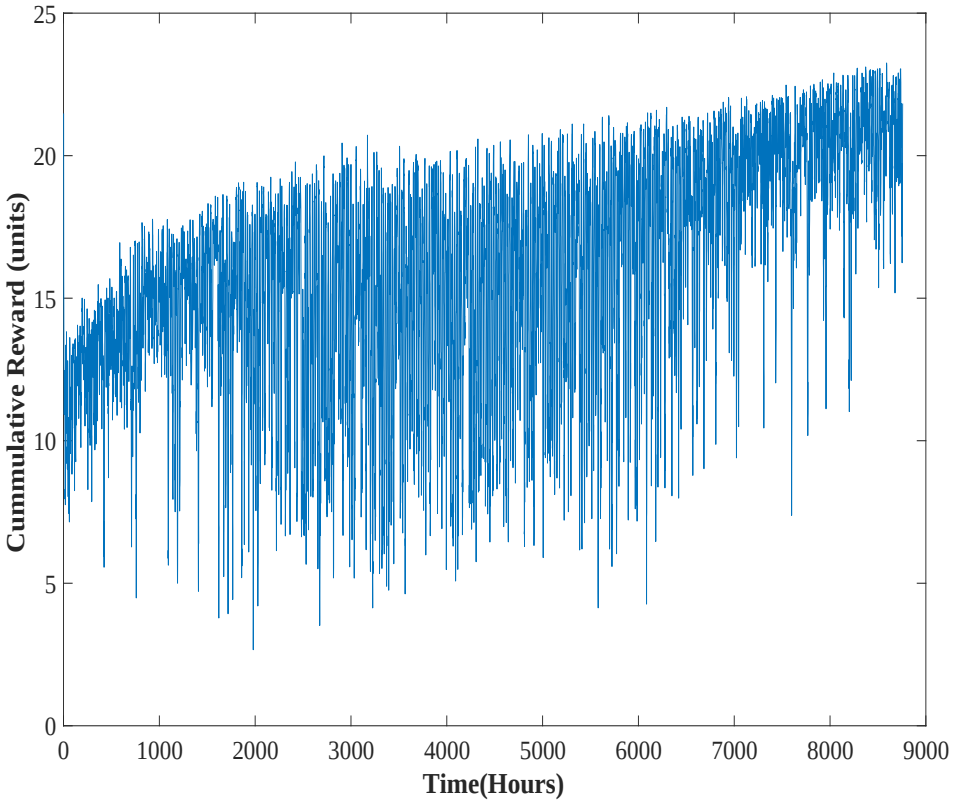

Fig. 6.7 Cumulative Reward at Epoch 2

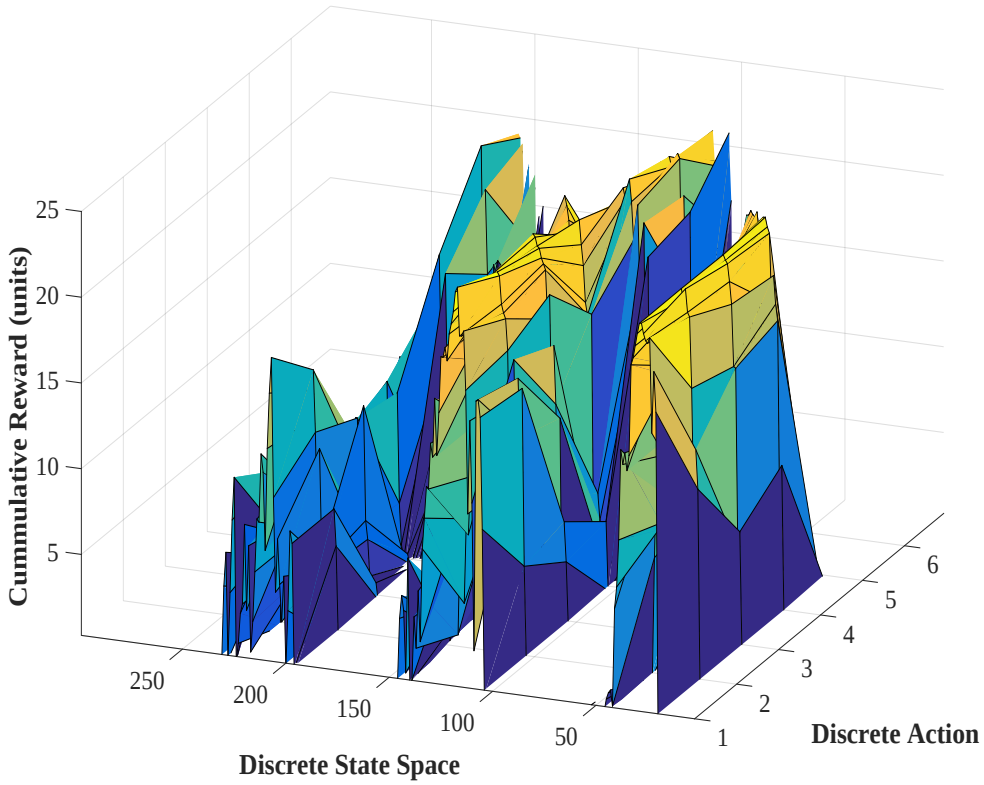

Fig. 6.8 3D Surface Plot of the RL Cumulative Reward after the Final Training

6.3.1.2 RL+Adaptive PoPA Performance

The RL+Adaptive PoPA had only one violation of S_{Lo} under the non-Gaussian uncertainty case study which occurred at the 45^{th} h as shown in Figure 6.9. Also, the DSL was never activated. However, the FC and EL were activated 28 and 20 times respectively in a bid to track the Adaptive PoPA's PGCC as shown in Figure 6.10, and the HT and WT responses are shown in Figure 6.11. Furthermore, under the Gaussian uncertainty case study, the RL had an improved performance as no violation occurred as shown in Table 6.1.

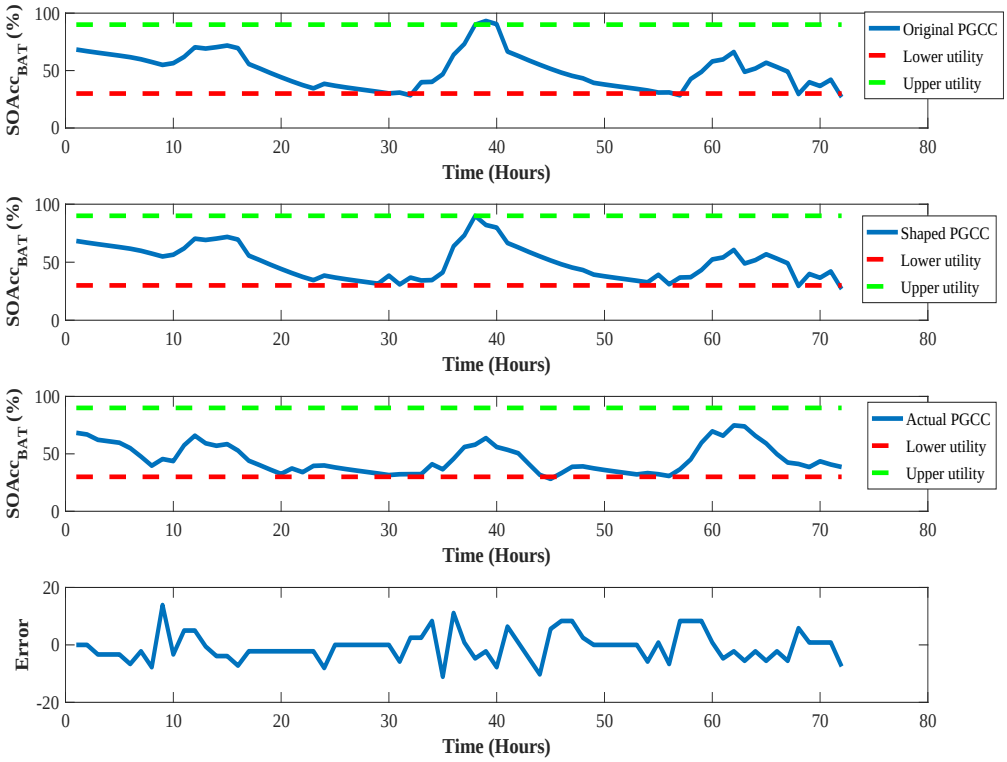

Fig. 6.9 Performance of the RL+Adaptive PoPA strategy over 72h

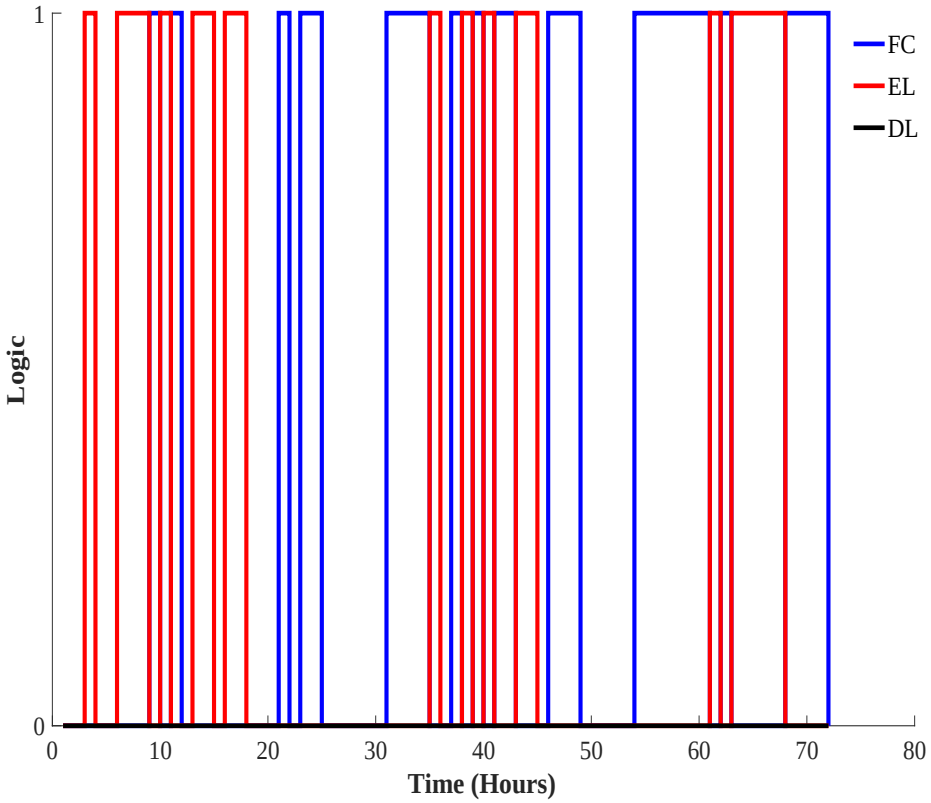

Fig. 6.10 RL+Adaptive PoPA converter logic over 72h

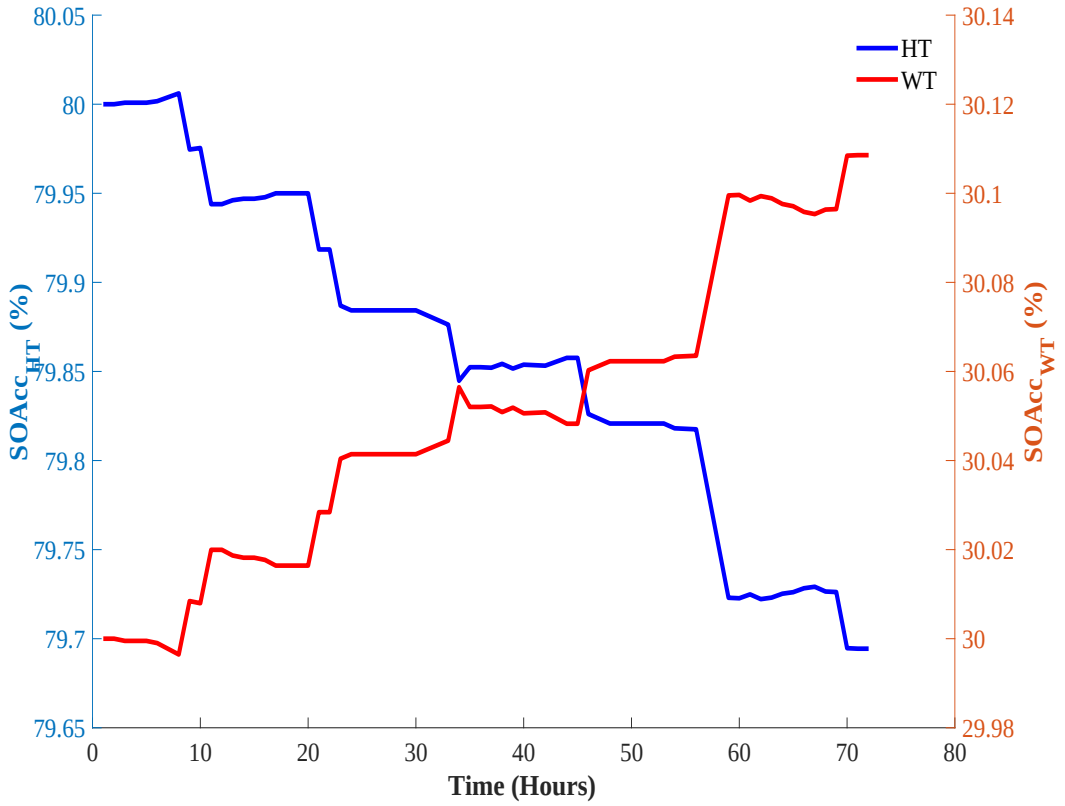

Fig. 6.11 RL+Adaptive PoPA HT and WT response over 72h

6.3.2 DRL+Adaptive PoPA

6.3.2.1 Training of the DRL Intelligent Agent

The Q-Table with dimension 270 by 7, which was realised at the final training session in section 6.2.1 was approximated using a DNN with 1 input, 10 hidden sigmoid layers and 7 outputs. Before the training, the data set is randomly divided up into training, testing and validation samples in proportions of 70%, 15% 15% respectively. The approximation of the Q-Table is implemented using the Levenberg-Marquard back-propagation training method in MATLAB with the NN toolbox. The training, validation and testing regression coefficients of correlation were 0.95, 0.96, and 0.95 respectively with an average of 0.95 as shown in

Figure 6.12. Therefore the coefficients of correlation show a strong relationship with the training data set without over-fitting and can be used for generalization. Furthermore, from Figure 6.13, the mean squared error (MSE) performance validation score which was 4.2, occurred at the 76^{th} epoch out of 82 epochs used to training the DNN.

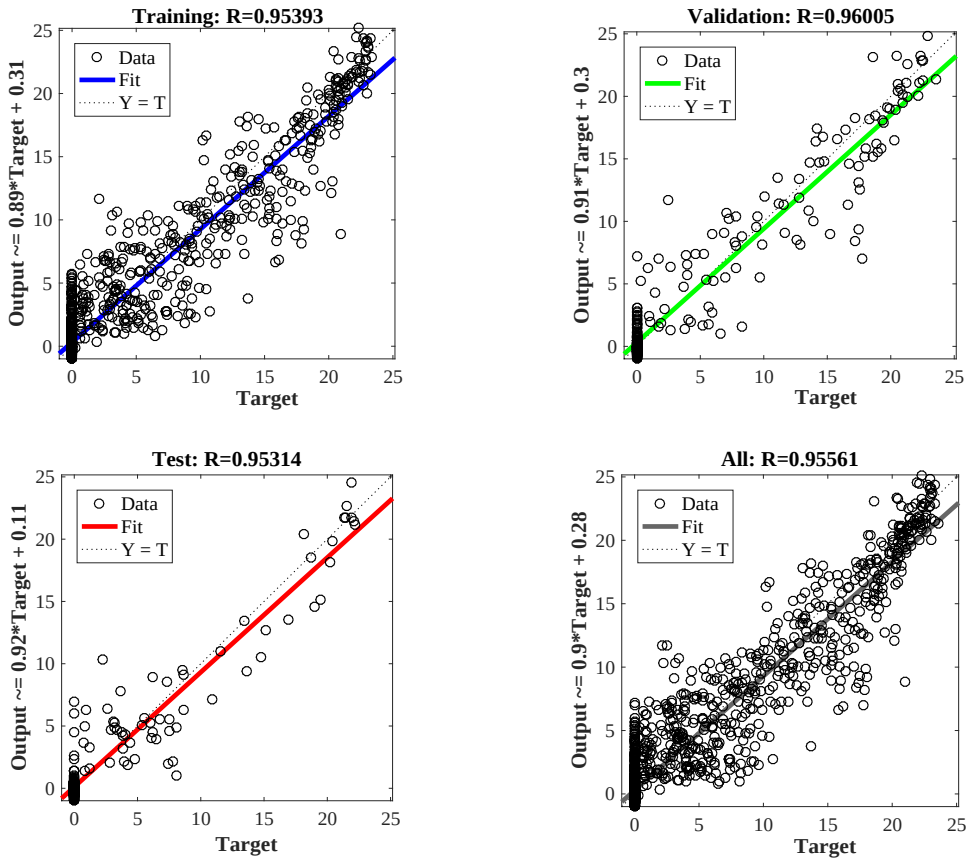

Fig. 6.12 DRL+Adaptive Training Regression Plot

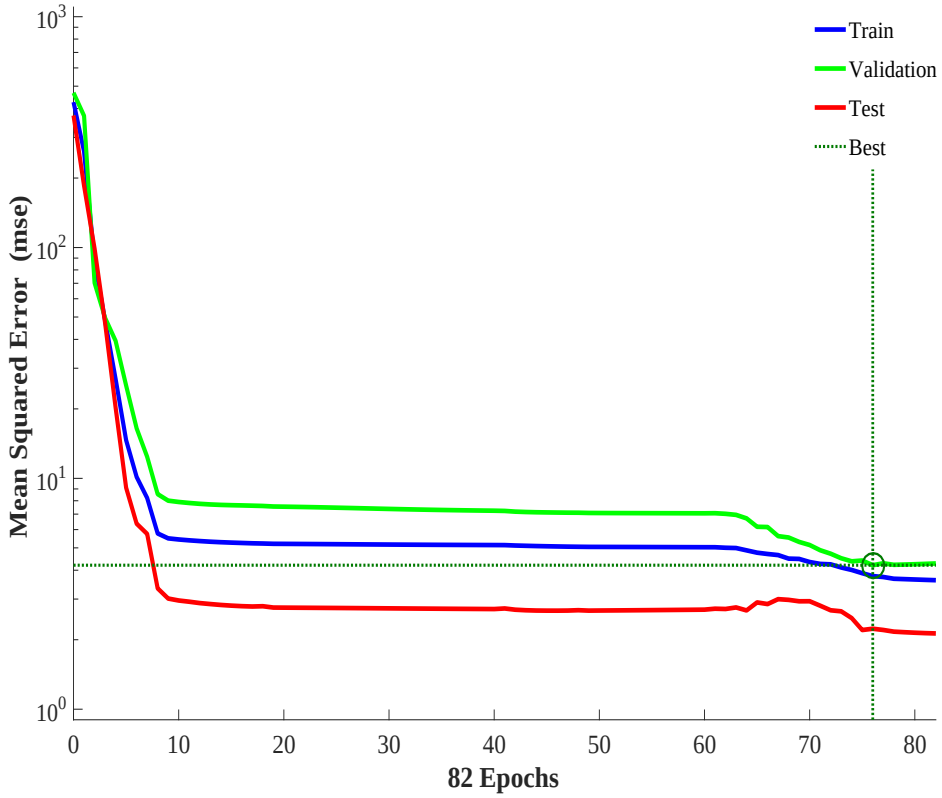

Fig. 6.13 MSE Performance validation of the DRL+Adaptive

6.3.2.2 DRL+Adaptive PoPA Performance

The DRL had only one violation of the S_{Up} under the non-Gaussian uncertainty case study at the 37th h as shown in Figure 6.14. The FC and EL were activated 29 and 28 times respectively in order to counteract the effects of uncertainty as shown in Figure 6.15 with corresponding HT and WT response shown in Figure 6.16. However, under the Gaussian uncertainty case study, the S_{Up} violation increased as it was violated twice as shown in Table 6.1.

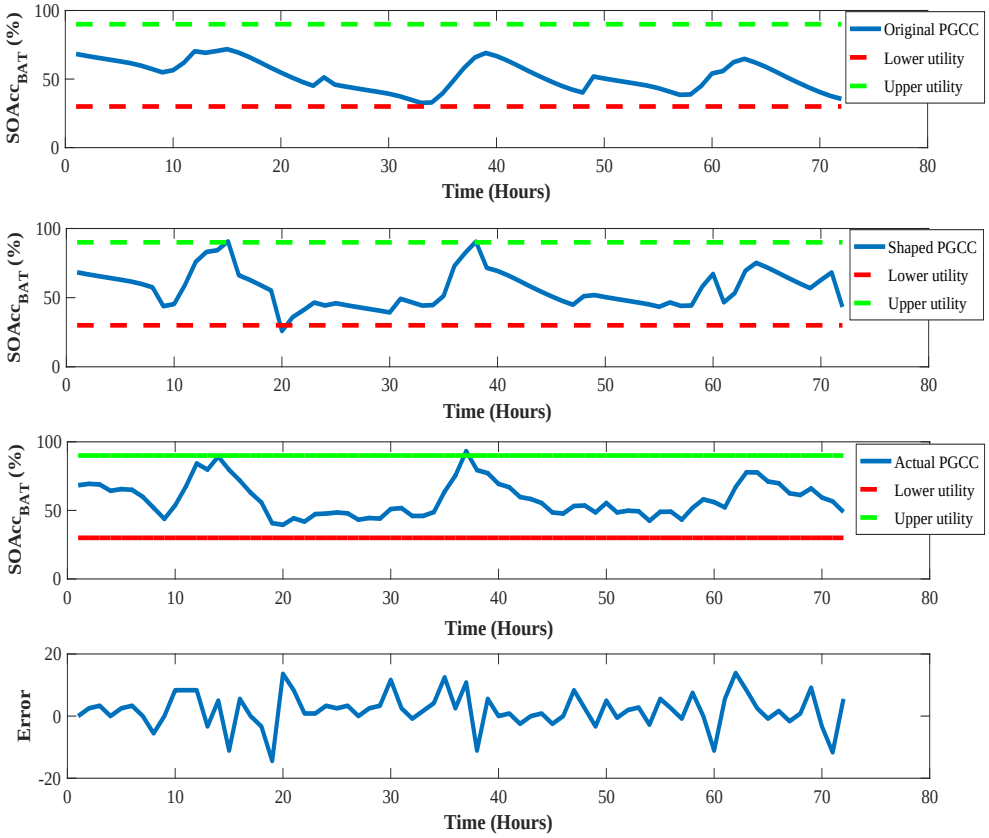

Fig. 6.14 Performance of the DRL+Adaptive PoPA strategy over 72h

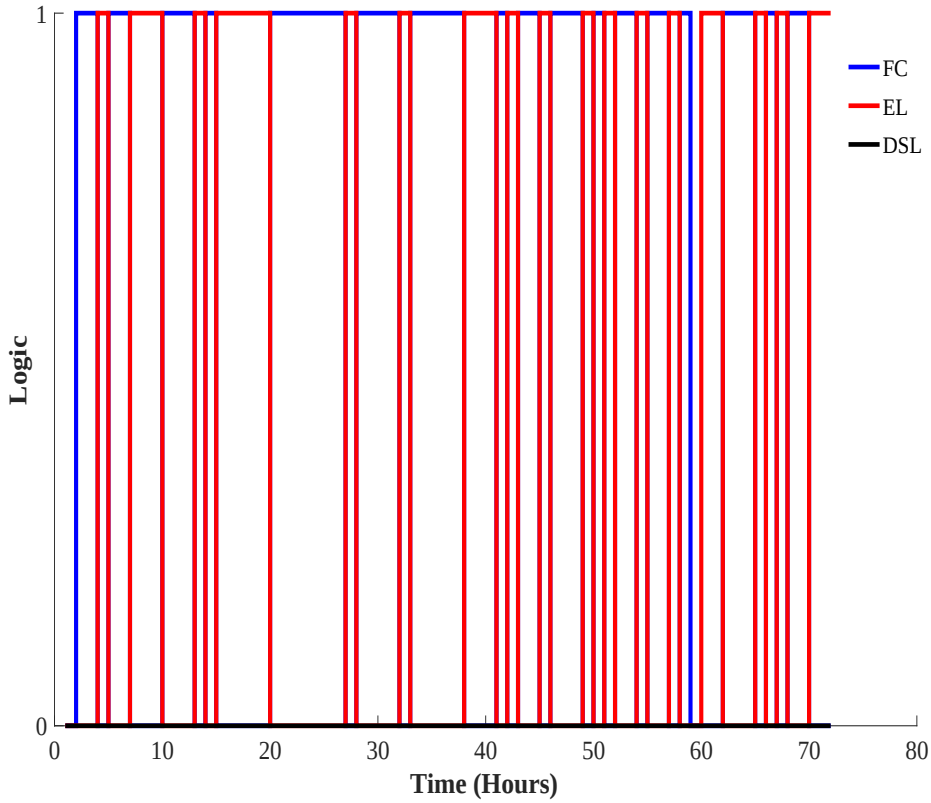

Fig. 6.15 Converter Logic with DRL+Adaptive PoPA over 72h

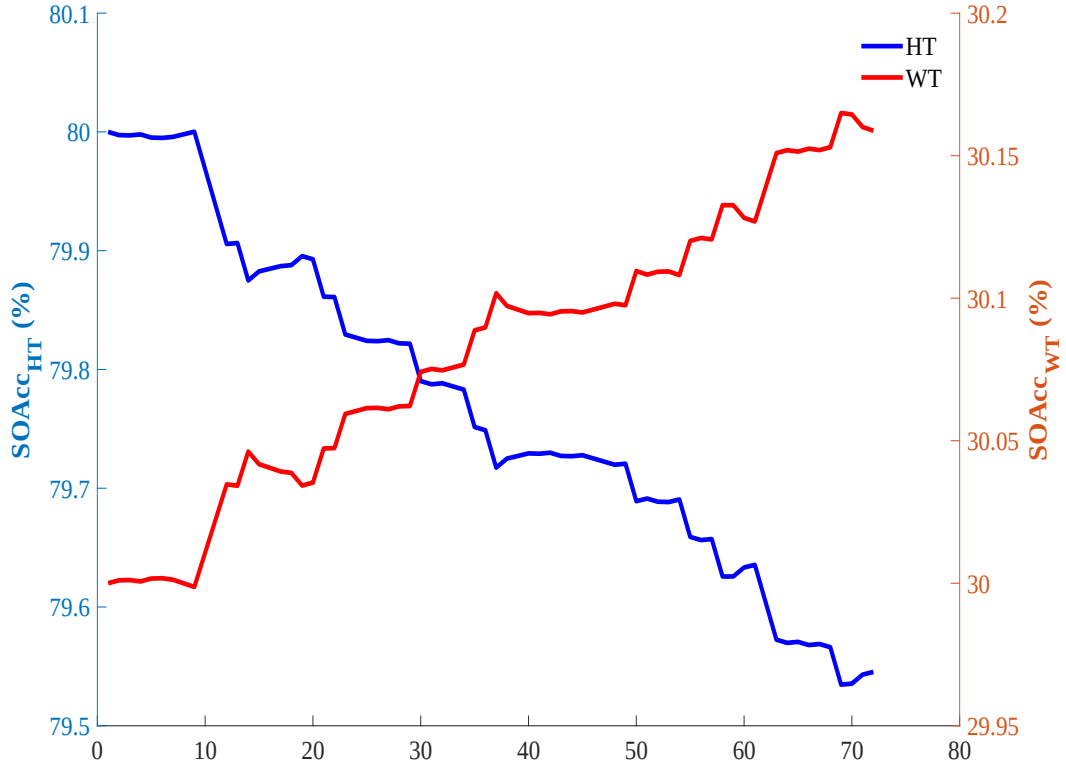

Fig. 6.16 HT and WT response with DRL+Adaptive PoPA over 72h

6.3.3 A2C+P PoPA

The A2C+P PoPA had only 6 violations concerning the S_{Up} and none with regards to violating the S_{Lo} under the non-Gaussian uncertainty scenario as shown in Figure 6.17. As shown in Figure 6.18 the FC was activated 30 times while the EL was activated only once at the 40th h. Figure 6.19 depicts the corresponding HT and WT response. Therefore, the A2C+P PoPA had the least FC and EL activation compared to the DRL+Adaptive and RL+Adaptive which had significantly more activation cycles. The A2C+P PoPA had 18 violations under the Gaussian uncertainty case study with respect to the S_{Lo} as shown in Table 6.1. However

the progressive violation of S_{Lo} did not activate the DSL, as the $SOAcc_{BAT}$ never dipped below the 20% which is the propositional logic constraint which activates the DSL.

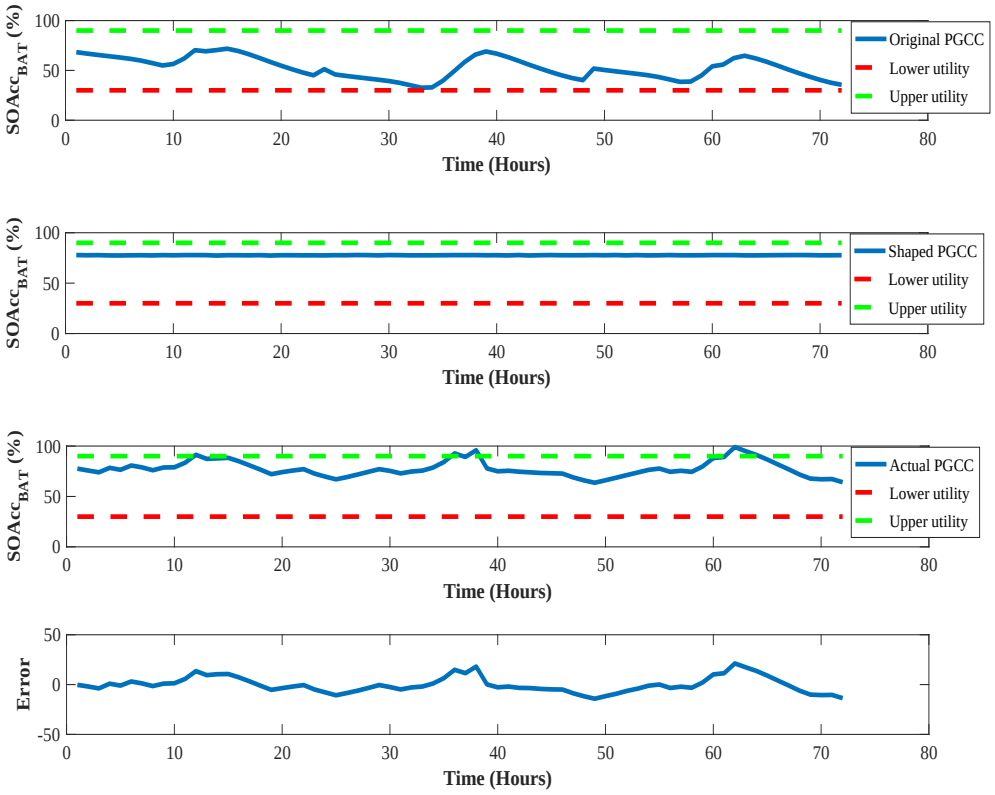

Fig. 6.17 Performance of the A2C+P PoPA strategy over 72h

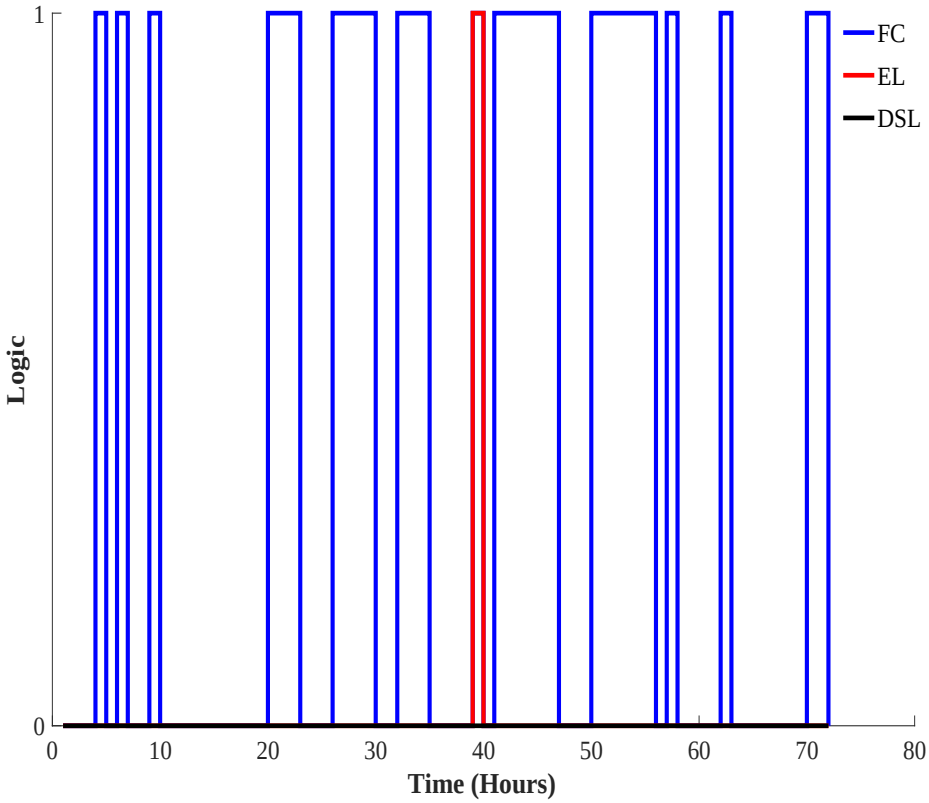

Fig. 6.18 HT and WT response with A2C+P PoPA over 72h

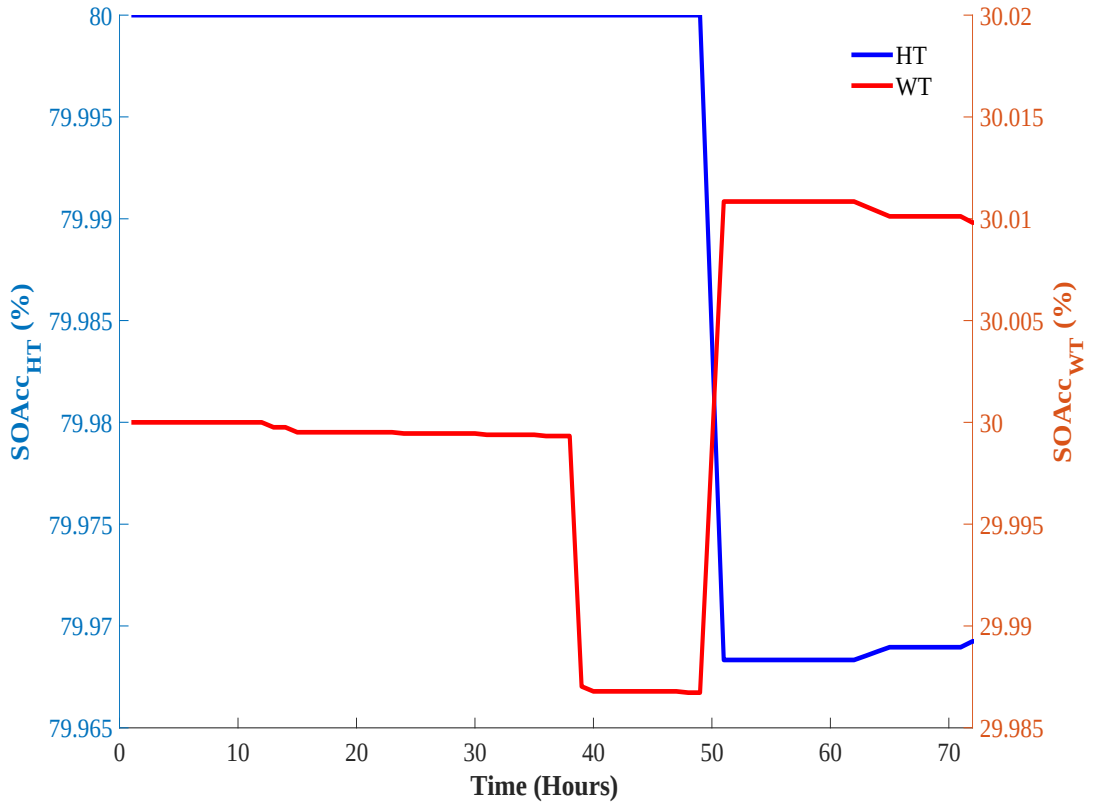

Fig. 6.19 HT and WT response with A2C+P PoPA over 72h

6.4 Summary

The RL+Adaptive, DRL+Adaptive and A2C+P PoPA have been presented in this Chapter. As shown in Table 6.1 the performance of the RL+Adaptive, DRL+Adaptive and A2C+P PoPA are presented. The RL and DRL adaptive both had only one violation of the S_{Lo} and S_{Up} respectively, whereas the A2C+P had 6 violations of the S_{Up} under non-Gaussian uncertainty. While the RL+Adaptive PoPA had a better performance when the uncertainty was Gaussian the DRL+Adaptive PoPA had violated the S_{Up} twice and the A2C+P had 18 violations of the S_{Lo}. Though the overall performance of the RL+Adaptive PoPA and DRL+Adaptive PoPA did not outshine that of the probabilistic methods presented in Chapter 5, these machine

learning based PoPA approaches excluding the A2C+P PoPA, have shown significantly better performance than the Kalman+Adaptive, Adaptive and the DA PoPA presented in Chapter 4. Nevertheless, further investigation over a period of 8760h will be performed in Chapter 7 with all these proposed methods.

Table 6.1 Summary of performance over 72 h analysis with RL+Adaptive, DRL+Adaptive and A2C+P PoPA algorithms.

Indices		RL+Adaptive PoPA	DRL+Adaptive PoPA	A2C+P PoPA
Non-Gaussian Uncertainty	Lower Pinch Violation	1	0	0
	Upper Pinch Violation	0	1	6
	DSL Activation	0	0	0
Gaussian Uncertainty	Lower Pinch Violation	0	0	18
	Upper Pinch Violation	0	2	0
	DSL Activation	0	0	0

Chapter 7

Results and Discussion

The proposed methods are evaluated against the DA-PoPA, which is the most recent state of the art over 8760 h with the HT sized at $15m^3$ capacity under non-Gaussian and Gaussian load uncertainty. The PV uncertainty is of normally distributed throughout the investigation. The performances of the methods are investigated and analysed on a long term basis over 8760 h. Also, a sensitivity The BAT, HT, and WT are initialised to 80%, 80% and 30% respectively. Throughout this Chapter, percentage increase or decrease are discussed are benchmarked against the performance of the DA PoPA. The HESS parameters are shown in Table 7.1.

Table 7.1 HESS Microgrid Parameters [27]

System Components	Specification
Load (peak)	2200 W
PV (66.64 W rated power)	217
DSL	2210 W
BAT	3000 Ah / 12 V
FC	3000 W
EL	4000 W
HT	30 bar, 15 m^3
$\eta_{CV}, \eta_{PV}, \eta_{FC}, \eta_{EL}$	0.95, 0.10, 0.87, 0.87

The performance indices utilised in this Chapter to evaluate the energy management approaches are with respect to violating the S^{l}_{Lo} (30%), S^{l}_{Up} (90%) Pinch constraints and DSL activation as defined in Chapter 4, section 4.3.

7.1 Long term (8760h) Operation

7.1.1 Non-Gaussian Uncertainty with HT Capacity of $15m^3$

The results showing the performances of the deterministic methods; DA, Adaptive and Kalman+Adaptive PoPA are presented in Table 7.2a. The performances of the probabilistic methods; P+Adaptive, RLS+P without bias and RLS+P with a biased linear model are presented in Table 7.2b. While the machine learning-based PoPA methods; RL, DRL and A2C+P are presented in Table 7.2c.

7.1.1.1 DA PoPA

From Table 7.2a, the $SOAcc_{BAT}$ controlled by the DA PoPA violated the $S_{Up}(SOAcc^{n}_{BAT} > 90\%)$ and $S_{Lo}(SOAcc^{n}_{BAT}<30\%)$ pinch limits 756 and 804 times respectively with the EL activated 265 times. Consequently, as a result of over-discharging the $SOAcc_{BAT}$ beyond 20%, the DSL was activated 229 times, and the FC was activated 264 times. The $SOAcc^{n}_{BAT}$, $SOAcc^{n}_{HT}$ responses and corresponding evolution of the probability of S_{LO} and S_{Up} violation over the 8760 h are shown in Figures 7.1, 7.2 and 7.3. From Figure 7.1, the $SOAcc^{n}_{BAT}$ controlled by the DA PoPA showed sensitivity to RES intermittency. During the first three and last month's where RES is considerably intermittent due to the partial absence of sunshine, the $SOAcc^{n}_{BAT}$, frequently dipped below the S_{Lo} even so below 20%. Also, during the months of peak sunshine, the $SOAcc^{n}_{BAT}$ frequently violated the S_{Up}. This was largely due to the effect of uncertainty, which introduced forecast error making the DA-PoPA energy targeting inadequate. Nevertheless, the performance of the DA PoPA with regards to violating the

S_{Lo} was only better than the RLS+P (A=Ax+B). Similarly, the DA performed better than P+Adaptive and A2C+P PoPA concerning S_{Up} violation only.

7.1.1.2 A2C+P PoPA

The A2C+P PoPA method which had the worst S_{Up} violation of 908 times had a very low S_{Lo} violation of 55 times which was only comparable to the performances of the RL +Adaptive and DRL+Adaptive PoPA which both had 51 and 11 times as shown in Table 7.2c. The $SOAcc^{n}_{BAT}$, controlled by the A2C+P PoPA EMS violated the S_{Up} steadily as shown in Figure 7.27 and consequently the probability of S_{Up} violation maintained a steep rise with S_{Lo} constant at zero until 8000h as shown in Figure 7.29. The $A2C+P$ activated the DSL 19 times and the FC 4226 times while the EL was never activated as shown in Table 7.2c. The corresponding response of the $SOAcc^{n}_{HT}$ is shown in Figure ref A2C6.3, which was 66.3% at 8760 h.

7.1.1.3 RLS+P PoPA (y=Ax+B)

Furthermore, RLS+P (y=Ax+B) which had the worst S_{Lo} violation of 1217 times, consequently also activated the DSL 673 times and the FC 2754 times. Thus, benchmarked against the performance of the DA PoPA utilising the RLS+P (y=Ax+B), led to 51.4% in S_{Lo} violation, 194% and 432% increase in DSL and FC activation as shown in Table 7.2b. Thus, despite a decently sized HT of $15m^3$ (initialised with $SOAcc^{n}_{HT}$ at 80%) the $SOAcc^{n}_{HT}$ violated the 10% constraint limit on the HT; hence, causing the unavailability of the FC in periods requiring energy supply as shown in Figure 7.17. Nevertheless, the RLS+P (y=Ax+B) activated the PV 8582 times, which was the record high and also a 7.2% increase compared to the DA PoPA which activated the PV 8004 times as shown in Table 7.2b. However, Figure 7.18 which shows the progression of the probability of violating the S_{Lo} and S_{Up} insightfully reveals that the bulk of the S_{Lo} violation occurred after 5979 h as seen by the immediate steep

rise in the S_{Lo} probability of violation from 4% to 14% due to lack of H_2 carrier in the HT. Therefore, investigating further with HT capacity of $25m^3$ confirms this assertion as the S_{Lo} violation reduces to 197 times which is a 75.5% decrease as shown in Table 7.2b. Also, the S_{Up} violation and DSL activation were decreased by 42.2% and 67.7% as well. Typical of a robust approach; the RLS+P (A=Ax+B) algorithm requires more allocation of H_2 resources, which will consequently increase operational cost in contrast to the rest of the methods.

7.1.1.4 P+Adaptive PoPA

The probabilistic approach P+Adaptive PoPA which violated the S_{Lo} and S_{Up} 321 and 828 times, was only better in performance than the A2C+P and RLS+P (y=Ax+B) concerning the S_{Up} and DA-PoPA concerning the S_{Lo} indices. The DSL, FC and EL were activated by the P+Adaptive PoPA EMS 126, 1935, and 926 times respectively, as shown in Table 7.2b. Therefore, the consequence of the P+Adaptive PoPA using the FC robustly to maintain the PGCC bound led to premature exhaustion of the H_2 in the HT as the $SOAcc^n_{HT}$ dipped below 10% at 7500 h, as seen in Figure 7.11. Consequently, the FC to become unavailable for dispatch at 7500h. Nevertheless, as shown in Figure 7.10, the P+Adaptive PoPA showed sensitivity in curtailing the excessive overcharging of the BAT. Furthermore, the probability of violating the S_{Up} had a steep rise even in the months of poor sunshine and even so steeper in the periods of peak sunshine, as shown in Figure 7.12. Therefore, an adaptive mechanism to correct the prior distribution should suffice as this would adjust the prior distribution or the estimated PGCC bound based on the residual error to match the reality.

7.1.1.5 Adaptive PoPA

The adaptive PoPA violated the S_{Up} 271 times and as well violated the S_{Lo} 303 times. However, the DSL was activated only once in 8760h, as shown in Table 7.2a. Nevertheless the performance of the Adaptive PoPA with regards to S_{Lo} violation was only better than

that of the P+Adaptive and the DA PoPA which translated to a 66% decrease in the violation against the DA PoPA. Furthermore, a 66% decrease in the violation of the S_{Up} and 6% increase in PV penetration were achieved with the Adaptive PoPA. However, the FC and EL were activated 95% and 150% more than that of the DA PoPA due to the closed-loop feedback mechanism, which aimed at negating the uncertainty. Figures 7.4, 7.5 and 7.6 shows the $SOAcc_{BAT}$, $SOAcc_{HT}$ and the probability of violating the pinch limits respectively.

7.1.1.6 RLS+P PoPA (y=Ax)

In Table 7.2b, the RLS+P is shown to have had an enhanced performance compared to the P+RLS as the S_{Lo} which was violated 198 times and S_{Up} 666 times amounted to a 15% and 20% reduction respectively. Consequently, despite a 75% reduction in the S_{Lo} violation, the S_{Up} violation only improved by 12% against the performance of the DA-PoPA. Nevertheless, the improvement is as a result of the residual error correction factor, which was based on the simplest linear model y=Ax. Again, with the RLS+P (y=Ax) PoPA, the effect of the robust bound led to the accelerated exhaustion of the H_2 as shown in Figure 7.14 only after which the violation of the S_Lo had a steep rise from 2.2% to 7% as shown in 7.15. The response of the BAT over 8760 h is shown in Figure 7.13.

7.1.1.7 Kalman+Adaptive PoPA

The Kalman+Adaptive PoPA had 64 S_{Lo} and 265 S_{Up} violations, which constituted 92% and 65% reduction respectively in comparison to the performance of the DA PoPA. Furthermore, the DSL was never activated, as shown in Table 7.2a. Although the DRL+Adaptive and A2C+adaptive PoPA had fewer violations of 11 and 55 times compared to the Kalman +Adaptive PoPA, only the RL+Adaptive had superior performance concerning both pinch limits. The activation of the FC, EL and PV were 521%, 255% and 6% respectively compared

to the DA PoPA. Figure 7.7, 7.8 and 7.9, shows the $SOAcc_{HT}$, $SOAcc_{HT}$ and the probability of violating the pinch limits respectively.

7.1.1.8 RL +Adaptive PoPA

The RL+Adaptive had the best performance with regards to clipping the $SOAcc_{BAT}$ from violating the S_{Lo} which was a 70% decrease compared to the performance of the DA PoPA. Consequently, the DSL was never activated; hence, a 100% reduction in fossil fuel emission was achieved. Also, concerning the S_{Lo} violation, the performance of the RL+Adaptive, which attained a 94% reduction was only second to the 99% reduction achieved by the DRL+Adaptive PoPA when compared to the DA PoPA. However, the remarkable performance of the RL+Adaptive PoPA was accompanied by 1184% and 1237% increase in FC and EL activation frequency in contrast to that of the DA PoPA. Nevertheless, this increased frequency is justified. Figure 7.19, 7.20 and 7.21, shows the $SOAcc_{HT}$, $SOAcc_{HT}$ and the probability of violating the pinch limits respectively. Furthermore, the cumulative reward plot is shown in Figure 7.22 and the the red line represents the smoothed average of the cumulative reward. Also, Figure 7.23 depicts the corresponding 3D surface plot of the Q-Table derived from the 8760 h operation of the HESS with a maximum reward of 25.5 units.

7.1.1.9 DRL+Adaptive PoPA

The DRL +Adaptive PoPA had the best performance concerning the violation of the S_{Lo}. The probability of violating the S_{Up} has an impulse rise from 0 to 0.01 between 300 h to 400 h. Thereafter, the S_{Lo} is maintained at 0.01% until 6000h, and concurrently, probability of the S_{Up} violation gradually increased and became steeper between 2000h: 6500h, as shown in Figure 7.26. Nevertheless, in counteracting the effects of uncertainty, the DRL+Adaptive PoPA activated the FC the most by 5038 times as against 296 and 577 times with DA and Adaptive PoPA respectively, as shown in Table 7.2c. Similarly, the EL was activated 3503

times, which was only fewer than the RL+Adaptive PoPA's 3802 times and a 1208% increase concerning the performance of the DA PoPA. Nevertheless, the DSL was never activated; hence, a 100% decrease in fossil fuel emission impact. The BAT and HT response are shown in Figure 7.24 and Figure 7.26, respectively.

7.1.1.10 Summary

The deterministic PoPA methods; Adaptive, Kalman+Adaptive, the probabilistic PoPA methods; P+Adaptive RLS-P PoPA (y=Ax), RLS-P PoPA (y=Ax+B) and the machine learning-based PoPA methods; RL+Adaptive, DRL+Adaptive, A2C+P, have all been compared under non-Gaussian stochastic load and Gaussian stochastic PV scenario. Therefore, benchmarking these methods against the performance of the DA PoPA, the most performing methods on all front; Adaptive, Kalman+Adaptive, RL+Adaptive, DRL+Adaptive, RLS-P PoPA (y=Ax) PoPA led to a reduction in S_{Lo} violation by 66%, 92%, 94%, 99% and 75% as well as a decrease in the upper limit violation by 60%, 65%, 70%, 38% and 12% respectively. The reduction in S_{Up} violation by the Adaptive, Kalman+Adaptive, RL+Adaptive, DRL+Adaptive, RLS-P PoPA (y=Ax) methods led to an increase in PV penetration by $6\%, 6\%$ and $7\%, 4\%$ and 1% respectively, primarily due to the decreased violation of the PV (ON/OFF) protection constraint. These safety constraints can be found in the APPENDIX. Additionally, the DSL was activated only once with the Adaptive PoPA and was never activated with the Kalman, RL+Adaptive and DRL+Adaptive PoPA. Consequently, a reduction in fossil fuel emission by $99.59\%, 100\%$ and $100\%, 66\%$ and 100% was achieved with the Adaptive, Kalman+Adaptive, RL+Adaptive, DRL+Adaptive, RLS-P PoPA (y=Ax) EMS respectively.

Also, the activation of the FC and EL with the Adaptive PoPA was seen to have increased by 95% and 150% and similarly for the Kalman +Adaptive PoPA, it was 520% and 255% respectively, compared to the DA-PoPA.

The RL+Adaptive which had the highest PV penetration of 7% consequently also had the highest increase in EL activation, which was 1273%. Similarly, the DRL+Adaptive PoPA had the highest FC activation frequency which was at 1602% as well as the least S_{Lo} violation of 99% compared to the performance of the DA PoPA as summarised in Figure 7.30.

The A2C+P PoPA which had a decent third-best performance concerning the S_{Lo} violation of 55 times and accompanied by the DSL being activated 19 times, had the worst performance concerning violating the S_{Up} 908 times which is a 20% increase in contrast to the DA PoPA. Similarly, the probabilistic method RLS-P PoPA which utilised a simple linear model (y=Ax+B), had the worst performance concerning the S_{Lo} only because of excessive usage of the H_2 carrier which was revealed when the HT was increased from $15m^3$ to $25m^3$. Therefore, increasing the complexity of the simple residual error correction based on the error correction can introduce over-fitting on past information which may not match the reality and conversely result in overly tracking of the error due to energy uncertainty. Thus, the RLS-P PoPA (y=Ax), which used the simplest linear model, had a more decent performance. Although the probabilistic approach requires accurate information on the distributions of the uncertainty.Nevertheless, the recursive error correction mechanism, which is based on the ordinary least squares approach, provides an unbiased estimate on the forecast error caused by uncertainty.

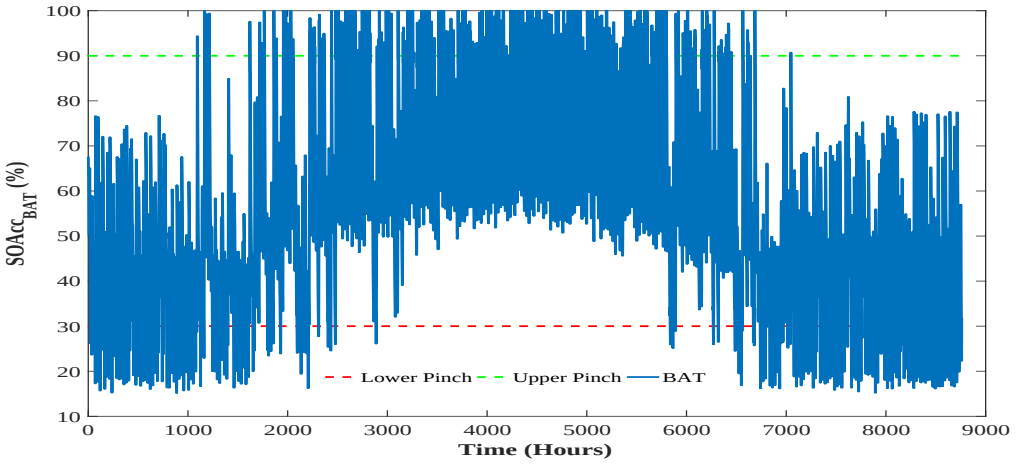

Fig. 7.1 8760h BAT response with DA PoPA

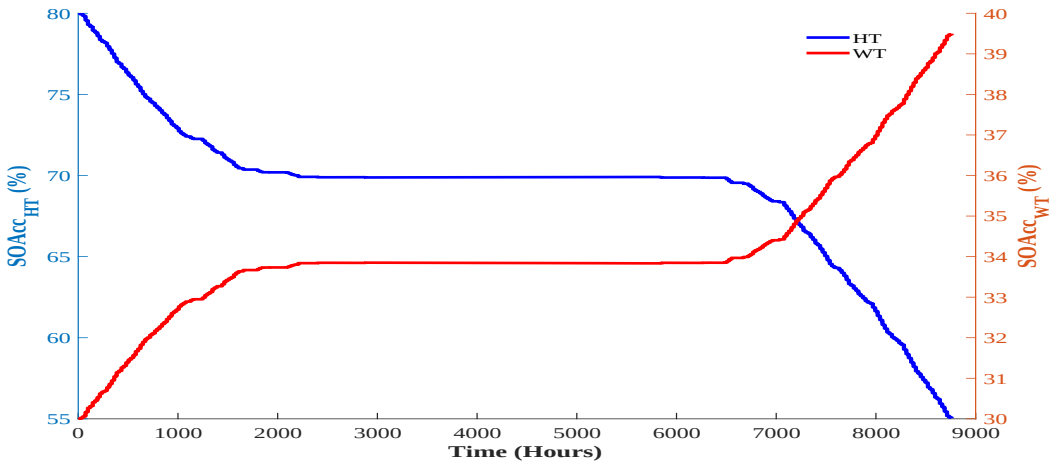

Fig. 7.2 HT and WT response for 8760h with DA PoPA

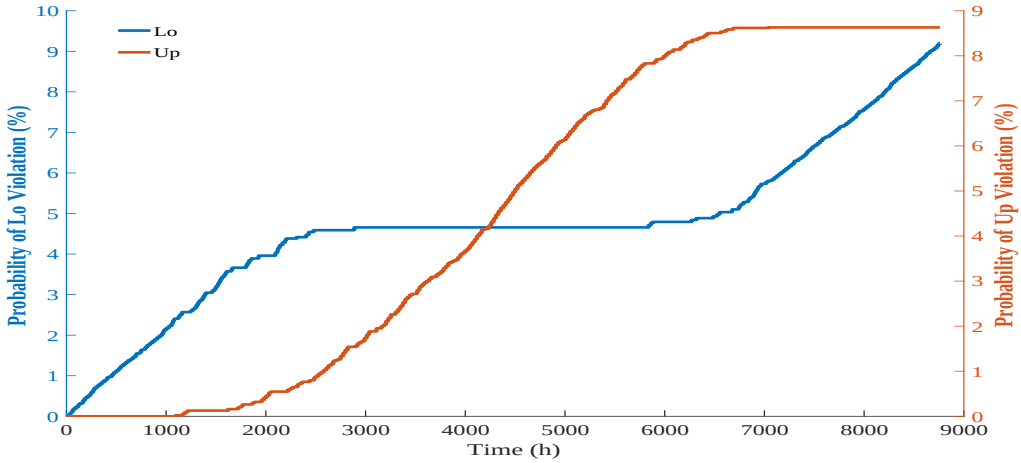

Fig. 7.3 Probability of Lo and Up violation in 8760h with DA PoPA

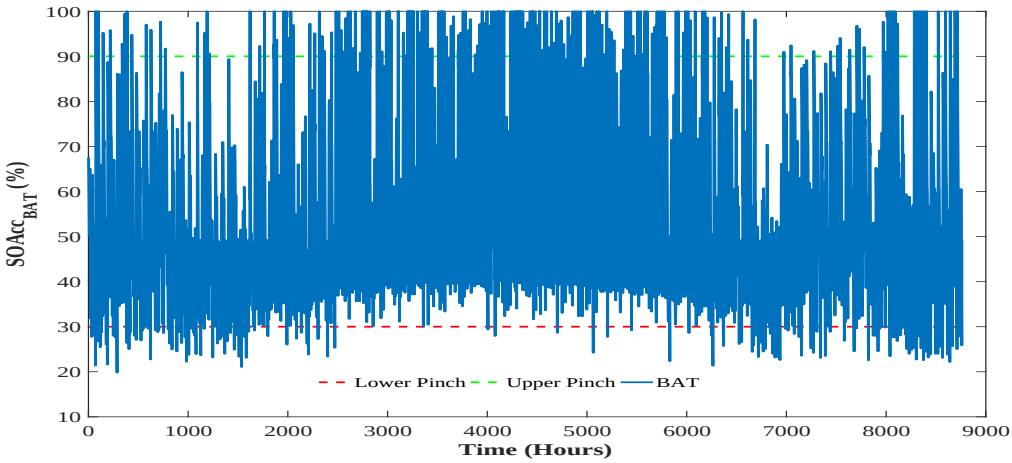

Fig. 7.4 8760h BAT response with Adaptive PoPA

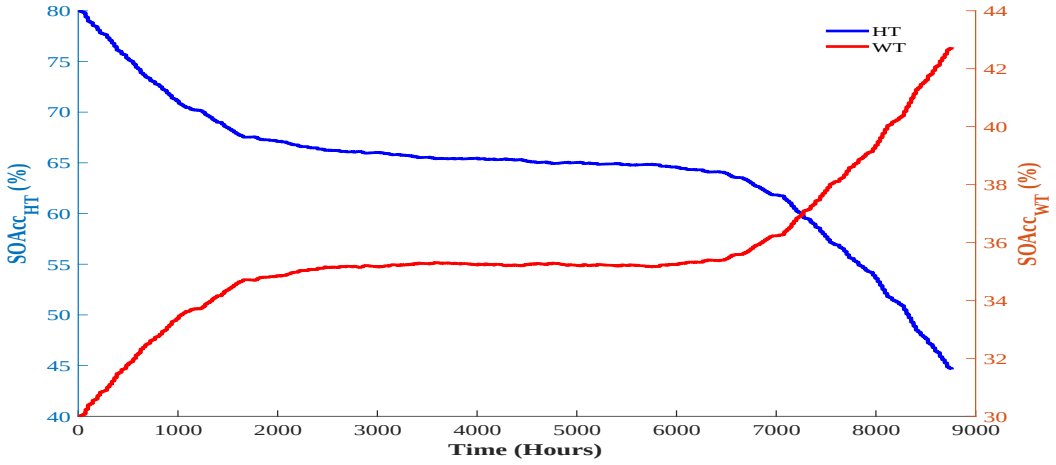

Fig. 7.5 HT and WT response for 8760h with Adaptive PoPA

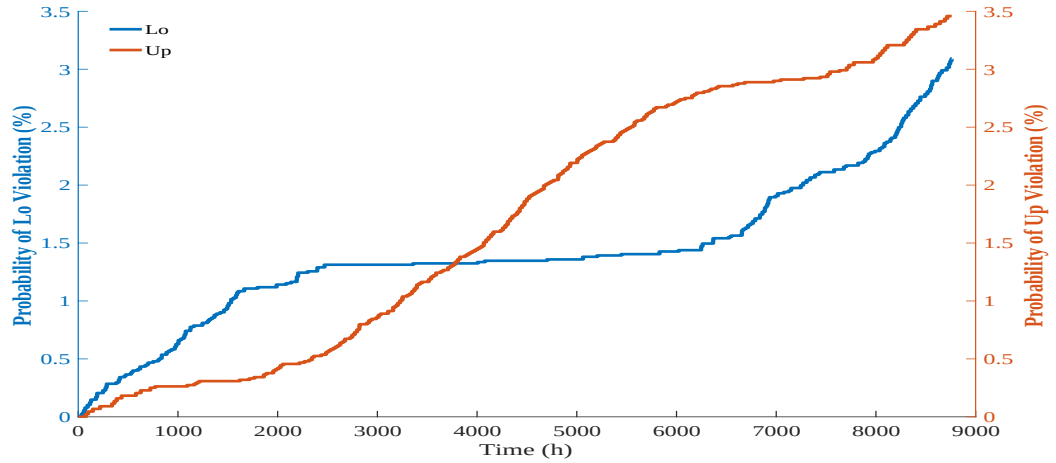

Fig. 7.6 Probability of Lo and Up violation in 8760h with Adaptive PoPA

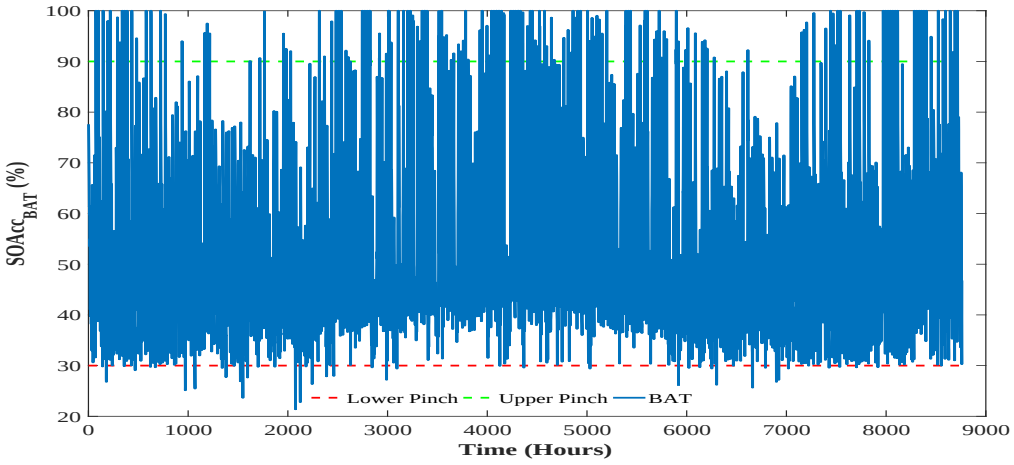

Fig. 7.7 8760h BAT response with Kalman+Adaptive PoPA

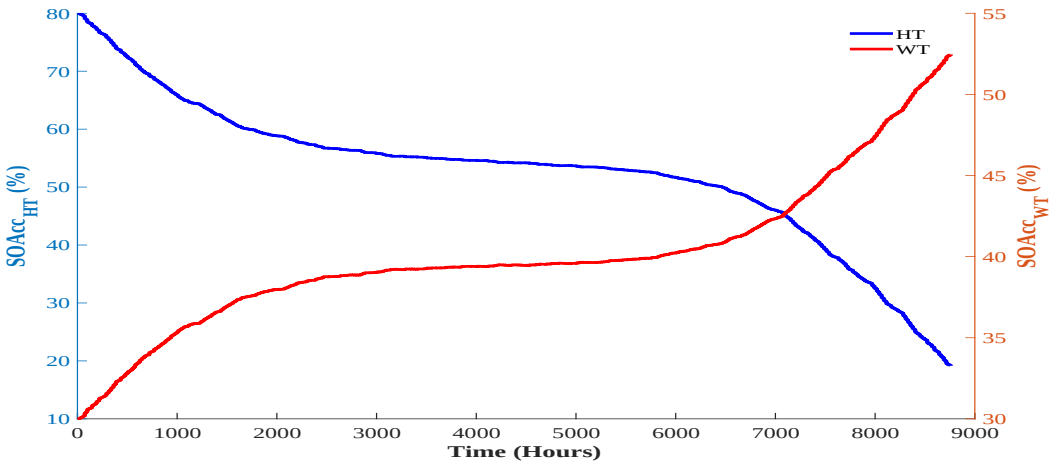

Fig. 7.8 HT and WT response for 8760h with Kalman+Adaptive PoPA

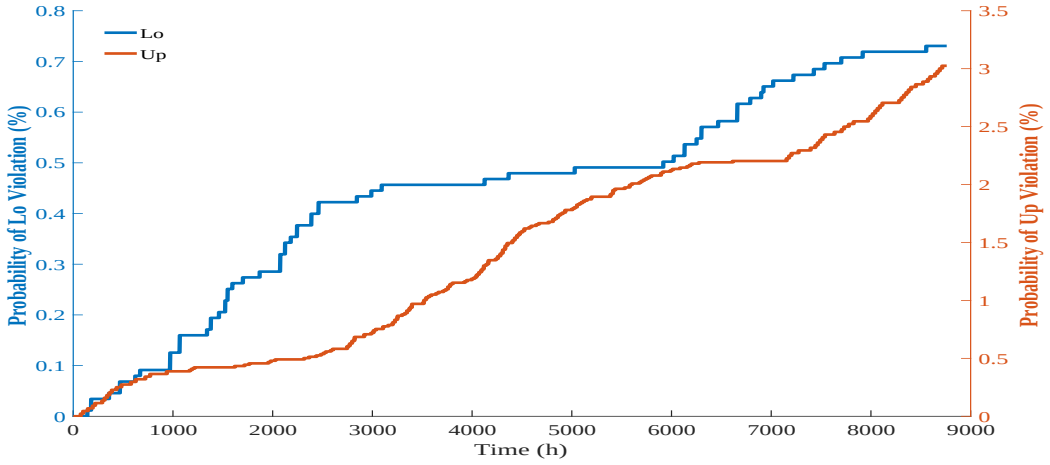

Fig. 7.9 Probability of Lo and Up violation in 8760h with Kalman+Adaptive PoPA

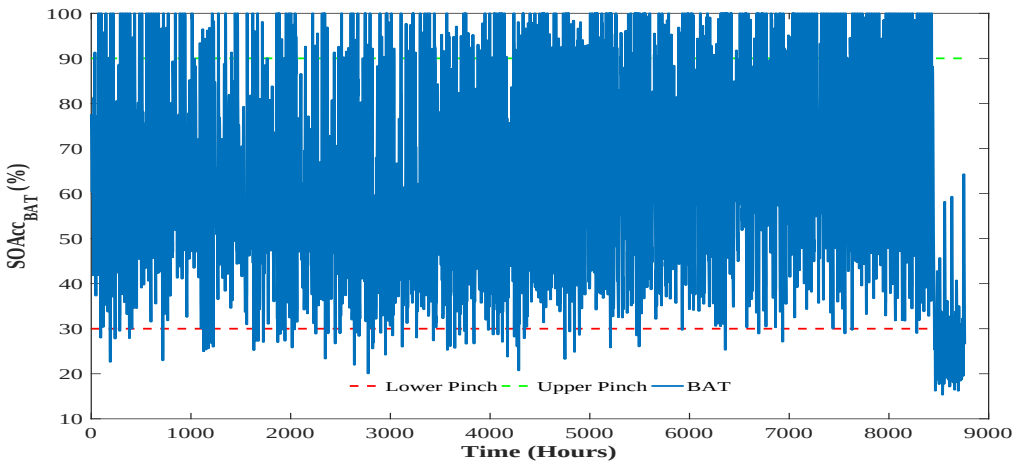

Fig. 7.10 8760h BAT response with P-PoPA

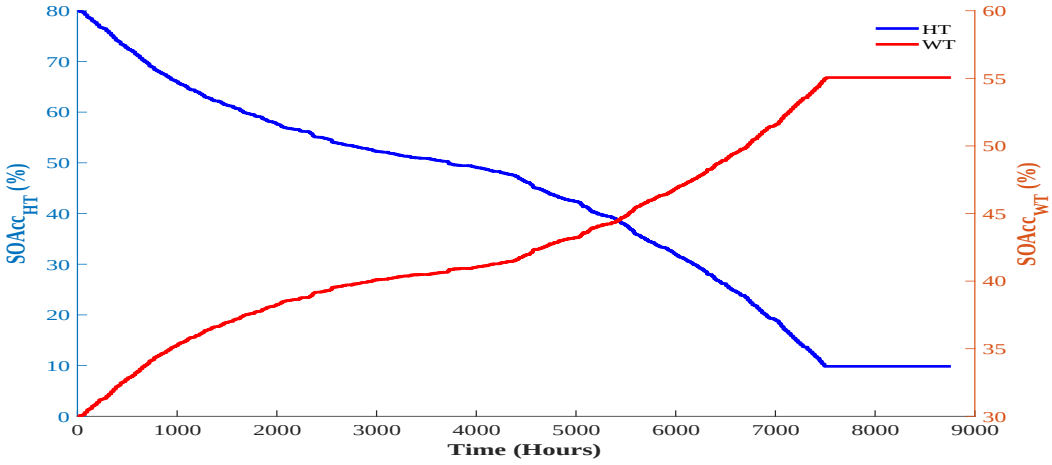

Fig. 7.11 HT and WT response for 8760h with P-PoPA

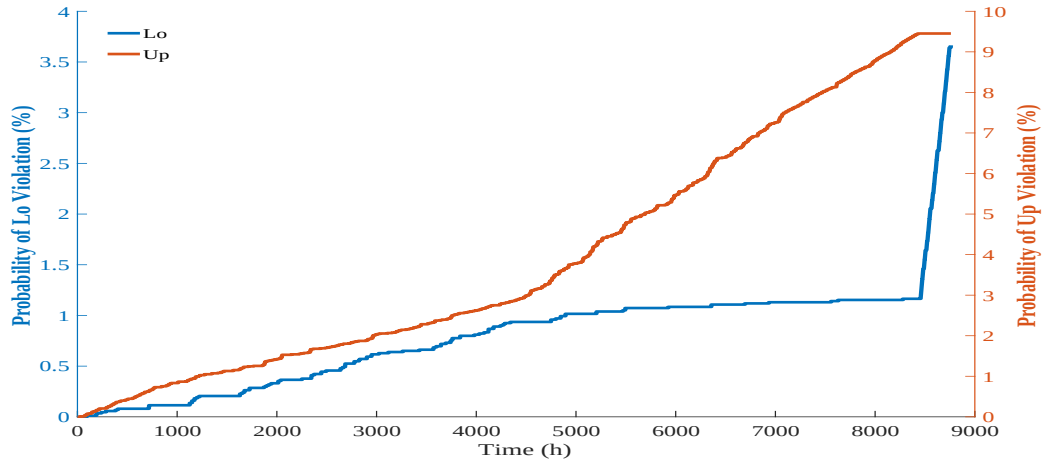

Fig. 7.12 Probability of Lo and Up violation in 8760h with P-PoPA

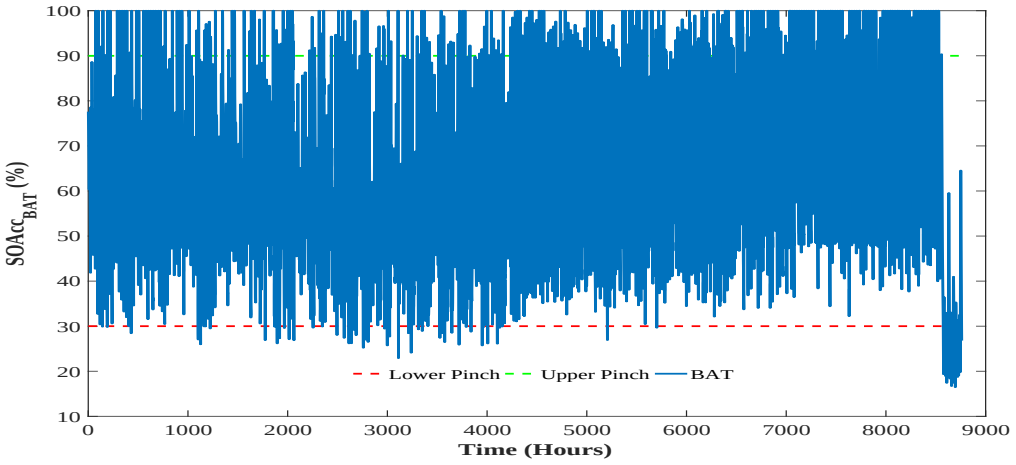

Fig. 7.13 8760h BAT response with RLS+P PoPA

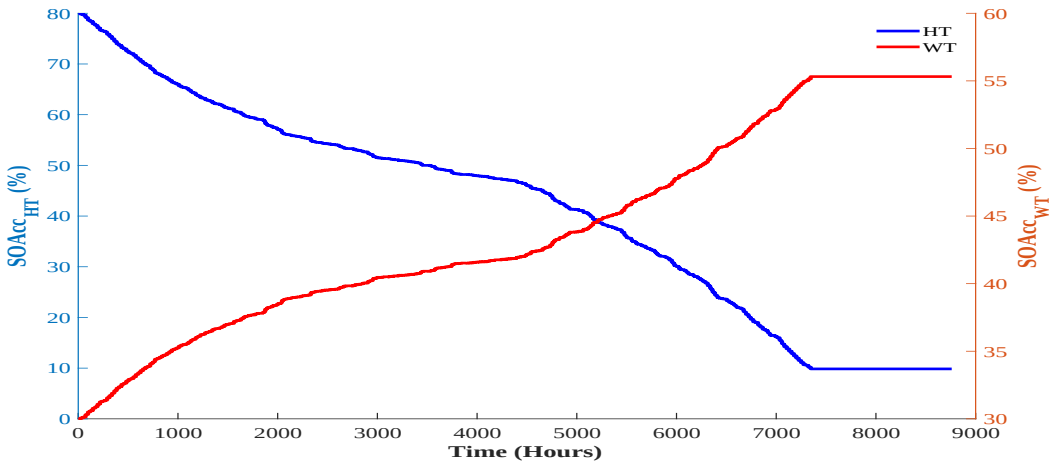

Fig. 7.14 HT and WT response for 8760h with RLS+P PoPA

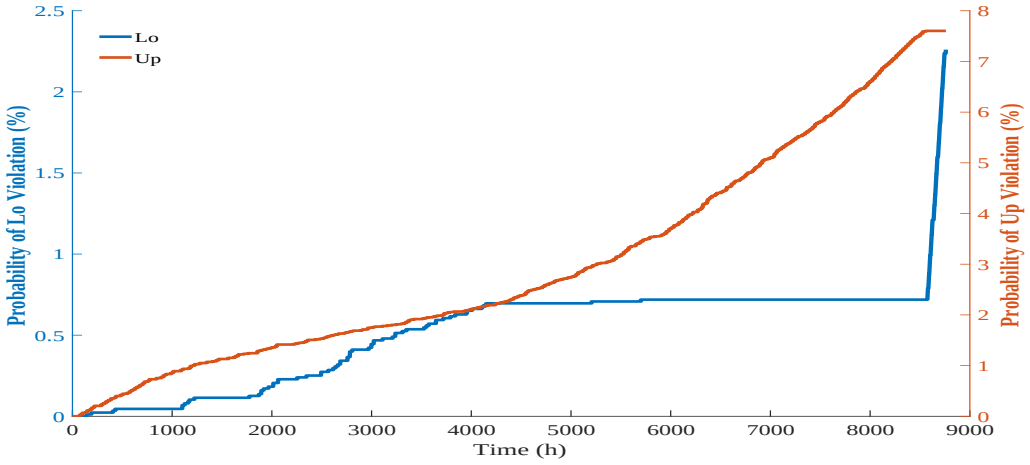

Fig. 7.15 Probability of Lo and Up violation in 8760h with RLS+P PoPA

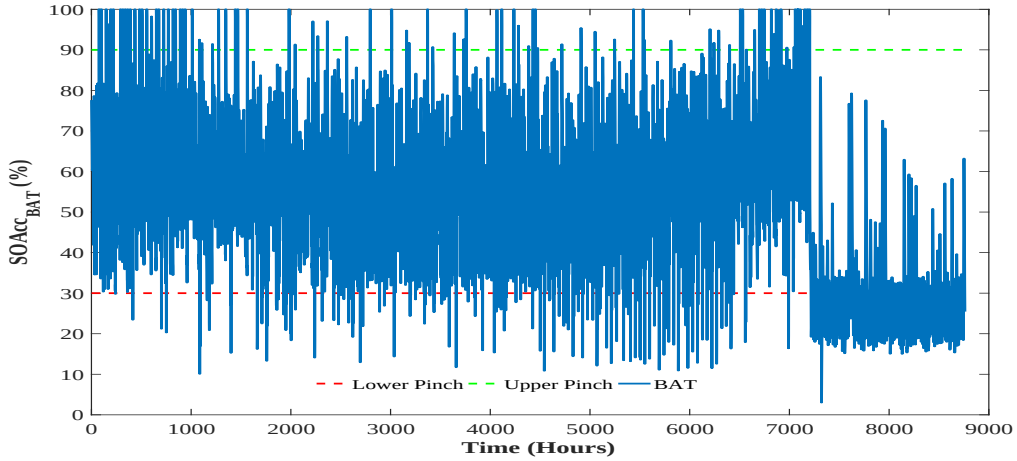

Fig. 7.16 8760h BAT response with RLS+P PoPA with bias

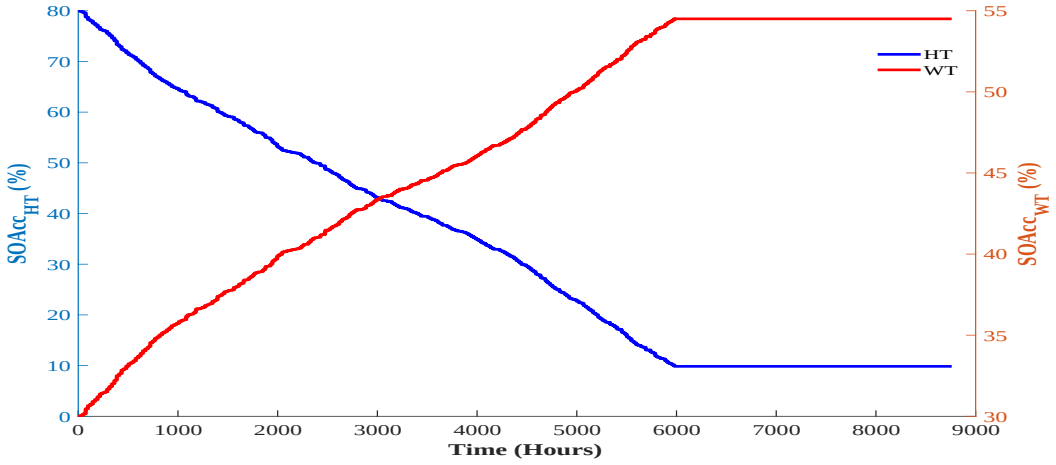

Fig. 7.17 HT and WT response for 8760h with RLS+P PoPA with bias

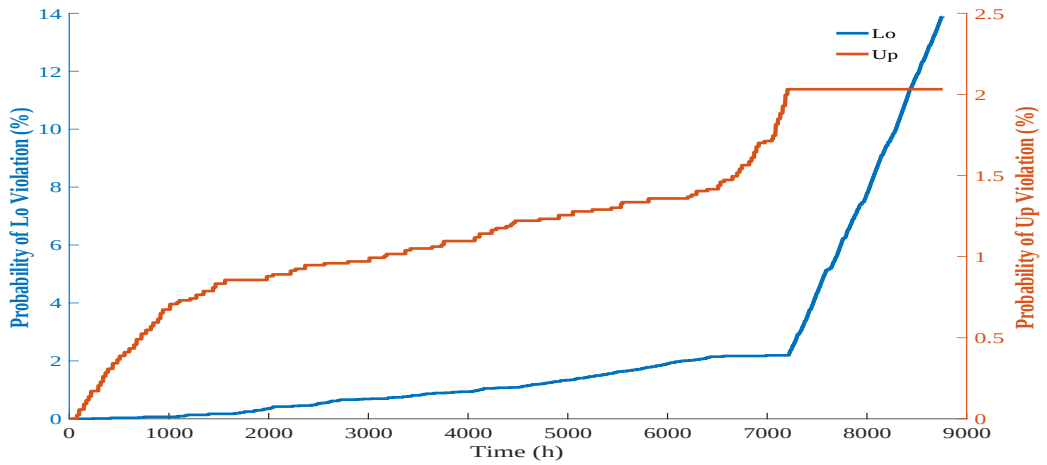

Fig. 7.18 Probability of Lo and Up violation in 8760h with RLS+P PoPA with bias

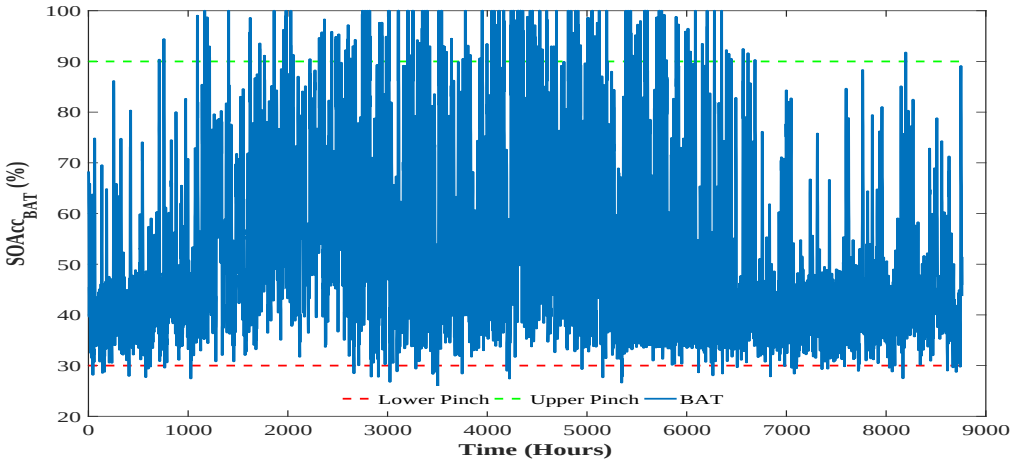

Fig. 7.19 8760h BAT response with RL+Adaptive PoPA

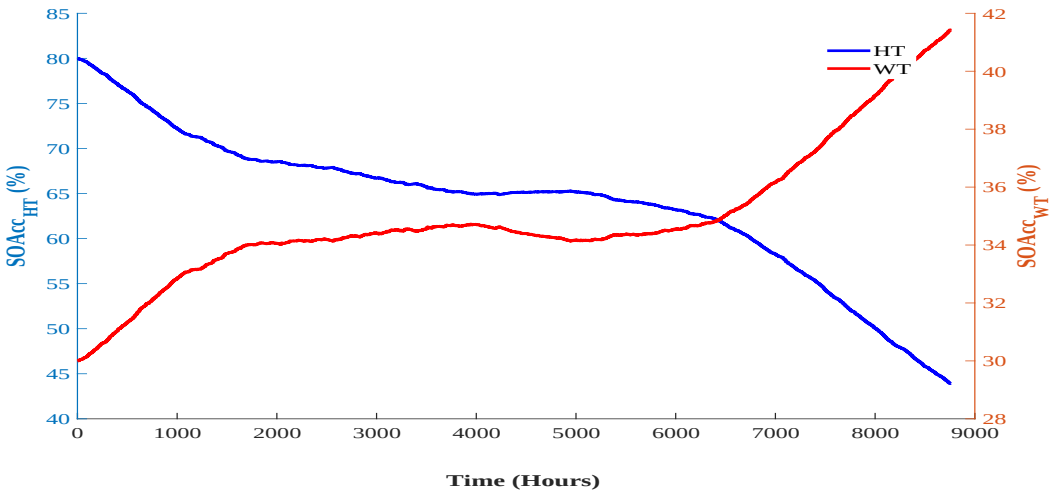

Fig. 7.20 HT and WT response for 8760h with RL+Adaptive PoPA

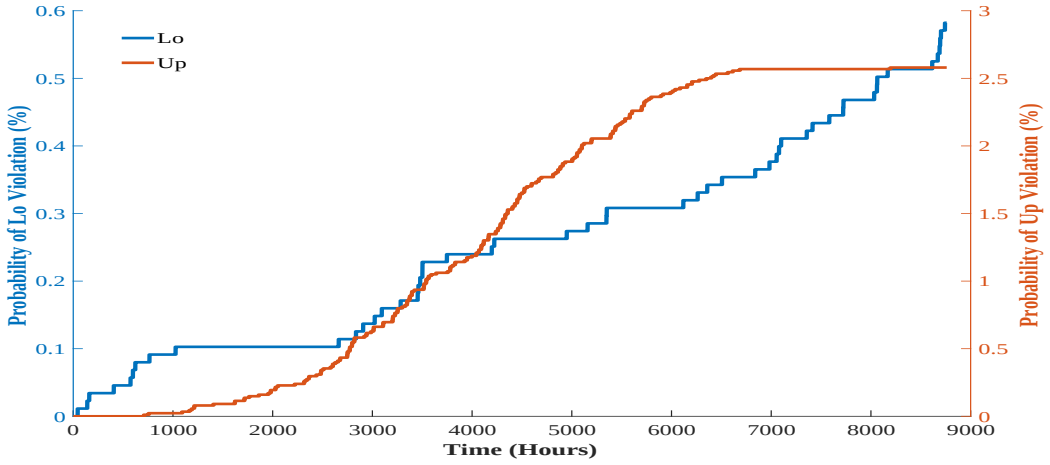

Fig. 7.21 Probability of Lo and Up violation in 8760h with RL+Adaptive PoPA

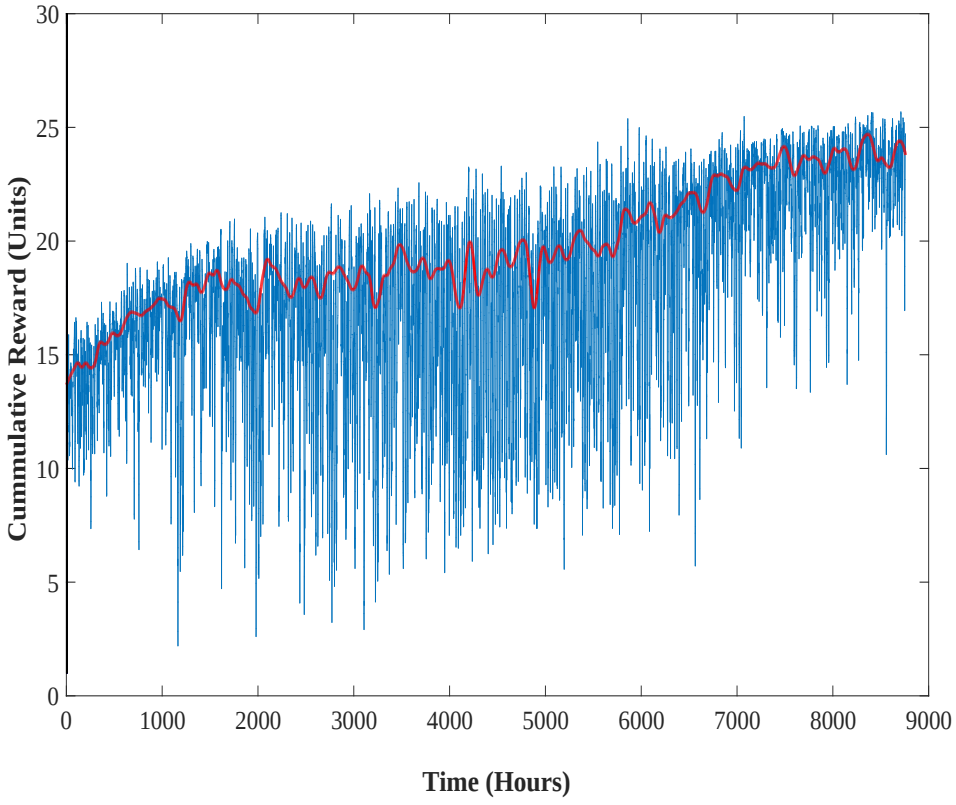

Fig. 7.22 Cumulative Reward during the operation of the HESS

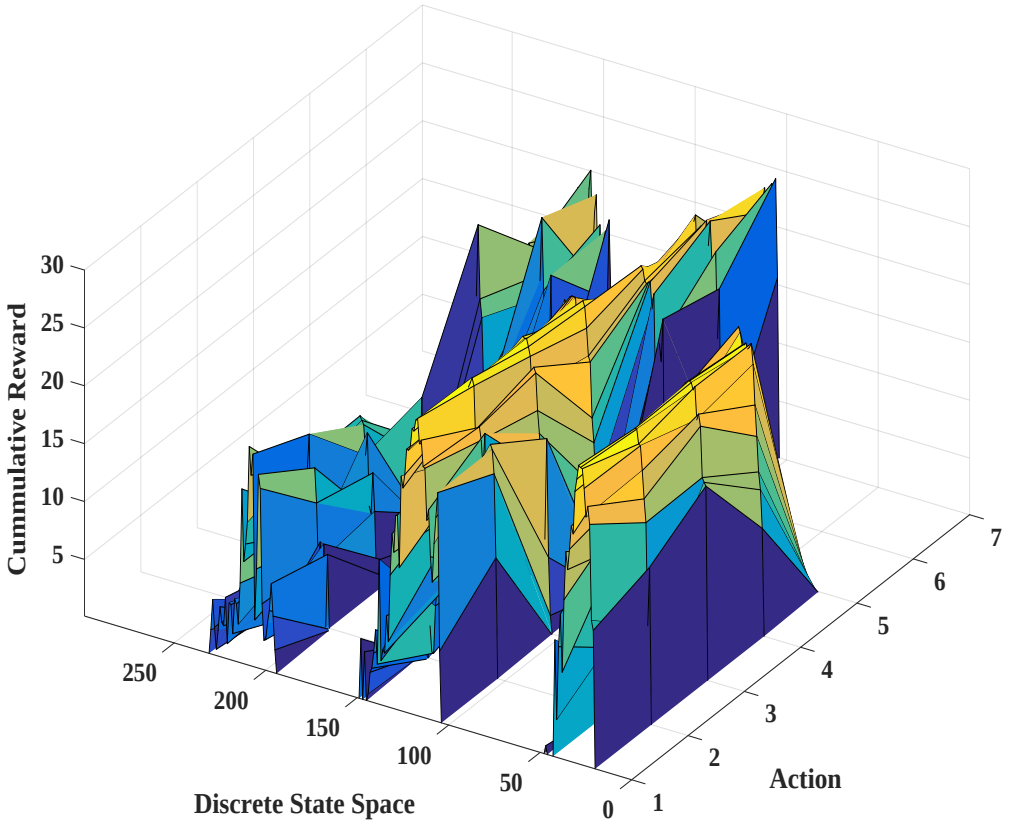

Fig. 7.23 3D Surface Plot of the RL Cumulative Reward after 8760 h operation of the HESS

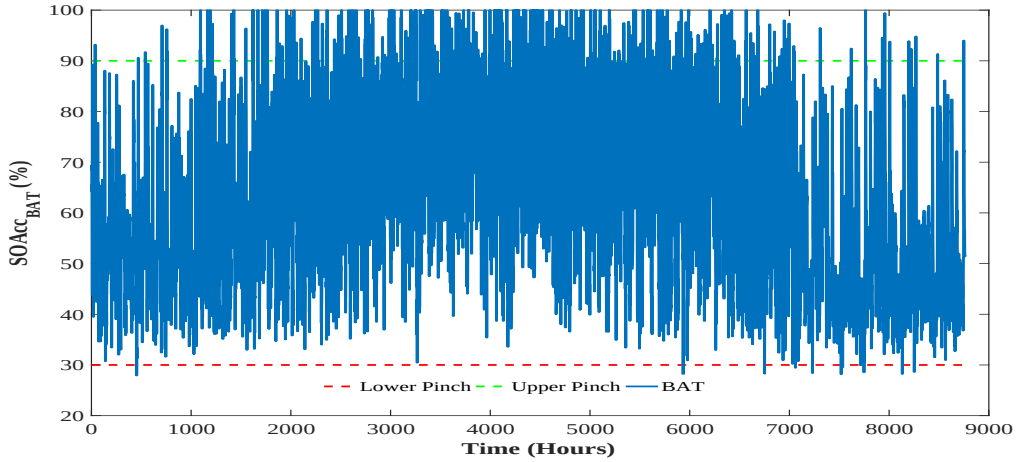

Fig. 7.24 8760h BAT response with DRL+Adaptive PoPA

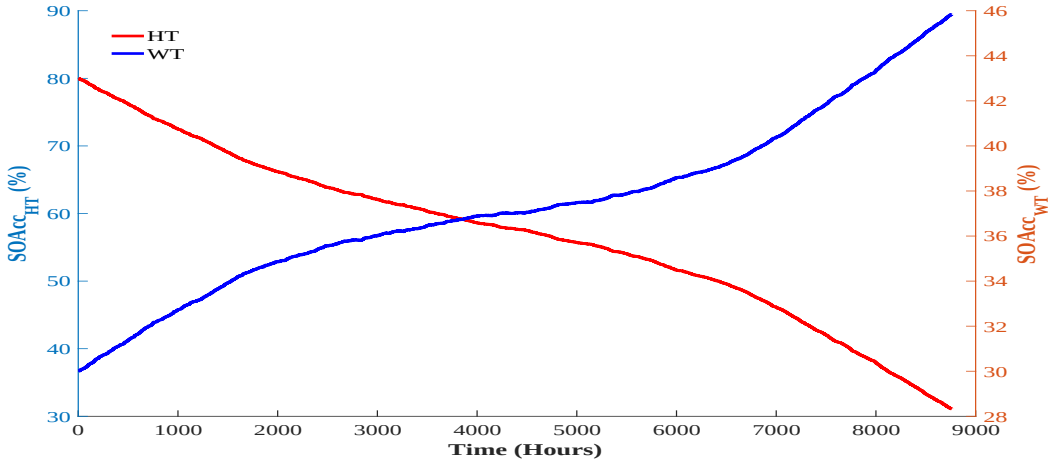

Fig. 7.25 HT and WT response for 8760h with DRL+Adaptive PoPA

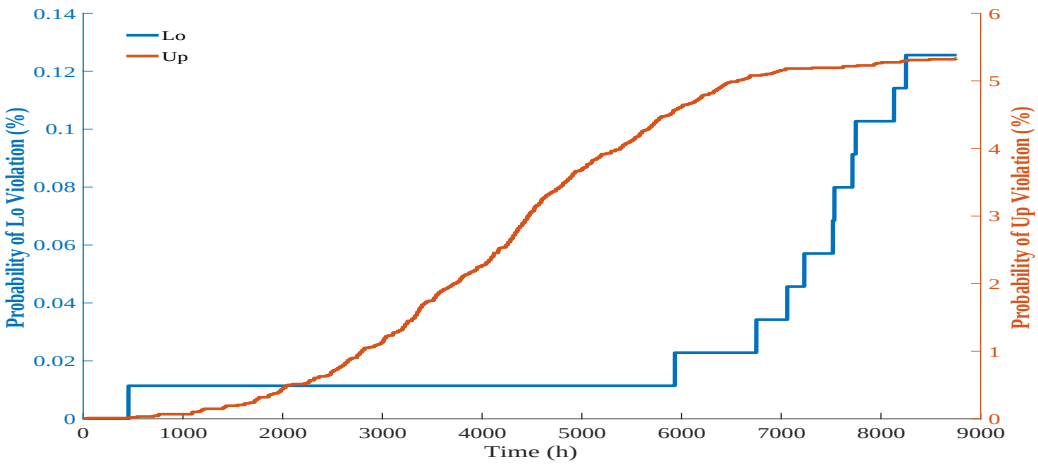

Fig. 7.26 Probability of Lo and Up violation in 8760h with DRL+Adaptive PoPA

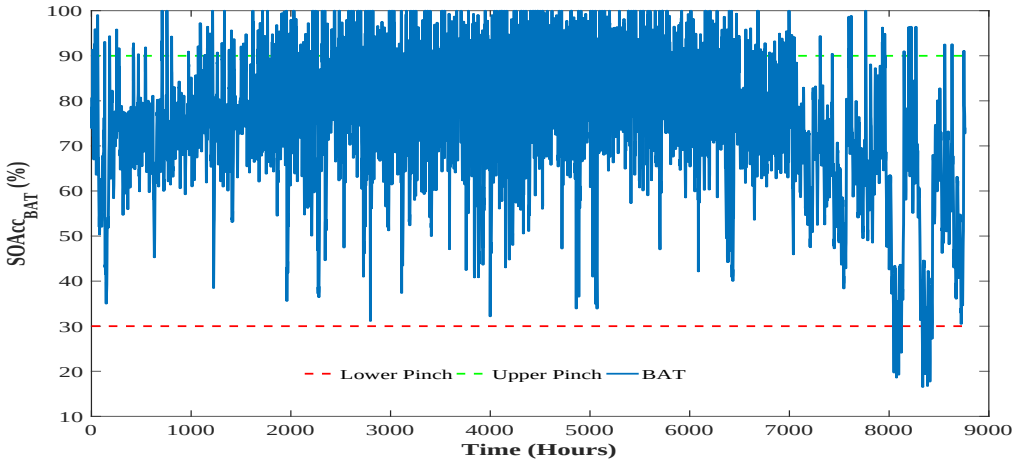

Fig. 7.27 8760h BAT response with A2C+P PoPA

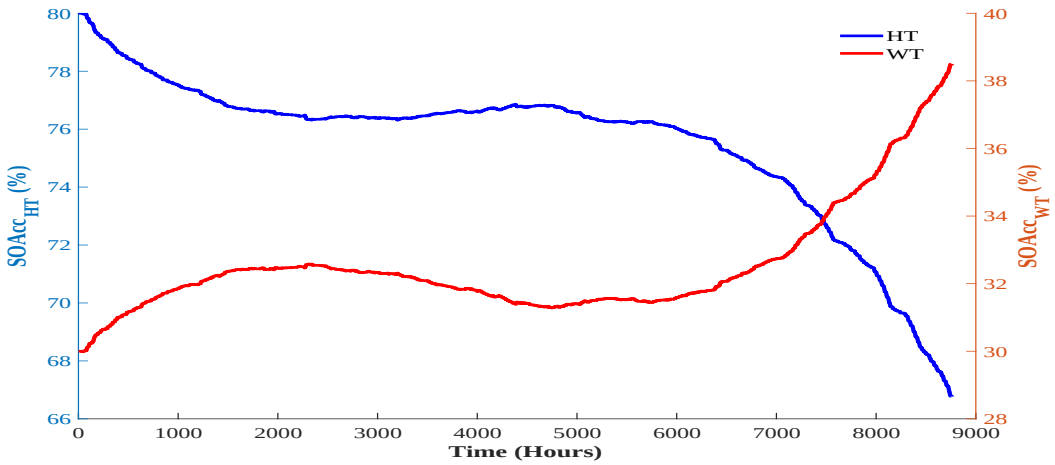

Fig. 7.28 HT and WT response for 8760h with A2C+P PoPA

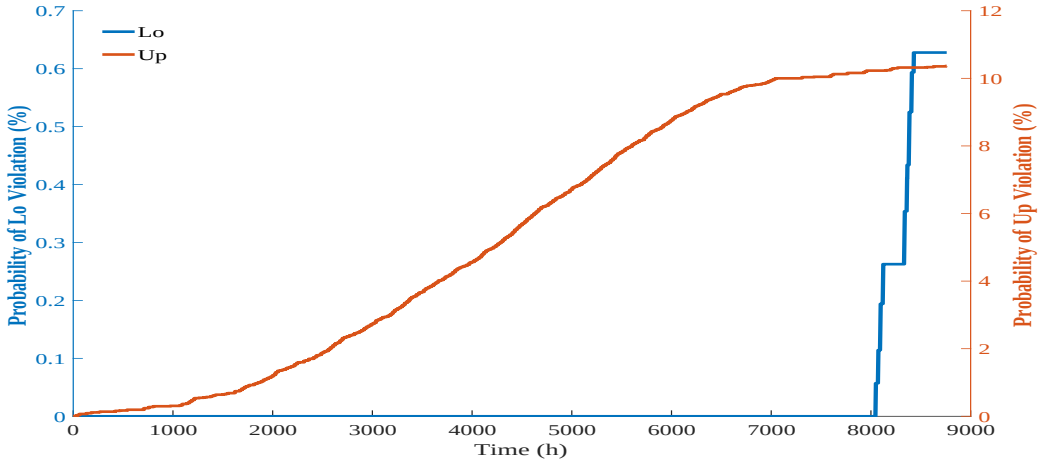

Fig. 7.29 Probability of Lo and Up violation in 8760h with A2C+P PoPA

7.1.2 Gaussian Uncertainty with HT Capacity of $15m^3$

7.1.2.1 A2C+P PoPA

The A2C+P despite being the most computationally intensive and supposedly the most robust algorithm which has been proposed, had the worst S_{Lo} and DSL performance which resulted in 2200 S_{Lo} violations and the DSL being activated 1073 times as shown in Figure 7.36. The stochastic effect of the uncertainty, continuous hyper-dimensional input state and continuous action, coupled with a mismatch between the actual probability density of the uncertainty and the probabilistic model used to train the A2C+P, can result in such suboptimal performance. Nevertheless, the A2C+P had a better S_{Up} violation performance than the DA and the P+Adaptive which had the second and worst performance respectively.

7.1.2.2 DA-PoPA

The DA PoPA which had 867 S_{Lo} violations, 777 S_{Up} violations and activated the DSL 108 times recorded the worst S_{Lo} performance which was only second to the A2C+P PoPA as shown in Figure 7.36. However, the S_{Up} violation performance was only better than that of

the P+Adaptive, which was the worst. Nevertheless, the DA-PoPA had the least FC and EL activation of 264 times and 265 times, respectively, as shown in Figure 7.36.

7.1.2.3 RLS-P PoPA (y=Ax+B)

The RLS-P PoPA with biased had the second worse S_{Lo} performance, which was only better than the A2C+P PoPA, as shown in Figure 7.36. Nonetheless, a further investigation which was carried out by increasing the HT capacity from $15m^3$ to 25^m3 revealed the main reason for the suboptimal performance of the RLS-P with a biased linear model was as a result of limited H_2 resources. Therefore, with the HT at $25m^3$, the RLS-P PoPA with a first-order residual linear model, had an improved performance as the S_{Lo} violation and DSL activation 1023 reduced from1023 to 235 times and from 510 to 86 times respectively. However, the S_{Up} violation increased from 217 to 448 times. Nevertheless, the RLS-P PoPA with a first-order linear residual model as with a typical probabilistic approach introduces robustness which is only achieved at the cost of increased usage of H_2 resources, hence, with the approach is omitted from further investigation.

7.1.2.4 P+Adaptive PoPA

The P+Adaptive PoPA had a better performance index of 202 times concerning the S_{Lo} compared to the DA and adaptive PoPA, which both had 876 and 209 violations. However, the P+Adaptive had the worst S_{Up} violation of 813 times, which was a 5% increase compared to the DA PoPA's performance. Also, the DSL was activated 104 times, which was only marginally better than the DA PoPA's performance of 108 times, as shown in Figure 7.36.

7.1.2.5 Adaptive PoPA

Though the Adaptive PoPA had 209 S_{Lo} violations, which was a 76% decrease in contrast to the DA PoPA's performance, and the DSL was never activated. Furthermore, the Adaptive

PoPA had a better S_{Lo} and S_{Up} violation performance of 209 and 287 times respectively compared to the DA which had 867 and 777 and the A2C+P PoPA which had 2200 and 746 times respectively as shown in Figure 7.36. Nevertheless, the Adaptive which had a better $S_{U}p$ violation performance than the DA, also performed better than the RLS-P PoPA with linear bias model concerning the $S_{U}p$ violation as shown in Figure 7.36.

7.1.2.6 RLS-P PoPA (y=Ax)

The RLS-P PoPA with the simplest residual error linear model (y=Ax), had the second-best S_{Lo} performance of 15 times which was a tremendous improvement to the P+Adaptive PoPA which had 202 S_{Lo} violations as shown in Figure 7.36. Also, comparing the with the performance of the DA to the RLS-P PoPA (y=Ax), the S_{Lo} violation was reduced by 98%, and the S_{Up} violation was also decreased by 22%. Furthermore, DSL was never activated; hence, a 100% reduction in fossil fuel emission was achieved with the RLS-PoPA. The FC and EL which were activated 1480 and 900 times was only utilised more compared to the DA and Adaptive PoPA EMS as shown in Figure 7.36.

7.1.2.7 Kalman+Adaptive PoPA

The Kalman+Adaptive PoPA violated the S_{Lo} 94 times, amounted to 89% decrease in contrast to the DA PoPA. The S_{Up} and S_{Lo} violations of the Kalman+Adaptive PoPA was only better than the DA, Adaptive, P+Adaptive and A2C+P PoPA. The FC and EL activations were 1607 and 1113 times, respectively, without the DSL being activated, as shown in Figure 7.36. The increased frequency of FC and EL activation, which were 509% and 320% respectively in contrast to the DA PoPA's, is obviously as a result of counteracting the projected uncertainty.

7.1.2.8 RL+Adaptive PoPA

The RL +Adaptive PoPA despite having the highest PV penetration of 7% increase consequently had the best S_{Up} violation performance, which was a 72% decrease in contrast to the DA-PoPA. Furthermore, the DSL was never activated, and therefore, fossil fuel usage and emission were reduced by 100%. However, the enhanced performance comes at a trade-off with a higher frequency of FC and EL activation, which was only less than the DRL+Adaptive PoPA.

7.1.2.9 DRL+Adaptive PoPA

The DRL+Adaptive PoPA had the best S_{Lo} violation of 12 times, which was a 99% decrease compared to the DA PoPA's performance and consequently, the DSL was never activated. Nevertheless, the DRL had a S_{Up} performance indices, which was only better than the DA, P+Adaptive and the RLS-P PoPA as shown in Figure 7.36. Furthermore, in counteracting the effects of uncertainty, the FC and EL had the most activation of 1810% and 1195% increase shown in Figure 7.30 with the DRL +Adaptive PoPA EMS.

7.1.2.10 Summary

The proposed methods were compared with the HT sized to $15m^3$ under Gaussian uncertainty. The Adaptive PoPA which utilised closed-loop feedback to counteract the effects of uncertainty had a better performance than the DA PoPA and the A2C+P PoPA. The Kalman+Adaptive PoPA had a marginally better performance overall than the Adaptive PoPA. The A2C+P PoPA algorithm, which is the most computationally intensive and utilises two DNN (Actor-Critic) within the RL based probabilistic PoPA framework, had the worst performance overall. The suboptimal performance of the A2C+P PoPA could be many of several technical reasons which range from the hyper-parameters tuning of the NN, limited training of the NN with a vast amount of data for proper generalisation and the presence of

stochasticity in the continuous state input. Since the A2C+P PoPA necessitates a substantial computational burden, the A2C+P PoPA has been omitted from further investigation. Therefore, the suboptimal performance of the A2C+P PoPA will be investigated in the future. The machine learning approaches which utilised the deterministic Adaptive PoPA; RL+Adaptive and DRL+Adaptive had the best S_{Up} and S_{Lo} performances respectively. In conclusion, the Probabilistic based Adaptive PoPA EMSs; P+Adaptive, RLS-P (y=Ax) particularly the RLS-P PoPA (y=Ax+B) was shown to have robust performance only if the HT is sized greater than $25m^3$ as the probabilistic bounds necessitate a trade-off in resources for robustness to uncertainty. Nevertheless, the RLS-P PoPA with a biased linear model will be omitted from further investigation since its performance is impacted the most by the unavailability of H_2 carrier.

Table 7.2 Performance metrics of the PoPA methods for one year (8760 Hrs) under Non-Gaussian uncertainty with HT capacity of $15m^3$

(a) Investigation of DA, Adaptive and KL+Adaptive PoPA

Performance Indices	Day - Ahead PoPA	Adaptive PoPA	Kalman+Adaptive PoPA
Lower Pinch violation ($SOAcc^n_{BAT}$ < 30%)	804	271	64
Upper Pinch violation ($SOAcc^n_{BAT}$ >90%)	756	303	265
FC start-stop (cycles/year)	296	577	1837
EL start-stop (cycles/year)	262	654	931
DSL start-stop (cycles/year)	229	1	0
PV start-stop (cycles/year)	8004	8457	8495

(b) P+Adaptive PoPA, RLS-P PoPA, RLS-P PoPA with bias

Performance Indices	P+Adaptive PoPA	RLS-P PoPA (Y = Ax)	RLS-P PoPA (Y = Ax+B)
Lower Pinch violation ($SOAcc^n_{BAT}$ < 30%)	321	198	1217
Upper Pinch violation ($SOAcc^n_{BAT}$ >90%)	828	666	178
FC start-stop (cycles/year)	1935	2281	1574
EL start-stop (cycles/year)	926	1253	1356
DSL start-stop (cycles/year)	126	79	673
PV start-stop (cycles/year)	7932	8094	8582

(c) Investigation of RL+Adaptive PoPA, DRL+Adaptive PoPA and A2C+P PoPA

Perfomace Indices	RL+Adaptive PoPA	DRL+Adaptive PoPA	A2C+P PoPA
Lower Pinch violation ($SOAcc^n_{BAT}$ < 30%)	51	11	55
Upper Pinch violation ($SOAcc^n_{BAT}$ >90%)	226	467	908
FC start-stop (cycles/year)	3802	5038	4226
EL start-stop (cycles/year)	3503	3426	0
DSL start-stop (cycles/year)	0	0	19
PV start-stop (cycles/year)	8534	8293	7852

Table 7.3 Performance metrics of the PoPA methods for one year (8760 Hrs) under Gaussian uncertainty with HT capacity of $15m^3$

(a) Investigation of DA, Adaptive and KL+Adaptive PoPA

Perfomace Indices	**Day - Ahead PoPA**	**Adaptive PoPA**	**Kalman+Adaptive PoPA**
Lower Pinch violation ($SOAcc^n_{BAT}$ < 30%)	867	209	94
Upper Pinch violation ($SOAcc^n_{BAT}$ >90%)	777	287	229
FC start-stop (cycles/year)	264	550	1607
EL start-stop (cycles/year)	265	264	1113
DSL start-stop (cycles/year)	108	0	0
PV start-stop (cycles/year)	7983	8473	8544

(b) P+Adaptive PoPA, RLS-P PoPA, RLS-P PoPA with bias

Performance Indices	**P+PoPA**	**RLS-P+PoPA Y = Ax)**	**RLS-P+PoPA Y = Ax+B)**
Lower Pinch violation ($SOAcc^n_{BAT}$ < 30%)	202	15	1023
Upper Pinch violation ($SOAcc^n_{BAT}$ >90%)	813	609	217
FC start-stop (cycles/year)	2290	1480	2754
EL start-stop (cycles/year)	1149	900	1411
DSL start-stop (cycles/year)	104	0	510
PV start-stop (cycles/year)	7947	8151	8543

(c) Investigation of RL+Adaptive PoPA, DRL+Adaptive PoPA and A2C+P PoPA

Perfomace Indices	RL+Adaptive **PoPA**	DRL+Adaptive **PoPA**	A2C+P **- PoPA**
Lower Pinch violation ($SOAcc^n_{BAT}$ < 30%)	38	12	2200
Upper Pinch violation ($SOAcc^n_{BAT}$ >90%)	216	470	746
FC start-stop (cycles/year)	3087	5043	110
EL start-stop (cycles/year)	3111	3433	916
DSL start-stop (cycles/year)	0	0	1073
PV start-stop (cycles/year)	8490	8290	8014

7.2 Sensitivity Analysis of the PoPA Schemes to HT sizes

7.2.1 Non-Gaussian Case Study

A sensitivity analysis was carried out to investigate the impact of H_2 resources availability with the EMSs under non-Gaussian uncertainty by varying the HT capacity between 15, 10

and 7.5m^3 as shown in Figure 7.31 and between 5, 2.5 and 1m^3 as shown in Figure 7.32. The performances indices concerning S_{Up}, S_{Lo} violations and DSL activation of the proposed EMSs, are benchmarked and reported as percent change (increase or decrease) against the performance of DA PoPA with HT capacity of 15m^3 under non-Gaussian uncertainty, as shown in Figures 7.33-7.35respectively. A percentage increase is indicated by a positive magnitude and a percentage decrease has been indicated by a negative magnitude. Nevertheless, the A2C+PoPA algorithm, which has the most significant computational complexity necessitates the need for a state of the art computer processor considerably faster than an intel *i*5 and with a RAM greater than 64GB. Therefore, the A2C+P has now been omitted from further investigation in the sensitivity analysis, as the investigation will be carried out in future work when the computational assets become available. Also, the RLS-P PoPA which utilised the linear model (y=Ax+B) has been omitted, mainly due to excessive resources constraint, which required the HT to be sized more significantly than 25m^3 in contrast to the rest proposed PoPA methods.

The RL+Adaptive PoPA scheme with HT capacity at 10m^3, had the fewest S_{Lo} and S_{Up} violations of 68 and 256 times respectively, with the DSL never activated as depicted in Figure 7.31. Particularly, the RL+Adaptive PoPA which had the most significant reduction in S_{Lo} violation for all sizes, except at 1m^3 where the Kalman +Adaptive had a 1% improvement from the RL+Adaptive' 77% decrease as shown in Figure 7.33. Though for HT capacity of 5m^3 the RLS+P and RL+Adaptive both had a similar performance of 64% decrease in S_{Lo} violation, at 1m^3 the RL+Adaptive, P+Adaptive, RL+Adaptive PoPA all had the same performance of 77% decrease as shown in Figure 7.34. However, the performance of the P+Adaptive PoPA, which had 1371 S_{Lo} violation and 601 DSL activation was the worse performing in the 10m^3 HT size category. The RLS-P PoPA had the second-worst S_{Lo} violation and DSL activation of 1241 and 601 times, respectively, as shown in Figure 7.31. Although the P+Adaptive PoPA had the least performing in regards to S_{Up} violation at HT

sizes 15 and $10m^3$, the DRL+Adaptive had the least reduction in S_{Up} violation for all sizes below $10m^3$ as shown in Figure 7.33. With a reduction in HT capacity from 15 to $10m^3$, the P+Adaptive and the RLS+P PoPA significantly had the most DSL activation which was 210% and 193% respectively as shown in Figure 7.35. This underscores the trade-off of the robustness, which requires more resources compared to the rest of the methods.

The best performing in the $10m^3$ HT size, were the RL+Adaptive and Adaptive PoPA which never activated the DSL and was closely followed by the Kalman+Adaptive and then the DRL +Adaptive which had a 93% and 59% reduction as shown in Figure 7.35. The DA-PoPA's violation of the S_{Lo} and S_{Lo} as well as the activation of the DSL remained unchanged at 804,756 and 299 times respectively despite the reduction in HT capacity from $15m^3$ - $5m^3$ as shown in Figure 7.31-7.35. Nevertheless, except for HT sized at $15m^3$ where the P+Adaptive had the worst violation of 828 times, the DA PoPA significantly had the worst S_{Up} violation of 756 times for the rest of all the HT sizes below $15m^3$. The Kalman Adaptive PoPA which had the second-best performance, had S_{Lo} and S_{Up} violation of 264 and 87 times, although the DSL was activated 15 times with HT at $10m^3$ in contrast to it never being activated with the HT sized at $15m^3$.

Decreasing the HT capacity from 10 to $7.5m^3$, the RL+Adaptive PoPA activated the DSL 85 times in contrast to once by the Adaptive PoPA, as shown in Figure 7.31. Nevertheless, for HT sizes 10 and $7.5m^3$, the RL+Adaptive had the best performance amounting to 92% and 70% decrease in S_{Lo} violation. The RL+Adaptive PoPA also had the best performance which was only second the DRL+Adaptive when the HT capacity was $15m^3$. The Adaptive PoPA's performance concerning S_{Up} and S_{Lo} violation as well as DSL activation, which remained unchanged with HT capacity varied from 15 to $7.5m^3$ noted the best fossil fuel impact at $7.5m^3$, as the DSL was never activated as shown in Figure 7.35.

The performance of the Adaptive PoPA for the S_{Lo} violation was the best for HT capacity of $5m^3$ and was only second to the performance of the DA PoPA for HT capacity of $2.5m^3$

and $1m^3$ as shown in Figure 7.33. Furthermore, the Adaptive PoPA had the best fossil fuel reduction in the HT capacity of $7.5m^3$ as the DSL was activated only once compared with the RL+Adaptive PoPA which had the best performance concerning the S_{Lo} and S_{Up} violation but activated the DSL 85 times. The least performing remained the P+Adaptive and the RLS+P PoPA with 276% and 252% increase in the use of fossil fuel resources respectively.

The DA PoPA despite having its most significant change in performance considering HT capacities of $2.5m^3$ and $1m^3$, was, however, had the least the S_{Lo} violations of 75% and 153% increase respectively as shown in Figure 7.34. In contrast, the P+Adaptive PoPA had the worst S_{Lo} violation of 297% for HT capacity of $2.5m^3$ as well as 354% for HT capacity of $1m^3$ respectively, as shown in Figure 7.34. The RL+Adaptive and Kalman +Adaptive PoPA exhibited a significant change in performance when the HT was changed from 7.5 to $5m^3$. While the DRL+Adaptive PoPA exhibited a significant change when the HT was changed from 10 to $7.5m^3$. Similarly, the P+Adaptive which had the least and second least performance S_{Lo} violation at sizes less than $15m^3$, exhibited a significant change in performance when the tank size was changed from 15 to $10m^3$ as shown in Figures 7.31-7.35.

7.2.2 Summary

From the investigation and analysis, as the HT capacity was decreased from 15 to $1m^3$ in steps of $2.5m^3$, the S_{Up} violation indicated a decreasing trend while an increasing trend was revealed with the S_{Lo} violation and the DSL activation. The PoPA methods have all shown varying degrees of strengths and weakness against the DA-PoPA benchmark over HT sizes of 15 to $1m^3$ and should primarily be considered for applications with necessary trade-off depending on the HT capacity or H_2 autonomy, computational complexity and interest in the specific performance indices. Though, the DA-PoPA's violation of the S_{Up} remained considerably unchanged despite the HT size variation. This clearly underscored the weakness of the DA-PoPA to counteract uncertainty in the event of unanticipated excess or deficit

energy not considered prior to the daily energy target planning. Nevertheless, with negligible trade off in DSL performance, the RL+Adaptive PoPA is arguably the optimal PoPA method when the HT is decently sized in the range of $15m^3$ to $7.5m^3$.

In conclusion, the probabilistic methods; P+Adaptive and RLS+P PoPA, which required a larger amount of H_2 resources for a robust preventive strategy on the overall, had an enhanced performance only when the H_2 was adequately available (i.e. HT > $15m^3$) as shown in Figures 7.31-7.35. The P+Adaptive and RLS+P PoPA had the most significant change in performance when the HT capacity was change from $15m^3$ to $10m^3$. Similarly, Kalman+Adaptive, RL+Adaptive and DRL+Adaptive were impacted the most when the HT capacity was change from $15m^3$ to $5m^3$ and the Adaptive PoPA at $2.5m^3$.

7.2.3 Gaussian Case Study

A sensitivity analysis was performed in order to investigate the behaviour of the proposed methods with limited availability of H_2 resources by varying the HT capacity from 15 to $7.5m^3$ and from 5 to $1m^3$ in steps of $2.5m^3$ as shown in Figures 7.36-7.37 respectively, under Gaussian uncertainty. The results of the proposed methods are presented as a percentage change (increase or decrease) benchmarked against the DA-PoPA method, which was sized with HT capacity of $15m^3$ under Gaussian uncertainty. A percentage increase is indicated by a positive magnitude, and a decrease is indicated by a negative magnitude. The performances for the HT capacity range 15 to $1m^3$ concerning the S_{Up} and S_{Lo} violations are shown in Figures 7.38 - 7.39 respectively while the DSL activation are shown in Figure 7.35. The A2C and the RLS+P PoPA with a linear bias model (y=Ax+B) have both been excluded from the sensitivity analysis for the same reasons which were highlighted in section 7.2.1.

The performance of the DA, Adaptive, Kalman +Adaptive and RL+Adaptive PoPA, remained unchanged when the HT was decreased from $15m^3$ to $10m^3$, and more so, the performance of the DA-PoPA remained consistent throughout the investigation despite

dropping the HT capacity from 15 to $1m^3$. Interestingly, the performance of the DA and Adaptive PoPA were similar to each other and remained unchanged with the HT sized at $7.5m^3$ and $5m^3$.as shown in Figures 7.36-7.40.

Generally, the DA-PoPA significantly had the worst performance concerning the S_{Up} violation for all HT sizes (10 to $1m^3$) except for $15m^3$ HT capacity, where the P+Adaptive PoPA had the worst performance amounting to a 5% increase. Nevertheless, the RL+Adaptive which realised a 72% and 96% decrease in S_{Up} and S_{Lo} violation respectively, had the best performance for $10m^3$ HT size, with Kalman+Adaptive PoPA having the second-best indices as shown in Figure 7.38-7.39. Furthermore, with the HT capacity at $10m^3$, the Adaptive, Kalman+Adaptive and RL+Adaptive never activated the DSL, while the DRL+Adaptive had a 12% reduction. The P+Adaptive and the RLS-P PoPA had the least and second least performance which was a 493% and 42% increase in DSL activation respectively with the HT sized at $10m^3$ as shown in Figure 7.40. Besides, the P+Adaptive showed the most significant sensitivity to a reduction in HT capacity, when the HT was re-sized to $10m^3$.

Decreasing the HT from 10 to $5m^3$ the performance of the DA remained unchanged. Similarly, the Kalman +Adaptive PoPA's performance remained unchanged with 10 to $7.5m^3$ HT capacity. Furthermore, the performance of the DA and Adaptive PoPA were significantly the same when the HT capacity was $7.5m^3$ and $5m^3$, as shown in Figure 7.36. The DA PoPA and the Adaptive PoPA had the worst S_{Up} violation at 0%, while the P+Adaptive which the most DSL activation and consequently the worst violation of the S_{Lo} constraint as shown in Figure 7.38-7.40. The RLS-P PoPA performed better concerning the S_{Lo} and SUp violations when the HT sized was $7.5m^3$. However, the DRL+Adaptive PoPA had a better performance than the RLS-P with regards to fewer DSL activation only. Nevertheless, the RLS-P performed better than the DA, Adaptive, P+Adaptive, and DRL+Adaptive PoPA concerning the S_{Lo} violation with the HT sized to $7.5m^3$, as shown in Figure 7.36. The DRL+Adaptive and RLS-P PoPA showed the most significant decline in performance with the

HT capacity varied from 10 to $7.5m^3$. The Kalman+Adaptive PoPA was the best performing concerning the S_{Up} violation with a 71% decrease and DSL never activated with the HT capacity at $7.5m^3$. However, the RL+Adaptive which had the next best performance with regards to DSL activation and S_{Up} violation, had the best performance with the S_{Lo} violation only, as shown in Figure 7.38-7.40.

Furthermore, with the HT size decreased from 7.5 to $5m^3$, the Kalman+Adaptive PoPA had the best performance with regards to reducing the S_{Lo} and S_{Lo} violation by 6% and 71% respectively. However, the DSL was activated 315% more than the DA and Adaptive PoPA. The DA and Adaptive PoPA had the same performance, which was a 0% change in the S_{Up} and S_{Lo} with the HT sized at $5m^3$ as shown in Figure 7.37-7.40. At HT sizes $2.5m^3$ the DA had the best performance in terms of the S_{Lo} and DSL activation which were both 0% nevertheless it had the worst S_{Lo} violation with respect to the performance of the rest proposed methods. The P+Adaptive PoPA had the best performance with respect to decreasing the violation of the $S_{U}p$ by 75% and 77% when the HT was sized to $2.5m^3$ and $1m^3$ respectively. Nevertheless, the P+Adaptive significantly violated S_{Lo} the most when HT size was $2.5m^3$, with a fossil fuel usage performance which was only better than the RLS-P and the Kalman+Adaptive PoPA for HT of $1m^3$.

7.2.4 Summary

The performances of the proposed methods have been investigated under Gaussian uncertainty with varying HT capacity from 15 to $1m^3$ in steps of $2.5m^3$ sizes. The performance of the DA PoPA remained unchanged over the range of HT capacities, typical of a DA strategy which does not account for any occurrence of uncertainty in-between the beginning and the end of the horizon. Nevertheless, despite the DA having a better S_{Lo} violation, as well as the fewest and DSL usage with HT sizes $2.5m^3$ and $1m^3$ it can be seen to have the worst S_{Up} violation. More so, whilst the rest of the proposed methods all exhibit a decreasing trend in

$S_U p$ violation with downsizing HT capacity, the DA PoPA which neglects uncertainty and consequently, the derivation of dynamic EMS inside a receding horizon does not show this trend. Therefore, for HT sizes $2.5m^3$ and $1m^3$, the Adaptive PoPA which had the next best performance is arguably the preferred EMS under Gaussian uncertainty for these sizes. For HT of $5m^3$, the adaptive PoPA though has a better performance with DSL usage had the same performance as the DA PoPA, hence the Kalman +Adaptive PoPA though activated the DSL 315% more arguably had the best performance when considering a trade-off in overall performance indices. Nevertheless, the Kalman+Adaptive PoPA was the optimal EMS for a $7.5m^3$ HT size. For HT capacity $15m^3$ to $10m^3$ the RL+Adaptive PoPA is arguably the most optimal EMS, though is closely followed by the DRL+Adaptive and the Kalman +Adaptive PoPA which can be used with a trade-off in performance needs.

In conclusion, the performance of the DA PoPA correlates with its past performance under non-Gaussian uncertain, which was presented in Section 7.2.1 in this Chapter. The investigation revealed the consistent behaviour of the proposed PoPA when HT capacity is varied from $15m^3$ to $1m^3$ under Gaussian and non-Gaussian uncertainty. The Kalman +Adaptive PoPA showed improvement in performance under the Gaussian uncertainty when the HT was sized greater then $5m^3$. The probabilistic methods; P+Adaptive PoPA and RLS-P+PoPA perform significantly optimally when the HT is sized greater than $15m^3$. Finally, Figure 7.41 presents a concise summary of the performance and recommendation of the proposed algorithms.

EMS	Percentage change in the performance of the proposed methods with respect to the DA PoPA under Non-Gaussian uncertainty and the HT sized at 15m^3						
	Lower Pinch violation ($SOAcc^n_{BAT}$ < 30%)	Upper Pinch violation ($SOAcc^n_{BAT}$>90%)	FC start-stop (cycles/year)	EL start-stop (cycles/year)	DSL start-stop (cycles/year)	PV start-stop (cycles/year)
Adaptive PoPA	-66%	-60%	95%	150%	-100%	6%
Kalman+Adaptive PoPA	-92%	-65%	521%	255%	-100%	6%
RL+Adaptive PoPA	-94%	-70%	1184%	1237%	-100%	7%
P+Adaptive PoPA	-60%	10%	554%	253%	-45%	-1%
RLS-P PoPA (y=Ax)	-75%	-12%	671%	378%	-66%	1%
DRL+Adaptive PoPA	-99%	-38%	1602%	1208%	-100%	4%

EMS	Percentage change in the performance of the proposed methods with respect to the DA PoPA under Gaussian uncertainty and the HT sized at 15m^3					
	Lower Pinch violation ($SOAcc^n_{BAT}$ < 30%)	Upper Pinch violation ($SOAcc^n_{BAT}$>90%)	FC start-stop (cycles/year)	EL start-stop (cycles/year)	DSL start-stop (cycles/year)	PV start-stop (cycles/year)
Adaptive PoPA	-76%	-63%	108%	174%	-100%	6%
Kalman+Adaptive PoPA	-89%	-71%	509%	320%	-100%	7%
RL+Adaptive PoPA	-96%	-72%	1069%	1074%	-100%	6%
P+Adaptive PoPA	-77%	5%	767%	334%	-4%	0%
RLS-P PoPA (y=Ax)	-98%	-22%	461%	240%	-100%	7%
DRL+Adaptive PoPA	-99%	-40%	1810%	1195%	-100%	4%

Fig. 7.30 Summary of the percentage change in performance of the Proposed PoPA EMSs compared to the DA PoPA under the Non-Gaussian and Gaussian with HT capacity of $15m^3$

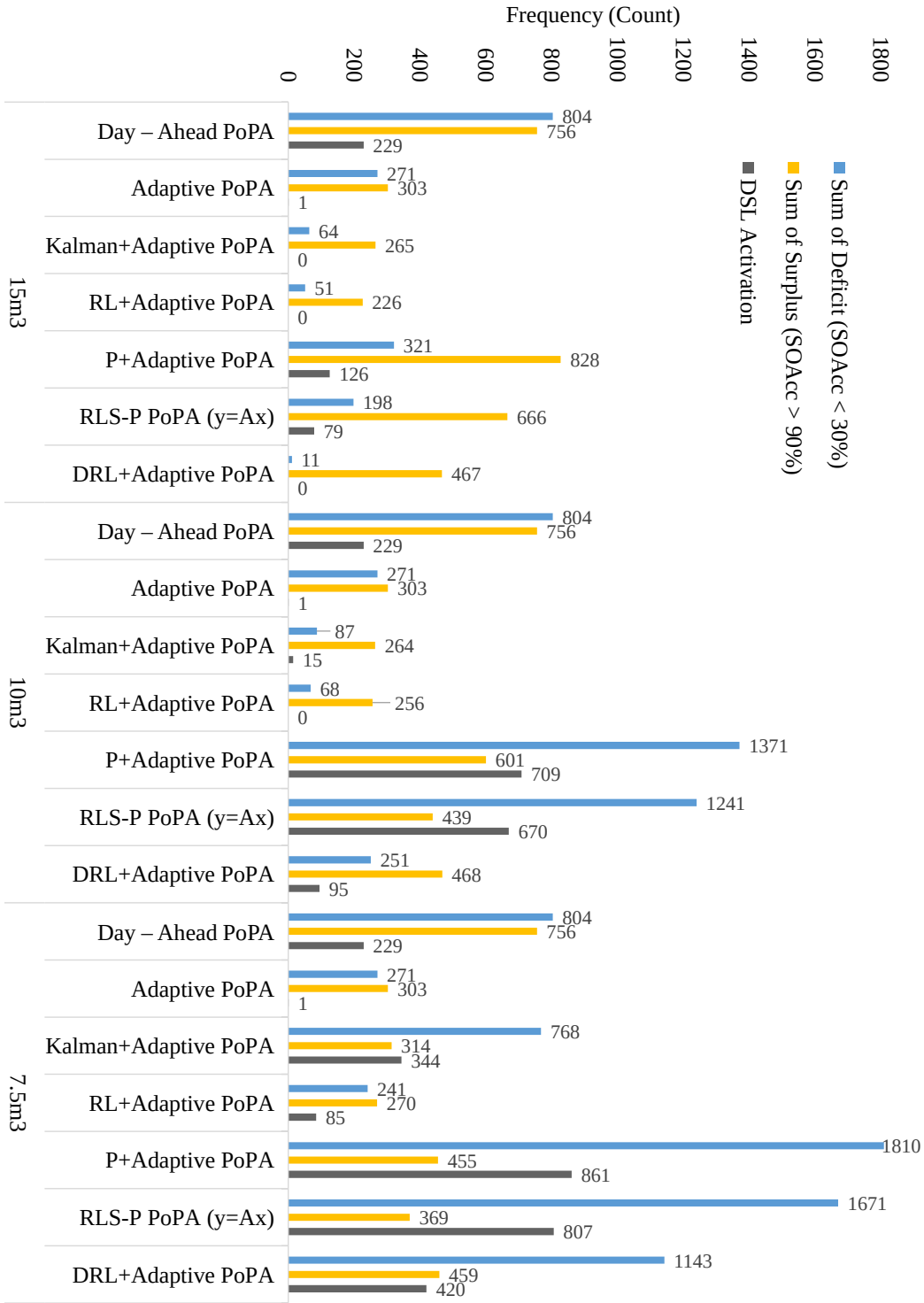

Fig. 7.31 Sensitivity analysis of the PoPA EMS Schemes with 15, 10 and 7.5m^3 HT capacity under non-Gaussian uncertainty

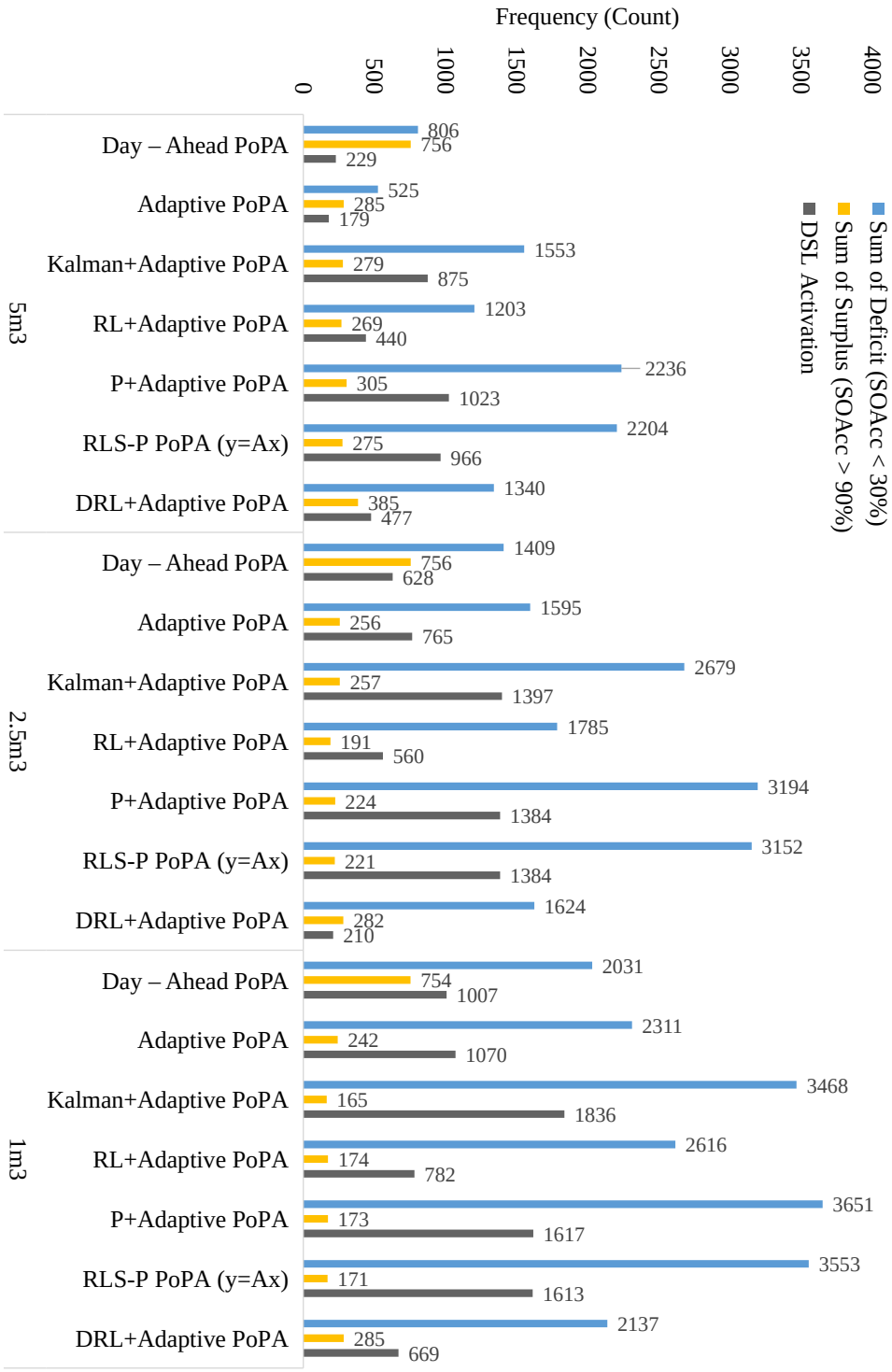

Fig. 7.32 Sensitivity analysis of the PoPA Energy Management Schemes with $5, 2.5$ and $1m^3$ HT capacity under non-Gaussian uncertainty

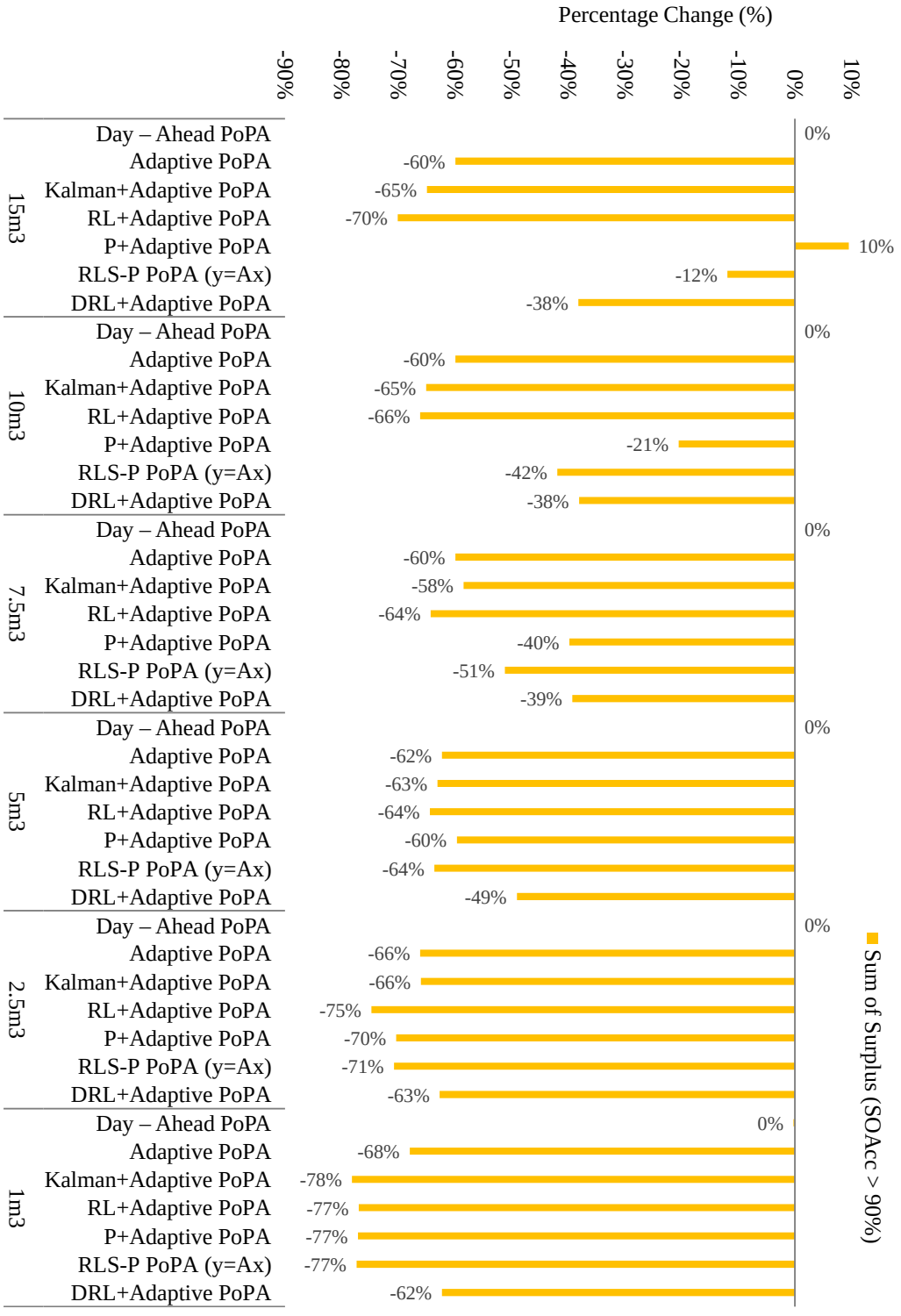

Fig. 7.33 Percentage Change in S_{Up} violation with the proposed PoPA methods from the DA PoPA benchmark with HT Capacity of $15m^3$ under non-Gaussian uncertainty

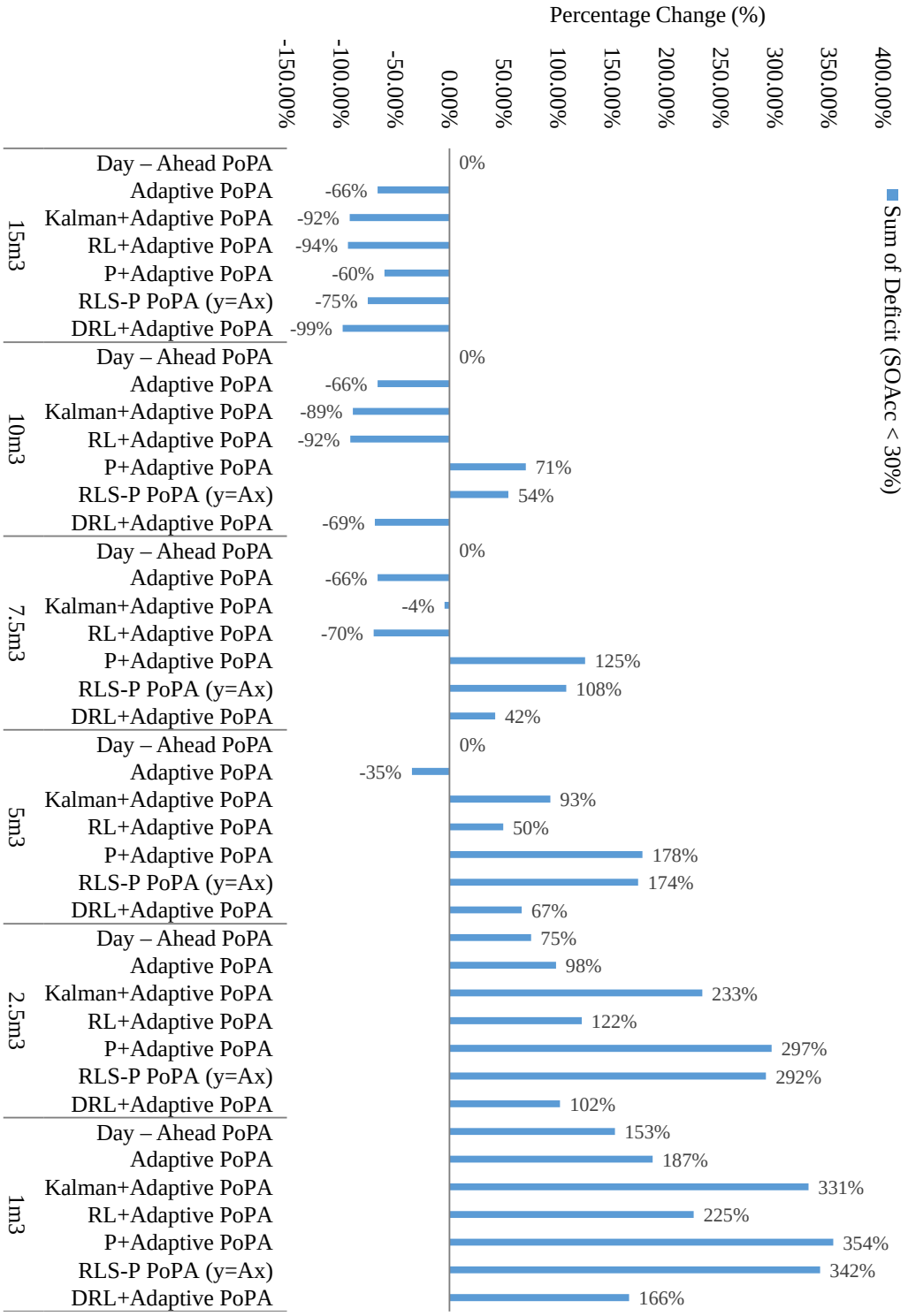

Fig. 7.34 Percentage Change in S_{Lo} violation with the proposed PoPA methods from the DA PoPA benchmark with HT Capacity of $15m^3$ under non-Gaussian uncertainty

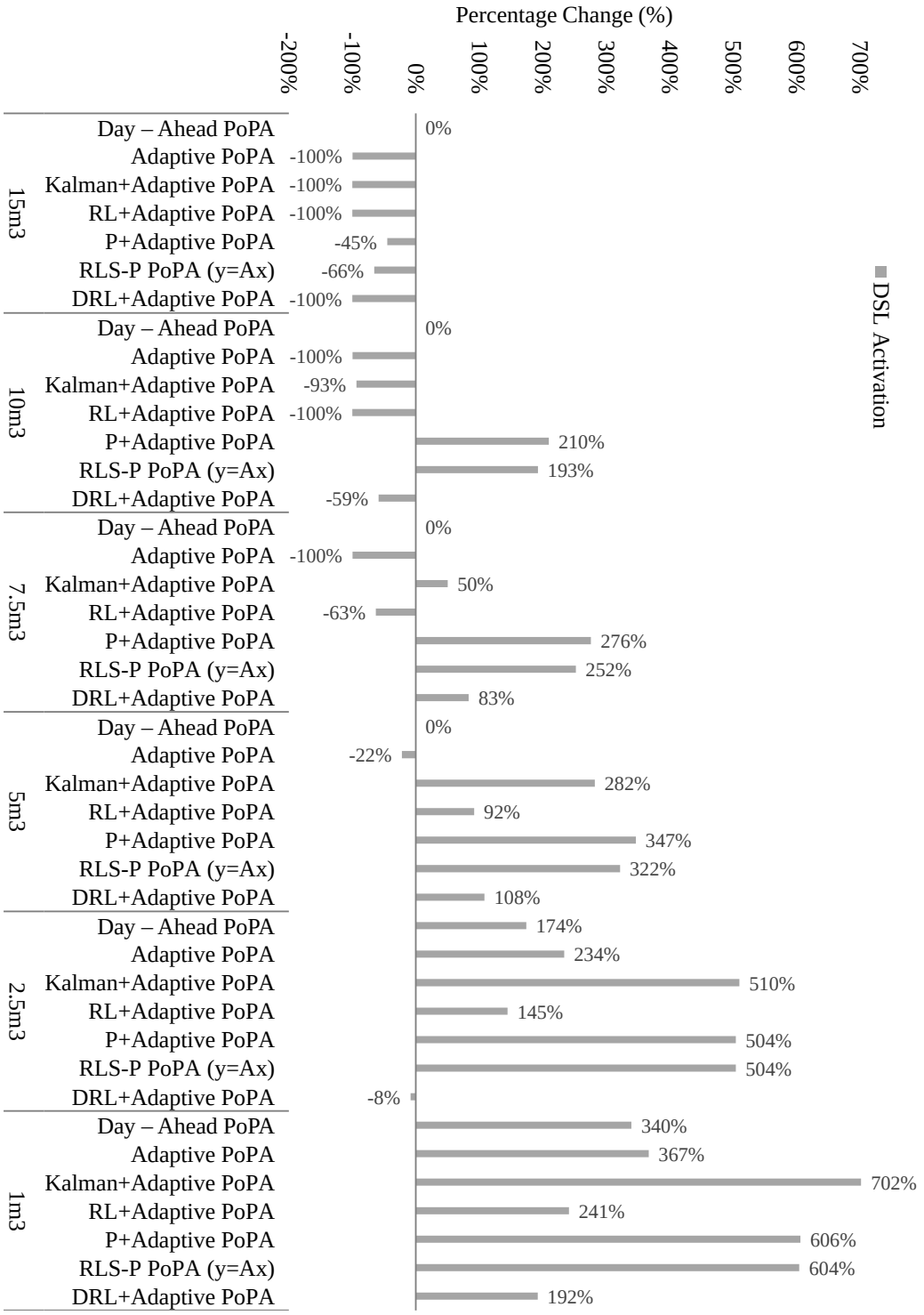

Fig. 7.35 Percentage Change in DSL activation with the proposed PoPA methods from the DA PoPA benchmark with HT Capacity of $15m^3$ under non-Gaussian uncertainty

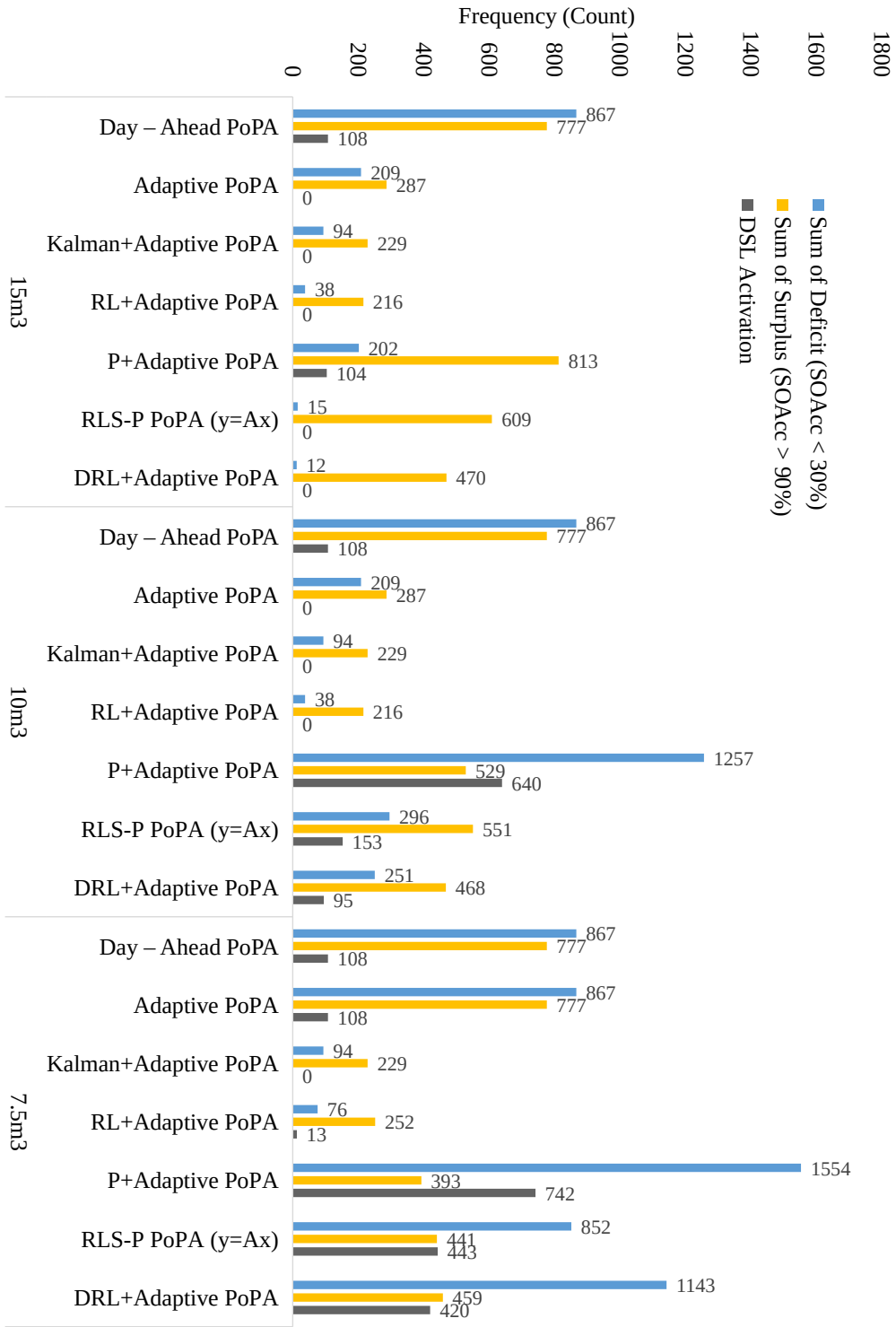

Fig. 7.36 Sensitivity analysis of the PoPA EMS Schemes with $15, 10$ and $7.5m^3$ HT capacity under Gaussian uncertainty

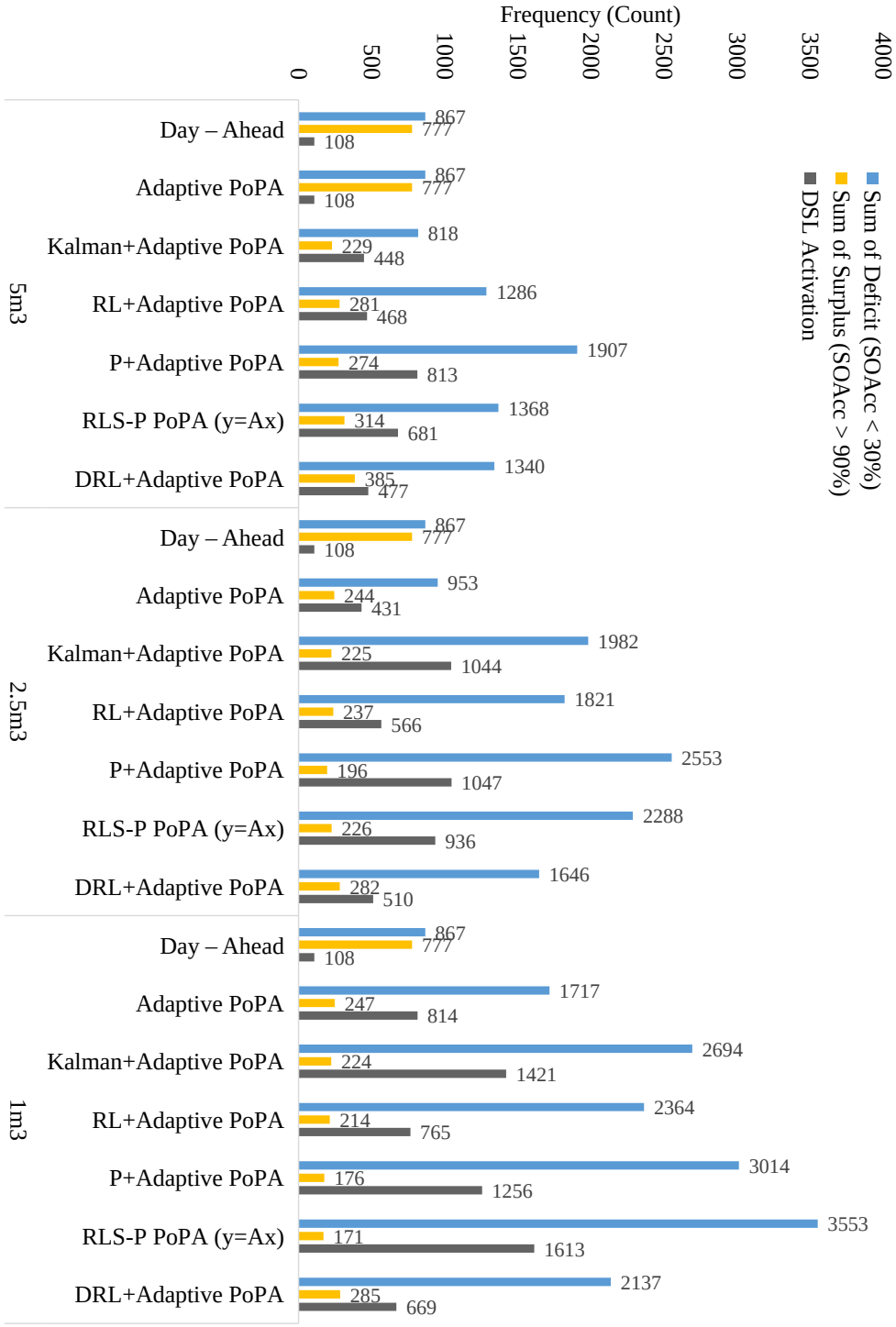

Fig. 7.37 Sensitivity analysis of the PoPA Energy Management Schemes with $5, 2.5$ and $1m^3$ HT capacity under Gaussian uncertainty

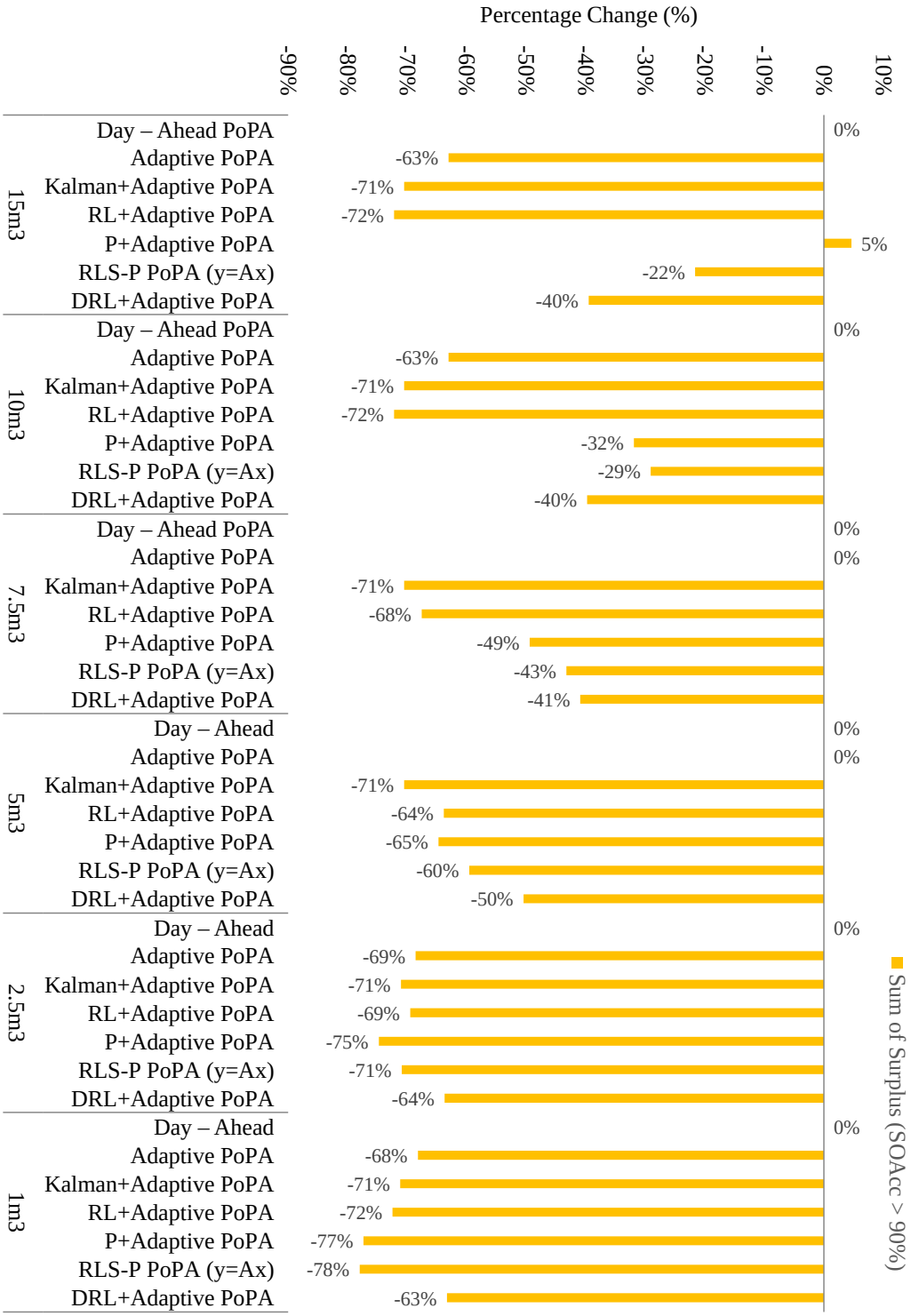

Fig. 7.38 Percentage Change in S_{Up} violation with the proposed PoPA methods from the DA PoPA benchmark with HT Capacity of $15m^3$ under Gaussian uncertainty

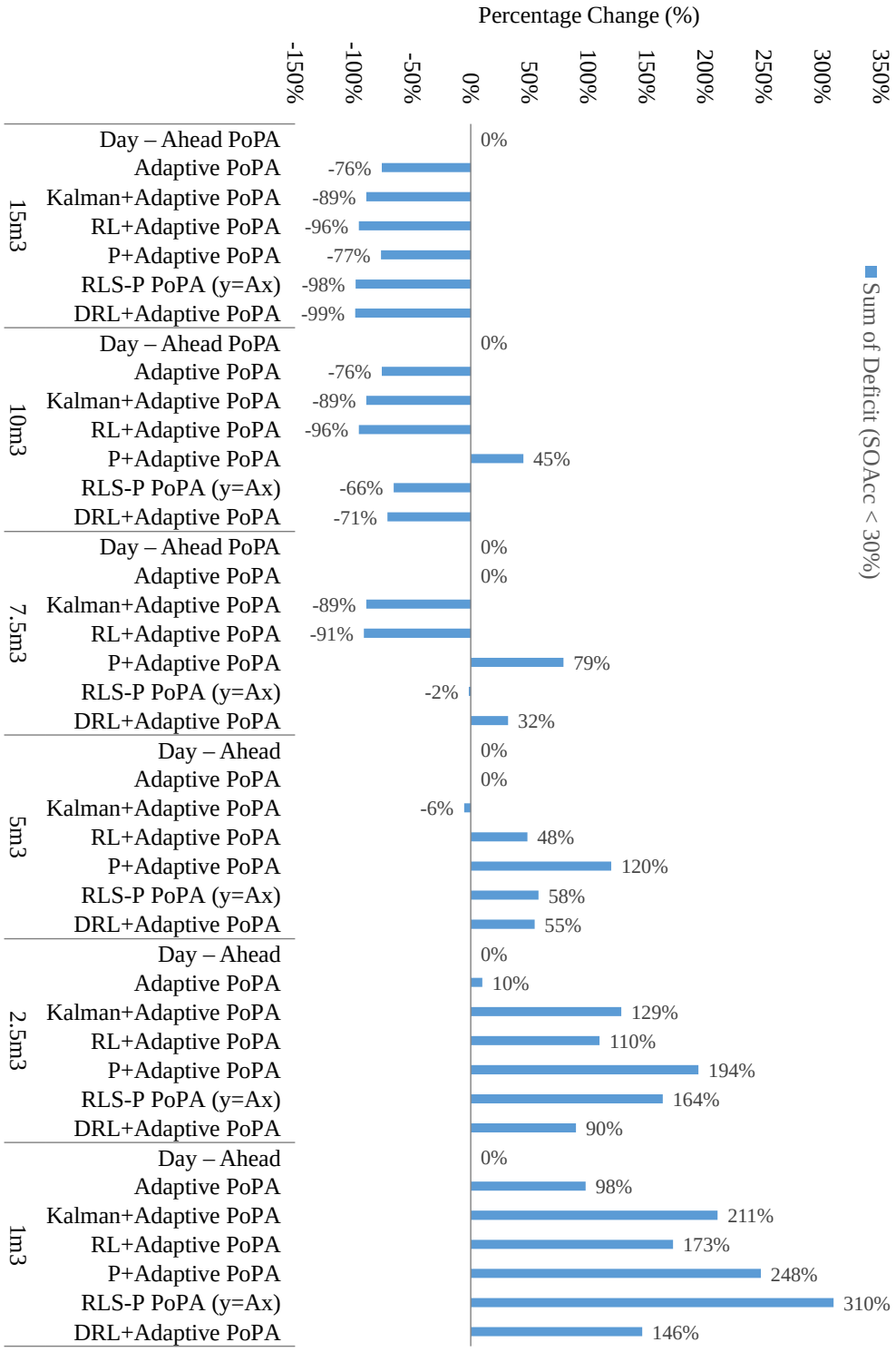

Fig. 7.39 Percentage Change in S_{Lo} violation with the proposed PoPA methods from the DA PoPA benchmark with HT Capacity of $15m^3$ under Gaussian uncertainty

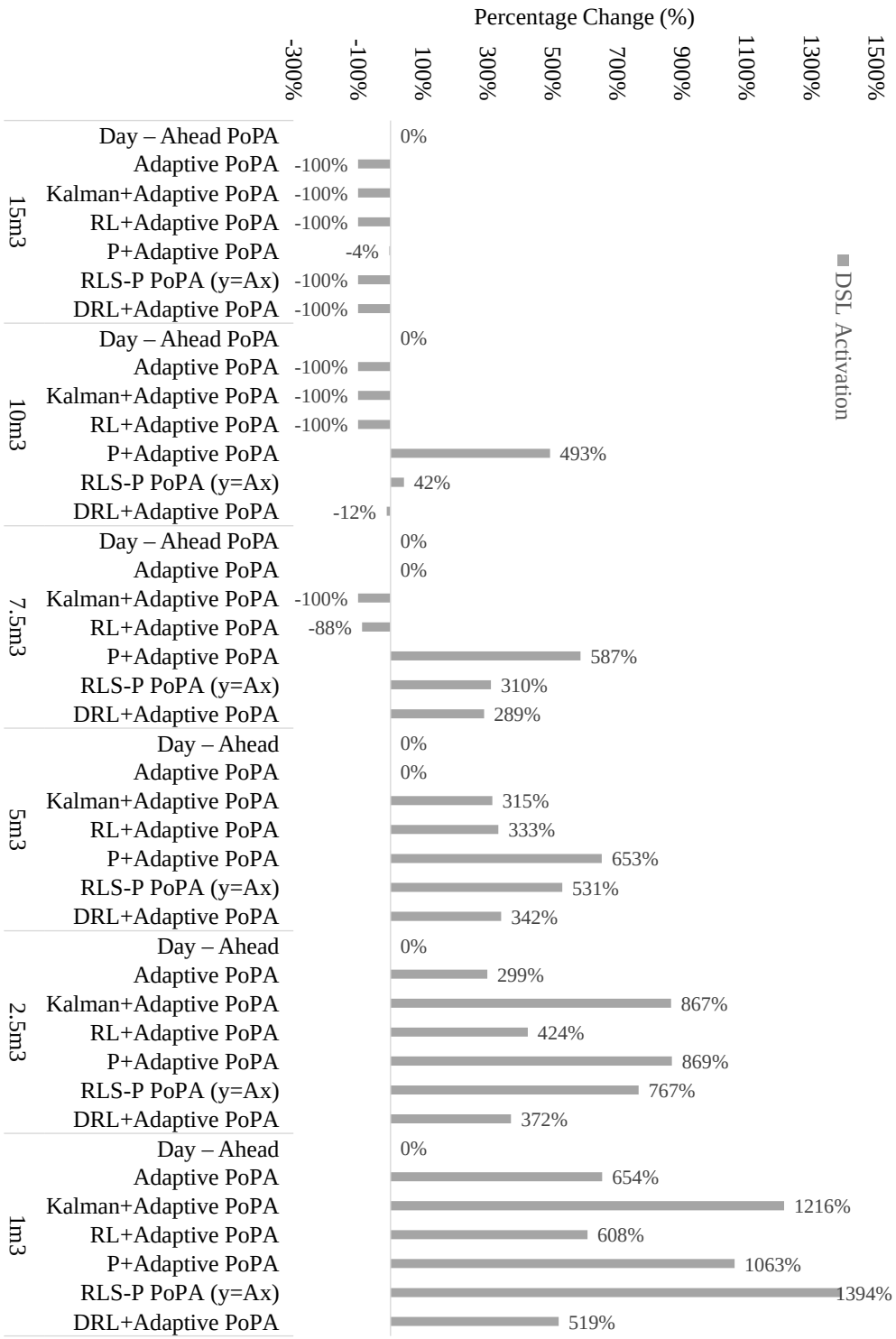

Fig. 7.40 Percentage Change in DSL activation with the proposed PoPA methods from the DA PoPA benchmark with HT Capacity of $15m^3$ under Gaussian uncertainty

Algorithm	Simulation processing Time for 8760h	Computational complexity	Summary
DA PoPA	12.313s	Extremely low	Use only if the magnitude of uncertainty is entirely absent or less than the *SOAcc* will not result in a violation of the Pinch limits.
Adaptive PoPA	38.118 s	Very low	Use if uncertainty is not persistent or H_2 resources is inadequate.
Kalman+Adaptive PoPA	70.193 s	Low	Use if the uncertainty is Gaussian and a decent level of accuracy is required.
RL +Adaptive PoPA	3 mins	Moderate	Use for the best accuracy with deterministic Load and PV profiles and H_2 resources is significantly adequate.
Probabilistic Adaptive PoPA	Depends on the number of scenarios (Typically, 6hrs for 1000 scenarios)	Very High	Use for enhanced robustness when probability density of the Load and PV profiles are available and H_2 resources is adequate.
RLS Probabilistic Adaptive PoPA	Depends on the number of scenarios (Typically, 6hrs for 1000 scenarios)	Very High	Use for enhanced robustness and improved accuracy when probability density function or adequate historical of the Load and PV profiles are known and available respectively. However, as with robust approach over budgeting and increase in cost of resources can occur.
DNN+Adaptive PoPA		High	The neural network function approximators
A2C+Probabilistic PoPA	Depends on the number of scenarios (Typically, 12hrs for 1000 scenarios)	Very High	This algorithm is the most complicated of them all and should only be used when the historical data is sufficiently large enough to train the two deep neural network function approximators. Nevertheless, this algorithm has not been thoroughly tested due to computational burden which imposes the need for a state of the art computational processor and RAM greater than that of a Pentium core i5 and 64GB RAM respectively.

Fig. 7.41 Summary of the performance and recommendation of the proposed PoPA algorithms

Chapter 8

Conclusion

In this thesis, several graphical insight based EMSs algorithms in a deterministic, probabilistic-RLS-Monte Carlo-chance constrained and RL Adaptive PoPA frameworks have been developed, compared and analyzed. The graphical EMSs were proposed in order to optimally control and coordinate the flow of energy and/or materials between heterogeneous HESS assets while considering the effects of uncertainty. The highlight of this study is that the RL+Adaptive and DRL+Adaptive PoPA utilising a machine learning approach had the best performance with respect to the violation of S_{Lo} and S_{Up} respectively when the HT was sized adequately above $7m^3$.

The effect of forecast uncertainty especially in off-grid HESS, results in the detrimental violation of the systems operating constraints, particularly when the EMS is planned using a DA approach. From a practical perspective the consequence of violating S_{Up} of the BAT due to inaccurate energy targeting, would perhaps result in excessive overcharging, overheating and even burning/explosion. Similarly, violating S_{Lo}, results in the BAT discharging beyond the optimal DOD which reduces the C_{BAT} and life cycle as well as increases GHG emission via the use of a DSL backup supply being is a non-renewable resource. Furthermore, effectively maintaining the reliability and operating constraints in an off-grid HESS, at minimum

resources cost are essentially the main objectives of an optimal EMS, and particularly in this thesis.

Hence, first, a deterministic Adaptive PoPA approach is exploited which is computationally efficient and requires minimum information regarding the parameters of the HESS. The Adaptive PoPA via a graphical insight based PGCC tool is realised in a receding horizon model predictive control framework in order to deal with electrical load demand uncertainty and RES variability which distort the forecast PGCC. The Adaptive PoPA via a simple state feedback mechanism compares real and forecast $SoAcc_{BAT}$ PGCC deviation at every sampling time interval (k). Hence, where the magnitude of deviation is greater than the 5% preset threshold value, re-computation of the PGCC is carried out using the latest $SOAcc_{BAT}$. Nevertheless, this strategy despite having the least computational complexity of $\mathcal{O}(Log(N.L))$ was found to be inadequate in the event of successive recurring uncertainty which increased the violation of the S_{Lo} and S_{Up} operating constraints. A sensitivity analysis showed the Adaptive PoPA is the significantly the preferred algorithm for use with HT capacity less than $5m^3$.

The Adaptive Pinch analysis was modified into a probabilistic adaptive Pinch which incorporated statistical inference to deal with uncertainty caused by the stochastic load variability by satisfying the certainty constraints. The method was validated using the Monte Carlo simulation which entailed a uniformly random sampling of the load distribution as the actual load.

The Kalman+Adaptive PoPA which entails estimating the likelihood of uncertainty derived from minimising the mean squared error between the actual and predict the State of charge of the Battery, improved the Adaptive PoPA. However, this strategy was sensitive to the probability density function of the uncertainty as the performance of the Kalman +Adaptive PoPA showed a superior improvement with uncertainty drawn out of a Gaussian PDF compared to a non-Gaussian PDF.

The PoPA is a conservative approach thus it requires accurate and precise model parameters and information to guide against erroneous EMS control and decision making in the HESS. Therefore the probabilistic Adaptive PoPA framework was proposed to proffer robustness using a chance constrained bounded PGCC.

The probabilistic Adaptive PoPA framework which requires the most computation, due to the analysis performed by generating n random scenarios via a Monte Carlo simulation from historical data, has a more superior performance than the deterministic PoPA. The deterministic algorithms have a computational complexity of $\mathcal{O}(Log(N.L))$, while the Probabilistic PoPA algorithms are $\mathcal{O}(Log(n.L.N))$. Generally, the probabilistic PoPA EMSs in contrast to the deterministic PoPA algorithms require a much larger budgeting of resources in order to proffer robustness. Therefore this trade-off between robustness and H_2 resources made the RLS-P PoPA with bias unsuitable for deployment when the HT capacity is less than $15m^3$. The RLS-P PoPA which utilised the simplest linear model (y=Ax) improved the performance of the standard P+Adaptive PoPA algorithm which did not use a residual error correction mechanism. Nevertheless, the improvement became marginally significant as the HT capacity decreased beyond $5m^3$.

Thirdly, reinforcement learning strategies; Tabular dyna-Q learning, deep Q network, and a deep actor critic network were formulated within the aforementioned deterministic and probabilistic Adaptive PoPA frameworks. The RL+Adaptive method incorporating a learning agent was shown to maximise the expected reward by acting optimally if the identified pinch targets are met. However, RL+Adaptive Pinch which had the best performance S_{Up} violation when the HT was sized greater then $7m^3$, showed increased violation of the limits when the HT was sized less than $7m^3$. Nevertheless, the RL+Adaptive Pinch has been modified to incorporate an abstract reward system regardless of hydrogen availability. Hence, the advantage of the abstract reward formulation is easily seen since despite the reduction in Hydrogen tank size from $15m^3$ to $1m^3$ the agent is capable of learning the optimal policy.

The DRL+Adaptive which used a deep neural network to generalise the training experience of the tabular based RL+Adaptive PoPA had the best performance with regards to the S_{Lo} violation. Similarly, like the RL+Adaptive PoPA, the DRL+Adaptive performance declined with HT capacity decreased beyond $7m^3$. The A2C+P PoPA which is still in the development stage, had a decent performance only with the non-Gaussian uncertainty. However, the A2C+P PoPA which was omitted from the sensitivity analysis due to computational burden constraint, had the performance which was the worst for the Gaussian uncertainty case study. The sub-optimal performance requires acute investigation as factors which range from limited training data set, improper tuning of the networks hyper-parameters can influence the behaviour of deep neural net.

As it is evident in the sensitivity analysis performed, there is the need to either outsource or resize the MG to cause excess energy. This also underscores the importance of sizing the micro grid a priori against uncertainty typically with sizing method A1 or with a MCS approach so as to cause excess energy for storage. Nevertheless, the techno-economic consideration of this work has therefore been chiefly related to reliability with respect to the Lo and excess energy lost in terms of the Up utility violation.

The DA-PoPA despite the HT capacity, maintained the same frequency of upper pinch violation, due to the lack of a state feedback loop necessary to deal with uncertainty. The Adaptive PoPA thus utilising the state feedback, corrects for the forecast error which was only better than the DA-PoPA when the tank was sized decently between 15 to 5 m3. The Kalman Adaptive pinch utilising an uncertainty estimator as well as the feed-back loop performed better than the DA and Adaptive PoPA and was only second to the RL+Adaptive PoPA and DRL+Adaptive schemes. Nevertheless, the RL+Adaptive PoPA provided a more favourable and practical framework for dealing with uncertainty due to load and weather variability.

In conclusion, the sensitivity analysis showed the algorithms conform to the 'no free launch theory' as no particular algorithm can satisfy all scenarios, rather these proposed algorithms should be used as fit for purpose.

- Future Work

As shown in the thesis, the approach utilizing reinforcement learning can reliably guarantee optimal operation in an uncertain situation as an agent learns the optimal sequence of action for every system state. Therefore, future work will integrate demand side response for load shifting (from peak periods to off peak) into the proposed RL+Adaptive PoPA framework via a co-operative multi-agent approach in order to effectively achieve much more systems resource savings.

Appendix A

Energy Storage Technology

A.1 Energy Storages

The use of multiple complementary energy storage types for reliability is the current trend, and excess energy from the PV-Battery system can be converted and stored for future usage. The integration of hybrid energy storages enhances efficiency as the frequent utilisation of dump load for absorbing excess energy will be avoided. According to [29], there are several factors which must be considered when choosing an Energy storage system ESS for an application. These include; capital cost, power, and energy rating and density, efficiency, self-discharge losses, depth of discharge, ramp rate, life cycle. A few popular integrated energy storages are discussed below.

A.1.1 Pumped Hydro Storage (PHS)

This form of storage is the most widely used technology as it is responsible for over 120GW of generated electricity worldwide and also represents 99 percent of the total electrical storage capacity in the world. The principle of operation is that water is pumped from a ground-level reservoir tank to an overhead tank which represents stored energy in the form of potential

energy during the off-peak period. This is analogous to the charging of a battery. During the off-peak period, the stored water at potential is released into hydro turbines, which in turn drives a generator to produce electrical energy. The PHS is the most mature ES technology [159], and also it has the most significant energy and power capacity with installed capacities ranging from 2000 to 3000 MW globally. Nevertheless, PHS is commonly sized within the range of 1000 MW to 1500 MW [29, 160].

A.1.2 Compressed Air Energy Storage (CAES)

This technology has been in use since the 19th century. It involves the use of a compressor to compress air during the off-peak period for storage in an underground (rock structures, mines) or a pipe or vessel above the ground. When energy is required, natural gas is combusted in the presence of the previously stored up compressed air in a modified gas turbine [29]. Besides PHS, CAES is the only technology which is commercially available technology with the capability of delivering 100MW from a single unit [159]. Nevertheless, it is essential to note that only two of such plants exist, one is at Huntorf, Germany, and the other is in Alabama, USA [29, 161].

A.1.3 Flywheel Energy Storage (FES)

This storage system has been in existence since the 1970s. It consists of a large mass of steel usually cylindrical in shape, attached by bearings to a mechanical rotor. The rotational energy in the form of kinetic energy is stored in the steel mass during the charging process as its speed of about 20000-50000 rpm is maintained. During the discharge process, the flywheel drives the rotor as a generator to produce electricity [29]

A.1.4 Batteries

These are electrochemical energy storage devices which convert chemical energy to electrical energy. Secondary batteries are rechargeable as the internal chemical reaction is reversible, unlike with the primary batteries. The electrical characteristics of a battery are dependent on the topology in which the nominal low voltage cells are connected. The topology can either be in series or parallel or as a combination of both. Some of the most popular batteries in use for RES are Lead Acid (LA), Lithium-ion (Li-on), Sodium sulphide (NaS), Nickel Cadmium (NiCd), Nickel Metal Hybrid (NiMH). The NiCd Battery suffers from memory loss effect and depends on DOD. Hence it is not reliable for long time usage [162, 29]. Though the Li-on battery is more expensive, it has the longest life span as well as the highest power and energy density compared to the other battery types.

The flow batteries have recently been built in the Mega Wattage range. In the flow battery, the electrolyte is stored in an external containment and pumped for the electrochemical reaction when required. The power and energy ratings are functions of the area of the stacked cells and amount of electrolyte. Typical varieties are Vanadium Redox Battery (VRB)[163, 164], Polysulphide Bromide (PSB) [165, 166] and Zinc Bromine (ZnBr) [167, 168]. They possess a very promising potential for applications requiring large scale energy storage integration.

Appendix B

HESS Propositional Logic

Connection	Symbol	Logic proposition for HESS
$BAT \leftarrow PV$	$\varepsilon_{PV}(k)$	$\bigcap_{c}[\varepsilon_{PV}^{c}(k)], \in \{Avl, Req, Gen\}$
	$\varepsilon_{PV}^{Avl}(k)$	1
	$\varepsilon_{PV}^{Req}(k)$	$q_{PV}^{SOAcc\ BAT}(k)$
	$\varepsilon_{PV}^{Gen}(k)$	1
	$q_{PV}^{SOAcc\ BAT}(k)$	$SOAcc_{BAT}(k) < S_{LO}^{BAT \leftarrow PV}(k)$
$BAT \leftarrow DSL$	$\varepsilon_{DSL}(k)$	$\bigcap_{c}[\varepsilon_{DSL}^{c}(k)], \in \{Avl, Req, Gen\}$
	$\varepsilon_{DSL}^{Avl}(k)$	1
	$\varepsilon_{DSL}^{Req}(k)$	$q_{DSL}^{SOAcc\ BAT}(k)$
	$\varepsilon_{DSL}^{Gen}(k)$	1
	$q_{DSL}^{SOAcc\ BAT}(k)$	$SOAcc_{BAT}(k) < S_{LO}^{BAT \leftarrow DSL}(k) \vee \left[\begin{matrix}[S_{LO}^{BAT \leftarrow DSL}(k) < SOAcc_{BAT}(k) < S_{UP}^{BAT \leftarrow DSL}(k)] \wedge \\ [\varepsilon_{DSL}(k-1)]\end{matrix}\right]$
$BAT \leftarrow FC$	$\varepsilon_{FC}(k)$	$\bigcup_{c}[\varepsilon_{FC}^{c}(k)] \wedge \varepsilon_{FC}^{Avl}(k),\ c \in \{Req, Gen\}$
	$\varepsilon_{FC}^{Avl}(k)$	$\bigcap_{l}[a_{FC}^{SOAcc\ l}(k)], l \in \{HT, WT\}$
	$\varepsilon_{FC}^{Req}(k)$	$q_{FC}^{SOAcc\ BAT}(k)$
	$\varepsilon_{FC}^{Gen}(k)$	$\rho_{FC}^{U_c}$
	$\rho_{FC}^{U_c}$	$\underset{\rightarrow}{U_c}(SOAcc_{BAT}(k))$
	$q_{FC}^{SOAcc\ BAT}(\mathrm{k})$	$SOAcc_{BAT}(t) < S_{LO}^{BAT \leftarrow FC}(k)$
	$a_{FC}^{SOAcc\ WT}(k)$	$SOAcc_{WT}(t) < S_{UP}^{WT \leftarrow FC}(k)$
	$a_{FC}^{SOAcc\ FT}(k)$	$SOAcc_{FT}(t) > S_{LO}^{FC \leftarrow HT}(k)$
$BAT \rightarrow EL$	$\varepsilon_{EL}(k)$	$\bigcup_{c}[\varepsilon_{EL}^{c}(k)] \cap \varepsilon_{PV}^{Avl}(k),\ c \in \{Req, Gen\}$
	$\varepsilon_{EL}^{Avl}(k)$	$\bigcap_{l}[a_{EL}^{SOAcc\ l}(k)], l \in \{BAT, HT\}$
	$\varepsilon_{EL}^{Req}(k)$	$q_{EL}^{SOAcc\ BAT}(k)$
	$\varepsilon_{EL}^{Gen}(k)$	$\rho_{EL}^{U_c}$
	$a_{EL}^{SOAcc\ BAT}(k)$	$SOAcc_{BAT}(k) > S_{LO}^{BAT \rightarrow EL}(k)$
	$a_{EL}^{SOAcc\ FT}(k)$	$SOAcc_{FT}(k) < S_{UP}^{EL \rightarrow HT}(k)$
	$q_{EL}^{SOAcc\ WT}(k)$	$SOAcc_{WT}(k) > S_{LO}^{EL \leftarrow WT}(k)$
	$\rho_{EL}^{U_c}$	$\underset{\rightarrow}{U_c}(SOAcc_{BAT}(k))$

Appendix C

Pseudo Codes for Adaptive, Kalman and RL PoPA

Pseudo Codes for the Proposed Algorithms

a. Pseudo Code for Adaptive PoPA

1. Define the entire time span and intervals.
2. Define the initial systems state and EMS propositions
3. For all intervals k
   Perform within the prediction horizon the following procedures:
4. if $(k - N) = 23 \vee \Delta H(k) > (\xi == 5\%)$
   - 4.1.1 Repeat while Loop, L < =24 $\wedge$ $(S_{max} > S_{Up}^{l} \vee S_{min} < S_{Lo}^{l})$
   - 4.2 Compute the PGCC with dispatch control sequence U_c according to equations (1)
   - 4.3 Determine $S_{min} = \underset{k\in[k,k+1,\dots,N]}{min}\ SOAcc_l^m(k)$ and $S_{max} = \underset{k\in[k,k+1,\dots,N]}{max}\ SOAcc_l^m(k)$
     - 4.3.1 If $S_{min} < S_{Lo}^{l}$
       a. Determine the energy $MOES = Lo - S_{min}$ required to shift the PGCC (Such that, $SOAcc_l^{m,1}(k_1) = (SOAcc_l^{m,0}(k_1) + MOES) < S_{Up}^{l}$)
       b. $U_c = FC\ :\ U_c(SOAcc_l^m) = [U_k(S_{k+1}), \dots U_{N-1}(S_T), \mid S_{k+1\,:\,k\in[1,2,\dots,N]} < S_{Up}^{l}]$ In a memory location, store the control sequence U_c
       c. Activate the selected converter U_c to inject the energy determined in step 4.2.1(a) at k_1 then go to step 4.3.
     - 4.3.2 if $S_{max} > S_{Up}^{l}$
       a. Determine the amount of energy MEES = $S_{max} - S_{Up}^{l}$ (Such that, $SOAcc_l^{m,1}(k_1) = (SOAcc_l^{m,0}(k_1) - \text{MEES}) > S_{Lo}^{l}$ to shift the PGCC).
       b. Activate the selected converter U_c , $c \in \{\text{EL}\}$ to absorb the energy determined in step 4.2.2(a) at k_1 then go to step 4.3.
   - 4.4 Determine $SOAcc_l^{m,L}(N)$: L ∈ [0: 24]
     - 4.4.1 if $SOAcc_l^{m,L}(N-1) \cong SOAcc_l^{m,L}(k_1)$
       a. calculate $\Delta S = SOAcc_l^{m,L}(k_1) - SOAcc_l^{m,L}(N-1)$ (such that $SOAcc_l^{m,1}(N-1)$ $=SOAcc_l^{m,0}(N-1) \pm \Delta S$
       b. Activate the selected converter U_c to inject or absorb the energy $\pm\,\Delta S$ determined in step 4.3.1(a) at $N-1$.
       c. repeat from step 4 until L>24
5. Activate the determined control sequence in control horizon $U_c(SOAcc_l^n) : S_{Lo}^{l} < [U_k(S_{k+1}), \dots U_{N-1}(S_N), \mid S_{k+1\,:\,k\in[1,2,\dots,N]} < S_{Up}^{l}]$
6. **Determine state estimation error due to uncertainty:**
   $\Delta H(k) = |SOAcc_{BAT}^{n}(k|k-1) - SOAcc_{BAT}^{m}(k)|$
7. Update the model with the actual system state with (7) for new PGCC re-computation
8. Repeat from step 3 until k > 8760

b. Pseudo Code for Kalman+Adaptive PoPA algorithm

This follows steps 1 – 5 of the Adaptive PoPA algorithm, but with the inclusion of the Kalman filter.

7. Update the priori covariance estimate $\mathcal{P}_k = \left[\mathcal{I} - \mathcal{K}_{\mathcal{G}}\mathcal{I}\right]\mathcal{P}_{k-1}$
8. Determine the Kalman gain $K_{G(k)} = \mathcal{P}_k\, I^T\, [\mathcal{I}\,\mathcal{P}_k\,\mathcal{I}^T + \mathcal{R}_k]^{-1}$
9. Predict the system state with the most recent output measurement from (11):
$$SOAcc_l^m(k) = SOAcc_l^m(k|k-1) + \mathcal{K}_{\mathcal{G}}(SOAcc_l^n(k) - \mathcal{I}\,SOAcc_l^m(k|k-1))$$
10. Estimate the posterior covariance matrix $\mathcal{P}_{k+1} = A\,\mathcal{P}_k A^T + \mathcal{R}_k$
11. Repeat from step 3 while $k \leq 8760$

c. Pseudo Code for RL+Adaptive PoPA

This follows steps 1 – 6 of the first proposal, with the inclusion of the Q-learning state-action pair $Q(s,a)$.

5. Observe the systems state, s

6. For $k\sim = N$

   Switch ON/OFF dispatchable energy resources with the action selection policy $\pi\ (s)$ defined in (17) based on the state-action value function $Q(s,a)$.

   Else

   Override the action selected from policy $\pi\ (s)$ with AEEND EMS from Adaptive PoPA

   End

7. Observe $SOAcc_{BAT}^{n}$ and determine the reward, R according to (21)
8. Update $Q(s,a)$ based on equation (16)

   s$\leftarrow s'$

9. Randomly draw without replacement *n*-sample from memory $D \in <$ S, A, R, S', A' $>$ pairs of the most recent n-pinch limits violation experience due to uncertainty.
10. Update $Q(s,a)$ with the uncertainty experience
11. Repeat from step 3 until $k > 8760$

Appendix D

Adaptive Power Pinch Analysis .m Code

```
I_rad = dlmread('PV_POA.csv');          %Plane of Array for insolation
I_Rad=I_rad';
%I_Rad=[I_Rad(2688:8760),I_Rad(1:2687)];


Ng=0.96;
Nb=0.72;
Air_den=1.23    ;                        %Air density 1.23 Kg/m3
Cp=0.4;
Area_sw=3.24 ;                           %Wind Turbine Swept Area
WT_no=3;
WT_wind = dlmread('WT_Wind.csv');       %Velocity of Wind m/s
Wind_vel=WT_wind';


LD3=ones(1,8760)*1000;                   % Constant Load for a year

LD3_daily=24*1000;                         %Load per day

P_DSL3_BAT3= 2010;

%Counter=0 ;                             %counts the no.of iteration



%%

%%%%%%%%%%%%%%%%%%%%%%%%%%%%%%%%%%%%%%%% START OF MICROGRID 3 INITIALIZATION
%%%%%%%%%%%%%%%%%%%%%%%%%%%%%%%%%%%%%%%%%%%%%%%%%%%%%%%%%%%%

%INITIALIZING ACTIVATION STATES OF THE NODES
e_BAT3_LD3=1;
e_PV3_BAT3=0;                %PV3 is the solar panel in microgrid 3, WG2 is
the wind turbine in microgrid 3
e_WG2_BAT3=0;
e_BAT3_EL=0  ;                %EL is the ELectrolyser, WT is the Water Tank,
FC is the Fuel Cell
e_WT_EL=0    ;
e_EL_FT=0    ;                  %FT is the Hydrogen storage tank
e_FT_FC=0;
e_FC_BAT3=0;
e_FC_WT=0;
e_DSL3_BAT3=0;

e_BAT3_EL = e_EL_FT;

%ACTIVATION FOR WATER TANK TO ELECTROLYSER
e_WT_EL=e_EL_FT;

%ACTIVATION FOR FLOW TANK TO FUEL CELL
e_FC_BAT3 =e_FT_FC       ;                       %The Logic for SOC to
CONVERTER is the same as CONVERTER TO SOC
```

```
%ACTIVATION FOR FUEL CELL TO WATER TANK
e_FC_WT=e_FC_BAT3;

%INITIALIZING AVAILABILITY OVERRIDE
r_PV3_BAT3=0;
r_WG2_BAT3=0;
r_BAT3_EL=0;
r_WT_EL=0;
r_EL_FT=0;
r_FT_FC=0;
r_FC_WT=0;
r_FC_BAT3=0;
r_BAT3_LD3=0;
r_DSL3_BAT3=0;

%INITIALIZING GENERALITY CONSTRAINT FOR ACTIVATION (OVERRIDE)

g_PV3_BAT3=1;
g_WG2_BAT3=0;
g_BAT3_EL=1;
g_WT_EL=1;
g_EL_FT=1;
g_FT_FC=1;
g_FC_WT=1;
g_FC_BAT3=1;
g_BAT3_LD3=1;
g_DSL3_BAT3=1;



%
%INITIALIZING ACTIVATION STATES OF THE NODES
e_BAT3_LD3_A=1;
e_PV3_BAT3_A=0   ;               %PV3 is the solar panel in microgrid 3, WG2
is the wind turbine in microgrid 3
e_WG2_BAT3_A=0;
e_BAT3_EL_A=0    ;               %EL is the ELectrolyser, WT is the Water
Tank, FC is the Fuel Cell
e_WT_EL_A=0    ;
e_EL_FT_A=0    ;                 %FT is the Hydrogen storage tank
e_FT_FC_A=0;
e_FC_BAT3_A=0;
e_FC_WT_A=0;
e_DSL3_BAT3_A=0;

e_BAT3_EL_A = e_EL_FT_A;

%ACTIVATION FOR WATER TANK TO ELECTROLYSER
e_WT_EL_A=e_EL_FT_A;

%ACTIVATION FOR FLOW TANK TO FUEL CELL
e_FC_BAT3_A =e_FT_FC_A       ;                      %The Logic for SOC to
CONVERTER is the same as CONVERTER TO SOC

%ACTIVATION FOR FUEL CELL TO WATER TANK
```

```
e_FC_WT_A=e_FC_BAT3_A;
%

% %INITIALIZE SOCs EL AND FC
 SOC_BAT3_A=80  ;%70                                    %Tweek #SOC_BAT3 to alter
the SOC LEVEL FOR BATTERY 3
 SOC_H2_FT_A=90;%80
 SOC_H2O_WT_A=50;%30
%

% %VARIABLE DECLARATION FOR MEMORY
A_e_BAT3_LD3_A=zeros(1,8760);
A_e_PV3_BAT3_A= zeros(1,8760)      ;
A_e_WG2_BAT3_A=zeros(1,8760);
A_e_BAT3_EL_A=zeros(1,8760)       ;
A_e_WT_EL_A= zeros(1,8760);
A_e_EL_FT_A=zeros(1,8760)      ;
A_e_FT_FC_A=zeros(1,8760);
A_e_FC_WT_A=zeros(1,8760);
A_e_FC_BAT3_A=zeros(1,8760);
A_e_DSL3_BAT3_A=zeros(1,8760);
A_F_FC_WT_EL_A=zeros(1,8760);
A_F_EL_FT_FC_A=zeros(1,8760);
A_R_e_FC_BAT3=zeros(1,8760);
A_R_e_BAT3_EL=zeros(1,8760);
% %%%%%%%%%%%%%%%%%%%%%%%%%%%%%%%%%%%%%%%% END OF REAL SYSTEM MICROGRID 3
INITIALIZATION %%%%%%%%%%%%%%%%%%%%%%%%%%%%%%%%%%%%%%%%%%%%%%%%%%%%%%%%
%


% INITIALIZING BATTERY CAPACITY
% Battery3 capacity   3KAh*12V = 36KWh
BAT3_Cap=36000;


%INITIALIZING DIESEL GENERATOR3


%INITIALIZING FUEL CELL AND ELECTROLYSER DYNAMICS
polyn_EL=[-0.000001426704372 0.027954416509736 2.502267281445165];  %Transfer
function for Electrolyser
polyn_FC=[0.000000895442340 0.033197516886985 -0.278092554468687];  %Transfer
function for Fuel Cell

nc_EL=15;                              % no. of cells in the electrolyser
nc_FC=40;                              % no. of cells in the fuel cell
nF=0.87;                               % Efficiency
ne=2;                                  % no. of electron
F=96485;                               % Faraday's constant W/mol
P_BAT3_EL=4000;                            % Power required per time by the
Electrolyser
P_FC_BAT3=3000;                            % Max power the Fuel cell can
deliver

WT_Cap=2.1749e+03*2;
```

```
FT_Cap=974.3583*2;%2000*10

%INITIALIZE SOCs EL AND FC
SOC_BAT3=80  ;                                    %Tweek #SOC_BAT3 to alter the
SOC LEVEL FOR BATTERY 3
SOC_H2_FT=100;
SOC_H2O_WT=30;

%%%% ELECTROLYSER ACTIVATION %%%%%%%
EL_SUMMER=zeros(1,8760);
EL_SUMMER(1:8760)=1;
%EL_SUMMER(1:2160)=1;
%EL_SUMMER(6553:8760)=1;

%%%% FUEL CELL ACTIVATION %%%%%
FC_WINTER=zeros(1,8760);
FC_WINTER(1:8760)=1;%(100:8000)(2881:5832)

%VARIABLE DECLARATION FOR MEMORY
A_e_BAT3_LD3=zeros(1,8760);
A_e_PV3_BAT3= zeros(1,8760)      ;
A_e_WG2_BAT3=zeros(1,8760);
A_e_BAT3_EL=zeros(1,8760)       ;
A_e_WT_EL= zeros(1,8760);
A_e_EL_FT=zeros(1,8760)      ;
A_e_FT_FC=zeros(1,8760);
A_e_FC_WT=zeros(1,8760);
A_e_FC_BAT3=zeros(1,8760);
A_e_DSL3_BAT3=zeros(1,8760);
A_F_FC_WT_EL=zeros(1,8760);
A_F_EL_FT_FC=zeros(1,8760);

%
% A_r_PV3_BAT3=zeros(1,8760);
% A_r_WG2_BAT3=zeros(1,8760);
% A_r_BAT3_EL=zeros(1,8760);
% A_r_WT_EL=zeros(1,8760);
% A_r_EL_FT=zeros(1,24);
% A_r_FT_FC=zeros(1,24);
% A_r_FC_WT=zeros(1,8760);
% A_r_FC_BAT3=zeros(1,8760);
% A_r_BAT3_LD3=zeros(1,8760);
% A_r_DSL3_BAT3=zeros(1,8760);



A_g_FC_BAT3=zeros(1,8760);
A_g_EL_FT1=zeros(1,8760);
A_g_EL_FT2=zeros(1,8760);


%%%%%%%%%%%%%%%%%%%%%%%%%%%%%%%%%%%%%%%%%%%%%%%%%%%%%%%%%%%%%ACTUAL
%%%%%%%%%%%%%%%%%%%%%%%%%%%%%%%%%%%%%%%%%%%%%%%%%%%%%%%%%%%%%INITIALIZATION
%%%%%%%%%%%%%%%%%%%%%%%%%%%%%%%%%%%%%%%%%%%%%%%%%%%%%%%%%%%%%%%%%%%%%%%%%%%
%INITIALIZING ACTIVATION STATES OF THE NODES
```

```
e_BAT3_LD3_A=1;
e_PV3_BAT3_A=0   ;               %PV3 is the solar panel in microgrid 3, WG2
is the wind turbine in microgrid 3
e_WG2_BAT3_A=0;
e_BAT3_EL_A=0    ;               %EL is the ELectrolyser, WT is the Water
Tank, FC is the Fuel Cell
e_WT_EL_A=0    ;
e_EL_FT_A=0    ;                 %FT is the Hydrogen storage tank
e_FT_FC_A=0;
e_FC_BAT3_A=0;
e_FC_WT_A=0;
e_DSL3_BAT3_A=0;

e_BAT3_EL_A = e_EL_FT_A;

%ACTIVATION FOR WATER TANK TO ELECTROLYSER
e_WT_EL_A=e_EL_FT_A;

%ACTIVATION FOR FLOW TANK TO FUEL CELL
e_FC_BAT3_A =e_FT_FC_A       ;                      %The Logic for SOC to
CONVERTER is the same as CONVERTER TO SOC

%ACTIVATION FOR FUEL CELL TO WATER TANK
e_FC_WT_A=e_FC_BAT3_A;

% %INITIALIZE SOCs EL AND FC
 SOC_BAT3_A=80  ;                                %Tweek #SOC_BAT3 to alter
the SOC LEVEL FOR BATTERY 3
 SOC_H2_FT_A=100;
 SOC_H2O_WT_A=30;

% %VARIABLE DECLARATION FOR MEMORY
A_e_BAT3_LD3_A=zeros(1,8760);
A_e_PV3_BAT3_A= zeros(1,8760)      ;
A_e_WG2_BAT3_A=zeros(1,8760);
A_e_BAT3_EL_A=zeros(1,8760)       ;
A_e_WT_EL_A= zeros(1,8760);
A_e_EL_FT_A=zeros(1,8760)      ;
A_e_FT_FC_A=zeros(1,8760);
A_e_FC_WT_A=zeros(1,8760);
A_e_FC_BAT3_A=zeros(1,8760);
A_e_DSL3_BAT3_A=zeros(1,8760);
A_F_FC_WT_EL_A=zeros(1,8760);
A_F_EL_FT_FC_A=zeros(1,8760);
A_R_e_FC_BAT3=zeros(1,8760);
A_R_e_BAT3_EL=zeros(1,8760);


%%%%%%%%%%%%%%%%%%%%%%%%%%%%%%%%%%%%%%%%%%%%%%%%%%%%%%%%%%%%%%%%%%%%%%%%%%%
```

```
%%
%%%%%%%%%%%%%%%%%%%%%%%%%%%%%%%%%%%%%%%%%%%%%%%%%%%%%%%%%%%%%%%%%%%%%%%%%%%%%%%
%%%%%%
%%
%% PREDICTION USED TO DETERMINE PGCC

EL_ON1=zeros(24,24);
EL_ON2=zeros(24,24);
FC_ON=zeros(24,24);


startt=1;
start=1;
stop=24;
Counter=0;
Counter2=0;


k=1;

PINCH_DATA=[];
A_SOC_BAT3=zeros(1,240)
Recall=zeros(1,240)





LD3_A=repmat(Actual_load,1,365);

ran_PV=repmat(noise_for_PV,1,365);
P_BAT3_EL=zeros(1,8760)*P_BAT3_EL;
P_FC_BAT3=zeros(1,8760)*P_FC_BAT3;
A_g_EL_FT=zeros(1,8760);
% P_BAT3_EL(1)=4000;
% P_FC_BAT3(1)=3000;

A_SOC_ref=zeros(1,8760);
A_IAE=zeros(1,8760);
A_FC_ATTEMPT=zeros(1,8760);
A_EL_ATTEMPT=zeros(1,8760);
A_Power_FC=zeros(1,8760);
number_count=0;
EPL=zeros(1,8760);
A_t_violation_EL=zeros(1,24);
Unserved_load=0;
```

```
Lost_Energy=0;
Excess_Energy_lost=0;


 WT_Cap=2.1749e+03*300;%15;
 FT_Cap=974.3583*150;%10;%2000*10



LD3=dlmread('LOAD_AVERAGE.csv')*0.5;


while k<=8760%71%719%8760
for k=1:1:8761%72%720%8761% %determines the number of hours to run the Pinch
analysis
%for k=start:1:stop

    Counter2=Counter2+1;

     if(stop-start)==23||(A_SOC_BAT3(k-1)<30||A_SOC_BAT3(k-1)>90)||
(A_SOC_BAT3(k-1)>5+A_SOC_BAT3_A(k-1) || A_SOC_BAT3(k-1)<-5+A_SOC_BAT3_A(k-1))
% &&SOC_BAT3>10/100*SOC_BAT3_A %Do recalculation only if the deviation is
state>10%(A_SOC_BAT3(k-1)<30||A_SOC_BAT3(k-1)>90)||

     P_BAT3_EL(k:end)=0;
%      P_FC_BAT3(k:end)=0;
     end

   for l=1:1:24
       start=k;
       if k==1
          stop=24;
       startt=1;
       end
        if k==1625%73%36%20||k==24||40 %48&&l==1%41%24
       %  pause(2)
        %display('paused for 0.5 Seconds')
       end

 if (stop-start)==23||(A_SOC_BAT3(k-1)<30||A_SOC_BAT3(k-1)>90)||
(A_SOC_BAT3(k-1)>5+A_SOC_BAT3_A(k-1) || A_SOC_BAT3(k-1)<-5+A_SOC_BAT3_A(k-1))
% &&SOC_BAT3>10/100*SOC_BAT3_A %Do recalculation only if the deviation is
state>10%(A_SOC_BAT3(k-1)<30||A_SOC_BAT3(k-1)>90)||
  %Power_FC=0;  %reset the MOES if the horizon changes

  %P_FC_BAT3=zeros(1,8760);
 if start>1
SOC_BAT3=A_SOC_BAT3_A(start-1)  ;                                  %Tweek
#SOC_BAT3 to alter the SOC LEVEL FOR BATTERY 3
SOC_H2_FT=A_SOC_H2_FT_A(start-1);
SOC_H2O_WT=A_SOC_H2O_WT_A(start-1);
% e_BAT3_EL = A_e_BAT3_EL_A(start-1);
% e_FC_BAT3=  A_e_FC_BAT3_A(start-1);
```

```
e_BAT3_LD3= A_e_BAT3_LD3_A(start-1)  ;
e_PV3_BAT3= A_e_PV3_BAT3_A(start-1)  ;
e_WG2_BAT3=  A_e_WG2_BAT3_A(start-1) ;

e_WT_EL = A_e_WT_EL_A(start-1);
e_EL_FT = A_e_EL_FT_A(start-1);
e_FT_FC= A_e_FT_FC_A(start-1);
e_FC_WT=  A_e_FC_WT_A(start-1);


e_DSL3_BAT3= A_e_DSL3_BAT3_A(start-1);

%ACTIVATION FOR BATTERY TO ELECTROLYSER
%e_BAT3_EL = e_EL_FT;

%ACTIVATION FOR WATER TANK TO ELECTROLYSER
e_WT_EL=e_EL_FT;

%ACTIVATION FOR FLOW TANK TO FUEL CELL
e_FT_FC=e_FC_BAT3;                              %The Logic for SOC to
CONVERTER is the same as CONVERTER TO SOC

%ACTIVATION FOR FUEL CELL TO WATER TANK
e_FC_WT=e_FC_BAT3;
 end
%%%%%%%%%%%%%%%%%%%%%%%%

 if start==1
SOC_BAT3=80 ;
SOC_H2O_WT=30;
SOC_H2_FT=100   ;
%INITIALIZING ACTIVATION STATES OF THE NODES
e_BAT3_LD3=1;
e_PV3_BAT3=0   ;                %PV3 is the solar panel in microgrid 3, WG2 is
the wind turbine in microgrid 3
e_WG2_BAT3=0;
e_BAT3_EL=0    ;                %EL is the ELectrolyser, WT is the Water Tank,
FC is the Fuel Cell
e_WT_EL=0    ;
e_EL_FT=0    ;                  %FT is the Hydrogen storage tank
e_FT_FC=0;
e_FC_BAT3=0;
e_FC_WT=0;
e_DSL3_BAT3=0;

e_BAT3_EL = e_EL_FT;

% ACTIVATION FOR WATER TANK TO ELECTROLYSER
e_WT_EL=e_EL_FT;

% ACTIVATION FOR FLOW TANK TO FUEL CELL
e_FC_BAT3 =e_FT_FC       ;                       %The Logic for SOC to
CONVERTER is the same as CONVERTER TO SOC
```

```
% ACTIVATION FOR FUEL CELL TO WATER TANK
e_FC_WT=e_FC_BAT3;
   end




 for j=k:1:stop %j=start:1:stop
%    if start==1 %stop-start==23 &&
%        c=-1;
%    else
%        c=0;
%    end
if k>0
    if
k==stop&&l>1&&ceil(Pinch_Data(stop))~=ceil(Pinch_Data(startt))&&(Pinch_Data(s
tartt)>=30&&Pinch_Data(startt)<=90)
    sss=-1;%0
else
    sss=0;
    end
end
%Counter=Counter+1
%%%%%% MICROGRID3 %%% MICROGRID 3 %%%%%% MICROGRID3 %%% MICROGRID 3 %%%%%%
MICROGRID3 %%% MICROGRID 3

%%%%%ITERATION %%%% ITERATION

%INSTANTENOUS LOAD POWER

P_BAT3_LD3=LD3(j);


%POWER FROM PV SYSTEM
PV3_no=217;
Area_PV3=0.52*PV3_no        ;           %Area for 70W solar panel

P_PV3_BAT3=Area_PV3*I_Rad(j)*0.1 ;     % 0.1 is efficiency for
polycrystalline

%POWER WIND TURBINE GENERATOR

P_WG2_BAT3= 0.5 * Air_den *Area_sw  * Cp* ((Wind_vel(j))^3) * Ng * Nb*WT_no ;



%FUEL CELL AND ELECTROLYSER POWER FLOW

I_EL=polyval(polyn_EL,P_BAT3_EL(j))  ;       % Power flow as a function of
Power supplied to the electroliser
I_FC=polyval(polyn_FC,P_FC_BAT3(j))  ;     % Power flow as a function of
Power supplied to the electroliser
```

```
%*e_BAT3_EL *e_FC_BAT3*

Fout_FC_WT_H2O= e_FC_WT * 0.85 * nc_FC * 3600* I_FC  / (nF*ne*F)  ;      %
The flow of H2O from FC to WT +VE flow since it goes in to the Water Tank
%A_Fout_FC_WT_H2O(k,j)=Fout_FC_WT_H2O;


Fout_EL_FT_H2= e_EL_FT * nF*nc_EL *  3600* I_EL/(ne*F)  ;                  %
The flow of H2 from EL to FT   +VE flow since it goes into a Flow Tnak
%A_Fout_EL_FT_H2(k,j)=Fout_EL_FT_H2;


Fout_FT_FC_H2= e_FT_FC * nc_FC * 3600 *I_FC /(nF*ne*F)   ;                 %
The flow of H2 out of the FT to the FC  based on the needs of the  FC i.e
*eff -VE flow since it flows out
%A_Fout_FT_FC_H2(k,j)=Fout_FT_FC_H2;


Fout_WT_H2O= e_WT_EL* 1.3 * nF * nc_EL * 3600 * I_EL /(ne*F) ;        % The
flow of H2O from the WT to the EL based on what the EL needs. The Flow is -VE
since it depletes the Water Tank
%A_Fout_WT_H2O(k,j)=Fout_WT_H2O;

%%WATER TANK AND FLOW TANK MAX CAPACITY CALCULATION
%WT_Cap=1.3*24*(I_FC*nc_FC*nF)*3600/(ne*F)
%Calculate at max Power then set it manually.  Water Tank capacity should
hold moles/hr for 24hrs

%FT_Cap=1.3*24*(I_EL*nc_EL*nF)*3600/(ne*F)                              %Storage
Tank capacity should hold moles/hr for 24hrs
R=normrnd(0,2)*10;

%NET ENERGY FLOW OF POWER STORED IN THE BATTERY
A_P_PV3_BAT3(j)=P_PV3_BAT3;
A_P_WG2_BAT3(j)=P_WG2_BAT3;
P_RES3=(e_PV3_BAT3*P_PV3_BAT3)
+(e_WG2_BAT3*P_WG2_BAT3)+(e_DSL3_BAT3*P_DSL3_BAT3)+(A_g_FC_BAT3(j+sss)*P_FC_B
AT3(j+sss));
A_P_RES3(j)=P_RES3;
P_BAT3= P_RES3-(e_BAT3_LD3*P_BAT3_LD3)-(A_g_EL_FT(j+sss)*P_BAT3_EL(j+sss));
if P_BAT3<=0
   Deficit_P_BAT3=1;
else
    Deficit_P_BAT3=0;
end
A_Deficit_P_BAT3(j)=Deficit_P_BAT3;


if P_BAT3>LD3(j)&&SOC_BAT3>90&&SOC_H2_FT>90 && SOC_H2O_WT>40
    Surplus_P_BAT3=1;
else
    Surplus_P_BAT3=0;
end
```

```
A_Surplus_P_BAT3(j)=Surplus_P_BAT3;


A_P_BAT3(j)=(P_BAT3/BAT3_Cap)*100 ;
SOC_BAT3=SOC_BAT3+(P_BAT3/BAT3_Cap)*100 ;
if SOC_BAT3<=0;
    SOC_BAT3=0;
end
if SOC_BAT3>=100
    SOC_BAT3=100;
end

A_SOC_BAT3(j)=SOC_BAT3;
if SOC_BAT3<30
   Deficit_SOC_BAT3=1;
else
   Deficit_SOC_BAT3=0;
end
 A_Deficit_SOC_BAT3(j)= Deficit_SOC_BAT3;

 if j<=1
     c=1;
 else
     c=0;
 end

% WATER STORED IN THE WATER TANK
 FC_WT_EL=100*(Fout_FC_WT_H2O - Fout_WT_H2O)/WT_Cap;
SOC_H2O_WT= SOC_H2O_WT +FC_WT_EL;
if SOC_H2O_WT>=100
    SOC_H2O_WT=100;
end
    if  SOC_H2O_WT<=0
        SOC_H2O_WT=0;
    end
A_SOC_H2O_WT(j)=SOC_H2O_WT;
A_F_FC_WT_EL(j)=FC_WT_EL;

%HYDROGEN STORED IN THE FLOW TANK
EL_FT_FC=100*(Fout_EL_FT_H2 - Fout_FT_FC_H2)/FT_Cap;
SOC_H2_FT=SOC_H2_FT + EL_FT_FC;
if SOC_H2_FT>=100                          %LIMITS FOR SOC OF WATER TANK AND
FLOW TANK
    SOC_H2_FT=100;
end
if SOC_H2_FT<=0
    SOC_H2_FT=0;
end
A_SOC_H2_FT(j)=SOC_H2_FT;
A_F_EL_FT_FC(j)=EL_FT_FC;

%ACTIVATION FOR PV TO BATTERY
str_PV3_BAT3=0      ;                     % start charging battery if SOC max
is < 90%
stp_PV3_BAT3=90;
```

```
if SOC_BAT3<stp_PV3_BAT3
    q_PV3_BAT3=1;
else
    q_PV3_BAT3=0;
end
e_req_PV3_BAT3=q_PV3_BAT3  ;            %The logic determines when the
battery SOC is below the stop point then the Battery makes a request

a_PV3_BAT3=1;
e_avail_PV3_BAT3= a_PV3_BAT3 || r_PV3_BAT3;
e_PV3_BAT3= e_avail_PV3_BAT3 && e_req_PV3_BAT3 && g_PV3_BAT3;


%ACTIVATION FOR WIND TURBINE WG2 TO BATTERY BAT3
str_WG2_BAT3=0   ;                        % start charging battery if SOC max
is < 90%
stp_WG2_BAT3=90;

if SOC_BAT3<stp_WG2_BAT3
    q_WG2_BAT3=1;
else
    q_WG2_BAT3=0;
end
e_req_WG2_BAT3=q_WG2_BAT3    ;          %The logic determines when the
battery SOC is below the stop point then the Battery makes a request
a_WG2_BAT3=1;
e_avail_WG2_BAT3 = a_WG2_BAT3 || r_WG2_BAT3;

e_WG2_BAT3 = e_avail_WG2_BAT3 && e_req_WG2_BAT3 && g_WG2_BAT3;

%ACTIVATION FOR DIESEL TO BATTERY
str_DSL3_BAT3=20;
stp_DSL3_BAT3=30;
if k<=1
    c=1;
else
    c=0;
end
if SOC_BAT3<str_DSL3_BAT3 %||
[SOC_BAT3>str_DSL3_BAT3&&SOC_BAT3<stp_DSL3_BAT3] && A_e_DSL3_BAT3(j+c-1)==1
q_DSL3_BAT3=1;
else
q_DSL3_BAT3=0;
end
e_req_DSL3_BAT3 =q_DSL3_BAT3;

a_DSL3_BAT3=1       ;                          %Availability logic for
Diesel generator

e_avail_DSL3_BAT3 = a_DSL3_BAT3 || r_DSL3_BAT3;

e_DSL3_BAT3= e_avail_DSL3_BAT3 && e_req_DSL3_BAT3 && g_DSL3_BAT3;
```

```
%ACTIVATION FOR FUEL CELL TO BATTERY
if FC_WINTER(k)==1
    FC_ON_WINTER=1;
else
    FC_ON_WINTER=0;
end
str_FC_BAT3=99  ;      %90                  %start and stop min and max
threshold to make request by Battery for Fuel cell to supply power
stp_FC_BAT3=80;
if FC_ON_WINTER==1 && SOC_BAT3<str_FC_BAT3  %|| SOC_BAT3>str_FC_BAT3 &&
SOC_BAT3<stp_FC_BAT3 && A_e_FC_BAT3(j-1+c)==1       %i==[2881:5832] ensures
Summer operation only
    q_FC_BAT3=1 ;
else
    q_FC_BAT3=0;
end
e_req_FC_BAT3 =   q_FC_BAT3;

  str_FC_WT=90      ;                              %start and stop min and max
threshold to make request for Fuel cell to supply power to Battery based on
Water Tank not full and Flow tank above minimum
  stp_FC_WT=90;

if SOC_H2O_WT<str_FC_WT
  a1_FC_WT=1;
else
  a1_FC_WT=0;
end

str_FT_FC =10   ;                                   %start and stop SOC
HYDROGEN FLOW TANK REQUIRED to supply FUEL CELL
stp_FT_FC =10;
if SOC_H2_FT>str_FT_FC
  a2_FT_FC=1;
else
  a2_FT_FC=0;
end

e_avail_FC_BAT3= a1_FC_WT && a2_FT_FC ; %|| r_FT_FC;


e_FC_BAT3 =  A_g_FC_BAT3(j-1+c);

%ACTIVATION FOR BATTERY TO LOAD
% e_BAT3_LD3=e_avail_BAT3_LD3 && e_avail_BAT3_LD3  && g_BAT3_LD3


%ACTIVATION FOR ELECTROLYSER TO FLOW TANK
str_EL_FT = 99       ;%90                    %start and stop SOC for engaging
the ELECTROLYSER TO SUPPLY FLOW TANK
stp_EL_FT= 100;
if SOC_H2_FT<str_EL_FT                  %FT MAKES REQUEST FOR H2 SUPPLY FROM
ELECTROLYSER
    q_EL_FT=1;
```

```
else
    q_EL_FT=0;
end
e_req_EL_FT= q_EL_FT;


if EL_SUMMER(k)==1                    %Scan the array if the index is equal to
1 then logic is true else it is false for zero
    EL_ON_SUMMER=1;
    else
    EL_ON_SUMMER=0;
end

str_BAT3_EL= 70   ;                    %start and stop SOC for engaging the
BATTERY TO SUPPLY ELECTROLYSER
stp_BAT3_EL =33;
% if Counter<=1
%     c=2;
% else
%     c=0;
% end             %This corrects the indexing by assuming the past was zero
if EL_ON_SUMMER==1 && SOC_BAT3>str_BAT3_EL || SOC_BAT3<str_BAT3_EL &&
SOC_BAT3>stp_BAT3_EL %&& A_e_EL_FT(j+c-1)==1  %i==[2881:5832] ensures Winter
operation only
  a1_BAT3_EL = 1;
else

  a1_BAT3_EL=0;
end


str_WT_EL =10   ;                      %start and stop SOC WATER TANK
REQUIRED to supply ELEctrolyser
stp_WT_EL =10;
if SOC_H2O_WT>str_WT_EL
  a2_EL_FT=1;
else
  a2_EL_FT=0;
end


e_avail_EL_FT= a1_BAT3_EL && a2_EL_FT ; %|| r_EL_FT;
e_EL_FT=(A_g_EL_FT1(j-1+c) || A_g_EL_FT2(j-1+c));


%ACTIVATION FOR BATTERY TO ELECTROLYSER
e_BAT3_EL = e_EL_FT;

%ACTIVATION FOR WATER TANK TO ELECTROLYSER
e_WT_EL=e_EL_FT;

%ACTIVATION FOR FLOW TANK TO FUEL CELL
e_FT_FC=e_FC_BAT3   ;                          %The Logic for SOC to
CONVERTER is the same as CONVERTER TO SOC
```

```
%ACTIVATION FOR FUEL CELL TO WATER TANK
e_FC_WT=e_FC_BAT3;

A_e_BAT3_LD3(j)=e_BAT3_LD3;
A_e_PV3_BAT3(j)= e_PV3_BAT3;
A_e_WG2_BAT3(j)=e_WG2_BAT3;
A_e_BAT3_EL(j)=e_BAT3_EL ;
A_e_WT_EL(j)= e_WT_EL ;
A_e_EL_FT(j)=e_EL_FT  ;
A_e_FT_FC(j)=e_FT_FC;
A_e_FC_WT(j)=e_FC_WT;
A_e_FC_BAT3(j)=e_FC_BAT3;
A_e_DSL3_BAT3(j)=e_DSL3_BAT3;

%%%%%%%%%%%%%%%%%%%% END OF MG3 LOW LEVEL PMS
%%%%%%%%%%%%%%%%%%%%%%%%%%%%%%%%%%


Pinch_Data(j)=SOC_BAT3;
%PINCH_DATA(l,j,k)=SOC_BAT3;
 if l==1 && startt==k
 Pinch_Data_Raw_before_shaping(j)=SOC_BAT3; %first recompution L=1
 end
 if l==2 && startt==k
 Pinch_Data_Raw_before_shaping2(j)=SOC_BAT3; %first recompution L=1
 end
 if l==3 && startt==k
 Pinch_Data_Raw_before_shaping3(j)=SOC_BAT3; %first recompution L=1
 end
 if l==4 && startt==k
 Pinch_Data_Raw_before_shaping4(j)=SOC_BAT3; %first recompution L=1
 end
 if l==5 && startt==k
 Pinch_Data_Raw_before_shaping5(j)=SOC_BAT3; %first recompution L=1
 end
 if l==6 && startt==k
 Pinch_Data_Raw_before_shaping6(j)=SOC_BAT3; %first recompution L=1
 end
 if l==7 && startt==k
 Pinch_Data_Raw_before_shaping7(j)=SOC_BAT3; %first recompution L=1
 end
 if l==8 && startt==k
 Pinch_Data_Raw_before_shaping8(j)=SOC_BAT3; %first recompution L=1
 end
 if l==9 && startt==k
 Pinch_Data_Raw_before_shaping9(j)=SOC_BAT3; %first recompution L=1
 end
  if l==10 && startt==k
 Pinch_Data_Raw_before_shaping10(j)=SOC_BAT3; %first recompution L=1
  end
  if l==11 && startt==k
 Pinch_Data_Raw_before_shaping11(j)=SOC_BAT3; %first recompution L=1
  end
```

```
   if l==24 && startt==k
 Pinch_Data_Raw_after_shaping(j)=SOC_BAT3 ;%first recomputation when L=24
   end
if l==24
 PINCH_DIAG(k,j)=SOC_BAT3;   % Extract the recomputation from here
end
Pinch_shaping(l,j)=SOC_BAT3;% insight  array vector to the iterative shaping
via PoPA
Pinch_shaping(l,j)=SOC_BAT3;
% PINCH_DATAA(Counter2,j)=SOC_BAT3;
 end
%run this loop while Smin and Smax violation exist

      Recomp=1; %signal for recomputation
Recomputation(k)=Recomp;

%PINCH ANALYSIS AND DETERMINATION OF G OVERIDE

%%START PINCH%%
SOC_BAT3_min=30;          %Minimum and Maximum Pinch Targets
SOC_BAT3_max=90;
S_UP=90;
S_LO=30;
S_min=min(Pinch_Data(start:stop-1));
S_max=max(Pinch_Data(start:stop-1));
if S_min<SOC_BAT3_min
    [~, t_violation]=min(Pinch_Data(start:stop-1));
   t_violation=t_violation+start-1;% corrects the index of the minimum
violation
   %t_violation= find(Pinch_Data(1:stop)==S_min)     ;           % time of
violation of the Lower pinch

   E_target =(SOC_BAT3_min - S_min)*(BAT3_Cap/100);%*P_FC_BAT3));
   t_duration = ceil(E_target);%/BAT3_Cap;             %Time duration needed
based on allowable amount of energy from battery per hour
%    if t_violation-1<start
%       t_violation=start+1
%    end
%
%   A_g_FC_BAT3(t_violation)= 1;
%   P_FC_BAT3(t_violation)=E_target;%

%%DAY_AHEAD PoPA CUMMULATIVE ACTION
  A_g_FC_BAT3(start)=1;
  %Power_FC=E_target;
  %Power_FC=Power_FC+E_target;% MOES cummulative from all previous violation
  %A_Power_FC(startt,l)=Power_FC;
  P_FC_BAT3(start)=E_target+P_FC_BAT3(start);
  if (P_FC_BAT3(start)/BAT3_Cap*100)+Pinch_shaping(1,start)>S_UP
      P_FC_BAT3(start)=P_FC_BAT3(start)-
((Pinch_shaping(1,start)+(P_FC_BAT3(start)*100/BAT3_Cap)-S_UP))*BAT3_Cap/100
; % limits the FC for MOES to Upper Pinch limit
  end
%   if P_FC_BAT3(start)>6000
%      P_FC_BAT3(start)=6000;% Limits FC power to the maximum capcity
```

```
%   end

elseif   S_max>SOC_BAT3_max
    [~, t_violation_EL]=max(Pinch_shaping(1,start:stop-1));% to change from
day ahead to adaptive use start intead of startt which is the begining of the
horizon

        %t_violation_EL= max(find(Pinch_Data(1:stop)==S_max))     ;

        %%A_g_EL_FT1(start:stop-1)= Pinch_Data(start:stop-1)>SOC_BAT3_max;
former

Ex_target=(S_max - SOC_BAT3_max)*(BAT3_Cap/(100));     % former
% A_g_EL_FT1(t_violation_EL)=1;
% P_BAT3_EL(t_violation_EL)=abs(Ex_target);%

%%DAY_AHEAD PoPA CUMMULATIVE ACTION
    t_violation_EL=t_violation_EL+start-1; %start-1
    Ex_target=(S_max - SOC_BAT3_max)*(BAT3_Cap/(100));% former
%     Power_EL=Ex_target;
%     Power_EL=Power_EL+Ex_target;% MAE cummulative from previous violation
    A_g_EL_FT1(t_violation_EL)=1;
    P_BAT3_EL(t_violation_EL)=Ex_target+P_BAT3_EL(t_violation_EL);

   if Pinch_Data(t_violation_EL)-
(P_BAT3_EL(t_violation_EL)/BAT3_Cap)*100<S_LO    % Limits the energy
extracted by the EL to be less than or equal to the lower Pinch
     if Pinch_Data(t_violation_EL)-
(P_BAT3_EL(t_violation_EL)/BAT3_Cap)>0||Pinch_Data(t_violation_EL)-
(P_BAT3_EL(t_violation_EL)/BAT3_Cap)==0 % if the value is positive

         P_BAT3_EL(t_violation_EL)=((Pinch_Data(t_violation_EL)-
P_BAT3_EL(t_violation_EL))+ (S_LO-(Pinch_Data(t_violation_EL)-
P_BAT3_EL(t_violation_EL))))*BAT3_Cap/100;

        %P_BAT3_EL(t_violation_EL)=((Pinch_Data(t_violation_EL)-
P_BAT3_EL(t_violation_EL))+ (S_LO-(Pinch_Data(t_violation_EL)-
P_BAT3_EL(t_violation_EL))))*BAT3_Cap/100;

     elseif Pinch_Data(t_violation_EL)-(P_BAT3_EL(t_violation_EL)/BAT3_Cap)<0
% for negative power violation limit of the EL
          P_BAT3_EL(t_violation_EL)=(Pinch_Data(t_violation_EL)-
(P_BAT3_EL(t_violation_EL)/BAT3_Cap)+(S_LO+(abs(Pinch_Data(t_violation_EL)-
(P_BAT3_EL(t_violation_EL)/BAT3_Cap)))))*BAT3_Cap/100;
    % Pinch_Data(t_violation_EL)=(Pinch_Data(t_violation_EL)-
(P_BAT3_EL(t_violation_EL)/BAT3_Cap)+(S_LO+(abs(Pinch_Data(t_violation_EL)-
(P_BAT3_EL(t_violation_EL)/BAT3_Cap)))))*BAT3_Cap/100;

     end
   end


%     if P_BAT3_EL(t_violation_EL)>4000
%        P_BAT3_EL(t_violation_EL)=4000; %Limits EL power to max capacity
```

```
%     end

else

if
ceil(Pinch_Data(stop))~=50&&(Pinch_Data(startt)>=30&&Pinch_Data(startt)<=90)%
&&k==0%ceil(Pinch_Data(stop))~=ceil(Pinch_Data(startt))&&(Pinch_Data(startt)>
=30&&Pinch_Data(startt)<=90)
    EE_target=(Pinch_Data(stop) - 50)*(BAT3_Cap/(100));

    if EE_target<0 %&& P_FC_BAT3(stop-1)>abs(EE_target)
           A_g_FC_BAT3(stop-1)=1;
           A_g_EL_FT2(stop-1)=0;
           A_g_EL_FT1(stop-1)=0;
           P_FC_BAT3(stop-1)=abs(EE_target);
          % P_FC_BAT3(stop-1)=P_FC_BAT3(stop-1)-abs(EE_target);% has to be
cummulative if not it will mismatch. if needed was 50KW and was match the
begining and error occurs u want to integrate by supplying what is needed now
+wat was there before.
           P_BAT3_EL(stop-1)=0;
%
%      if P_FC_BAT3(stop-1)>6000
%         P_FC_BAT3(stop-1)=6000;% Limits FC power to the maximum capcity
%      end


     else
        if EE_target>0 && P_FC_BAT3(stop-1)~=0 && P_FC_BAT3(stop-
1)>abs(EE_target)
          A_g_EL_FT2(stop-1)=0;
          A_g_FC_BAT3(stop-1)=1;
          P_BAT3_EL(stop-1)=0;%+P_BAT3_EL(stop-1)% you want to integrate the
energy with wat was already matched if error occurs
          P_FC_BAT3(stop-1)=P_FC_BAT3(stop-1)-EE_target;% to reduce the
Energy previously set you need to remove it from the exixting energy

%           if P_FC_BAT3(stop-1)>6000
%              P_FC_BAT3(stop-1)=6000;% Limits FC power to the maximum
capcity
%           end

        elseif EE_target>0 && P_FC_BAT3(stop-1)~=0 && P_FC_BAT3(stop-
1)<EE_target
         A_g_EL_FT2(stop-1)=1;
         A_g_FC_BAT3(stop-1)=0;
         P_BAT3_EL(stop-1)=EE_target-P_FC_BAT3(stop-1);%
         P_FC_BAT3(stop-1)=0;

%           if P_BAT3_EL(stop-1)>4000
%              P_BAT3_EL(stop-1)=4000; Limits % EL power to max capacity
%           end

        else
           A_g_EL_FT2(stop-1)=1;
           A_g_FC_BAT3(stop-1)=0;
```

```
           P_BAT3_EL(stop-1)=EE_target;%+P_BAT3_EL(stop-1)% you want to
integrate the energy with wat was already matched if error occurs
           P_FC_BAT3(stop-1)=0;

%           if P_BAT3_EL(stop-1)>4000
%              P_BAT3_EL(stop-1)=4000;  % Limits EL power to max capacity
%           end

        end
     end

end
end

% if Pinch_Data(stop-1)~=Pinch_Data(startt)
%     E_target=  (Pinch_Data(stop-1) -
Pinch_Data(startt))*(BAT3_Cap/(100*P_FC_BAT3));
%      if E_target<0
%            A_g_FC_BAT3(stop-1)=1;
%             A_g_EL_FT2(stop-1)=0;
%      else
%          E_target>0
%          A_g_EL_FT2(stop-1)=1;
%           A_g_FC_BAT3(stop-1)=0;
%      end
%
% end
%%%%%%%%%%%%%%%%%%%%%%%%%%%%%%%%%%%%  END OF PINCH %%%%%%%%%%%%%%%%



A_g_EL_FT=A_g_EL_FT1;
A_g_EL_FT=A_g_EL_FT2~=0;

A_g_EL_FT=A_g_EL_FT1+A_g_EL_FT2;


 end
   end


%%%%%%%%%%%%%%%%%%%%%%%%%%%% E.N.D OF M.P.C
%%%%%%%%%%%%%%%%%%%%%%%%%%%%%%%%%%%%%%%%%%%%%%%%%%%%



if k==1%||stop-start==21||stop-start==22
    e=1;
else
    e=0;
end

if    k==1%  k<8760%     tweek to alter availability
 e_avail_EL_FT_A=1;
```

```
e_avail_FC_BAT3_A=1;
end

EL_max=15000;
FC_max=15000;
if A_g_EL_FT(k-1+e)>EL_max  %Constrain the max power of EL
   A_g_EL_FT(k-1+e)=EL_max;
end
if A_g_FC_BAT3(k-1+e)>FC_max
     A_g_FC_BAT3(k-1+e)=FC_max;
end

%ACTIVATION FOR BATTERY TO ELECTROLYSER
e_EL_FT_A=A_g_EL_FT(k-1+e)*e_avail_EL_FT_A;

%ACTIVATION FOR WATER TANK TO ELECTROLYSER
e_WT_EL_A=e_EL_FT_A;

%ACTIVATION FOR FLOW TANK TO FUEL CELL
e_FT_FC_A=A_g_FC_BAT3(k-1+e)*e_avail_FC_BAT3_A;
%The Logic for SOC to CONVERTER is the same as CONVERTER TO SOC
e_FC_BAT3_A=e_FT_FC_A;
%ACTIVATION FOR FUEL CELL TO WATER TANK
e_FC_WT_A=A_g_FC_BAT3(k-1+e)*e_avail_FC_BAT3_A;




%%%%%% MICROGRID3 %%% MICROGRID 3 %%%%%% MICROGRID3 %%% MICROGRID 3 %%%%%%
MICROGRID3 %%% MICROGRID 3

%%%%%ITERATION %%%% ITERATION

%INSTANTENOUS LOAD POWER

P_BAT3_LD3_A=LD3_A(k);
% P_BAT3_LD3_A=random('norm', 1230, 378,1,1);

%POWER FROM PV SYSTEM
PV3_no=217;
Area_PV3=0.52*PV3_no ;           %Area for 70W solar panel
 if k>startt+7 && k<stop-8
     %Random=random('norm', 0, 10,1,1);
    Random;
 else
     Random=0;
 end

P_PV3_BAT3_A=Area_PV3*0.1 *(I_Rad(k)+ran_PV(k)) ;%+Random);  ;%   % 0.1 is
efficiency for polycrystalline
%P_PV3_BAT3=Area_PV3*I_RADOM(k)*0.1 ;

% I_RADOM(k)=I_Rad(k)+Random
```

```
%
% REAL(k)=Area_PV3*I_Rad(k)*0.1
% DIST(k)=Area_PV3*I_RADOM(k)*0.1
%I_REAL(k)=I_Rad(k)




%POWER WIND TURBINE GENERATOR

P_WG2_BAT3_A= 0.5 * Air_den *Area_sw  * Cp* ((Wind_vel(k))^3) * Ng * Nb*WT_no
;



%FUEL CELL AND ELECTROLYSER POWER FLOW

I_EL=polyval(polyn_EL,P_BAT3_EL(k-1+e)*A_g_EL_FT(k-1+e)*e_avail_EL_FT_A)  ;
% Power flow as a function of Power supplied to the electroliser
I_FC=polyval(polyn_FC,P_FC_BAT3(k-1+e)*A_g_FC_BAT3(k-1+e)*e_avail_FC_BAT3_A);
% Power flow as a function of Power supplied to the electroliser

%*e_BAT3_EL *e_FC_BAT3*
e_FC_WT_A=e_FC_BAT3_A;
Fout_FC_WT_H2O_A= e_FC_WT_A * 0.85 * nc_FC * 3600* I_FC  / (nF*ne*F)  ;
% The flow of H2O from FC to WT +VE flow since it goes in to the Water Tank
A_Fout_FC_WT_H2O_A(k)=Fout_FC_WT_H2O_A;


Fout_EL_FT_H2_A= e_EL_FT_A * nF*nc_EL *  3600* I_EL/(ne*F)  ;
% The flow of H2 from EL to FT   +VE flow since it goes into a Flow Tnak
A_Fout_EL_FT_H2_A(k)=Fout_EL_FT_H2_A;


Fout_FT_FC_H2_A= e_FT_FC_A * nc_FC * 3600 *I_FC /(nF*ne*F)   ;
% The flow of H2 out of the FT to the FC  based on the needs of the  FC i.e
*eff -VE flow since it flows out
A_Fout_FT_FC_H2_A(k)=Fout_FT_FC_H2_A;


Fout_WT_H2O_A= e_WT_EL_A* 1.3 * nF * nc_EL * 3600 * I_EL /(ne*F) ;        %
The flow of H2O from the WT to the EL based on what the EL needs. The Flow is
-VE since it depletes the Water Tank
A_Fout_WT_H2O_A(k)=Fout_WT_H2O_A;

%%WATER TANK AND FLOW TANK MAX CAPACITY CALCULATION
%WT_Cap=1.3*24*(I_FC*nc_FC*nF)*3600/(ne*F)
%Calculate at max Power then set it manually.  Water Tank capacity should
hold moles/hr for 24hrs


%FT_Cap=1.3*24*(I_EL*nc_EL*nF)*3600/(ne*F)                              %Storage
Tank capacity should hold moles/hr for 24hrs
```

```
A_FC_ATTEMPT(k)=e_avail_FC_BAT3_A*A_g_FC_BAT3(k-1+e);
A_EL_ATTEMPT(k)=e_avail_EL_FT_A*A_g_EL_FT(k-1+e);
%NET ENERGY FLOW OF POWER STORED IN THE BATTERY
if stop-start==23
    c=-1;
else
    c=0;
end

A_P_PV3_BAT3_A(k)=(e_PV3_BAT3_A*P_PV3_BAT3_A);
A_P_WG2_BAT3_A(k)=P_WG2_BAT3_A;
A_P_BAT3_AA(k)=SOC_BAT3_A*BAT3_Cap/100;
A_P_DSL3_A(k)=(e_DSL3_BAT3_A*P_DSL3_BAT3);
A_P_EL_A(k)=(e_avail_EL_FT_A*A_g_EL_FT(k-1+e)*P_BAT3_EL(k-1+e));
A_P_FC_A(k)=(e_avail_FC_BAT3_A*A_g_FC_BAT3(k-1+e)*P_FC_BAT3(k-1+e));


P_RES3_A=(e_PV3_BAT3_A*P_PV3_BAT3_A)
+(e_WG2_BAT3_A*P_WG2_BAT3_A)+(e_DSL3_BAT3_A*P_DSL3_BAT3)+(e_avail_FC_BAT3_A*A
_g_FC_BAT3(k-1+e)*P_FC_BAT3(k-1+e));%(r_FC_BAT3*P_FC_BAT3);%%
A_P_RES3_A(k)=P_RES3_A;
P_BAT3_A= P_RES3_A -
(((e_BAT3_LD3_A*P_BAT3_LD3_A))+(e_avail_EL_FT_A*A_g_EL_FT(k-1+e)*P_BAT3_EL(k-
1+e)));%( r_BAT3_EL*P_BAT3_EL);%
A_LD3_A(k)=P_BAT3_LD3_A;
%%
%LOLP CALCULATION
ENERGY_in_SYSTEM(k)=(SOC_BAT3_A*BAT3_Cap/100)+P_RES3_A ;
if ((SOC_BAT3_A*BAT3_Cap/100)+P_RES3_A)<(BAT3_Cap*30/100)
    DEFICIT=((SOC_BAT3_A*BAT3_Cap/100)+P_RES3_A);
    LOAD_D=(((e_BAT3_LD3_A*P_BAT3_LD3_A))+(e_avail_EL_FT_A*A_g_EL_FT(k-
1+e)*P_BAT3_EL(k-1+e)));
    number_count=number_count+1;
else
    DEFICIT=0;
    LOAD_D=0;
end
DEFICIT_A(k)=DEFICIT;
LOAD_D_A(k)=LOAD_D;

if P_BAT3_A<0 &&SOC_BAT3_A<30
    UnServed_load=(P_BAT3_A)+Unserved_load;
end

%%
A_P_BAT3_A(k)=(P_BAT3_A/BAT3_Cap)*100 ;
SOC_BAT3_A=SOC_BAT3_A +(P_BAT3_A/BAT3_Cap)*100 ;
if SOC_BAT3_A<=0;
    SOC_BAT3_A=0;
end
if SOC_BAT3_A>=100
    Excess=SOC_BAT3_A +((P_BAT3_A/BAT3_Cap)*100)-100;%Calculate Excess Energy
not saved in the battery
    Excess_Energy_lost=(Excess*BAT3_Cap)/100+Excess_Energy_lost;
    SOC_BAT3_A=100;
```

```
end
A_SOC_BAT3_A(k)=SOC_BAT3_A;

if SOC_BAT3_A<30
   Deficit_SOC_BAT3_A=1;
else
   Deficit_SOC_BAT3_A=0;
end
 A_Deficit_SOC_BAT3_A(k)= Deficit_SOC_BAT3_A;


% WATER STORED IN THE WATER TANK
 FC_WT_EL_A=100*(Fout_FC_WT_H2O_A - Fout_WT_H2O_A)/WT_Cap;
SOC_H2O_WT_A= SOC_H2O_WT_A +FC_WT_EL_A;
if SOC_H2O_WT_A>=100
    SOC_H2O_WT_A=100;
end
    if  SOC_H2O_WT_A<=0
        SOC_H2O_WT_A=0;
    end
A_SOC_H2O_WT_A(k)=SOC_H2O_WT_A;
A_F_FC_WT_EL_A(k)=FC_WT_EL_A;

%HYDROGEN STORED IN THE FLOW TANK
EL_FT_FC_A=100*(Fout_EL_FT_H2_A - Fout_FT_FC_H2_A)/FT_Cap;
SOC_H2_FT_A=SOC_H2_FT_A + EL_FT_FC_A;
if SOC_H2_FT_A>=100                          %LIMITS FOR SOC OF WATER TANK
AND FLOW TANK
    SOC_H2_FT_A=100;
end
if SOC_H2_FT_A<=0
    SOC_H2_FT_A=0;
end
A_SOC_H2_FT_A(k)=SOC_H2_FT_A;
A_F_EL_FT_FC_A(k)=EL_FT_FC_A;

%ACTIVATION FOR PV TO BATTERY
str_PV3_BAT3=0      ;                    % start charging battery if SOC max
is < 90%
stp_PV3_BAT3=90;

if SOC_BAT3_A<stp_PV3_BAT3
    q_PV3_BAT3_A=1;
else
    q_PV3_BAT3_A=0;
end
e_req_PV3_BAT3_A=q_PV3_BAT3_A  ;            %The logic determines when the
battery SOC is below the stop point then the Battery makes a request

a_PV3_BAT3_A=1;
e_avail_PV3_BAT3_A= a_PV3_BAT3_A || r_PV3_BAT3_A;
e_PV3_BAT3_A= e_avail_PV3_BAT3_A && e_req_PV3_BAT3_A && g_PV3_BAT3;


%ACTIVATION FOR WIND TURBINE WG2 TO BATTERY BAT3
```

```
str_WG2_BAT3=0;                          % start charging battery if SOC max is
< 90%
stp_WG2_BAT3=90;

if SOC_BAT3_A<stp_WG2_BAT3
    q_WG2_BAT3_A=1;
else
    q_WG2_BAT3_A=0;
end
e_req_WG2_BAT3_A=q_WG2_BAT3_A ;          %The logic determines when the
battery SOC is below the stop point then the Battery makes a request
a_WG2_BAT3_A=1;
e_avail_WG2_BAT3_A = a_WG2_BAT3_A || r_WG2_BAT3_A;

e_WG2_BAT3_A = e_avail_WG2_BAT3_A && e_req_WG2_BAT3_A && g_WG2_BAT3;

%ACTIVATION FOR DIESEL TO BATTERY
str_DSL3_BAT3=20;
stp_DSL3_BAT3=30;
if k<=1
    c=1;
else
    c=0;
end

if SOC_BAT3_A<str_DSL3_BAT3 ||
[SOC_BAT3_A>str_DSL3_BAT3&&SOC_BAT3_A<stp_DSL3_BAT3] && A_e_DSL3_BAT3_A(k+c-
1)==1
q_DSL3_BAT3_A=1;
else
q_DSL3_BAT3_A=0;
end
e_req_DSL3_BAT3_A =q_DSL3_BAT3_A;

a_DSL3_BAT3_A=1  ;                           %Availability logic for Diesel
generator

e_avail_DSL3_BAT3_A = a_DSL3_BAT3_A || r_DSL3_BAT3_A;

e_DSL3_BAT3_A= e_avail_DSL3_BAT3_A && e_req_DSL3_BAT3_A && g_DSL3_BAT3;


%ACTIVATION FOR FUEL CELL TO BATTERY

str_FC_BAT3=90;                         %start and stop min and max threshold
to make request by Battery for Fuel cell to supply power
stp_FC_BAT3=80;
if SOC_BAT3_A<str_FC_BAT3  || SOC_BAT3_A>str_FC_BAT3 &&
SOC_BAT3_A<stp_FC_BAT3 && A_e_FC_BAT3_A(k+c-1)==1       %i==[2881:5832]
ensures Summer operation only
    q_FC_BAT3_A=1 ;
else
    q_FC_BAT3_A=0;
end
e_req_FC_BAT3_A =   q_FC_BAT3_A;
```

```
  str_FC_WT_A=90 ;                                %start and stop min and max
threshold to make request for Fuel cell to supply power to Battery based on
Water Tank not full and Flow tank above minimum
  stp_FC_WT_A=90;

if SOC_H2O_WT_A<str_FC_WT_A
  a1_FC_WT_A=1;
else
  a1_FC_WT_A=0;
end

str_FT_FC =10   ;                                    %start and stop SOC
HYDROGEN FLOW TANK REQUIRED to supply FUEL CELL
stp_FT_FC =10;
if SOC_H2_FT_A>str_FT_FC
  a2_FT_FC_A=1;
else
  a2_FT_FC_A=0;
end

e_avail_FC_BAT3_A= a1_FC_WT_A && a2_FT_FC_A;  %|| r_FT_FC;

%e_FC_BAT3 = e_avail_FC_BAT3 && e_req_FC_BAT3 &&A_g_FC_BAT3(k);
% e_FC_BAT3 = e_avail_FC_BAT3 && (r_FC_BAT3 ||A_g_FC_BAT3(k));% ;
% e_FC_BAT3 = e_avail_FC_BAT3 &&(r_FC_BAT3  ~);

%e_FC_BAT3_A = e_req_FC_BAT3_A && A_g_FC_BAT3(k) ;



%ACTIVATION FOR BATTERY TO LOAD
% e_BAT3_LD3=e_avail_BAT3_LD3 && e_avail_BAT3_LD3  && g_BAT3_LD3


%ACTIVATION FOR ELECTROLYSER TO FLOW TANK
str_EL_FT = 90       ;                    %start and stop SOC for engaging
the ELECTROLYSER TO SUPPLY FLOW TANK
stp_EL_FT= 100;
if SOC_H2_FT_A<str_EL_FT                  %FT MAKES REQUEST FOR H2 SUPPLY
FROM ELECTROLYSER
    q_EL_FT_A=1;
else
    q_EL_FT_A=0;
end
e_req_EL_FT_A= q_EL_FT_A;


str_BAT3_EL= 40   ;                    %start and stop SOC for engaging the
BATTERY TO SUPPLY ELECTROLYSER
stp_BAT3_EL =33;
if SOC_BAT3_A>str_BAT3_EL || SOC_BAT3_A<str_BAT3_EL && SOC_BAT3_A>stp_BAT3_EL
&& A_e_EL_FT_A(k+c-1)>=1  %i==[2881:5832] ensures Winter operation only
  a1_BAT3_EL_A = 1;
```

```
else

  a1_BAT3_EL_A=0;
end


str_WT_EL =10   ;                       %start and stop SOC WATER TANK
REQUIRED to supply ELEctrolyser
stp_WT_EL =10;
if SOC_H2O_WT_A>str_WT_EL
  a2_EL_FT_A=1;
else
  a2_EL_FT_A=0;
end

e_avail_EL_FT_A = a1_BAT3_EL_A && a2_EL_FT_A ;% || r_EL_FT;
%e_EL_FT_A = e_req_EL_FT_A && (A_g_EL_FT1(k-1+c)&& A_g_EL_FT2(k-1+c)) ;

%ACTIVATION FOR BATTERY TO ELECTROLYSER
e_BAT3_EL_A = e_EL_FT_A;

%ACTIVATION FOR WATER TANK TO ELECTROLYSER
e_WT_EL_A=e_EL_FT_A;

%ACTIVATION FOR FLOW TANK TO FUEL CELL
e_FT_FC_A=e_FC_BAT3_A   ;                               %The Logic for SOC to
CONVERTER is the same as CONVERTER TO SOC

%ACTIVATION FOR FUEL CELL TO WATER TANK
e_FC_WT=e_FC_BAT3;

A_e_BAT3_LD3_A(k)=e_BAT3_LD3_A;
A_e_PV3_BAT3_A(k)= e_PV3_BAT3_A;
A_e_WG2_BAT3_A(k)=e_WG2_BAT3_A;
A_e_BAT3_EL_A(k)=e_BAT3_EL_A ;
A_e_WT_EL_A(k)= e_WT_EL_A ;
A_e_EL_FT_A(k)=e_EL_FT_A  ;
A_e_FT_FC_A(k)=e_FT_FC_A;
A_e_FC_WT_A(k)=e_FC_WT_A;
%A_e_FC_BAT3_A(k)=e_FC_BAT3_A;
A_e_DSL3_BAT3_A(k)=e_DSL3_BAT3_A;
% % %

%%%%%%%%%%%%%%%%%%%%%%%%%%%%%%%%%% FEEDBACK THE STATES OF SOC AND LOGIC
%%%%%%%%%%%%%%%%%%%%%%%%%%%%%%%%%% TO PINCH SECTION

% e_BAT3_LD3=e_BAT3_LD3_A;
% e_PV3_BAT3= e_PV3_BAT3_A;
% e_WG2_BAT3=e_WG2_BAT3_A;
% e_BAT3_EL=e_BAT3_EL_A ;
% e_WT_EL= e_WT_EL_A;
% e_EL_FT=e_EL_FT_A;
% e_FT_FC=e_FT_FC_A;
% e_FC_WT=e_FC_WT_A;
% e_FC_BAT3=e_FC_BAT3_A;
```

```
% e_DSL3_BAT3=e_DSL3_BAT3_A;
%
% SOC_H2O_WT=SOC_H2O_WT_A;
%
% SOC_H2_FT=SOC_H2_FT_A;
%
% SOC_BAT3=SOC_BAT3_A;


% %%%%%%%%%%%%%%%%%%%% END OF ACTUAL SYSTEM
%%%%%%%%%%%%%%%%%%%%%%%%%%%%%%%%%%

%%%%%%%%%%%%%%%%%%%%%%%%COUNTER INCREMENTAL LOOP%%%%%%%%%%
  if k==stop
  startt=stop+1;
  stop=stop+24;

 end

%  Counter=Counter+1;
%  if Counter ==25
%      Counter=1;
%  end
%%%%%%%%%%%%%%%%%%%%%%%%%%%%%%%%%%%%%%%%%%%%%%%%%%%%
ii(k)=k;

sstart(k)=start;









%%%%%%%%%%%%%%%% IAE CALC %%%%%%%%%%%%%%
SOC_ref=Pinch_Data(k);
if Pinch_Data(k)<30||SOC_BAT3_A<30
    SOC_ref=30;
end
if Pinch_Data(k)>90||SOC_BAT3_A>90
    SOC_ref=90;
end

A_SOC_ref(k)=SOC_ref;
IAE=abs(SOC_ref-SOC_BAT3_A)/SOC_ref;% change between system and model
A_IAE(k)=IAE;

if SOC_BAT3_A>90&&e_avail_EL_FT_A*A_g_EL_FT(k-1+e)*P_BAT3_EL(k-1+e)<1
    EPL(k)=(SOC_BAT3_A-90)*BAT3_Cap/100;
end

end
tt=1:k;
plot(tt,A_SOC_ref(1:k),tt,A_SOC_BAT3_A) %
```

```
IAE_a=sum(A_IAE)/k
LOLP=(sum(DEFICIT_A)/sum(LOAD_D_A))/number_count

end
```

Appendix E

Reinforcement Learning Adaptive PoPA .m Code

```
rng('default')

% DONT TOUCH YOU NEED TO INCREASE PICH MIN LEVEL AND REDUCE PINCH MAX BY 2%
% RESPECTIVELY



%Dont Temper with this Version for recalculates when there is error between
model and system Pinch analysis in the whole Year
%find(Recall(1,1:k)==1)% finds where adaptive recalculation occurred
%Adaptive MPC PINCH recalculates every time there is difference between
%model and Actual system


%PREDICTION TOP LEVEL INITIALIZATION FOR PV AND WIND DATA INPUT
I_rad = dlmread('PV_POA.csv');          %Plane of Array for insolation
I_Rad=I_rad';

Ng=0.96;
Nb=0.72;
Air_den=1.23    ;                        %Air density 1.23 Kg/m3
Cp=0.4;
Area_sw=3.24 ;                           %Wind Turbine Swept Area
WT_no=3;
WT_wind = dlmread('WT_Wind.csv');       %Velocity of Wind m/s
Wind_vel=WT_wind';


LD3=ones(1,8760)*1000;                   % Constant Load for a year
LD3_daily=24*1000;                         %Load per day
P_DSL3_BAT3= 2210;

%Counter=0 ;                             %counts the no.of iteration



%%

%%%%%%%%%%%%%%%%%%%%%%%%%%%%%%%%%%%%%%% START OF MICROGRID 3 INITIALIZATION
%%%%%%%%%%%%%%%%%%%%%%%%%%%%%%%%%%%%%%%%%%%%%%%%%%%%%%%%%%%%%%%%%%%%%%%%%%

%INITIALIZING ACTIVATION STATES OF THE NODES
e_BAT3_LD3=1;
e_PV3_BAT3=0;                %PV3 is the solar panel in microgrid 3, WG2 is
the wind turbine in microgrid 3
e_WG2_BAT3=0;
e_BAT3_EL=0  ;                %EL is the ELectrolyser, WT is the Water Tank,
FC is the Fuel Cell
e_WT_EL=0    ;
e_EL_FT=0    ;                  %FT is the Hydrogen storage tank
e_FT_FC=0;
e_FC_BAT3=0;
e_FC_WT=0;
```

```
e_DSL3_BAT3=0;

e_BAT3_EL = e_EL_FT;

%ACTIVATION FOR WATER TANK TO ELECTROLYSER
e_WT_EL=e_EL_FT;

%ACTIVATION FOR FLOW TANK TO FUEL CELL
e_FC_BAT3 =e_FT_FC       ;                        %The Logic for SOC to
CONVERTER is the same as CONVERTER TO SOC

%ACTIVATION FOR FUEL CELL TO WATER TANK
e_FC_WT=e_FC_BAT3;

%INITIALIZING AVAILABILITY OVERRIDE
r_PV3_BAT3=0;
r_WG2_BAT3=0;
r_BAT3_EL=0;
r_WT_EL=0;
r_EL_FT=0;
r_FT_FC=0;
r_FC_WT=0;
r_FC_BAT3=0;
r_BAT3_LD3=0;
r_DSL3_BAT3=0;

%INITIALIZING GENERALITY CONSTRAINT FOR ACTIVATION (OVERRIDE)

g_PV3_BAT3=1   ;
g_WG2_BAT3=0;
g_BAT3_EL=1      ;
g_WT_EL=1    ;
g_EL_FT=1      ;
g_FT_FC=1;
g_FC_WT=1;
g_FC_BAT3=1;
g_BAT3_LD3=1;
g_DSL3_BAT3=1;



%
%INITIALIZING ACTIVATION STATES OF THE NODES
e_BAT3_LD3_A=1;
e_PV3_BAT3_A=0   ;               %PV3 is the solar panel in microgrid 3, WG2
is the wind turbine in microgrid 3
e_WG2_BAT3_A=0;
e_BAT3_EL_A=0    ;               %EL is the ELectrolyser, WT is the Water
Tank, FC is the Fuel Cell
e_WT_EL_A=0    ;
e_EL_FT_A=0    ;                 %FT is the Hydrogen storage tank
e_FT_FC_A=0;
e_FC_BAT3_A=0;
e_FC_WT_A=0;
e_DSL3_BAT3_A=0;
```

```
e_BAT3_EL_A = e_EL_FT_A;

%ACTIVATION FOR WATER TANK TO ELECTROLYSER
e_WT_EL_A=e_EL_FT_A;

%ACTIVATION FOR FLOW TANK TO FUEL CELL
e_FC_BAT3_A =e_FT_FC_A       ;                        %The Logic for SOC to
CONVERTER is the same as CONVERTER TO SOC

%ACTIVATION FOR FUEL CELL TO WATER TANK
e_FC_WT_A=e_FC_BAT3_A;
%

% %INITIALIZE SOCs EL AND FC
 SOC_BAT3_A=70  ;                                  %Tweek #SOC_BAT3 to alter
the SOC LEVEL FOR BATTERY 3
 SOC_H2_FT_A=80;
 SOC_H2O_WT_A=30;
%

% %VARIABLE DECLARATION FOR MEMORY
A_e_BAT3_LD3_A=zeros(1,8760);
A_e_PV3_BAT3_A= zeros(1,8760)      ;
A_e_WG2_BAT3_A=zeros(1,8760);
A_e_BAT3_EL_A=zeros(1,8760)       ;
A_e_WT_EL_A= zeros(1,8760);
A_e_EL_FT_A=zeros(1,8760)      ;
A_e_FT_FC_A=zeros(1,8760);
A_e_FC_WT_A=zeros(1,8760);
A_e_FC_BAT3_A=zeros(1,8760);
A_e_DSL3_BAT3_A=zeros(1,8760);
A_F_FC_WT_EL_A=zeros(1,8760);
A_F_EL_FT_FC_A=zeros(1,8760);
A_R_e_FC_BAT3=zeros(1,8760);
A_R_e_BAT3_EL=zeros(1,8760);
% %%%%%%%%%%%%%%%%%%%%%%%%%%%%%%%%%%%%%% END OF REAL SYSTEM MICROGRID 3
INITIALIZATION %%%%%%%%%%%%%%%%%%%%%%%%%%%%%%%%%%%%%%%%%%%%%%%%%%%%%%
%

% INITIALIZING BATTERY CAPACITY
% Battery3 capacity   3KAh*12V = 36KWh
BAT3_Cap=36000;


%INITIALIZING DIESEL GENERATOR3


%INITIALIZING FUEL CELL AND ELECTROLYSER DYNAMICS
polyn_EL=[-0.000001426704372 0.027954416509736 2.502267281445165];  %Transfer
function for Electrolyser
polyn_FC=[0.000000895442340 0.033197516886985 -0.278092554468687];  %Transfer
function for Fuel Cell
```

```
nc_EL=15;                               % no. of cells in the electrolyser
nc_FC=40;                               % no. of cells in the fuel cell
nF=0.87;                                % Efficiency
ne=2;                                   % no. of electron
F=96485;                                % Faraday's constant W/mol
P_BAT3_EL=4000;                             % Power required per time by the
Electrolyser
P_FC_BAT3=3000;                             % Max power the Fuel cell can
deliver

WT_Cap=2.1749e+03*300;
FT_Cap=974*300%974.3583*10;%

%INITIALIZE SOCs EL AND FC
SOC_BAT3=70  ;                                      %Tweek #SOC_BAT3 to alter the
SOC LEVEL FOR BATTERY 3
SOC_H2_FT=80;
SOC_H2O_WT=30;

%%%% ELECTROLYSER ACTIVATION %%%%%%%
EL_SUMMER=zeros(1,8760);
EL_SUMMER(1:8760)=1;
%EL_SUMMER(1:2160)=1;
%EL_SUMMER(6553:8760)=1;

%%%% FUEL CELL ACTIVATION %%%%%
FC_WINTER=zeros(1,8760);
FC_WINTER(1:8760)=1;%(100:8000)(2881:5832)

%VARIABLE DECLARATION FOR MEMORY
A_e_BAT3_LD3=zeros(1,8760);
A_e_PV3_BAT3= zeros(1,8760)      ;
A_e_WG2_BAT3=zeros(1,8760);
A_e_BAT3_EL=zeros(1,8760)       ;
A_e_WT_EL= zeros(1,8760);
A_e_EL_FT=zeros(1,8760)      ;
A_e_FT_FC=zeros(1,8760);
A_e_FC_WT=zeros(1,8760);
A_e_FC_BAT3=zeros(1,8760);
A_e_DSL3_BAT3=zeros(1,8760);
A_F_FC_WT_EL=zeros(1,8760);
A_F_EL_FT_FC=zeros(1,8760);

%
% A_r_PV3_BAT3=zeros(1,8760);
% A_r_WG2_BAT3=zeros(1,8760);
% A_r_BAT3_EL=zeros(1,8760);
% A_r_WT_EL=zeros(1,8760);
% A_r_EL_FT=zeros(1,24);
% A_r_FT_FC=zeros(1,24);
% A_r_FC_WT=zeros(1,8760);
% A_r_FC_BAT3=zeros(1,8760);
% A_r_BAT3_LD3=zeros(1,8760);
% A_r_DSL3_BAT3=zeros(1,8760);
```

```
A_g_FC_BAT3=zeros(1,8760);
A_g_EL_FT1=zeros(1,8760);
A_g_EL_FT2=zeros(1,8760);


%%%%%%%%%%%%%%%%%%%%%%%%%%%%%%%%%%%%%%%%%%%%%%%%%%%%%%%%%%%%%%ACTUAL
%%%%%%%%%%%%%%%%%%%%%%%%%%%%%%%%%%%%%%%%%%%%%%%%%%%%%%%%%%%%%%INITIALIZATION
%%%%%%%%%%%%%%%%%%%%%%%%%%%%%%%%%%%%%%%%%%%%%%%%%%%%%%%%%%%%%%%%%%%%%%%%%%%%
%INITIALIZING ACTIVATION STATES OF THE NODES
e_BAT3_LD3_A=1;
e_PV3_BAT3_A=0   ;                %PV3 is the solar panel in microgrid 3, WG2
is the wind turbine in microgrid 3
e_WG2_BAT3_A=0;
e_BAT3_EL_A=0    ;                %EL is the ELectrolyser, WT is the Water
Tank, FC is the Fuel Cell
e_WT_EL_A=0    ;
e_EL_FT_A=0    ;                  %FT is the Hydrogen storage tank
e_FT_FC_A=0;
e_FC_BAT3_A=0;
e_FC_WT_A=0;
e_DSL3_BAT3_A=0;

e_BAT3_EL_A = e_EL_FT_A;

%ACTIVATION FOR WATER TANK TO ELECTROLYSER
e_WT_EL_A=e_EL_FT_A;

%ACTIVATION FOR FLOW TANK TO FUEL CELL
e_FC_BAT3_A =e_FT_FC_A       ;                  %The Logic for SOC to
CONVERTER is the same as CONVERTER TO SOC

%ACTIVATION FOR FUEL CELL TO WATER TANK
e_FC_WT_A=e_FC_BAT3_A;

% %INITIALIZE SOCs EL AND FC
 SOC_BAT3_A=70  ;                              %Tweek #SOC_BAT3 to alter
the SOC LEVEL FOR BATTERY 3
 SOC_H2_FT_A=80;
 SOC_H2O_WT_A=30;

% %VARIABLE DECLARATION FOR MEMORY
A_e_BAT3_LD3_A=zeros(1,8760);
A_e_PV3_BAT3_A= zeros(1,8760)      ;
A_e_WG2_BAT3_A=zeros(1,8760);
A_e_BAT3_EL_A=zeros(1,8760)       ;
A_e_WT_EL_A= zeros(1,8760);
A_e_EL_FT_A=zeros(1,8760)      ;
A_e_FT_FC_A=zeros(1,8760);
A_e_FC_WT_A=zeros(1,8760);
A_e_FC_BAT3_A=zeros(1,8760);
A_e_DSL3_BAT3_A=zeros(1,8760);
A_F_FC_WT_EL_A=zeros(1,8760);
A_F_EL_FT_FC_A=zeros(1,8760);
```

```
A_R_e_FC_BAT3=zeros(1,8760);
A_R_e_BAT3_EL=zeros(1,8760);


%%%%%%%%%%%%%%%%%%%%%%%%%%%%%%%%%%%%%%%%%%%%%%%%%%%%%%%%%%%%%%%%%%%%%%%%%%%%
EL_ON1=zeros(24,24);
EL_ON2=zeros(24,24);
FC_ON=zeros(24,24);


startt=1;
start=1;
stop=24;
Counter=0;
Counter2=0;


k=1;

PINCH_DATA=[];
A_SOC_BAT3=zeros(1,240)
Recall=zeros(1,240)

%%%%%%%%%%%%%%%%%%%%%%% Q-Learning INIT %%%%%%%%%%%%%%%%%%%%%%%%%%%%%%%%

ACTION=[1 2 3 4 5 6 7]';
Q_Table=rand(270,length(ACTION))+1;

ep=0.8  ;  % epsilon   % tweek depending on how true the reward was in real
time

Alpha=0.9;
gamma=0.9;


ACTION_1_COUNT=0;
ACTION_2_COUNT=0;
ACTION_3_COUNT=0;
ACTION_4_COUNT=0;


LD3_A=repmat(Actual_load,1,365);
% LD3=dlmread('LOAD_Max.csv');
LD3=dlmread('LOAD_AVERAGE.csv')*0.5;
LD3_A=dlmread('ACTUAL_LD_S2.csv')*1.5;
%LD3=ones(1,8760)*1000;

% LD3_A=LD3;

WT_Cap=2.1749e+03*300;
FT_Cap=974*300;%974.3583*10;%

 while k<=8760%719
for k=1:1:8760%720 %determines the number of hours to run the Pinch analysis
```

```
%for k=start:1:stop

    Counter2=Counter2+1;

   for l=1:1:10
       start=k;
       if k==1
           stop=24;
       startt=1;
       end
%          if k==24
%          pause(1)
%        end
%
 if (stop-start)==23 ||(A_SOC_BAT3(k-1)<30||A_SOC_BAT3(k-1)>90)||
(A_SOC_BAT3(k-1)>5+A_SOC_BAT3_A(k-1) || A_SOC_BAT3(k-1)<-5+A_SOC_BAT3_A(k-1))
% &&SOC_BAT3>10/100*SOC_BAT3_A %Do recalculation only if the deviation is
state>10%
 if start>1
SOC_BAT3=A_SOC_BAT3_A(start-1)  ;                                    %Tweek
#SOC_BAT3 to alter the SOC LEVEL FOR BATTERY 3
SOC_H2_FT=A_SOC_H2_FT_A(start-1);
SOC_H2O_WT=A_SOC_H2O_WT_A(start-1);

e_BAT3_LD3= A_e_BAT3_LD3_A(start-1)  ;
e_PV3_BAT3= A_e_PV3_BAT3_A(start-1)  ;
e_WG2_BAT3=  A_e_WG2_BAT3_A(start-1) ;
e_BAT3_EL = A_e_BAT3_EL_A(start-1);
e_WT_EL = A_e_WT_EL_A(start-1);
e_EL_FT  = A_e_EL_FT_A(start-1);
e_FT_FC= A_e_FT_FC_A(start-1);
e_FC_WT=  A_e_FC_WT_A(start-1);
e_FC_BAT3=  A_e_FC_BAT3_A(start-1);
e_DSL3_BAT3= A_e_DSL3_BAT3_A(start-1);

%ACTIVATION FOR BATTERY TO ELECTROLYSER
e_BAT3_EL = e_EL_FT;

%ACTIVATION FOR WATER TANK TO ELECTROLYSER
e_WT_EL=e_EL_FT;

%ACTIVATION FOR FLOW TANK TO FUEL CELL
e_FT_FC=e_FC_BAT3;                              %The Logic for SOC to
CONVERTER is the same as CONVERTER TO SOC

%ACTIVATION FOR FUEL CELL TO WATER TANK
e_FC_WT=e_FC_BAT3;
 end
%%%%%%%%%%%%%%%%%%%%%%%%

 if start==1
SOC_BAT3=70 ;
SOC_H2O_WT=30;
SOC_H2_FT=80   ;
%INITIALIZING ACTIVATION STATES OF THE NODES
```

```
e_BAT3_LD3=1;
e_PV3_BAT3=0    ;               %PV3 is the solar panel in microgrid 3, WG2 is
the wind turbine in microgrid 3
e_WG2_BAT3=0;
e_BAT3_EL=0     ;               %EL is the ELectrolyser, WT is the Water Tank,
FC is the Fuel Cell
e_WT_EL=0     ;
e_EL_FT=0     ;                 %FT is the Hydrogen storage tank
e_FT_FC=0;
e_FC_BAT3=0;
e_FC_WT=0;
e_DSL3_BAT3=0;

e_BAT3_EL = e_EL_FT;

% ACTIVATION FOR WATER TANK TO ELECTROLYSER
e_WT_EL=e_EL_FT;

% ACTIVATION FOR FLOW TANK TO FUEL CELL
e_FC_BAT3 =e_FT_FC       ;                        %The Logic for SOC to
CONVERTER is the same as CONVERTER TO SOC

% ACTIVATION FOR FUEL CELL TO WATER TANK
e_FC_WT=e_FC_BAT3;
   end




 for j=k:1:stop %j=start:1:stop

%Counter=Counter+1
%%%%%% MICROGRID3 %%% MICROGRID 3 %%%%%% MICROGRID3 %%% MICROGRID 3 %%%%%%
MICROGRID3 %%% MICROGRID 3

%%%%%ITERATION %%%% ITERATION

%INSTANTENOUS LOAD POWER
P_BAT3_LD3=LD3(j);


%POWER FROM PV SYSTEM
PV3_no=217;
Area_PV3=0.52*PV3_no        ;           %Area for 70W solar panel

P_PV3_BAT3=Area_PV3*I_Rad(j)*0.1 ;     % 0.1 is efficiency for
polycrystalline

%POWER WIND TURBINE GENERATOR

P_WG2_BAT3= 0.5 * Air_den *Area_sw  * Cp* ((Wind_vel(j))^3) * Ng * Nb*WT_no ;
```

```
%FUEL CELL AND ELECTROLYSER POWER FLOW

I_EL=polyval(polyn_EL,P_BAT3_EL)  ;       % Power flow as a function of Power
supplied to the electroliser
I_FC=polyval(polyn_FC,P_FC_BAT3)    ;     % Power flow as a function of Power
supplied to the electroliser

%*e_BAT3_EL *e_FC_BAT3*

Fout_FC_WT_H2O= e_FC_WT * 0.85 * nc_FC * 3600* I_FC  / (nF*ne*F)  ;      %
The flow of H2O from FC to WT +VE flow since it goes in to the Water Tank
%A_Fout_FC_WT_H2O(k,j)=Fout_FC_WT_H2O;


Fout_EL_FT_H2= e_EL_FT * nF*nc_EL *  3600* I_EL/(ne*F)  ;                  %
The flow of H2 from EL to FT   +VE flow since it goes into a Flow Tnak
%A_Fout_EL_FT_H2(k,j)=Fout_EL_FT_H2;


Fout_FT_FC_H2= e_FT_FC * nc_FC * 3600 *I_FC /(nF*ne*F)   ;                 %
The flow of H2 out of the FT to the FC  based on the needs of the  FC i.e
*eff -VE flow since it flows out
%A_Fout_FT_FC_H2(k,j)=Fout_FT_FC_H2;


Fout_WT_H2O= e_WT_EL* 1.3 * nF * nc_EL * 3600 * I_EL /(ne*F) ;        % The
flow of H2O from the WT to the EL based on what the EL needs. The Flow is -VE
since it depletes the Water Tank
%A_Fout_WT_H2O(k,j)=Fout_WT_H2O;

%%WATER TANK AND FLOW TANK MAX CAPACITY CALCULATION
%WT_Cap=1.3*24*(I_FC*nc_FC*nF)*3600/(ne*F)
%Calculate at max Power then set it manually.  Water Tank capacity should
hold moles/hr for 24hrs

%FT_Cap=1.3*24*(I_EL*nc_EL*nF)*3600/(ne*F)                          %Storage
Tank capacity should hold moles/hr for 24hrs


%NET ENERGY FLOW OF POWER STORED IN THE BATTERY
A_P_PV3_BAT3(j)=P_PV3_BAT3;
A_P_WG2_BAT3(j)=P_WG2_BAT3;
P_RES3=(e_PV3_BAT3*P_PV3_BAT3)
+(e_WG2_BAT3*P_WG2_BAT3)+(e_DSL3_BAT3*P_DSL3_BAT3)+(e_FC_BAT3*P_FC_BAT3);
A_P_RES3(j)=P_RES3;
P_BAT3= P_RES3-(e_BAT3_LD3*P_BAT3_LD3)-(e_BAT3_EL*P_BAT3_EL);
if P_BAT3<=0
   Deficit_P_BAT3=1;
else
    Deficit_P_BAT3=0;
end
A_Deficit_P_BAT3(j)=Deficit_P_BAT3;
```

```
if P_BAT3>LD3(j)&&SOC_BAT3>90&&SOC_H2_FT>90 && SOC_H2O_WT>40
    Surplus_P_BAT3=1;
else
    Surplus_P_BAT3=0;
end
A_Surplus_P_BAT3(j)=Surplus_P_BAT3;


A_P_BAT3(j)=(P_BAT3/BAT3_Cap)*100 ;
SOC_BAT3=SOC_BAT3+(P_BAT3/BAT3_Cap)*100 ;
if SOC_BAT3<=0;
    SOC_BAT3=0;
end
if SOC_BAT3>=100
    SOC_BAT3=100;
end

A_SOC_BAT3(j)=SOC_BAT3;
if SOC_BAT3<30
   Deficit_SOC_BAT3=1;
else
   Deficit_SOC_BAT3=0;
end
 A_Deficit_SOC_BAT3(j)= Deficit_SOC_BAT3;

 if j<=1
     c=1;
 else
     c=0;
 end

% WATER STORED IN THE WATER TANK
 FC_WT_EL=100*(Fout_FC_WT_H2O - Fout_WT_H2O)/WT_Cap;
SOC_H2O_WT= SOC_H2O_WT +FC_WT_EL;
if SOC_H2O_WT>=100
    SOC_H2O_WT=100;
end
    if  SOC_H2O_WT<=0
        SOC_H2O_WT=0;
    end
A_SOC_H2O_WT(j)=SOC_H2O_WT;
A_F_FC_WT_EL(j)=FC_WT_EL;

%HYDROGEN STORED IN THE FLOW TANK
EL_FT_FC=100*(Fout_EL_FT_H2 - Fout_FT_FC_H2)/FT_Cap;
SOC_H2_FT=SOC_H2_FT + EL_FT_FC;
if SOC_H2_FT>=100                          %LIMITS FOR SOC OF WATER TANK AND
FLOW TANK
    SOC_H2_FT=100;
end
if SOC_H2_FT<=0
    SOC_H2_FT=0;
end
A_SOC_H2_FT(j)=SOC_H2_FT;
```

```
A_F_EL_FT_FC(j)=EL_FT_FC;

%ACTIVATION FOR PV TO BATTERY
str_PV3_BAT3=0      ;                    % start charging battery if SOC max
is < 90%
stp_PV3_BAT3=90;

if SOC_BAT3<stp_PV3_BAT3
    q_PV3_BAT3=1;
else
    q_PV3_BAT3=0;
end
e_req_PV3_BAT3=q_PV3_BAT3  ;            %The logic determines when the
battery SOC is below the stop point then the Battery makes a request

a_PV3_BAT3=1;
e_avail_PV3_BAT3= a_PV3_BAT3 || r_PV3_BAT3;
e_PV3_BAT3= e_avail_PV3_BAT3 && e_req_PV3_BAT3 && g_PV3_BAT3;


%ACTIVATION FOR WIND TURBINE WG2 TO BATTERY BAT3
str_WG2_BAT3=0   ;                      % start charging battery if SOC max
is < 90%
stp_WG2_BAT3=90;

if SOC_BAT3<stp_WG2_BAT3
    q_WG2_BAT3=1;
else
    q_WG2_BAT3=0;
end
e_req_WG2_BAT3=q_WG2_BAT3    ;          %The logic determines when the
battery SOC is below the stop point then the Battery makes a request
a_WG2_BAT3=1;
e_avail_WG2_BAT3 = a_WG2_BAT3 || r_WG2_BAT3;

e_WG2_BAT3 = e_avail_WG2_BAT3 && e_req_WG2_BAT3 && g_WG2_BAT3;

%ACTIVATION FOR DIESEL TO BATTERY
str_DSL3_BAT3=20;
stp_DSL3_BAT3=30;
if k<=1
    c=1;
else
    c=0;
end
if SOC_BAT3<str_DSL3_BAT3 || [SOC_BAT3>str_DSL3_BAT3&&SOC_BAT3<stp_DSL3_BAT3]
%&& A_e_DSL3_BAT3(j+c-1)==1
q_DSL3_BAT3=1;
else
q_DSL3_BAT3=0;
end
e_req_DSL3_BAT3 =q_DSL3_BAT3;

a_DSL3_BAT3=1       ;                        %Availability logic for
Diesel generator
```

```
e_avail_DSL3_BAT3 = a_DSL3_BAT3 || r_DSL3_BAT3;

e_DSL3_BAT3= e_avail_DSL3_BAT3 && e_req_DSL3_BAT3 && g_DSL3_BAT3;


%ACTIVATION FOR FUEL CELL TO BATTERY
if FC_WINTER(k)==1
    FC_ON_WINTER=1;
else
    FC_ON_WINTER=0;
end
str_FC_BAT3=99  ;      %90                  %start and stop min and max
threshold to make request by Battery for Fuel cell to supply power
stp_FC_BAT3=80;
if FC_ON_WINTER==1 && SOC_BAT3<str_FC_BAT3  || SOC_BAT3>str_FC_BAT3 &&
SOC_BAT3<stp_FC_BAT3 && A_e_FC_BAT3(j-1+c)==1       %i==[2881:5832] ensures
Summer operation only
    q_FC_BAT3=1 ;
else
    q_FC_BAT3=0;
end
e_req_FC_BAT3 =   q_FC_BAT3;

  str_FC_WT=90      ;                              %start and stop min and max
threshold to make request for Fuel cell to supply power to Battery based on
Water Tank not full and Flow tank above minimum
  stp_FC_WT=90;

if SOC_H2O_WT<str_FC_WT
  a1_FC_WT=1;
else
  a1_FC_WT=0;
end

str_FT_FC =10   ;                                   %start and stop SOC
HYDROGEN FLOW TANK REQUIRED to supply FUEL CELL
stp_FT_FC =10;
if SOC_H2_FT>str_FT_FC
  a2_FT_FC=1;
else
  a2_FT_FC=0;
end

e_avail_FC_BAT3= a1_FC_WT && a2_FT_FC ; %|| r_FT_FC;


e_FC_BAT3 = e_req_FC_BAT3 && A_g_FC_BAT3(j+c);

%ACTIVATION FOR BATTERY TO LOAD
% e_BAT3_LD3=e_avail_BAT3_LD3 && e_avail_BAT3_LD3  && g_BAT3_LD3


%ACTIVATION FOR ELECTROLYSER TO FLOW TANK
```

```
str_EL_FT = 99       ;%90                    %start and stop SOC for engaging
the ELECTROLYSER TO SUPPLY FLOW TANK
stp_EL_FT= 100;
if SOC_H2_FT<str_EL_FT                   %FT MAKES REQUEST FOR H2 SUPPLY FROM
ELECTROLYSER
    q_EL_FT=1;
else
    q_EL_FT=0;
end
e_req_EL_FT= q_EL_FT;


if EL_SUMMER(k)==1                    %Scan the array if the index is equal to
1 then logic is true else it is false for zero
    EL_ON_SUMMER=1;
    else
    EL_ON_SUMMER=0;
end

str_BAT3_EL= 70   ;                    %start and stop SOC for engaging the
BATTERY TO SUPPLY ELECTROLYSER
stp_BAT3_EL =33;
% if Counter<=1
%     c=2;
% else
%     c=0;
% end             %This corrects the indexing by assuming the past was zero
if EL_ON_SUMMER==1 && SOC_BAT3>str_BAT3_EL || SOC_BAT3<str_BAT3_EL &&
SOC_BAT3>stp_BAT3_EL && A_e_EL_FT(j+c-1)==1  %i==[2881:5832] ensures Winter
operation only
  a1_BAT3_EL = 1;
else

  a1_BAT3_EL=0;
end


str_WT_EL =10   ;                      %start and stop SOC WATER TANK
REQUIRED to supply ELEctrolyser
stp_WT_EL =10;
if SOC_H2O_WT>str_WT_EL
  a2_EL_FT=1;
else
  a2_EL_FT=0;
end


e_avail_EL_FT= a1_BAT3_EL && a2_EL_FT ; %|| r_EL_FT;
e_EL_FT=e_req_EL_FT&&(A_g_EL_FT1(j+c) || A_g_EL_FT2(j+c));


%ACTIVATION FOR BATTERY TO ELECTROLYSER
e_BAT3_EL = e_EL_FT;

%ACTIVATION FOR WATER TANK TO ELECTROLYSER
```

```
e_WT_EL=e_EL_FT;

%ACTIVATION FOR FLOW TANK TO FUEL CELL
e_FT_FC=e_FC_BAT3   ;                                %The Logic for SOC to
CONVERTER is the same as CONVERTER TO SOC

%ACTIVATION FOR FUEL CELL TO WATER TANK
e_FC_WT=e_FC_BAT3;

A_e_BAT3_LD3(j)=e_BAT3_LD3;
A_e_PV3_BAT3(j)= e_PV3_BAT3;
A_e_WG2_BAT3(j)=e_WG2_BAT3;
A_e_BAT3_EL(j)=e_BAT3_EL ;
A_e_WT_EL(j)= e_WT_EL ;
A_e_EL_FT(j)=e_EL_FT  ;
A_e_FT_FC(j)=e_FT_FC;
A_e_FC_WT(j)=e_FC_WT;
A_e_FC_BAT3(j)=e_FC_BAT3;
A_e_DSL3_BAT3(j)=e_DSL3_BAT3;

%%%%%%%%%%%%%%%%%%%% END OF MG3 LOW LEVEL PMS
%%%%%%%%%%%%%%%%%%%%%%%%%%%%%%%%%%


Pinch_Data(j)=SOC_BAT3;
%PINCH_DATA(l,j,k)=SOC_BAT3;
   if l==10 && startt==k
 Pinch_Data_Raw(j)=SOC_BAT3;
end

% PINCH_DATA(k,j)=SOC_BAT3;
% PINCH_DATAA(Counter2,j)=SOC_BAT3;
 end
%run this loop while Smin and Smax violation exist


%PINCH ANALYSIS AND DETERMINATION OF G OVERIDE

%%START PINCH%%
SOC_BAT3_min=31 ;          %Minimum and Maximum Pinch Targets
SOC_BAT3_max=89;
S_min=min(Pinch_Data(start:stop));

if S_min<SOC_BAT3_min

   t_violation= find(Pinch_Data(1:stop)==S_min)     ;           % time of
violation of the Lower pinch

   E_target = (SOC_BAT3_min - S_min)*(BAT3_Cap/(100*P_FC_BAT3));
   t_duration = ceil(E_target)/BAT3_Cap;             %Time duration needed
based on allowable amount of energy from battery per hour
   if t_violation-1<1
      t_violation=2
   end
```

```
   A_g_FC_BAT3(t_violation-1)= 1;


else

  S_max=max(Pinch_Data(start:stop));

  A_g_EL_FT1(1,start:stop-2)=  Pinch_Data(start:stop-2)>SOC_BAT3_max;

end

if
ceil(Pinch_Data(stop))~=50&&(Pinch_Data(startt)>=30&&Pinch_Data(startt)<=90)%
Pinch_Data(stop)~=Pinch_Data(startt)&&Pinch_Data(startt)>=30
    EE_target=(Pinch_Data(stop) - Pinch_Data(startt))*(BAT3_Cap/(100));
     if EE_target<0
           A_g_FC_BAT3(stop)=1;
            A_g_EL_FT2(stop)=0;

     else
         EE_target>0
         A_g_EL_FT2(stop)=1;
          A_g_FC_BAT3(stop)=0;

     end

end


% if Pinch_Data(stop-1)~=Pinch_Data(startt)
%     E_target=  (Pinch_Data(stop-1) -
Pinch_Data(startt))*(BAT3_Cap/(100*P_FC_BAT3));
%      if E_target<0
%            A_g_FC_BAT3(stop-1)=1;
%             A_g_EL_FT2(stop-1)=0;
%      else
%          E_target>0
%          A_g_EL_FT2(stop-1)=1;
%           A_g_FC_BAT3(stop-1)=0;
%      end
%
% end
%%%%%%%%%%%%%%%%%%%%%%%%%%%%%%%%%%%%  END OF PINCH %%%%%%%%%%%%%%%%



A_g_EL_FT=A_g_EL_FT1+A_g_EL_FT2;
%A_g_EL_FT=A_g_EL_FT2~=0;

      Recal=1;
Recall(k)=Recal;
```

```
end
   end


%%%%%%%%%%%%%%%%%%%%%%%%%%%% E.N.D OF M.P.C
%%%%%%%%%%%%%%%%%%%%%%%%%%%%%%%%%%%%%%%%%%%%

%%%%%%%%%%%%%%%%%%%%%%%%%%%% Q _ LEARNING %%%%%%%%%%%%%%%%%%%%%%%%%%%%%%%%

%         if k==30
%         pause(5)
%     end




%%%%%%%%%%%%%%%%%%%%%%%%%%%%%%%% EXPLORE A NEW ACTION %%%%%%%%%%%%%%%%%%%%
%
% if k<=1
% SOC_BAT3_A =A_SOC_BAT3(1)  ;
% e_avail_EL_FT_A= e_EL_FT ;
% e_avail_FC_BAT3_A=e_FC_BAT3_A;
% end
[aa bb]=size(Pinch_Data);%(A_SOC_BAT3);
Pinch_now=Pinch_Data(k) ;
if bb>k+1
Pinch_now=Pinch_Data(k);
else
Pinch_now=Pinch_Data(k) ;
end

State= QQ_State_error_typeX(Pinch_now,SOC_BAT3_A)    ;      % calibrates the
state of the BAttery's SOC to a range of states

% State
Prob_sel=sum(rand>cumsum([0 1-ep ep])) ;     %Type of action selector whether
to read from table (exploit) or try exploration random action

% WHEN THE CONVERGENCE OF TABLE OCCURS UPDATE EPSILON TO 1
%IF REWARD IS NOT MET OVER 3 TIMES DECREASE EPSILON

% if
%     Action_sel=1
% else
%
% else
% if A_g_EL_FT1(k)==1 && A_g_FC_BAT3(k)==0
%     Action_sel=3
%
% end
% end
% end
 if SOC_BAT3_A<40||SOC_BAT3_A>85
    Prob_sel=2;
```

```
 end

    if Prob_sel ==1              %random action selected based on epsilon
    if A_g_FC_BAT3(k-1+c)==0 && A_g_EL_FT1(k-1+c)==0
      Action_sel=datasample(ACTION(1),1)   ;
    end
    if A_g_FC_BAT3(k-1+c)==1 && A_g_EL_FT1(k-1+c)==0
       Action_sel=datasample(ACTION(4),1)   ;
    end
    if A_g_FC_BAT3(k-1+c)==0 && A_g_EL_FT1(k-1+c)==1
    Action_sel=datasample(ACTION(7),1)   ;
    end
     Action_sel=datasample(ACTION(1:7),1) ;  % overide


    if SOC_BAT3_A<31
        Action_sel=datasample(ACTION(4),1)  ;
    elseif SOC_BAT3_A>31&&SOC_BAT3_A<40
          Action_sel=datasample(ACTION(1:4),1)  ;
    end
    if SOC_BAT3_A>89
        Action_sel=datasample(ACTION(7),1)  ;
    end

    else
    if Prob_sel==2
    [state1
,Q_action_max]=max(Q_Table(QQ_State_error_typeX(Pinch_now,SOC_BAT3_A),:)) ;
%max action from previous learning
    Action_sel=Q_action_max;
    end
    if SOC_BAT3_A>30&&SOC_BAT3_A<40
     [state1
,Q_action_max]=max(Q_Table(QQ_State_error_typeX(Pinch_now,SOC_BAT3_A),1:4)) ;
%max action from previous learning
   Action_sel=Q_action_max;
    end
    if SOC_BAT3_A>70
        [state1
,Q_action_max]=max(Q_Table(QQ_State_error_typeX(Pinch_now,SOC_BAT3_A),[1,5:7]
)) ;
          if Q_action_max==1
             Action_sel=Q_action_max;
          elseif    Q_action_max>1
              Action_sel=Q_action_max+3; %corrects the action index
          end
     end


     if SOC_BAT3_A<31
        Action_sel=datasample(ACTION(4),1)  ;
    end
     if SOC_BAT3_A>89
       Action_sel=datasample(ACTION(7),1)  ;
```

```
      end
     end

   Action_sell(k)=Action_sel;
       %% Take action on the logic based on the whatever action has been
selected

 if  Action_sel==1
     r_BAT3_EL=0;
     r_FC_BAT3=0;
 end
  if Action_sel==2
     r_BAT3_EL=0;
     r_FC_BAT3=0.1;
  end
   if Action_sel==3
     r_BAT3_EL=0;
     r_FC_BAT3=0.3;
  end
   if Action_sel==4
     r_BAT3_EL=0;
     r_FC_BAT3=1;
  end

   if Action_sel==5
     r_BAT3_EL=0.3;
     r_FC_BAT3=0;
   end

   if Action_sel==6
     r_BAT3_EL=.5;
     r_FC_BAT3=0;
   end

   if Action_sel==7
     r_BAT3_EL=1;
     r_FC_BAT3=0;
   end




%    if Action_sel==4
%      r_BAT3_EL=1;
%      r_FC_BAT3=1;
%    end


%The Logic of availability to carry out an action is set, No need to learn on
an action that wasn't carried out
%e_EL_FT_A=r_BAT3_EL &&e_avail_EL_FT_A    %( e_req_EL_FT_A ||  );
% if k<=1
%    c=1;
% e_req_EL_FT_A=1
%
```

```
% e_req_FC_BAT3_A=1
% else
%    c=0
% end




%e_EL_FT_A = e_avail_EL_FT_A && e_req_EL_FT_A
||(e_avail_EL_FT_A&&(A_g_EL_FT1(k-1+c) || A_g_EL_FT2(k-
1+c)));%e_avail_EL_FT_A
%e_EL_FT_A=e_avail_EL_FT_A&&(A_g_EL_FT1(k-1+c) || A_g_EL_FT2(k-1+c));
% e_EL_FT_A=e_avail_EL_FT_A && r_BAT3_EL
% e_BAT3_EL_A= e_EL_FT_A;
% A_R_e_BAT3_EL(k)= e_BAT3_EL_A;


% e_FC_BAT3_A = e_avail_FC_BAT3_A && r_FC_BAT3 ;  %;%(e_req_FC_BAT3 );
% %e_FC_BAT3_A = e_req_FC_BAT3_A  && A_g_FC_BAT3(k+c);%e_avail_FC_BAT3_A
% %e_FC_BAT3_A =(e_avail_FC_BAT3_A && e_req_FC_BAT3_A ) ||
(e_avail_FC_BAT3_A&& A_g_FC_BAT3(k+c));
% %e_FC_BAT3_A =(e_avail_FC_BAT3_A&& A_g_FC_BAT3(k+c))
%
% A_R_e_FC_BAT3(k)=e_FC_BAT3_A;

% if e_FC_BAT3_A==1 &&e_BAT3_EL_A==0   %Learning Pinch directly
%    Action_sel=2
% end
% if e_FC_BAT3_A==1 &&e_BAT3_EL_A==0
%    Action_sel=3
% end

% if (r_BAT3_EL==1 && e_EL_FT_A~=1)&&( r_FC_BAT3==1 && e_FC_BAT3_A ~=1) %
This means if Action 4 EL and FC ON was selected it will be changed to Action
1
%    Action_sel =1
% end
% if(r_BAT3_EL==1 && e_EL_FT_A~=1)&&( r_FC_BAT3==1 && e_FC_BAT3_A ==1)
%      Action_sel =2
% end
% if(r_BAT3_EL==1 && e_EL_FT_A==1)&&( r_FC_BAT3==1 && e_FC_BAT3_A ~=1)
%     Action_sel =3
% end
%
% if(r_BAT3_EL==1 && e_EL_FT_A==1)&&( r_FC_BAT3==1 && e_FC_BAT3_A ==1)
%     Action_sel =4
% end



% V_L(k)=sum(A_SOC_BAT3_A<30);
% V_U(k)=sum(A_SOC_BAT3_A>90);
% if V_L(k)
% end
```

```
  Alpha=Alpha_gain/(1+k/2000);
  A_Alpha(k)=Alpha;
%
% if k>50
%     m=k
%     if k>1500
%     m=1500
%     end
%  ep=1/(1+500/k);
% end




%    E_target= (SOC_BAT3 - SOC_BAT3_A)*(BAT3_Cap/(100))
%    if E_target < 0
% %     P_FC_BAT3_A = abs(E_target);
% %    else
%     P_FC_BAT3_A = 3000;
%    end
%    if E_target>0
% %     P_BAT3_EL_A= E_target;
% %    else
%     P_BAT3_EL_A= 3000;
%    end



%State= Q_State_error_typeX(Pinch_Data(k),SOC_BAT3_A)    ;      % calibrates
the state of the BAttery's SOC to a range of states

State;



% if   A_g_FC_BAT3(k)==0 && A_g_EL_FT1(k)==0
%     Action_sel=1
% else
% if A_g_FC_BAT3(k)==1 && A_g_EL_FT1(k)==0
%   Action_sel=2
% else
% if A_g_EL_FT1(k)==1 && A_g_FC_BAT3(k)==0
%     Action_sel=3
%
% end
% end
% end
```

```
%%%%%% MICROGRID3 %%% MICROGRID 3 %%%%%% MICROGRID3 %%% MICROGRID 3 %%%%%%
MICROGRID3 %%% MICROGRID 3
ReplayQ(k,6)=SOC_BAT3_A;
%%%%%ITERATION %%%% ITERATION

%INSTANTENOUS LOAD POWER
P_BAT3_LD3_A=LD3(k);


%POWER FROM PV SYSTEM
PV3_no=217;
Area_PV3=0.52*PV3_no ;           %Area for 70W solar panel
%  if k>startt+7 && k<stop-8
%      %Random=random('norm', 0, 10,1,1);
%     Random;
%  else
%      Random=0;
%  end

P_PV3_BAT3_A=Area_PV3*0.1 *I_Rad(k) ;%+Random);  ;%   % 0.1 is efficiency for
polycrystalline
%P_PV3_BAT3=Area_PV3*I_RADOM(k)*0.1 ;

% I_RADOM(k)=I_Rad(k)+Random
%
% REAL(k)=Area_PV3*I_Rad(k)*0.1
% DIST(k)=Area_PV3*I_RADOM(k)*0.1
%I_REAL(k)=I_Rad(k)

%ACTIVATION FOR BATTERY TO ELECTROLYSER
 e_EL_FT_A=r_BAT3_EL;

%ACTIVATION FOR WATER TANK TO ELECTROLYSER
e_WT_EL_A=e_EL_FT_A;

%ACTIVATION FOR FLOW TANK TO FUEL CELL
e_FT_FC_A=r_FC_BAT3   ;                          %The Logic for SOC to
CONVERTER is the same as CONVERTER TO SOC

%ACTIVATION FOR FUEL CELL TO WATER TANK
e_FC_WT_A=r_FC_BAT3;
```

```
%POWER WIND TURBINE GENERATOR

P_WG2_BAT3_A= 0.5 * Air_den *Area_sw  * Cp* ((Wind_vel(k))^3) * Ng * Nb*WT_no
;

if  k==1%k<8761
e_avail_EL_FT_A=1;
e_avail_FC_BAT3_A=1;
end
A_e_avail_EL_FT_A(k)=e_avail_EL_FT_A;

A_e_avail_FC_BAT3_A(k)=e_avail_FC_BAT3_A;



if r_FC_BAT3>0&&e_avail_FC_BAT3_A==1
FC=1;
else
    FC=0;
end;
A_r_FC_BAT3(k)=FC;
if r_BAT3_EL>0 &&e_avail_EL_FT_A==1
   EL=1 ;
else
   EL=0;
end
A_r_BAT3_EL(k)=EL;

%FUEL CELL AND ELECTROLYSER POWER FLOW

I_EL=polyval(polyn_EL,P_BAT3_EL*r_BAT3_EL*e_avail_EL_FT_A)  ;       % Power
flow as a function of Power supplied to the electroliser
I_FC=polyval(polyn_FC,P_FC_BAT3*r_FC_BAT3*e_avail_FC_BAT3_A ) ;     % Power
flow as a function of Power supplied to the electroliser

%*e_BAT3_EL *e_FC_BAT3*
e_FC_WT_A=r_FC_BAT3;
Fout_FC_WT_H2O_A= e_FC_WT_A * 0.85 * nc_FC * 3600* I_FC  / (nF*ne*F)  ;
% The flow of H2O from FC to WT +VE flow since it goes in to the Water Tank
A_Fout_FC_WT_H2O_A(k)=Fout_FC_WT_H2O_A;


Fout_EL_FT_H2_A= e_EL_FT_A* nF*nc_EL *  3600* I_EL/(ne*F)  ;
% The flow of H2 from EL to FT   +VE flow since it goes into a Flow Tnak
A_Fout_EL_FT_H2_A(k)=Fout_EL_FT_H2_A;


Fout_FT_FC_H2_A= e_FT_FC_A * nc_FC * 3600 *I_FC /(nF*ne*F)   ;
% The flow of H2 out of the FT to the FC  based on the needs of the  FC i.e
*eff -VE flow since it flows out
A_Fout_FT_FC_H2_A(k)=Fout_FT_FC_H2_A;
```

```
Fout_WT_H2O_A= e_WT_EL_A* 1.3 * nF * nc_EL * 3600 * I_EL /(ne*F) ;        %
The flow of H2O from the WT to the EL based on what the EL needs. The Flow is
-VE since it depletes the Water Tank
A_Fout_WT_H2O_A(k)=Fout_WT_H2O_A;

%%WATER TANK AND FLOW TANK MAX CAPACITY CALCULATION
%WT_Cap=1.3*24*(I_FC*nc_FC*nF)*3600/(ne*F)
%Calculate at max Power then set it manually.  Water Tank capacity should
hold moles/hr for 24hrs

%FT_Cap=1.3*24*(I_EL*nc_EL*nF)*3600/(ne*F)                              %Storage
Tank capacity should hold moles/hr for 24hrs


%NET ENERGY FLOW OF POWER STORED IN THE BATTERY
if k<=1
    c=1;
else
    c=0;
end

Lr_FC_BAT3(k)=r_FC_BAT3;

Lr_BAT3_EL(k)=r_BAT3_EL;

A_P_PV3_BAT3_A(k)=P_PV3_BAT3_A;
A_P_WG2_BAT3_A(k)=P_WG2_BAT3_A;

[aa bb]=size(Pinch_Data);%(A_SOC_BAT3);

if stop-1==k
    r_BAT3_EL=A_g_EL_FT1(k+1); % use end logic instead of RL at terminal
    r_FC_BAT3=A_g_FC_BAT3(k+1);
end

P_RES3_A=(e_PV3_BAT3_A*P_PV3_BAT3_A)
+(e_WG2_BAT3_A*P_WG2_BAT3_A)+(e_DSL3_BAT3_A*P_DSL3_BAT3)+(e_avail_FC_BAT3_A
*r_FC_BAT3*P_FC_BAT3);%%%(A_g_FC_BAT3(k-1+c)*P_FC_BAT3);
A_P_RES3_A(k)=P_RES3_A;
P_BAT3_A= P_RES3_A -(e_BAT3_LD3_A*P_BAT3_LD3_A+ran(k)*0)-
(e_avail_EL_FT_A*r_BAT3_EL*P_BAT3_EL);%( A_g_EL_FT1(k-1+c)*P_BAT3_EL);%%
A_LD_sys(k)=(e_BAT3_LD3_A*P_BAT3_LD3_A+ran(k)*250);

A_P_BAT3_A(k)=(P_BAT3_A/BAT3_Cap)*100 ;

%%%%%%%%%%%%%%%%%%%%%%%%%%%%%%%%%%%%%%%%%%%%%%%%%%%%%%%%%%%%%%%%%%%%%%%%
P_NO_INT=(e_PV3_BAT3_A*P_PV3_BAT3_A)
+(e_WG2_BAT3_A*P_WG2_BAT3_A)+(e_DSL3_BAT3_A*P_DSL3_BAT3)-
(e_BAT3_LD3_A*P_BAT3_LD3_A+ran(k)*0);
SOC_BAT3_NO_INT=SOC_BAT3_A;
SOC_BAT3_NO_INT=SOC_BAT3_NO_INT +(P_NO_INT/BAT3_Cap)*100;
%%%%%%%%%%%%%%%%%%%%%%%%%%%%%%%%%%%%%%%%%%%%%%%%%%%%%%%%%%%%%%%%%%%%%%%%
```

```
SOC_BAT3_A=SOC_BAT3_A +(P_BAT3_A/BAT3_Cap)*100 ;
if SOC_BAT3_A<=0;
    SOC_BAT3_A=0;
end
if SOC_BAT3_A>=100
    SOC_BAT3_A=100;
end
A_SOC_BAT3_A(k)=SOC_BAT3_A;

if SOC_BAT3_A<30
   Deficit_SOC_BAT3_A=1;
else
   Deficit_SOC_BAT3_A=0;
end
 A_Deficit_SOC_BAT3_A(k)= Deficit_SOC_BAT3_A;


% WATER STORED IN THE WATER TANK
 FC_WT_EL_A=100*(Fout_FC_WT_H2O_A - Fout_WT_H2O_A)/WT_Cap;
SOC_H2O_WT_A= SOC_H2O_WT_A + FC_WT_EL_A;
if SOC_H2O_WT_A>=100
    SOC_H2O_WT_A=100;
end
    if  SOC_H2O_WT_A<=0
        SOC_H2O_WT_A=0;
    end
A_SOC_H2O_WT_A(k)=SOC_H2O_WT_A;
A_F_FC_WT_EL_A(k)=FC_WT_EL_A;

%HYDROGEN STORED IN THE FLOW TANK
EL_FT_FC_A=100*(Fout_EL_FT_H2_A - Fout_FT_FC_H2_A)/FT_Cap;
SOC_H2_FT_A=SOC_H2_FT_A + EL_FT_FC_A;
if SOC_H2_FT_A>=100                          %LIMITS FOR SOC OF WATER TANK
AND FLOW TANK
    SOC_H2_FT_A=100;
end
if SOC_H2_FT_A<=0
    SOC_H2_FT_A=0;
end
A_SOC_H2_FT_A(k)=SOC_H2_FT_A;
A_F_EL_FT_FC_A(k)=EL_FT_FC_A;

%ACTIVATION FOR PV TO BATTERY
str_PV3_BAT3=0      ;                     % start charging battery if SOC max
is < 90%
stp_PV3_BAT3=90;

if SOC_BAT3_A<stp_PV3_BAT3
    q_PV3_BAT3_A=1;
else
    q_PV3_BAT3_A=0;
end
e_req_PV3_BAT3_A=q_PV3_BAT3_A  ;            %The logic determines when the
battery SOC is below the stop point then the Battery makes a request
```

```
a_PV3_BAT3_A=1;
e_avail_PV3_BAT3_A= a_PV3_BAT3_A || r_PV3_BAT3_A;
e_PV3_BAT3_A= e_avail_PV3_BAT3_A && e_req_PV3_BAT3_A && g_PV3_BAT3;


%ACTIVATION FOR WIND TURBINE WG2 TO BATTERY BAT3
str_WG2_BAT3=0;                         % start charging battery if SOC max is
< 90%
stp_WG2_BAT3=90;

if SOC_BAT3_A<stp_WG2_BAT3
    q_WG2_BAT3_A=1;
else
    q_WG2_BAT3_A=0;
end
e_req_WG2_BAT3_A=q_WG2_BAT3_A ;          %The logic determines when the
battery SOC is below the stop point then the Battery makes a request
a_WG2_BAT3_A=1;
e_avail_WG2_BAT3_A = a_WG2_BAT3_A || r_WG2_BAT3_A;

e_WG2_BAT3_A = e_avail_WG2_BAT3_A && e_req_WG2_BAT3_A && g_WG2_BAT3;

%ACTIVATION FOR DIESEL TO BATTERY
str_DSL3_BAT3=20;
stp_DSL3_BAT3=30;
if k<=1
    c=1;
else
    c=0;
end

if SOC_BAT3_A<str_DSL3_BAT3 ||
[SOC_BAT3_A>str_DSL3_BAT3&&SOC_BAT3_A<stp_DSL3_BAT3] && A_e_DSL3_BAT3_A(k+c-
1)==1
q_DSL3_BAT3_A=1;
else
q_DSL3_BAT3_A=0;
end
e_req_DSL3_BAT3_A =q_DSL3_BAT3_A;

a_DSL3_BAT3_A=1  ;                           %Availability logic for Diesel
generator

e_avail_DSL3_BAT3_A = a_DSL3_BAT3_A || r_DSL3_BAT3_A;

e_DSL3_BAT3_A= e_avail_DSL3_BAT3_A && e_req_DSL3_BAT3_A && g_DSL3_BAT3;


%ACTIVATION FOR FUEL CELL TO BATTERY

str_FC_BAT3=90  ;                       %start and stop min and max threshold
to make request by Battery for Fuel cell to supply power
stp_FC_BAT3=80;
```

```
if SOC_BAT3_A<str_FC_BAT3  || SOC_BAT3_A>str_FC_BAT3 &&
SOC_BAT3_A<stp_FC_BAT3 %&& A_e_FC_BAT3_A(k+c-1)==1       %i==[2881:5832]
ensures Summer operation only
    q_FC_BAT3_A=1 ;
else
    q_FC_BAT3_A=0;
end
e_req_FC_BAT3_A =   q_FC_BAT3_A;

  str_FC_WT_A=90 ;                                %start and stop min and max
threshold to make request for Fuel cell to supply power to Battery based on
Water Tank not full and Flow tank above minimum
  stp_FC_WT_A=90;

if SOC_H2O_WT_A<str_FC_WT_A
  a1_FC_WT_A=1;
else
  a1_FC_WT_A=0;
end

str_FT_FC =10   ;                                    %start and stop SOC
HYDROGEN FLOW TANK REQUIRED to supply FUEL CELL
stp_FT_FC =10;
if SOC_H2_FT_A>str_FT_FC
  a2_FT_FC_A=1;
else
  a2_FT_FC_A=0;
end

e_avail_FC_BAT3_A= a1_FC_WT_A && a2_FT_FC_A;  %|| r_FT_FC;

%e_FC_BAT3 = e_avail_FC_BAT3 && e_req_FC_BAT3 &&A_g_FC_BAT3(k);
% e_FC_BAT3 = e_avail_FC_BAT3 && (r_FC_BAT3 ||A_g_FC_BAT3(k));% ;
% e_FC_BAT3 = e_avail_FC_BAT3 &&(r_FC_BAT3  ~);

%e_FC_BAT3_A = e_req_FC_BAT3_A && A_g_FC_BAT3(k) ;



%ACTIVATION FOR BATTERY TO LOAD
% e_BAT3_LD3=e_avail_BAT3_LD3 && e_avail_BAT3_LD3  && g_BAT3_LD3


%ACTIVATION FOR ELECTROLYSER TO FLOW TANK
str_EL_FT = 90       ;                      %start and stop SOC for engaging
the ELECTROLYSER TO SUPPLY FLOW TANK
stp_EL_FT= 100;
if SOC_H2_FT_A<str_EL_FT                    %FT MAKES REQUEST FOR H2 SUPPLY
FROM ELECTROLYSER
    q_EL_FT_A=1;
else
    q_EL_FT_A=0;
end
e_req_EL_FT_A= q_EL_FT_A;
```

```
str_BAT3_EL= 30   ;                    %start and stop SOC for engaging the
BATTERY TO SUPPLY ELECTROLYSER
stp_BAT3_EL =33;
if SOC_BAT3_A>str_BAT3_EL || SOC_BAT3_A<str_BAT3_EL && SOC_BAT3_A>stp_BAT3_EL
%&& A_e_EL_FT_A(k+c-1)>=1  %i==[2881:5832] ensures Winter operation only
  a1_BAT3_EL_A = 1;
else

  a1_BAT3_EL_A=0;
end


str_WT_EL =10   ;                      %start and stop SOC WATER TANK
REQUIRED to supply ELEctrolyser
stp_WT_EL =10;
if SOC_H2O_WT_A>str_WT_EL
  a2_EL_FT_A=1;
else
  a2_EL_FT_A=0;
end

e_avail_EL_FT_A = a1_BAT3_EL_A && a2_EL_FT_A ;% || r_EL_FT;
%e_EL_FT_A = e_req_EL_FT_A &&  (A_g_EL_FT1(k-1+c)&& A_g_EL_FT2(k-1+c)) ;

%ACTIVATION FOR BATTERY TO ELECTROLYSER
e_BAT3_EL_A = e_EL_FT_A;

%ACTIVATION FOR WATER TANK TO ELECTROLYSER
e_WT_EL_A=e_EL_FT_A;

%ACTIVATION FOR FLOW TANK TO FUEL CELL
e_FT_FC_A=e_FC_BAT3_A   ;                          %The Logic for SOC to
CONVERTER is the same as CONVERTER TO SOC

%ACTIVATION FOR FUEL CELL TO WATER TANK
e_FC_WT=e_FC_BAT3;

A_e_BAT3_LD3_A(k)=e_BAT3_LD3_A;
A_e_PV3_BAT3_A(k)= e_PV3_BAT3_A;
A_e_WG2_BAT3_A(k)=e_WG2_BAT3_A;
A_e_BAT3_EL_A(k)=e_BAT3_EL_A ;
A_e_WT_EL_A(k)= e_WT_EL_A ;
A_e_EL_FT_A(k)=e_EL_FT_A  ;
A_e_FT_FC_A(k)=e_FT_FC_A;
A_e_FC_WT_A(k)=e_FC_WT_A;
%A_e_FC_BAT3_A(k)=e_FC_BAT3_A;
A_e_DSL3_BAT3_A(k)=e_DSL3_BAT3_A;
% % %

%%%%%%%%%%%%%%%%%%%%%%%%%%%%%%%%%% FEEDBACK THE STATES OF SOC AND LOGIC
%%%%%%%%%%%%%%%%%%%%%%%%%%%%%%%%%% TO PINCH SECTION
```

```
% e_BAT3_LD3=e_BAT3_LD3_A;
% e_PV3_BAT3= e_PV3_BAT3_A;
% e_WG2_BAT3=e_WG2_BAT3_A;
% e_BAT3_EL=e_BAT3_EL_A ;
% e_WT_EL= e_WT_EL_A;
% e_EL_FT=e_EL_FT_A;
% e_FT_FC=e_FT_FC_A;
% e_FC_WT=e_FC_WT_A;
% e_FC_BAT3=e_FC_BAT3_A;
% e_DSL3_BAT3=e_DSL3_BAT3_A;
%
% SOC_H2O_WT=SOC_H2O_WT_A;
%
% SOC_H2_FT=SOC_H2_FT_A;
%
% SOC_BAT3=SOC_BAT3_A;


% %%%%%%%%%%%%%%%%%%%% END OF ACTUAL SYSTEM
%%%%%%%%%%%%%%%%%%%%%%%%%%%%%%%%%%

%%%%%%%%%%%%%%%%%%%%%%%%COUNTER INCREMENTAL LOOP%%%%%%%%%%
  if k==stop
  startt=stop+1;
  stop=stop+24;
 end

%  Counter=Counter+1;
%  if Counter ==25
%      Counter=1;
%  end
%%%%%%%%%%%%%%%%%%%%%%%%%%%%%%%%%%%%%%%%%%%%%%%%%%%%
ii(k)=k;

sstart(k)=start;







%%%%%%%%%%%%%%%% Q L STEP AHEAD PREDICITON %%%%%%%%%%%%%%%% %%%%%%%%%%%%%%%
%%%%%%%%%%%%%%%% ACTION ON FIRST PREDICITON %%%%%%%%%%%%%%%%%%%%%%%%%%%%%%%

%INSTANTENOUS LOAD POWER
P_BAT3_LD3=LD3(k+1);


%POWER FROM PV SYSTEM
PV3_no=217;
Area_PV3=0.52*PV3_no  ;           %Area for 70W solar panel
if k>start+7 && k<stop-8
    Random=random('norm', 0, 1,1,1);
else
```

```
    Random=1;
end
P_PV3_BAT3=Area_PV3*0.1*I_Rad(k+1); %+ Random) ;     % 0.1 is efficiency for
polycrystalline
%P_PV3_BAT3=Area_PV3*I_RADOM(k+1)*0.1 ;

%POWER WIND TURBINE GENERATOR

P_WG2_BAT3= 0.5 * Air_den *Area_sw  * Cp* ((Wind_vel(k+1))^3) * Ng * Nb*WT_no
;



%FUEL CELL AND ELECTROLYSER POWER FLOW

I_EL=polyval(polyn_EL,P_BAT3_EL)  ;       % Power flow as a function of Power
supplied to the electroliser
I_FC=polyval(polyn_FC,P_FC_BAT3)    ;     % Power flow as a function of Power
supplied to the electroliser

%*e_BAT3_EL *e_FC_BAT3*

Fout_FC_WT_H2O_B= e_FC_WT * 0.85 * nc_FC * 3600* I_FC  / (nF*ne*F)  ;      %
The flow of H2O from FC to WT +VE flow since it goes in to the Water Tank
A_Fout_FC_WT_H2O_B(k)=Fout_FC_WT_H2O_B;


Fout_EL_FT_H2_B = e_EL_FT * nF*nc_EL *  3600* I_EL/(ne*F)  ;
% The flow of H2 from EL to FT   +VE flow since it goes into a Flow Tnak
A_Fout_EL_FT_H2(k)=Fout_EL_FT_H2_B;


Fout_FT_FC_H2_B= e_FT_FC * nc_FC * 3600 *I_FC /(nF*ne*F)   ;
% The flow of H2 out of the FT to the FC  based on the needs of the  FC i.e
*eff -VE flow since it flows out
A_Fout_FT_FC_H2_B(k)=Fout_FT_FC_H2_B;


Fout_WT_H2O_B= e_WT_EL* 1.3 * nF * nc_EL * 3600 * I_EL /(ne*F) ;        % The
flow of H2O from the WT to the EL based on what the EL needs. The Flow is -VE
since it depletes the Water Tank
A_Fout_WT_H2O_B(k)=Fout_WT_H2O_B;

%%WATER TANK AND FLOW TANK MAX CAPACITY CALCULATION
%WT_Cap=1.3*24*(I_FC*nc_FC*nF)*3600/(ne*F)
%Calculate at max Power then set it manually.  Water Tank capacity should
hold moles/hr for 24hrs

%FT_Cap=1.3*24*(I_EL*nc_EL*nF)*3600/(ne*F)                          %Storage
Tank capacity should hold moles/hr for 24hrs


%NET ENERGY FLOW OF POWER STORED IN THE BATTERY     edit the variables so
```

```
%it doesnt conflict the actual system you just need to compare the soc the
%pinch for that interval

P_RES3_B=(e_PV3_BAT3*P_PV3_BAT3)
+(e_WG2_BAT3*P_WG2_BAT3)+(e_DSL3_BAT3*P_DSL3_BAT3)+(0*P_FC_BAT3);
P_BAT3_B= P_RES3_B-(e_BAT3_LD3*P_BAT3_LD3)-(0*P_BAT3_EL);

A_P_BAT3_B(k)=(P_BAT3_B/BAT3_Cap)*100 ;

SOC_BAT3_B1=SOC_BAT3_A+(P_BAT3_B/BAT3_Cap)*100 ;
if SOC_BAT3_B1<=0;
    SOC_BAT3_B1=0;
end
if SOC_BAT3_B1>=100
    SOC_BAT3_B1=100;
end

B1_SOC_BAT3(k)=SOC_BAT3_B1;

% WATER STORED IN THE WATER TANK
 FC_WT_EL=100*(Fout_FC_WT_H2O - Fout_WT_H2O)/WT_Cap;
SOC_H2O_WT_B1= SOC_H2O_WT_A +FC_WT_EL;
if SOC_H2O_WT_B1>=100
    SOC_H2O_WT_B1=100;
end
    if  SOC_H2O_WT_B1<=0
        SOC_H2O_WT_B1=0;
    end
B1_SOC_H2O_WT(k)=SOC_H2O_WT_B1;


%HYDROGEN STORED IN THE FLOW TANK
EL_FT_FC=100*(Fout_EL_FT_H2 - Fout_FT_FC_H2)/FT_Cap;
SOC_H2_FT_B1=SOC_H2_FT_A + EL_FT_FC;
if SOC_H2_FT_B1>=100                          %LIMITS FOR SOC OF WATER TANK
AND FLOW TANK
    SOC_H2_FT_B1=100;
end
if SOC_H2_FT_B1<=0
    SOC_H2_FT_B1=0;
end
B1_SOC_H2_FT(k)=SOC_H2_FT_B1;
%%%%%%%%%%%%%%%%%%%%%%%%%%%%%%%% END OF ACTION 1 PREDICITON %%%%%%%%%%%%%%%

%%%%%%%%%%%%%%%%%%%%%%%%%%%%%%% ACTION 2 ON  PREDICITON %%%%%%%%%%



[aa bb]=size(Pinch_Data);%(A_SOC_BAT3);
if bb>k+1
Pinch_now=Pinch_Data(k);
Pinch_after=Pinch_Data(k+1);
else
Pinch_after=Pinch_Data(k);
Pinch_now=Pinch_Data(k) ;
```

```
end

if k==1
    P_BAT3_EL_B=P_BAT3_EL;
    P_FC_BAT3_B=P_FC_BAT3;
end


E_Action = (Pinch_after-SOC_BAT3_A )*(BAT3_Cap/(100));
if E_Action<0
   P_BAT3_EL_B = E_Action ;
else
    P_FC_BAT3_B=E_Action;
end
P_RES3=(e_PV3_BAT3*P_PV3_BAT3)
+(e_WG2_BAT3*P_WG2_BAT3)+(e_DSL3_BAT3*P_DSL3_BAT3)+(1*P_FC_BAT3);
P_BAT3= P_RES3-(e_BAT3_LD3*P_BAT3_LD3)-(0*P_BAT3_EL_B);

A_P_BAT3(k)=(P_BAT3/BAT3_Cap)*100 ;
SOC_BAT3_B2=SOC_BAT3_A+(P_BAT3/BAT3_Cap)*100 ;
if SOC_BAT3_B2<=0;
    SOC_BAT3_B2=0;
end
if SOC_BAT3_B2>=100
    SOC_BAT3_B2=100;
end

B2_SOC_BAT3(k)=SOC_BAT3_B2;

% WATER STORED IN THE WATER TANK
 FC_WT_EL=100*(Fout_FC_WT_H2O - Fout_WT_H2O)/WT_Cap;
SOC_H2O_WT_B2= SOC_H2O_WT_A +FC_WT_EL;
if SOC_H2O_WT_B2>=100
    SOC_H2O_WT_B2=100;
end
    if  SOC_H2O_WT_B2<=0
        SOC_H2O_WT_B2=0;
    end
B2_SOC_H2O_WT(k)=SOC_H2O_WT_B2;


%HYDROGEN STORED IN THE FLOW TANK
EL_FT_FC=100*(Fout_EL_FT_H2 - Fout_FT_FC_H2)/FT_Cap;
SOC_H2_FT_B2=SOC_H2_FT_A + EL_FT_FC;
if SOC_H2_FT_B2>=100                          %LIMITS FOR SOC OF WATER TANK
AND FLOW TANK
    SOC_H2_FT_B2=100;
end
if SOC_H2_FT_B2<=0
    SOC_H2_FT_B2=0;
end
B2_SOC_H2_FT(k)=SOC_H2_FT_B2;

%%%%%%%%%%%%%%%%%%%%%%%%%END OF ACTION 2 %%%%%%%%%%%%%%%%%%%%%%%%%%%%%%%%
```

```
%%%%%%%%%%%%%%%%%%%%%%%%%% ACTION 3 ON PREDICTION %%%%%%%%%%%%%%%%%%%%%%

P_RES3=(e_PV3_BAT3*P_PV3_BAT3)
+(e_WG2_BAT3*P_WG2_BAT3)+(e_DSL3_BAT3*P_DSL3_BAT3)+(0*P_FC_BAT3);
P_BAT3= P_RES3-(e_BAT3_LD3*P_BAT3_LD3)-(1*P_BAT3_EL);

A_P_BAT3(k)=(P_BAT3/BAT3_Cap)*100 ;
SOC_BAT3_B3=SOC_BAT3_A+(P_BAT3/BAT3_Cap)*100 ;
if SOC_BAT3_B3<=0;
    SOC_BAT3_B3=0;
end
if SOC_BAT3_B3>=100
    SOC_BAT3_B3=100;
end

B3_SOC_BAT3(k)=SOC_BAT3_B3;

% WATER STORED IN THE WATER TANK
 FC_WT_EL=100*(Fout_FC_WT_H2O - Fout_WT_H2O)/WT_Cap;
SOC_H2O_WT_B3= SOC_H2O_WT_A +FC_WT_EL;
if SOC_H2O_WT_B3>=100
    SOC_H2O_WT_B3=100;
end
    if  SOC_H2O_WT_B3<=0
        SOC_H2O_WT_B3=0;
    end
B3_SOC_H2O_WT(k)=SOC_H2O_WT_B3;


%HYDROGEN STORED IN THE FLOW TANK
EL_FT_FC=100*(Fout_EL_FT_H2 - Fout_FT_FC_H2)/FT_Cap;
SOC_H2_FT_B3=SOC_H2_FT + EL_FT_FC;
if SOC_H2_FT_B3>=100                          %LIMITS FOR SOC OF WATER TANK
AND FLOW TANK
    SOC_H2_FT_B3=100;
end
if SOC_H2_FT_B3<=0
    SOC_H2_FT_B3=0;
end
B3_SOC_H2_FT(k)=SOC_H2_FT_B3;


%%%%%%%%%%%%%%%%%%%%%%%% END OF ACTION 3 ON PREDICITON %%%%%%%%%%%%%%%%%%%%%%




State_next= QQ_State_error_typeX_next(Pinch_after,SOC_BAT3_A) ; % Update the
Value function


%REWARD FOR THE ACTUAL ACTION
```

```
% Actual_Reward=RewardX3(Pinch_now,A_SOC_BAT3_A(k-1+c),SOC_BAT3_A,Action_sel)
if Pinch_now<31
Pinch_now=31;
end
if Pinch_now>89
Pinch_now=89;
end
if Pinch_after<31
Pinch_after=31;
end
if Pinch_after>89
Pinch_after=89;
end


SOC_old=A_SOC_BAT3_A(k-1+c);
SOC_new=SOC_BAT3_A;

if SOC_new<30&&SOC_old<30 && SOC_old>SOC_new ||SOC_new<30   ;% Penalise the
actionSOC_old>SOC_new &&&& SOC_new>90
%    Penalty=(abs(SOC_new - SOC_old));%^2*0.5; % tunes sensitivity to failure

elseif SOC_new>90&&SOC_old>90&&SOC_old<SOC_new ||SOC_new>90 ;% Penalise the
actionSOC_old>SOC_new &&&& SOC_new>90
%      Penalty=(abs(SOC_new - SOC_old));%^2*5; % tunes sensitivity to failure
else
%      Penalty=0;
end

% Penalty_A(k)=Penalty;
%  if Penalty>100
%      Penalty=100;
%  end
%%%%%%%%%%%%%%%%%%%%%%%%%%%%%%%%%%%%%%%%%%%%%%%%%%%% CALC THE EFFECT OF ALL
%%%%%%%%%%%%%%%%%%%%%%%%%%%%%%%%%%%%%%%%%%%%%%%%%%%% ACTIONS
ACT1=SOC_BAT3_NO_INT;
ACT2=SOC_BAT3_NO_INT+((P_FC_BAT3*0.1*100)/BAT3_Cap) ;
ACT3=SOC_BAT3_NO_INT+((P_FC_BAT3*0.3*100)/BAT3_Cap) ;
ACT4=SOC_BAT3_NO_INT+((P_FC_BAT3*1*100)/BAT3_Cap)   ;
ACT5=SOC_BAT3_NO_INT-((P_BAT3_EL*0.3*100)/BAT3_Cap) ;
ACT6=SOC_BAT3_NO_INT-((P_BAT3_EL*0.5*100)/BAT3_Cap) ;
ACT7=SOC_BAT3_NO_INT-((P_BAT3_EL*1*100)/BAT3_Cap)   ;

SOC_ACTION=[ACT1 ACT2 ACT3 ACT4 ACT5 ACT6 ACT7];
if Pinch_after>=30&&Pinch_after<80
Best_min_ACT=min(find(SOC_ACTION>=Pinch_after));
elseif Pinch_after>80&&Pinch_after<=90
       Best_min_ACT=min(find(SOC_ACTION<=Pinch_after));
end

if Action_sel==Best_min_ACT
   Actual_Reward=1;                        %Goal
elseif SOC_new<Pinch_after
    Actual_Reward=0-1*abs((SOC_new-Pinch_after)/Pinch_after)^2; %-W1
```

```
elseif SOC_new>Pinch_after
       Actual_Reward=1-1*abs((SOC_new-Pinch_after)/Pinch_after)^2;    %G-W1
elseif SOC_new>90&&SOC_old>90&&SOC_old<SOC_new ||SOC_new>90
       Actual_Reward=-1*abs((SOC_new-Pinch_after)/Pinch_after)^2 -10;    %-
(W1+W2) penalise persistent erroroneuos actions
elseif SOC_new<30&&SOC_old<30 && SOC_old>SOC_new ||SOC_new<30
       Actual_Reward=-1*abs((SOC_new-Pinch_after)/Pinch_after)^2 -10;
end

%%%%%%%%%%%%%%%%%%%%%%%%%%%%%%%%%%%%%%%%%%%%%%%%%%%%%%%%%%%%%%%%%%%%%%%%%%%%%%%%
%


%%%%%%%%%%%%%%%%%%%%%%%%%%%%%%%%%%%%%%%%%%%%%%%%%%%%%%%%%%%%%%%%%%%%%%%%%%%%%%%%
if SOC_new<30&&SOC_old>30||SOC_new>90&&SOC_old<90
   % Actual_Reward=1;
else
    %Actual_Reward=0;
end



% Actual_Reward=100-(abs(Pinch_after - SOC_BAT3_A) -Penalty);%(Pinch_after -
SOC_BAT3_A)^2*10

if SOC_new<30&&SOC_old>30||SOC_new>90&&SOC_old<90
%    Actual_Reward=-1000;
end


% if abs(Pinch_after - SOC_BAT3_A)<3
%     Actual_Reward=1000;
% elseif abs(Pinch_after - SOC_BAT3_A)>=3&& abs(Pinch_after - SOC_BAT3_A)<5
%     Actual_Reward=50;
% elseif abs(Pinch_after - SOC_BAT3_A)>=5
%     Actual_Reward=-2000;
% end

if SOC_new>30&&SOC_old<30||SOC_new<90&&SOC_old>90
%    Actual_Reward=1000;
end

if k==350
%     pause(2)
end


 if Actual_Reward<-1000
%  Actual_Reward=-1000;
 elseif Actual_Reward>2000
%       Actual_Reward=2000;
 end

% % if Pinch_now<A_SOC_BAT3_A(k-1+c)&& Action_sel==3
```

```
% %     Actual_Reward=100
% % else
% % if   Action_sel==1
% %      Actual_Reward=100-(Pinch_now-SOC_BAT3_B1)^2*10
% % elseif   Action_sel==2
% %     Actual_Reward=100-(Pinch_now-SOC_BAT3_B2)^2*10
% % end
% % end
% %
% % if Pinch_now>SOC_BAT3_A && Action_sel==2
% %     Actual_Reward=100
% % else
% % if   Action_sel==1
% %  Actual_Reward=100-(Pinch_now-SOC_BAT3_B1)^2*10
% % elseif   Action_sel==3
% %  Actual_Reward=100-(Pinch_now-SOC_BAT3_B3)^2*10
% % end
% % end
% %
% % if Pinch_now==SOC_BAT3_A && Action_sel==1
% %     Actual_Reward=100
% % else
% %      if   Action_sel==3
% %      Actual_Reward=100-(Pinch_now-SOC_BAT3_B3)^2*10
% % elseif   Action_sel==2
% %     Actual_Reward=100-(Pinch_now-SOC_BAT3_B2)^2*10
% % end
% % end
%
%
%
% % if Pinch_after>SOC_BAT3_A
% %     Action_sel_next=2;
% % end
% % if Pinch_after<SOC_BAT3_A
% %     Action_sel_next=3;
% % end
% % if Pinch_after==SOC_BAT3_A
% %     Action_sel_next=1;
% % end
%
%
%
% %REWARD FOR THE FIRST ACTION PREDICTED %%%%
%
Future_Reward_1=RewardX3_1(Pinch_after,SOC_BAT3_A,SOC_BAT3_B1,1);%SOC_BAT3_B1
,
% %REWARD FOR THE SECOND ACTION PREDICTED %%%%
% Future_Reward_2=RewardX3_2(Pinch_after,SOC_BAT3_A,SOC_BAT3_B2,2);
%
% %REWARD FOR THE THIRD ACTION PREDICTED %%%%
% Future_Reward_3=RewardX3_3(Pinch_after,SOC_BAT3_A,SOC_BAT3_B3,3);
%
%
% % UPDATE OF Q TABLE %%%%%%
%
%  %compare reward select best
```

```
%       Future_Reward=[Future_Reward_1, Future_Reward_2 ,Future_Reward_3];
%       Reward_Max=max(Future_Reward);
%       if Future_Reward(1,1)==Future_Reward(1,3)
%           Action_sel_next=2
%       else
     % Action_sel_next=find(Future_Reward(1:3)==Reward_Max)
%       end
%

abs_Qmax=max(abs(Q_Table(State_next,:)));           %Uses the absolute
maximum value of the Q_Table rather than the norminal max
abs_Action=find((abs(Q_Table(State_next,:)))==abs_Qmax);

Q_Table;

if e_avail_FC_BAT3_A==1 && e_avail_EL_FT_A==1 && bb>k+2%
Q_Table(State,Action_sel)=Q_Table(State,Action_sel)+ Alpha*(Actual_Reward +
gamma*max(Q_Table(State_next,:) - Q_Table(State,Action_sel)));
else
Q_Table(State,Action_sel)=Q_Table(State,Action_sel);%+ Alpha*(Actual_Reward -
Q_Table(State,Action_sel));
end

Q_T(k)=Q_Table(State,Action_sel);
Q_T_mean(k)=Q_T(k)/1000;
dQ_T(k)=(abs(Q_T(k))- abs(Q_T(k-1+c)));%/abs(Q_T(k-1+c));

% if k>1&& abs(dQ_T(k-1)-dQ_T(k))>1000 &&Alpha<0.06       %%%ADAPTIVE
LEARNING RATE
%     Alpha=Alpha+0.01;
%     if Alpha>0.1
%         Alpha=0.1;
%     end
% end

% tz=1:1:8759;
% ys = smooth(tz,Q_T,0.025,'rloess');
% plot(tz,Q_T)
% plot(tz,Q_T,tz,ys)



ReplayQ(k,1)=State;
ReplayQ(k,2)=Action_sel;
ReplayQ(k,3)=State_next;
ReplayQ(k,4)=Actual_Reward;
ReplayQ(k,5)=Alpha*(Actual_Reward + gamma*max(Q_Table(State_next,:) -
Q_Table(State,Action_sel)));
ReplayQ(k,7)=SOC_BAT3_A; %after action
ReplayQ(k,8)=Prob_sel;
ReplayQ(k,9)=Pinch_now;
ReplayQ(k,10)=Pinch_after;

 if bb>k+1
     Qmax=max(Q_Table);
```

```
     Qmax_past=0;
     [Length_Repl ~]=size(ReplayQ);

%     while Qmax>Qmax_past-0.01%|Qmax>0.01+Qmax_past
Alpha_RR=Alpha;%0.05
   for N=1:2%100
       xx=0;
%       if k==1000
%           xx=1000;
%       end
%           if k==3000
%           xx=2000;
%           end
%           if k==4000
%               xx=3000;
%           end
%           if k==6000
%               xx=4000;
%
%           end
%               if k== 8000
%                   xx=5000;
%               end

        Alpha_R=Alpha_RR/(1+N/100);

         if startt>200
             xk=Length_Repl-100;
         else
             xk=startt;
         end
         Replay_sel=ReplayQ(xk:Length_Repl,:);
         Replay_sel=sortrows(Replay_sel,-5);
         Length_Repl1=size(Replay_sel);



         V_U=find(A_SOC_BAT3_A>90) ; % use the index of upper violation to
replay
         V_L=find(A_SOC_BAT3_A<30);
         Vu=size(V_U);
         vl=size(V_L);
          Replay_sel=ReplayQ([V_U,V_L],:);
%             Replay_sel=ReplayQ([V_U],:);
           Replay_sel=sortrows(Replay_sel,7);
           Length_Repl1=size(Replay_sel);
           if Length_Repl1>200
             xk=Length_Repl1-100;
         else
             xk=1;
         end
%

for M=xk:1:Length_Repl1
```

```
%          Replay_sel=sortrows(ReplayQ,-5);%ReplayQ;%
%        Qmax_past=max(Q_Table);
           M=datasample(xk:Length_Repl1,1 ,'Replace',false);

Q_Table(Replay_sel(M,1),Replay_sel(M,2))=Q_Table(Replay_sel(M,1),Replay_sel(M
,2))+Alpha_R*Replay_sel(M,5);
%         Qmax=max(Q_Table);
end
%  Alpha_R=0.02;

 end

 end


if  Action_sel==1
      ACTION_1_COUNT=ACTION_1_COUNT+1;
    else
        ACTION_1_COUNT=ACTION_1_COUNT;
    end

    if Action_sel==2
         ACTION_2_COUNT=ACTION_2_COUNT+1;
    else
        ACTION_2_COUNT=ACTION_2_COUNT ;
    end

    if Action_sel==3
         ACTION_3_COUNT=ACTION_3_COUNT+1;
    else
        ACTION_3_COUNT=ACTION_3_COUNT   ;
    end

%     if Action_sel==4
%          ACTION_4_COUNT=ACTION_4_COUNT+1
%     else
%         ACTION_4_COUNT=ACTION_4_COUNT
%     end


%%%%%%%%%%%%%%% IAE CALC %%%%%%%%%%%%%%
SOC_ref=Pinch_Data(k);
if Pinch_Data(k)<30||SOC_BAT3_A<30
    SOC_ref=30;
end
if Pinch_Data(k)>90||SOC_BAT3_A>90
    SOC_ref=90;
end

A_SOC_ref(k)=SOC_ref;
A_NET_ref(k)=(SOC_ref/100)*BAT3_Cap;
A_NET_ref_A(k)=(SOC_BAT3_A/100)*BAT3_Cap;
IAE=abs(SOC_ref-SOC_BAT3_A)/SOC_ref;% change between system and model
A_IAE(k)=IAE;
```

```
% tt=1:8760;
% A_SOC_ref(8760)=30
% plot(tt,A_SOC_ref,tt,A_SOC_BAT3_A) %

%    %%%%%%%%%%%%%%%% IAE CALC %%%%%%%%%%%%%%
% SOC_ref=Pinch_Data(k);
% if Pinch_Data(k)<30%||SOC_BAT3_A<30
%     SOC_ref=30;
% end
% if Pinch_Data(k)>90%||SOC_BAT3_A>90
%     SOC_ref=90;
% end
%
% A_SOC_ref(k)=SOC_ref;
% IAE=abs(SOC_ref-SOC_BAT3_A)/SOC_ref;% change between system and model
% A_IAE(k)=IAE;
% %IAE_avg=sum(A_IAE)/8760;
end



end
```

Appendix F

RLS Probabilistic Adaptive PoPA .m Code

```
rng('default')

%Dont Temper with this Version for recalculates when there is error between
model and system Pinch analysis in the whole Year
%find(Recall(1,1:k)==1)% finds where adaptive recalculation occurred
%Adaptive MPC PINCH recalculates every time there is difference between
%model and Actual system.


%PREDICTION TOP LEVEL INITIALIZATION FOR PV AND WIND DATA INPUT
I_rad = dlmread('PV_POA.csv');          %Plane of Array for insolation
I_Rad=I_rad';
%I_Rad=[I_Rad(2688:8760),I_Rad(1:2687)];


Ng=0.96;
Nb=0.72;
Air_den=1.23    ;                        %Air density 1.23 Kg/m3
Cp=0.4;
Area_sw=3.24 ;                           %Wind Turbine Swept Area
WT_no=3;
WT_wind = dlmread('WT_Wind.csv');       %Velocity of Wind m/s
Wind_vel=WT_wind';


LD3=ones(1,8760)*1000;                   % Constant Load for a year

LD3_daily=24*1000;                         %Load per day

P_DSL3_BAT3= 2010;

%Counter=0 ;                             %counts the no.of iteration



%%

%%%%%%%%%%%%%%%%%%%%%%%%%%%%%%%%%%%%%%%% START OF MICROGRID 3 INITIALIZATION
%%%%%%%%%%%%%%%%%%%%%%%%%%%%%%%%%%%%%%%%%%%%%%%%%%%%%%%%%%%%

%INITIALIZING ACTIVATION STATES OF THE NODES
e_BAT3_LD3=1;
e_PV3_BAT3=0;                %PV3 is the solar panel in microgrid 3, WG2 is
the wind turbine in microgrid 3
e_WG2_BAT3=0;
e_BAT3_EL=0  ;                %EL is the ELectrolyser, WT is the Water Tank,
FC is the Fuel Cell
e_WT_EL=0    ;
e_EL_FT=0    ;                  %FT is the Hydrogen storage tank
e_FT_FC=0;
e_FC_BAT3=0;
e_FC_WT=0;
e_DSL3_BAT3=0;
```

```
e_BAT3_EL = e_EL_FT;

%ACTIVATION FOR WATER TANK TO ELECTROLYSER
e_WT_EL=e_EL_FT;

%ACTIVATION FOR FLOW TANK TO FUEL CELL
e_FC_BAT3 =e_FT_FC       ;                      %The Logic for SOC to
CONVERTER is the same as CONVERTER TO SOC

%ACTIVATION FOR FUEL CELL TO WATER TANK
e_FC_WT=e_FC_BAT3;

%INITIALIZING AVAILABILITY OVERRIDE
r_PV3_BAT3=0;
r_WG2_BAT3=0;
r_BAT3_EL=0;
r_WT_EL=0;
r_EL_FT=0;
r_FT_FC=0;
r_FC_WT=0;
r_FC_BAT3=0;
r_BAT3_LD3=0;
r_DSL3_BAT3=0;

%INITIALIZING GENERALITY CONSTRAINT FOR ACTIVATION (OVERRIDE)

g_PV3_BAT3=1;
g_WG2_BAT3=0;
g_BAT3_EL=1;
g_WT_EL=1;
g_EL_FT=1;
g_FT_FC=1;
g_FC_WT=1;
g_FC_BAT3=1;
g_BAT3_LD3=1;
g_DSL3_BAT3=1;



%
%INITIALIZING ACTIVATION STATES OF THE NODES
e_BAT3_LD3_A=1;
e_PV3_BAT3_A=0   ;               %PV3 is the solar panel in microgrid 3, WG2
is the wind turbine in microgrid 3
e_WG2_BAT3_A=0;
e_BAT3_EL_A=0    ;               %EL is the ELectrolyser, WT is the Water
Tank, FC is the Fuel Cell
e_WT_EL_A=0    ;
e_EL_FT_A=0    ;                 %FT is the Hydrogen storage tank
e_FT_FC_A=0;
e_FC_BAT3_A=0;
e_FC_WT_A=0;
e_DSL3_BAT3_A=0;

e_BAT3_EL_A = e_EL_FT_A;
```

```
%ACTIVATION FOR WATER TANK TO ELECTROLYSER
e_WT_EL_A=e_EL_FT_A;

%ACTIVATION FOR FLOW TANK TO FUEL CELL
e_FC_BAT3_A =e_FT_FC_A       ;                      %The Logic for SOC to
CONVERTER is the same as CONVERTER TO SOC

%ACTIVATION FOR FUEL CELL TO WATER TANK
e_FC_WT_A=e_FC_BAT3_A;
%

% %INITIALIZE SOCs EL AND FC
 SOC_BAT3_A=80  ;%70                                 %Tweek #SOC_BAT3 to alter
the SOC LEVEL FOR BATTERY 3
 SOC_H2_FT_A=90;%80
 SOC_H2O_WT_A=50;%30
%

% %VARIABLE DECLARATION FOR MEMORY
A_e_BAT3_LD3_A=zeros(1,8760);
A_e_PV3_BAT3_A= zeros(1,8760)      ;
A_e_WG2_BAT3_A=zeros(1,8760);
A_e_BAT3_EL_A=zeros(1,8760)       ;
A_e_WT_EL_A= zeros(1,8760);
A_e_EL_FT_A=zeros(1,8760)      ;
A_e_FT_FC_A=zeros(1,8760);
A_e_FC_WT_A=zeros(1,8760);
A_e_FC_BAT3_A=zeros(1,8760);
A_e_DSL3_BAT3_A=zeros(1,8760);
A_F_FC_WT_EL_A=zeros(1,8760);
A_F_EL_FT_FC_A=zeros(1,8760);
A_R_e_FC_BAT3=zeros(1,8760);
A_R_e_BAT3_EL=zeros(1,8760);
% %%%%%%%%%%%%%%%%%%%%%%%%%%%%%%%%%%%%%%%% END OF REAL SYSTEM MICROGRID 3
INITIALIZATION %%%%%%%%%%%%%%%%%%%%%%%%%%%%%%%%%%%%%%%%%%%%%%%%%%%%%%%%
%


% INITIALIZING BATTERY CAPACITY
% Battery3 capacity   3KAh*12V = 36KWh
BAT3_Cap=36000;%20000;%


%INITIALIZING DIESEL GENERATOR3


%INITIALIZING FUEL CELL AND ELECTROLYSER DYNAMICS
polyn_EL=[-0.000001426704372 0.027954416509736 2.502267281445165];  %Transfer
function for Electrolyser
polyn_FC=[0.000000895442340 0.033197516886985 -0.278092554468687];  %Transfer
function for Fuel Cell

nc_EL=15;                           % no. of cells in the electrolyser
```

```
nc_FC=40;                           % no. of cells in the fuel cell
nF=0.87;                            % Efficiency
ne=2;                               % no. of electron
F=96485;                            % Faraday's constant W/mol
P_BAT3_EL=4000;                          % Power required per time by the
Electrolyser
P_FC_BAT3=3000;                          % Max power the Fuel cell can
deliver

WT_Cap=2.1749e+03*2;
FT_Cap=974.3583*2;%2000*10

%INITIALIZE SOCs EL AND FC
SOC_BAT3=80  ;                                %Tweek #SOC_BAT3 to alter the
SOC LEVEL FOR BATTERY 3
SOC_H2_FT=100;
SOC_H2O_WT=30;

%%%% ELECTROLYSER ACTIVATION %%%%%%%
EL_SUMMER=zeros(1,8760);
EL_SUMMER(1:8760)=1;
%EL_SUMMER(1:2160)=1;
%EL_SUMMER(6553:8760)=1;

%%%% FUEL CELL ACTIVATION %%%%%
FC_WINTER=zeros(1,8760);
FC_WINTER(1:8760)=1;%(100:8000)(2881:5832)

%VARIABLE DECLARATION FOR MEMORY
A_e_BAT3_LD3=zeros(1,8760);
A_e_PV3_BAT3= zeros(1,8760)      ;
A_e_WG2_BAT3=zeros(1,8760);
A_e_BAT3_EL=zeros(1,8760)       ;
A_e_WT_EL= zeros(1,8760);
A_e_EL_FT=zeros(1,8760)       ;
A_e_FT_FC=zeros(1,8760);
A_e_FC_WT=zeros(1,8760);
A_e_FC_BAT3=zeros(1,8760);
A_e_DSL3_BAT3=zeros(1,8760);
A_F_FC_WT_EL=zeros(1,8760);
A_F_EL_FT_FC=zeros(1,8760);


A_g_FC_BAT3=zeros(1,8760);
A_g_EL_FT1=zeros(1,8760);
A_g_EL_FT2=zeros(1,8760);


%%%%%%%%%%%%%%%%%%%%%%%%%%%%%%%%%%%%%%%%%%%%%%%%%%%%%%%%%%%%%%ACTUAL
%%%%%%%%%%%%%%%%%%%%%%%%%%%%%%%%%%%%%%%%%%%%%%%%%%%%%%%%%%%%%%INITIALIZATION
%%%%%%%%%%%%%%%%%%%%%%%%%%%%%%%%%%%%%%%%%%%%%%%%%%%%%%%%%%%%%%%%%%%%%%%%%%%
%INITIALIZING ACTIVATION STATES OF THE NODES
e_BAT3_LD3_A=1;
e_PV3_BAT3_A=0   ;                %PV3 is the solar panel in microgrid 3, WG2
is the wind turbine in microgrid 3
```

```
e_WG2_BAT3_A=0;
e_BAT3_EL_A=0    ;               %EL is the ELectrolyser, WT is the Water
Tank, FC is the Fuel Cell
e_WT_EL_A=0    ;
e_EL_FT_A=0    ;                 %FT is the Hydrogen storage tank
e_FT_FC_A=0;
e_FC_BAT3_A=0;
e_FC_WT_A=0;
e_DSL3_BAT3_A=0;

e_BAT3_EL_A = e_EL_FT_A;

%ACTIVATION FOR WATER TANK TO ELECTROLYSER
e_WT_EL_A=e_EL_FT_A;

%ACTIVATION FOR FLOW TANK TO FUEL CELL
e_FC_BAT3_A =e_FT_FC_A       ;                      %The Logic for SOC to
CONVERTER is the same as CONVERTER TO SOC

%ACTIVATION FOR FUEL CELL TO WATER TANK
e_FC_WT_A=e_FC_BAT3_A;

% %INITIALIZE SOCs EL AND FC
 SOC_BAT3_A=80  ;                                 %Tweek #SOC_BAT3 to alter
the SOC LEVEL FOR BATTERY 3
 SOC_H2_FT_A=100;
 SOC_H2O_WT_A=30;

% %VARIABLE DECLARATION FOR MEMORY
A_e_BAT3_LD3_A=zeros(1,8760);
A_e_PV3_BAT3_A= zeros(1,8760)      ;
A_e_WG2_BAT3_A=zeros(1,8760);
A_e_BAT3_EL_A=zeros(1,8760)       ;
A_e_WT_EL_A= zeros(1,8760);
A_e_EL_FT_A=zeros(1,8760)      ;
A_e_FT_FC_A=zeros(1,8760);
A_e_FC_WT_A=zeros(1,8760);
A_e_FC_BAT3_A=zeros(1,8760);
A_e_DSL3_BAT3_A=zeros(1,8760);
A_F_FC_WT_EL_A=zeros(1,8760);
A_F_EL_FT_FC_A=zeros(1,8760);
A_R_e_FC_BAT3=zeros(1,8760);
A_R_e_BAT3_EL=zeros(1,8760);


%%%%%%%%%%%%%%%%%%%%%%%%%%%%%%%%%%%%%%%%%%%%%%%%%%%%%%%%%%%%%%%%%%%%%%%%%%%%


EL_ON1=zeros(24,24);
EL_ON2=zeros(24,24);
FC_ON=zeros(24,24);


startt=1;
```

```
start=1;
stop=24;
Counter=0;
Counter2=0;


k=1;

PINCH_DATA=[];
A_SOC_BAT3=zeros(1,240);
Recall=zeros(1,240);


ran=repmat(Rando,1,365);
ran=repmat(noise_for_load,1,365);


P_BAT3_EL=zeros(1,8760)*P_BAT3_EL;
P_FC_BAT3=zeros(1,8760)*P_FC_BAT3;
A_g_EL_FT=zeros(1,8760);
% P_BAT3_EL(1)=4000;
% P_FC_BAT3(1)=3000;

A_SOC_ref=zeros(1,8760);
A_IAE=zeros(1,8760);
A_FC_ATTEMPT=zeros(1,8760);
A_EL_ATTEMPT=zeros(1,8760);
A_Power_FC=zeros(1,8760);
number_count=0;
EPL=zeros(1,8760);
A_t_violation_EL=zeros(1,24);
Unserved_load=0;
Lost_Energy=0;
Excess_Energy_lost=0;


 WT_Cap=2.1749e+03*15;%15;%15;
 FT_Cap=974.3583*10;%50;%2000*10  FT_Cap =9.7436e+03




%history of Load distribution for the past year.

CCC=dlmread('LD_ARRAY.csv');
LDD=CCC;
LDD1=LDD(:,1:91);
LD1=repmat(LDD1,1,24);% replicates distribution of load for the entire Winter
season
LDD2=LDD(:,91:182);
LD2=repmat(LDD2,1,24); %Replicates distribution for SPRING
```

```
LDD3=LDD(:,182:273);
LD3=repmat(LDD3,1,24); %SUMMER
LDD4=LDD(:,273:362);
LD4=repmat(LDD4,1,24); %AUTUMN
LD_ARRAY=[LD1,LD2,LD3,LD4]*1.38%*1.38;% Combines the population of load
distribution for the entire year.
LD_ARRAY=LD_ARRAY';

LD3_A=repmat(Actual_load,1,365);% agussian

A=1;
B=0;
XxY1=1;
RLS=1;
l=0;
S_min=0;
S_max=0;
% LD3_A=dlmread('ACTUAL_LD.csv');
%$%%%%%%%%%%%%%%%%%%%%%%%%%%%%%%%%%%
counta=0;
counta_A=0;

 WT_Cap=2.1749e+03*300;%
 FT_Cap=974.3583*300;%

 %LD3_A=dlmread('ACTUAL_LD_S2.csv')*1.5;

 while k<=8760%71%719%8760
for k=1:1:8761%72%720%8761% %determines the number of hours to run the Pinch
analysis
%for k=start:1:stop

    Counter2=Counter2+1;

for xx=k:1:stop

    %Form a PDF using LD ARRAY at time K instance then Extract LD randomly
for PDF
    if k<2190
    r1=1; %Range to select load from Load CLUSTER 1
    r2=2190; %

    %elseif k>2190%&&k<4380
    elseif k<4380      %CLUSTER  2
        r1=2190;
        r2=4380;
    elseif k <6570      %CLUSTER 3
        r1=4380;
        r2=6570;
    elseif k>6570
        r1=6570;
        r2=8760;
    end
    counta=counta+1;
    if counta>24
```

```
        counta=1;
    end
    LD_PD=fitdist(LD_ARRAY(r1:r2,counta),'Kernel');
    LD3(xx)=mean(LD_ARRAY(r1:r2,counta));% for regular adaptive PoPA
    LD_R=random(LD_PD,1000,1);

%         LD3_A(xx)=random(LD_PD,1,1);

%     LD_RA=random(LD_PD,1000,1);
    A_LD_R(:,xx)=LD_R; % contains random sampled load PDF
end

if (stop-start)==23||(A_SOC_BAT3_A(k-1)<30||A_SOC_BAT3_A(k-
1)>90)||(Upper_b(end,k-1)>5+A_SOC_BAT3_A(k-1) ||Lower_b(end,k-1)<-
5+A_SOC_BAT3_A(k-1))% &&SOC_BAT3>10/100*SOC_BAT3_A %Do recalculation only if
the deviation is state>10%(A_SOC_BAT3(k-1)<30||A_SOC_BAT3(k-1)>90)||
%
%     P_BAT3_EL(k:end)=0;  %reset all Pinch logic if discrepancy occurs
%     P_FC_BAT3(k:end)=0;
 end
% end

%  for l=1:1:10
  while
S_min<30||S_max>90||S_min>90||S_max<30%||Smin>30&&Smax<90||Smin<30&&Smax<90||
Smin>30&&Smax<90
            l=l+1;

       start=k;
       if k==1
          stop=24;
       startt=1;
       end
        if k==72%1625%73%36%20||k==24||40 %48&&l==1%41%24
       pause(2)
        display('paused for 0.5 Seconds')
       end

 if (stop-start)==23||(A_SOC_BAT3_A(k-1)<30||A_SOC_BAT3_A(k-
1)>90)||(Upper_b(end,k-1)>5+A_SOC_BAT3_A(k-1) ||Lower_b(end,k-1)<-
5+A_SOC_BAT3_A(k-1)) % &&SOC_BAT3>10/100*SOC_BAT3_A %Do recalculation only if
the deviation is state>10%(A_SOC_BAT3(k-1)<30||A_SOC_BAT3(k-1)>90)||
  %Power_FC=0;  %reset the MOES if the horizon changes
%   P_BAT3_EL(k:end)=0;
%   P_FC_BAT3(k:end)=0;
  %P_FC_BAT3=zeros(1,8760);


  n=1000; %number of samples
for z=1:1:n %iterate for the number of times montecarlo is needed.

 if start>1
SOC_BAT3=A_SOC_BAT3_A(start-1) ;                                    %Tweek
#SOC_BAT3 to alter the SOC LEVEL FOR BATTERY 3
SOC_H2_FT=A_SOC_H2_FT_A(start-1);
```

```
SOC_H2O_WT=A_SOC_H2O_WT_A(start-1);
% e_BAT3_EL = A_e_BAT3_EL_A(start-1);
% e_FC_BAT3=  A_e_FC_BAT3_A(start-1);


e_BAT3_LD3= A_e_BAT3_LD3_A(start-1)  ;
e_PV3_BAT3= A_e_PV3_BAT3_A(start-1)  ;
e_WG2_BAT3=  A_e_WG2_BAT3_A(start-1) ;

e_WT_EL = A_e_WT_EL_A(start-1);
e_EL_FT = A_e_EL_FT_A(start-1);
e_FT_FC= A_e_FT_FC_A(start-1);
e_FC_WT=  A_e_FC_WT_A(start-1);


e_DSL3_BAT3= A_e_DSL3_BAT3_A(start-1);

%ACTIVATION FOR BATTERY TO ELECTROLYSER
%e_BAT3_EL = e_EL_FT;

%ACTIVATION FOR WATER TANK TO ELECTROLYSER
e_WT_EL=e_EL_FT;

%ACTIVATION FOR FLOW TANK TO FUEL CELL
e_FT_FC=e_FC_BAT3;                                  %The Logic for SOC to
CONVERTER is the same as CONVERTER TO SOC

%ACTIVATION FOR FUEL CELL TO WATER TANK
e_FC_WT=e_FC_BAT3;
 end
%%%%%%%%%%%%%%%%%%%%%%%

 if start==1
SOC_BAT3=80 ;
SOC_H2O_WT=30;
SOC_H2_FT=100   ;
%INITIALIZING ACTIVATION STATES OF THE NODES
e_BAT3_LD3=1;
e_PV3_BAT3=0   ;                %PV3 is the solar panel in microgrid 3, WG2 is
the wind turbine in microgrid 3
e_WG2_BAT3=0;
e_BAT3_EL=0    ;                %EL is the ELectrolyser, WT is the Water Tank,
FC is the Fuel Cell
e_WT_EL=0    ;
e_EL_FT=0    ;                  %FT is the Hydrogen storage tank
e_FT_FC=0;
e_FC_BAT3=0;
e_FC_WT=0;
e_DSL3_BAT3=0;

e_BAT3_EL = e_EL_FT;

% ACTIVATION FOR WATER TANK TO ELECTROLYSER
e_WT_EL=e_EL_FT;
```

```
% ACTIVATION FOR FLOW TANK TO FUEL CELL
e_FC_BAT3 =e_FT_FC       ;                        %The Logic for SOC to
CONVERTER is the same as CONVERTER TO SOC

% ACTIVATION FOR FUEL CELL TO WATER TANK
e_FC_WT=e_FC_BAT3;
   end




for j=k:1:stop %j=start:1:stop
%    if start==1 %stop-start==23 &&
%        c=-1;
%    else
%        c=0;
%    end


if k>0
    if
k==stop&&l>1&&ceil(Lower_b(l,stop))~=50&&(Lower_b(l,startt)>=30&&Lower_b(l,st
artt)<=90)
    sss=-1;%0
else
    sss=0;
    end
end
%Counter=Counter+1
%%%%%% MICROGRID3 %%% MICROGRID 3 %%%%%% MICROGRID3 %%% MICROGRID 3 %%%%%%
MICROGRID3 %%% MICROGRID 3



%%%%%ITERATION %%%% ITERATION

%INSTANTENOUS LOAD POWER
P_BAT3_LD3=A_LD_R(z,j);


%POWER FROM PV SYSTEM
PV3_no=217;
Area_PV3=0.52*PV3_no        ;           %Area for 70W solar panel

P_PV3_BAT3=Area_PV3*I_Rad(j)*0.1 ;     % 0.1 is efficiency for
polycrystalline

%POWER WIND TURBINE GENERATOR

P_WG2_BAT3= 0.5 * Air_den *Area_sw  * Cp* ((Wind_vel(j))^3) * Ng * Nb*WT_no ;
```

```
%FUEL CELL AND ELECTROLYSER POWER FLOW

I_EL=polyval(polyn_EL,P_BAT3_EL(j))  ;       % Power flow as a function of
Power supplied to the electroliser
I_FC=polyval(polyn_FC,P_FC_BAT3(j))  ;     % Power flow as a function of
Power supplied to the electroliser

%*e_BAT3_EL *e_FC_BAT3*

Fout_FC_WT_H2O= e_FC_WT * 0.85 * nc_FC * 3600* I_FC  / (nF*ne*F)  ;      %
The flow of H2O from FC to WT +VE flow since it goes in to the Water Tank
%A_Fout_FC_WT_H2O(k,j)=Fout_FC_WT_H2O;


Fout_EL_FT_H2= e_EL_FT * nF*nc_EL *  3600* I_EL/(ne*F)  ;                  %
The flow of H2 from EL to FT   +VE flow since it goes into a Flow Tnak
%A_Fout_EL_FT_H2(k,j)=Fout_EL_FT_H2;


Fout_FT_FC_H2= e_FT_FC * nc_FC * 3600 *I_FC /(nF*ne*F)   ;                 %
The flow of H2 out of the FT to the FC  based on the needs of the  FC i.e
*eff -VE flow since it flows out
%A_Fout_FT_FC_H2(k,j)=Fout_FT_FC_H2;


Fout_WT_H2O= e_WT_EL* 1.3 * nF * nc_EL * 3600 * I_EL /(ne*F) ;        % The
flow of H2O from the WT to the EL based on what the EL needs. The Flow is -VE
since it depletes the Water Tank
%A_Fout_WT_H2O(k,j)=Fout_WT_H2O;

%%WATER TANK AND FLOW TANK MAX CAPACITY CALCULATION
%WT_Cap=1.3*24*(I_FC*nc_FC*nF)*3600/(ne*F)
%Calculate at max Power then set it manually.  Water Tank capacity should
hold moles/hr for 24hrs

%FT_Cap=1.3*24*(I_EL*nc_EL*nF)*3600/(ne*F)                              %Storage
Tank capacity should hold moles/hr for 24hrs


%NET ENERGY FLOW OF POWER STORED IN THE BATTERY
A_P_PV3_BAT3(z,j)=P_PV3_BAT3;
A_P_WG2_BAT3(z,j)=P_WG2_BAT3;
P_RES3=(e_PV3_BAT3*P_PV3_BAT3)+(e_WG2_BAT3*P_WG2_BAT3)+(e_DSL3_BAT3*P_DSL3_BA
T3)+(A_g_FC_BAT3(j+sss)*P_FC_BAT3(j+sss));
A_P_RES3(z,j)=P_RES3;
P_BAT3= P_RES3-(e_BAT3_LD3*P_BAT3_LD3)-(A_g_EL_FT(j+sss)*P_BAT3_EL(j+sss));
if P_BAT3<=0
   Deficit_P_BAT3=1;
else
    Deficit_P_BAT3=0;
end
A_Deficit_P_BAT3(z,j)=Deficit_P_BAT3;
```

```
if P_BAT3>P_BAT3_LD3&&SOC_BAT3>90&&SOC_H2_FT>90 && SOC_H2O_WT>40
    Surplus_P_BAT3=1;
else
    Surplus_P_BAT3=0;
end
A_Surplus_P_BAT3(z,j)=Surplus_P_BAT3;


A_P_BAT3(z,j)=(P_BAT3/BAT3_Cap)*100 ;
SOC_BAT3=SOC_BAT3+(P_BAT3/BAT3_Cap)*100 ;
if SOC_BAT3<=0;
    SOC_BAT3=0;
end
if SOC_BAT3>=100
    SOC_BAT3=100;
end

A_SOC_BAT3(z,j)=SOC_BAT3;

if SOC_BAT3<30
   Deficit_SOC_BAT3=1;
else
   Deficit_SOC_BAT3=0;
end
 A_Deficit_SOC_BAT3(z,j)= Deficit_SOC_BAT3;

 if j<=1
     c=1;
 else
     c=0;
 end

% WATER STORED IN THE WATER TANK
 FC_WT_EL=100*(Fout_FC_WT_H2O - Fout_WT_H2O)/WT_Cap;
SOC_H2O_WT= SOC_H2O_WT +FC_WT_EL;
if SOC_H2O_WT>=100
    SOC_H2O_WT=100;
end
    if  SOC_H2O_WT<=0
        SOC_H2O_WT=0;
    end
A_SOC_H2O_WT(z,j)=SOC_H2O_WT;
A_F_FC_WT_EL(z,j)=FC_WT_EL;

%HYDROGEN STORED IN THE FLOW TANK
EL_FT_FC=100*(Fout_EL_FT_H2 - Fout_FT_FC_H2)/FT_Cap;
SOC_H2_FT=SOC_H2_FT + EL_FT_FC;
if SOC_H2_FT>=100                          %LIMITS FOR SOC OF WATER TANK AND
FLOW TANK
    SOC_H2_FT=100;
end
if SOC_H2_FT<=0
    SOC_H2_FT=0;
end
```

```
A_SOC_H2_FT(z,j)=SOC_H2_FT;
A_F_EL_FT_FC(z,j)=EL_FT_FC;

%ACTIVATION FOR PV TO BATTERY
str_PV3_BAT3=0      ;                       % start charging battery if SOC max
is < 90%
stp_PV3_BAT3=90;

if SOC_BAT3<stp_PV3_BAT3
    q_PV3_BAT3=1;
else
    q_PV3_BAT3=0;
end
e_req_PV3_BAT3=q_PV3_BAT3  ;            %The logic determines when the
battery SOC is below the stop point then the Battery makes a request

a_PV3_BAT3=1;
e_avail_PV3_BAT3= a_PV3_BAT3 || r_PV3_BAT3;
e_PV3_BAT3= e_avail_PV3_BAT3 && e_req_PV3_BAT3 && g_PV3_BAT3;


%ACTIVATION FOR WIND TURBINE WG2 TO BATTERY BAT3
str_WG2_BAT3=0   ;                          % start charging battery if SOC max
is < 90%
stp_WG2_BAT3=90;

if SOC_BAT3<stp_WG2_BAT3
    q_WG2_BAT3=1;
else
    q_WG2_BAT3=0;
end
e_req_WG2_BAT3=q_WG2_BAT3    ;          %The logic determines when the
battery SOC is below the stop point then the Battery makes a request
a_WG2_BAT3=1;
e_avail_WG2_BAT3 = a_WG2_BAT3 || r_WG2_BAT3;

e_WG2_BAT3 = e_avail_WG2_BAT3 && e_req_WG2_BAT3 && g_WG2_BAT3;

%ACTIVATION FOR DIESEL TO BATTERY
str_DSL3_BAT3=20;
stp_DSL3_BAT3=30;
if k<=1
    c=1;
else
    c=0;
end
if SOC_BAT3<str_DSL3_BAT3 %||
[SOC_BAT3>str_DSL3_BAT3&&SOC_BAT3<stp_DSL3_BAT3] && A_e_DSL3_BAT3(j+c-1)==1
q_DSL3_BAT3=1;
else
q_DSL3_BAT3=0;
end
e_req_DSL3_BAT3 =q_DSL3_BAT3;
```

```
a_DSL3_BAT3=1       ;                           %Availability logic for
Diesel generator

e_avail_DSL3_BAT3 = a_DSL3_BAT3 || r_DSL3_BAT3;

e_DSL3_BAT3= e_avail_DSL3_BAT3 && e_req_DSL3_BAT3 && g_DSL3_BAT3;


%ACTIVATION FOR FUEL CELL TO BATTERY
if FC_WINTER(k)==1
    FC_ON_WINTER=1;
else
    FC_ON_WINTER=0;
end
str_FC_BAT3=99  ;      %90                  %start and stop min and max
threshold to make request by Battery for Fuel cell to supply power
stp_FC_BAT3=80;
if FC_ON_WINTER==1 && SOC_BAT3<str_FC_BAT3  %|| SOC_BAT3>str_FC_BAT3 &&
SOC_BAT3<stp_FC_BAT3 && A_e_FC_BAT3(j-1+c)==1       %i==[2881:5832] ensures
Summer operation only
    q_FC_BAT3=1 ;
else
    q_FC_BAT3=0;
end
e_req_FC_BAT3 =   q_FC_BAT3;

  str_FC_WT=90      ;                             %start and stop min and max
threshold to make request for Fuel cell to supply power to Battery based on
Water Tank not full and Flow tank above minimum
  stp_FC_WT=90;

if SOC_H2O_WT<str_FC_WT
  a1_FC_WT=1;
else
  a1_FC_WT=0;
end

str_FT_FC =10   ;                                  %start and stop SOC
HYDROGEN FLOW TANK REQUIRED to supply FUEL CELL
stp_FT_FC =10;
if SOC_H2_FT>str_FT_FC
  a2_FT_FC=1;
else
  a2_FT_FC=0;
end

e_avail_FC_BAT3= a1_FC_WT && a2_FT_FC ; %|| r_FT_FC;


e_FC_BAT3 =  A_g_FC_BAT3(j-1+c);

%ACTIVATION FOR BATTERY TO LOAD
% e_BAT3_LD3=e_avail_BAT3_LD3 && e_avail_BAT3_LD3  && g_BAT3_LD3
```

```
%ACTIVATION FOR ELECTROLYSER TO FLOW TANK
str_EL_FT = 99       ;%90                    %start and stop SOC for engaging
the ELECTROLYSER TO SUPPLY FLOW TANK
stp_EL_FT= 100;
if SOC_H2_FT<str_EL_FT                  %FT MAKES REQUEST FOR H2 SUPPLY FROM
ELECTROLYSER
    q_EL_FT=1;
else
    q_EL_FT=0;
end
e_req_EL_FT= q_EL_FT;


if EL_SUMMER(k)==1                    %Scan the array if the index is equal to
1 then logic is true else it is false for zero
    EL_ON_SUMMER=1;
    else
    EL_ON_SUMMER=0;
end

str_BAT3_EL= 70   ;                    %start and stop SOC for engaging the
BATTERY TO SUPPLY ELECTROLYSER
stp_BAT3_EL =33;
% if Counter<=1
%     c=2;
% else
%     c=0;
% end             %This corrects the indexing by assuming the past was zero
if EL_ON_SUMMER==1 && SOC_BAT3>str_BAT3_EL || SOC_BAT3<str_BAT3_EL &&
SOC_BAT3>stp_BAT3_EL %&& A_e_EL_FT(j+c-1)==1  %i==[2881:5832] ensures Winter
operation only
  a1_BAT3_EL = 1;
else

  a1_BAT3_EL=0;
end


str_WT_EL =10   ;                      %start and stop SOC WATER TANK
REQUIRED to supply ELEctrolyser
stp_WT_EL =10;
if SOC_H2O_WT>str_WT_EL
  a2_EL_FT=1;
else
  a2_EL_FT=0;
end


e_avail_EL_FT= a1_BAT3_EL && a2_EL_FT ; %|| r_EL_FT;
e_EL_FT=(A_g_EL_FT1(j-1+c) || A_g_EL_FT2(j-1+c));


%ACTIVATION FOR BATTERY TO ELECTROLYSER
e_BAT3_EL = e_EL_FT;
```

```
%ACTIVATION FOR WATER TANK TO ELECTROLYSER
e_WT_EL=e_EL_FT;

%ACTIVATION FOR FLOW TANK TO FUEL CELL
e_FT_FC=e_FC_BAT3   ;                              %The Logic for SOC to
CONVERTER is the same as CONVERTER TO SOC

%ACTIVATION FOR FUEL CELL TO WATER TANK
e_FC_WT=e_FC_BAT3;

%store as z,j

A_e_BAT3_LD3(z,j)=e_BAT3_LD3;
A_e_PV3_BAT3(z,j)= e_PV3_BAT3;
A_e_WG2_BAT3(z,j)=e_WG2_BAT3;
A_e_BAT3_EL(z,j)=e_BAT3_EL ;
A_e_WT_EL(z,j)= e_WT_EL ;
A_e_EL_FT(z,j)=e_EL_FT  ;
A_e_FT_FC(z,j)=e_FT_FC;
A_e_FC_WT(z,j)=e_FC_WT;
A_e_FC_BAT3(z,j)=e_FC_BAT3;
A_e_DSL3_BAT3(z,j)=e_DSL3_BAT3;

%%%%%%%%%%%%%%%%%%%% END OF MG3 LOW LEVEL PMS
%%%%%%%%%%%%%%%%%%%%%%%%%%%%%%%%%%


Pinch_Data(z,j)=SOC_BAT3;
%PINCH_DATA(l,j,k)=SOC_BAT3;


%  if l==1 && startt==k
%  Pinch_Data_Raw_before_shaping(z,j)=SOC_BAT3; %first recompution L=1
%  end
%  if l==2 && startt==k
%  Pinch_Data_Raw_before_shaping2(z,j)=SOC_BAT3; %first recompution L=1
%  end
%  if l==3 && startt==k
%  Pinch_Data_Raw_before_shaping3(z,j)=SOC_BAT3; %first recompution L=1
%  end
%  if l==4 && startt==k
%  Pinch_Data_Raw_before_shaping4(z,j)=SOC_BAT3; %first recompution L=1
%  end
%  if l==5 && startt==k
%  Pinch_Data_Raw_before_shaping5(z,j)=SOC_BAT3; %first recompution L=1
%  end
%  if l==6 && startt==k
%  Pinch_Data_Raw_before_shaping6(z,j)=SOC_BAT3; %first recompution L=1
%  end
%  if l==7 && startt==k
%  Pinch_Data_Raw_before_shaping7(z,j)=SOC_BAT3; %first recompution L=1
%  end
%  if l==8 && startt==k
%  Pinch_Data_Raw_before_shaping8(z,j)=SOC_BAT3; %first recompution L=1
```

```
%  end
%  if l==9 && startt==k
%  Pinch_Data_Raw_before_shaping9(z,j)=SOC_BAT3; %first recompution L=1
%  end
%   if l==10 && startt==k
%  Pinch_Data_Raw_before_shaping10(z,j)=SOC_BAT3; %first recompution L=1
%   end
%   if l==11 && startt==k
%  Pinch_Data_Raw_before_shaping11(z,j)=SOC_BAT3; %first recompution L=1
%   end
%
%
%    if l==24 && startt==k
%  Pinch_Data_Raw_after_shaping(z,j)=SOC_BAT3 ;%first recomputation when L=24
%    end
% if l==24
%  PINCH_DIAG(k,j)=SOC_BAT3;   % Extract the recomputation from here
% end
% Pinch_shaping(l,j)=SOC_BAT3;% insight  array vector to the iterative
shaping via PoPA
% PINCH_DATAA(Counter2,j)=SOC_BAT3;

 end
 %%%%%%%%%%%%%%%%%%%%%%%%%%%%%% STATISTICAL ANALYSIS ON THE PINCH DATA %%%%

 end% for monte carlo simulation

parfor e=k:1:stop     %parallel for loop
    MC_mean=mean(Pinch_Data(:,e)); % calc for each col
    MC_std=std(Pinch_Data(:,e));

     Lower_bb(l,e)=MC_mean-(MC_std*1.96/sqrt(z));
    Upper_bb(l,e)=MC_mean+(MC_std*1.96/sqrt(z));
%
     cxc=cdfplot(Pinch_Data(:,e));

    xdata=get(cxc,'Xdata');

    ydata=get(cxc,'Ydata') ;

    pr_l(l,e)=max(find(xdata<31));

    L_V(l,e)=ydata(pr_l(l,e));

    xcx_l=find(ydata>0.01);

    Lower=xdata(xcx_l(1));
    Lower_b(l,e)=xdata(xcx_l(1));

    xcx_u=find(ydata>0.99);

    Upper=xdata(xcx_u(1));
    Upper_b(l,e)=xdata(xcx_u(1));
```

```
   end

%  if L_V(l,e)==0
%     break
%  end

%run this loop while Smin and Smax violation exist

    Recomp=1; %signal for recomputation
 Recomputation(k)=Recomp;

%PINCH ANALYSIS AND DETERMINATION OF G OVERIDE

%%START PINCH%%
SOC_BAT3_min=30 ;           %Minimum and Maximum Pinch Targets
SOC_BAT3_max=90;
S_UP=90;
S_LO=30;

% S_min=min(Pinch_Data(start:stop-1));
% S_max=max(Pinch_Data(start:stop-1));
if l==1
Lower_b(l,start:stop)=Lower_b(l,start:stop);%*A+B;%*XxY1;
% Upper_b(l,start:stop)=Upper_b(l,start:stop);%*XxY1;
end



S_min=min(Lower_b(l,start:stop))*A+B;
S_max=max(Upper_b(l,start:stop));


%%%%%%%%%%%%%%%%%%%%%%%%%%%%%%%%%%%%%%%%%%RESIDUAL ERROR CORRECTION
% Xxx=sum(Lower_b(1:100))
% yyy=sum(A_SOC_BAT_3_A(1:100))
% if k>2
% XxY(k)=sum(A_SOC_BAT3_A(startt:k-1))/sum(Lower_b(startt:k-1));
% Xxx=A_SOC_BAT3_A(k-1)/Lower_b(k);
% end
%Smin %Update the maximum taget using correction
% if k>25
% S_min = S_min*(XxY(k) + (Xxx-XxY(k))/k);%Update the minimum target using
the error correction
% end

% if k>2
% XxZ(k)=sum(A_SOC_BAT3_A(startt:k-1))/sum(Upper_b(startt:k-1));
% Xxy=A_SOC_BAT3_A(k-1)/Upper_b(k);
% end
%Smax %Update the maximum taget using correction
% if k>25
% % S_max = S_max*(XxZ(k) + (Xxy-XxZ(k))/k);%Update the minimum target using
the error correction
```

```
% end
%%%%%%%%%%%%%%%%%%%%%%%%%%%%%%%%%%%%%%%%%%%%%%%%%%%%%%%%%%%%%%%%%%%%%%%%%%%%


if S_min<=SOC_BAT3_min
    [~, t_violation]=min(Lower_b(1,start:stop-1));
   t_violation=t_violation+start-1;% corrects the index of the minimum
violation
   %t_violation= find(Pinch_Data(1:stop)==S_min)     ;           % time of
violation of the Lower pinch

   E_target =(SOC_BAT3_min - S_min)*(BAT3_Cap/100);%*P_FC_BAT3));
   t_duration = ceil(E_target);%/BAT3_Cap;             %Time duration needed
based on allowable amount of energy from battery per hour
%    if t_violation-1<start
%       t_violation=start+1
%    end
%
%   A_g_FC_BAT3(t_violation)= 1;
%   P_FC_BAT3(t_violation)=E_target;%

%%DAY_AHEAD PoPA CUMMULATIVE ACTION
  A_g_FC_BAT3(start)=1;
  %Power_FC=E_target;
  %Power_FC=Power_FC+E_target;% MOES cummulative from all previous violation
  %A_Power_FC(startt,l)=Power_FC;
  P_FC_BAT3(start)=E_target+P_FC_BAT3(start);
  if (P_FC_BAT3(start)/BAT3_Cap*100)+Lower_b(1,start)>S_UP
      P_FC_BAT3(start)=P_FC_BAT3(start)-
((Lower_b(1,start)+(P_FC_BAT3(start)*100/BAT3_Cap)-S_UP))*BAT3_Cap/100 ; %
limits the FC for MOES to Upper Pinch limit
  end
%   if P_FC_BAT3(start)>6000
%      P_FC_BAT3(start)=6000;% Limits FC power to the maximum capcity
%   end

elseif   S_max>SOC_BAT3_max
 if RLS==0
    Upper_b(l,start:stop)=Upper_b(l,start:stop); %activates correction factor
only once
 else
     Upper_b(l,start:stop)=Upper_b(l,start:stop)*A+B;%*A+B;%*XxY1;
 end


    [~, t_violation_EL]=max(Upper_b(1,start:stop-1));% to change from day
ahead to adaptive use start intead of startt which is the begining of the
horizon

        %t_violation_EL= max(find(Pinch_Data(1:stop)==S_max))     ;

        %%A_g_EL_FT1(start:stop-1)= Pinch_Data(start:stop-1)>SOC_BAT3_max;
former

Ex_target=(S_max - SOC_BAT3_max)*(BAT3_Cap/(100));     % former
```

```
% A_g_EL_FT1(t_violation_EL)=1;
% P_BAT3_EL(t_violation_EL)=abs(Ex_target);%

%%DAY_AHEAD PoPA CUMMULATIVE ACTION
    t_violation_EL=t_violation_EL+start-1; %start-1
    Ex_target=(S_max - SOC_BAT3_max)*(BAT3_Cap/(100));% former
%     Power_EL=Ex_target;
%     Power_EL=Power_EL+Ex_target;% MAE cummulative from previous violation
    A_g_EL_FT1(t_violation_EL)=1;
    P_BAT3_EL(t_violation_EL)=Ex_target+P_BAT3_EL(t_violation_EL);

   if Upper_b(l,t_violation_EL)-(P_BAT3_EL(t_violation_EL)/BAT3_Cap)*100<S_LO
% Limits the energy extracted by the EL to be less than or equal to the lower
Pinch
     if Upper_b(l,t_violation_EL)-
(P_BAT3_EL(t_violation_EL)/BAT3_Cap)>0||Upper_b(l,t_violation_EL)-
(P_BAT3_EL(t_violation_EL)/BAT3_Cap)==0 % if the value is positive

         P_BAT3_EL(t_violation_EL)=((Upper_b(l,t_violation_EL)-
P_BAT3_EL(t_violation_EL))+ (S_LO-(Upper_b(l,t_violation_EL)-
P_BAT3_EL(t_violation_EL))))*BAT3_Cap/100;

        %P_BAT3_EL(t_violation_EL)=((Pinch_Data(t_violation_EL)-
P_BAT3_EL(t_violation_EL))+ (S_LO-(Pinch_Data(t_violation_EL)-
P_BAT3_EL(t_violation_EL))))*BAT3_Cap/100;

     elseif Upper_b(l,t_violation_EL)-(P_BAT3_EL(t_violation_EL)/BAT3_Cap)<0
% for negative power violation limit of the EL
          P_BAT3_EL(t_violation_EL)=(Upper_b(l,t_violation_EL)-
(P_BAT3_EL(t_violation_EL)/BAT3_Cap)+(S_LO+(abs(Upper_b(l,t_violation_EL)-
(P_BAT3_EL(t_violation_EL)/BAT3_Cap)))))*BAT3_Cap/100;
    % Pinch_Data(t_violation_EL)=(Pinch_Data(t_violation_EL)-
(P_BAT3_EL(t_violation_EL)/BAT3_Cap)+(S_LO+(abs(Pinch_Data(t_violation_EL)-
(P_BAT3_EL(t_violation_EL)/BAT3_Cap)))))*BAT3_Cap/100;

     end
   end


%     if P_BAT3_EL(t_violation_EL)>4000
%        P_BAT3_EL(t_violation_EL)=4000; %Limits EL power to max capacity
%     end

else



    %%%%%%%%%%%%%% FROM ORIGINAL RLPOPA
%  if
ceil(Pinch_Data(stop))~=50&&(Pinch_Data(startt)>=30&&Pinch_Data(startt)<=90)%
Pinch_Data(stop)~=Pinch_Data(startt)&&Pinch_Data(startt)>=30
%     EE_target=(Pinch_Data(stop) - Pinch_Data(startt))*(BAT3_Cap/(100));
%      if EE_target<0
%            A_g_FC_BAT3(stop)=1;
```

```
%             A_g_EL_FT2(stop)=0;
%
%       else
%           EE_target>0
%           A_g_EL_FT2(stop)=1;
%            A_g_FC_BAT3(stop)=0;
%
%       end
    %%%%%%%%%%%%%%%%%%%%%%%%%%%ORIGINAL AEEND



if
ceil(Upper_b(l,stop))<50%&&(Lower_b(l,startt)>=30)%&&Lower_b(l,startt)<=90)%&
&k==0%ceil(Pinch_Data(stop))~=ceil(Pinch_Data(startt))&&(Pinch_Data(startt)>=
30&&Pinch_Data(startt)<=90)
    EE_target=(Upper_b(l,stop) - 50)*(BAT3_Cap/(100));

    if EE_target<0 %&& P_FC_BAT3(stop-1)>abs(EE_target)
           A_g_FC_BAT3(stop-1)=1;
           A_g_EL_FT2(stop-1)=0;
           A_g_EL_FT1(stop-1)=0;
           P_FC_BAT3(stop-1)=abs(EE_target);
          % P_FC_BAT3(stop-1)=P_FC_BAT3(stop-1)-abs(EE_target);% has to be
cummulative if not it will mismatch. if needed was 50KW and was match the
begining and error occurs u want to integrate by supplying what is needed now
+wat was there before.
           P_BAT3_EL(stop-1)=0;
%
%       if P_FC_BAT3(stop-1)>6000
%          P_FC_BAT3(stop-1)=6000;% Limits FC power to the maximum capcity
%       end


     else
        if EE_target>0 && P_FC_BAT3(stop-1)~=0 && P_FC_BAT3(stop-
1)>abs(EE_target)
          A_g_EL_FT2(stop-1)=0;
          A_g_FC_BAT3(stop-1)=1;
          P_BAT3_EL(stop-1)=0;%+P_BAT3_EL(stop-1)% you want to integrate the
energy with wat was already matched if error occurs
          P_FC_BAT3(stop-1)=P_FC_BAT3(stop-1)-EE_target;% to reduce the
Energy previously set you need to remove it from the exixting energy

%           if P_FC_BAT3(stop-1)>6000
%              P_FC_BAT3(stop-1)=6000;% Limits FC power to the maximum
capcity
%           end

        elseif EE_target>0 && P_FC_BAT3(stop-1)~=0 && P_FC_BAT3(stop-
1)<EE_target
         A_g_EL_FT2(stop-1)=1;
         A_g_FC_BAT3(stop-1)=0;
         P_BAT3_EL(stop-1)=EE_target-P_FC_BAT3(stop-1);%
         P_FC_BAT3(stop-1)=0;
```

```
%           if P_BAT3_EL(stop-1)>4000
%              P_BAT3_EL(stop-1)=4000; Limits % EL power to max capacity
%           end

        else
           A_g_EL_FT2(stop-1)=1;
           A_g_FC_BAT3(stop-1)=0;
           P_BAT3_EL(stop-1)=EE_target;%+P_BAT3_EL(stop-1)% you want to
integrate the energy with wat was already matched if error occurs
           P_FC_BAT3(stop-1)=0;

%           if P_BAT3_EL(stop-1)>4000
%              P_BAT3_EL(stop-1)=4000;  % Limits EL power to max capacity
%           end

        end
     end

end
end

% if Pinch_Data(stop-1)~=Pinch_Data(startt)
%     E_target=  (Pinch_Data(stop-1) -
Pinch_Data(startt))*(BAT3_Cap/(100*P_FC_BAT3));
%      if E_target<0
%            A_g_FC_BAT3(stop-1)=1;
%             A_g_EL_FT2(stop-1)=0;
%      else
%          E_target>0
%          A_g_EL_FT2(stop-1)=1;
%           A_g_FC_BAT3(stop-1)=0;
%      end
%
% end
%%%%%%%%%%%%%%%%%%%%%%%%%%%%%%%%%%%%  END OF PINCH %%%%%%%%%%%%%%%%



A_g_EL_FT=A_g_EL_FT1;
A_g_EL_FT=A_g_EL_FT2~=0;

A_g_EL_FT=A_g_EL_FT1+A_g_EL_FT2;



A_Lower_b(start:stop)=Lower_b(l,start:stop);
A_Upper_b(start:stop)=Upper_b(l,start:stop);

 end

if
l==50%(S_min>SOC_BAT3_min&&S_max<SOC_BAT3_max&&ceil(Upper_b(l,stop))>=50&&cei
l(Upper_b(l,stop))<70)==0||l==50%&&(Lower_b(l,startt)>=30))
```

```
    break;
end
 RLS=0;



   end


%%%%%%%%%%%%%%%%


 RLS=1 ;
 l=1;%reset L back to 1
 S_min=0;
 S_max=0; %reset the while loop
%%%%%%%%%%%%%%%%%%%%%%%%%%%%%% E.N.D OF M.P.C
%%%%%%%%%%%%%%%%%%%%%%%%%%%%%%%%%%%%%%%%%%%%%%%%



if k==1%||stop-start==21||stop-start==22
    e=1;
else
    e=0;
end

if    k==1%  k<8760%     tweek to alter availability
 e_avail_EL_FT_A=1;
e_avail_FC_BAT3_A=1;
end
%%%%%%%%%%%%%%%%%%%%%%%%%%%%%%%%%%%%%%%%%%%%%%%%%%%%%%%%%%%%%%%%%%%%%%%%%% LIMIT
%%%%%%%%%%%%%%%%%%%%%%%%%%%%%%%%%%%%%%%%%%%%%%%%%%%%%%%%%%%%%%%%%%%%%%%%%% CONVERTER
EL_max=15000;
EL_min=1000;
FC_max=15000;
FC_min=1000;
if P_BAT3_EL(k-1+e)>EL_max  %Constrain the max power of EL
   P_BAT3_EL(k-1+e)=EL_max;
elseif P_BAT3_EL(k-1+e)>0&&P_BAT3_EL(k-1+e)<EL_min;
       P_BAT3_EL(k-1+e)=EL_min;
end
if P_FC_BAT3(k-1+e)>FC_max
    P_FC_BAT3(k-1+e)=FC_max;
elseif P_FC_BAT3(k-1+e)>0&&P_FC_BAT3(k-1+e)<FC_min
    P_FC_BAT3(k-1+e)=FC_min;
end
%%%%%%%%%%%%%%%%%%%%%%%%%%%%%%%%%%%%%%%%%%%%%%%%%%%%%%%%%%%%%%%%%%%%%%%%%%%%%%%
%ACTIVATION FOR BATTERY TO ELECTROLYSER
e_EL_FT_A=A_g_EL_FT(k-1+e)*e_avail_EL_FT_A;

%ACTIVATION FOR WATER TANK TO ELECTROLYSER
e_WT_EL_A=e_EL_FT_A;
```

```
%ACTIVATION FOR FLOW TANK TO FUEL CELL
e_FT_FC_A=A_g_FC_BAT3(k-1+e)*e_avail_FC_BAT3_A;
%The Logic for SOC to CONVERTER is the same as CONVERTER TO SOC
e_FC_BAT3_A=e_FT_FC_A;
%ACTIVATION FOR FUEL CELL TO WATER TANK
e_FC_WT_A=A_g_FC_BAT3(k-1+e)*e_avail_FC_BAT3_A;



%%%%% MICROGRID3 %%% MICROGRID 3 %%%%% MICROGRID3 %%% MICROGRID 3 %%%%%
MICROGRID3 %%% MICROGRID 3

%%%%%ITERATION %%%% ITERATION

%INSTANTENOUS LOAD POWER
if k<2190
   lr=1000;
elseif k<4380
    lr=3000;
elseif k<6570
    lr=5000;
elseif k>6570
    lr=7000;
end


 counta_A=counta_A+1;
    if counta_A>24
       counta_A=1;
    end

% P_BAT3_LD3_A=datasample(LD_ARRAY(r1:r2,counta_A),1);%selects randomly a
load within the season% A_LD_R(lr,k);
P_BAT3_LD3_A=LD3_A(k);
A_LD(k)=P_BAT3_LD3;


%POWER FROM PV SYSTEM
% PV3_no=217;
Area_PV3=0.52*PV3_no ;           %Area for 70W solar panel
 if k>startt+7 && k<stop-8
     %Random=random('norm', 0, 10,1,1);
    Random;
 else
     Random=0;
 end

P_PV3_BAT3_A=Area_PV3*0.1 *(I_Rad(k)) ;%+Random);  ;%   % 0.1 is efficiency
for polycrystalline
P_PV3_BAT3_A=Area_PV3*0.1 *(I_Rad(k)+ran_PV(k));
%P_PV3_BAT3=Area_PV3*I_RADOM(k)*0.1 ;

% I_RADOM(k)=I_Rad(k)+Random
```

```
%
% REAL(k)=Area_PV3*I_Rad(k)*0.1
% DIST(k)=Area_PV3*I_RADOM(k)*0.1
%I_REAL(k)=I_Rad(k)




%POWER WIND TURBINE GENERATOR

P_WG2_BAT3_A= 0.5 * Air_den *Area_sw  * Cp* ((Wind_vel(k))^3) * Ng * Nb*WT_no
;



%FUEL CELL AND ELECTROLYSER POWER FLOW

I_EL=polyval(polyn_EL,P_BAT3_EL(k-1+e)*A_g_EL_FT(k-1+e)*e_avail_EL_FT_A)  ;
% Power flow as a function of Power supplied to the electroliser
I_FC=polyval(polyn_FC,P_FC_BAT3(k-1+e)*A_g_FC_BAT3(k-1+e)*e_avail_FC_BAT3_A);
% Power flow as a function of Power supplied to the electroliser

%*e_BAT3_EL *e_FC_BAT3*
e_FC_WT_A=e_FC_BAT3_A;
Fout_FC_WT_H2O_A= e_FC_WT_A * 0.85 * nc_FC * 3600* I_FC  / (nF*ne*F)  ;
% The flow of H2O from FC to WT +VE flow since it goes in to the Water Tank
A_Fout_FC_WT_H2O_A(k)=Fout_FC_WT_H2O_A;


Fout_EL_FT_H2_A= e_EL_FT_A * nF*nc_EL *  3600* I_EL/(ne*F)  ;
% The flow of H2 from EL to FT   +VE flow since it goes into a Flow Tnak
A_Fout_EL_FT_H2_A(k)=Fout_EL_FT_H2_A;


Fout_FT_FC_H2_A= e_FT_FC_A * nc_FC * 3600 *I_FC /(nF*ne*F)   ;
% The flow of H2 out of the FT to the FC  based on the needs of the  FC i.e
*eff -VE flow since it flows out
A_Fout_FT_FC_H2_A(k)=Fout_FT_FC_H2_A;


Fout_WT_H2O_A= e_WT_EL_A* 1.3 * nF * nc_EL * 3600 * I_EL /(ne*F) ;        %
The flow of H2O from the WT to the EL based on what the EL needs. The Flow is
-VE since it depletes the Water Tank
A_Fout_WT_H2O_A(k)=Fout_WT_H2O_A;

%%WATER TANK AND FLOW TANK MAX CAPACITY CALCULATION
%WT_Cap=1.3*24*(I_FC*nc_FC*nF)*3600/(ne*F)
%Calculate at max Power then set it manually.  Water Tank capacity should
hold moles/hr for 24hrs


%FT_Cap=1.3*24*(I_EL*nc_EL*nF)*3600/(ne*F)                              %Storage
Tank capacity should hold moles/hr for 24hrs
```

```
A_FC_ATTEMPT(k)=e_avail_FC_BAT3_A*A_g_FC_BAT3(k-1+e);
A_EL_ATTEMPT(k)=e_avail_EL_FT_A*A_g_EL_FT(k-1+e);
%NET ENERGY FLOW OF POWER STORED IN THE BATTERY
if stop-start==23
    c=-1;
else
    c=0;
end

A_P_PV3_BAT3_A(k)=(e_PV3_BAT3_A*P_PV3_BAT3_A);
A_P_WG2_BAT3_A(k)=P_WG2_BAT3_A;
A_P_BAT3_AA(k)=SOC_BAT3_A*BAT3_Cap/100;
A_P_DSL3_A(k)=(e_DSL3_BAT3_A*P_DSL3_BAT3);
A_P_EL_A(k)=(e_avail_EL_FT_A*A_g_EL_FT(k-1+e)*P_BAT3_EL(k-1+e));
A_P_FC_A(k)=(e_avail_FC_BAT3_A*A_g_FC_BAT3(k-1+e)*P_FC_BAT3(k-1+e));


P_RES3_A=(e_PV3_BAT3_A*P_PV3_BAT3_A)
+(e_WG2_BAT3_A*P_WG2_BAT3_A)+(e_DSL3_BAT3_A*P_DSL3_BAT3)+(e_avail_FC_BAT3_A*A
_g_FC_BAT3(k-1+e)*P_FC_BAT3(k-1+e));%(r_FC_BAT3*P_FC_BAT3);%%
A_P_RES3_A(k)=P_RES3_A;
P_BAT3_A= P_RES3_A -
(((e_BAT3_LD3_A*P_BAT3_LD3_A))+(e_avail_EL_FT_A*A_g_EL_FT(k-1+e)*P_BAT3_EL(k-
1+e)));%( r_BAT3_EL*P_BAT3_EL);%
%%
%LOLP CALCULATION
ENERGY_in_SYSTEM(k)=(SOC_BAT3_A*BAT3_Cap/100)+P_RES3_A ;
if ((SOC_BAT3_A*BAT3_Cap/100)+P_RES3_A)<(BAT3_Cap*30/100)
    DEFICIT=((SOC_BAT3_A*BAT3_Cap/100)+P_RES3_A);
    LOAD_D=(((e_BAT3_LD3_A*P_BAT3_LD3_A))+(e_avail_EL_FT_A*A_g_EL_FT(k-
1+e)*P_BAT3_EL(k-1+e)));
    number_count=number_count+1;
else
    DEFICIT=0;
    LOAD_D=0;
end
DEFICIT_A(k)=DEFICIT;
LOAD_D_A(k)=LOAD_D;

if P_BAT3_A<0 &&SOC_BAT3_A<30
    UnServed_load=(P_BAT3_A)+Unserved_load;
end

%%
A_P_BAT3_A(k)=(P_BAT3_A/BAT3_Cap)*100 ;
SOC_BAT3_A=SOC_BAT3_A +(P_BAT3_A/BAT3_Cap)*100 ;
if SOC_BAT3_A<=0;
    SOC_BAT3_A=0;
end
if SOC_BAT3_A>=100
    Excess=SOC_BAT3_A +((P_BAT3_A/BAT3_Cap)*100)-100;%Calculate Excess Energy
not saved in the battery
    Excess_Energy_lost=(Excess*BAT3_Cap)/100+Excess_Energy_lost;
    SOC_BAT3_A=100;

end
```

```
A_SOC_BAT3_A(k)=SOC_BAT3_A;

if SOC_BAT3_A<30
   Deficit_SOC_BAT3_A=1;
else
   Deficit_SOC_BAT3_A=0;
end
 A_Deficit_SOC_BAT3_A(k)= Deficit_SOC_BAT3_A;


% WATER STORED IN THE WATER TANK
 FC_WT_EL_A=100*(Fout_FC_WT_H2O_A - Fout_WT_H2O_A)/WT_Cap;
SOC_H2O_WT_A= SOC_H2O_WT_A +FC_WT_EL_A;
if SOC_H2O_WT_A>=100
    SOC_H2O_WT_A=100;
end
    if  SOC_H2O_WT_A<=0
        SOC_H2O_WT_A=0;
    end
A_SOC_H2O_WT_A(k)=SOC_H2O_WT_A;
A_F_FC_WT_EL_A(k)=FC_WT_EL_A;

%HYDROGEN STORED IN THE FLOW TANK
EL_FT_FC_A=100*(Fout_EL_FT_H2_A - Fout_FT_FC_H2_A)/FT_Cap;
SOC_H2_FT_A=SOC_H2_FT_A + EL_FT_FC_A;
if SOC_H2_FT_A>=100                          %LIMITS FOR SOC OF WATER TANK
AND FLOW TANK
    SOC_H2_FT_A=100;
end
if SOC_H2_FT_A<=0
    SOC_H2_FT_A=0;
end
A_SOC_H2_FT_A(k)=SOC_H2_FT_A;
A_F_EL_FT_FC_A(k)=EL_FT_FC_A;

%ACTIVATION FOR PV TO BATTERY
str_PV3_BAT3=0      ;                    % start charging battery if SOC max
is < 90%
stp_PV3_BAT3=90;

if SOC_BAT3_A<stp_PV3_BAT3
    q_PV3_BAT3_A=1;
else
    q_PV3_BAT3_A=0;
end
e_req_PV3_BAT3_A=q_PV3_BAT3_A  ;            %The logic determines when the
battery SOC is below the stop point then the Battery makes a request

a_PV3_BAT3_A=1;
e_avail_PV3_BAT3_A= a_PV3_BAT3_A || r_PV3_BAT3_A;
e_PV3_BAT3_A= e_avail_PV3_BAT3_A && e_req_PV3_BAT3_A && g_PV3_BAT3;


%ACTIVATION FOR WIND TURBINE WG2 TO BATTERY BAT3
```

```
str_WG2_BAT3=0;                          % start charging battery if SOC max is
< 90%
stp_WG2_BAT3=90;

if SOC_BAT3_A<stp_WG2_BAT3
    q_WG2_BAT3_A=1;
else
    q_WG2_BAT3_A=0;
end
e_req_WG2_BAT3_A=q_WG2_BAT3_A ;          %The logic determines when the
battery SOC is below the stop point then the Battery makes a request
a_WG2_BAT3_A=1;
e_avail_WG2_BAT3_A = a_WG2_BAT3_A || r_WG2_BAT3_A;

e_WG2_BAT3_A = e_avail_WG2_BAT3_A && e_req_WG2_BAT3_A && g_WG2_BAT3;

%ACTIVATION FOR DIESEL TO BATTERY
str_DSL3_BAT3=20;
stp_DSL3_BAT3=30;
if k<=1
    c=1;
else
    c=0;
end

if SOC_BAT3_A<str_DSL3_BAT3 ||
[SOC_BAT3_A>str_DSL3_BAT3&&SOC_BAT3_A<stp_DSL3_BAT3] && A_e_DSL3_BAT3_A(k+c-
1)==1
q_DSL3_BAT3_A=1;
else
q_DSL3_BAT3_A=0;
end
e_req_DSL3_BAT3_A =q_DSL3_BAT3_A;

a_DSL3_BAT3_A=1  ;                           %Availability logic for Diesel
generator

e_avail_DSL3_BAT3_A = a_DSL3_BAT3_A || r_DSL3_BAT3_A;

e_DSL3_BAT3_A= e_avail_DSL3_BAT3_A && e_req_DSL3_BAT3_A && g_DSL3_BAT3;


%ACTIVATION FOR FUEL CELL TO BATTERY

str_FC_BAT3=90;                         %start and stop min and max threshold
to make request by Battery for Fuel cell to supply power
stp_FC_BAT3=80;
if SOC_BAT3_A<str_FC_BAT3  || SOC_BAT3_A>str_FC_BAT3 &&
SOC_BAT3_A<stp_FC_BAT3 && A_e_FC_BAT3_A(k+c-1)==1       %i==[2881:5832]
ensures Summer operation only
    q_FC_BAT3_A=1 ;
else
    q_FC_BAT3_A=0;
end
e_req_FC_BAT3_A =   q_FC_BAT3_A;
```

```
  str_FC_WT_A=90 ;                                %start and stop min and max
threshold to make request for Fuel cell to supply power to Battery based on
Water Tank not full and Flow tank above minimum
  stp_FC_WT_A=90;

if SOC_H2O_WT_A<str_FC_WT_A
  a1_FC_WT_A=1;
else
  a1_FC_WT_A=0;
end

str_FT_FC =10   ;                                    %start and stop SOC
HYDROGEN FLOW TANK REQUIRED to supply FUEL CELL
stp_FT_FC =10;
if SOC_H2_FT_A>str_FT_FC
  a2_FT_FC_A=1;
else
  a2_FT_FC_A=0;
end

e_avail_FC_BAT3_A= a1_FC_WT_A && a2_FT_FC_A;  %|| r_FT_FC;

%e_FC_BAT3 = e_avail_FC_BAT3 && e_req_FC_BAT3 &&A_g_FC_BAT3(k);
% e_FC_BAT3 = e_avail_FC_BAT3 && (r_FC_BAT3 ||A_g_FC_BAT3(k));% ;
% e_FC_BAT3 = e_avail_FC_BAT3 &&(r_FC_BAT3  ~);

%e_FC_BAT3_A = e_req_FC_BAT3_A && A_g_FC_BAT3(k) ;



%ACTIVATION FOR BATTERY TO LOAD
% e_BAT3_LD3=e_avail_BAT3_LD3 && e_avail_BAT3_LD3  && g_BAT3_LD3


%ACTIVATION FOR ELECTROLYSER TO FLOW TANK
str_EL_FT = 90       ;                     %start and stop SOC for engaging
the ELECTROLYSER TO SUPPLY FLOW TANK
stp_EL_FT= 100;
if SOC_H2_FT_A<str_EL_FT                   %FT MAKES REQUEST FOR H2 SUPPLY
FROM ELECTROLYSER
    q_EL_FT_A=1;
else
    q_EL_FT_A=0;
end
e_req_EL_FT_A= q_EL_FT_A;


str_BAT3_EL= 40   ;                    %start and stop SOC for engaging the
BATTERY TO SUPPLY ELECTROLYSER
stp_BAT3_EL =33;
if SOC_BAT3_A>str_BAT3_EL || SOC_BAT3_A<str_BAT3_EL && SOC_BAT3_A>stp_BAT3_EL
&& A_e_EL_FT_A(k+c-1)>=1  %i==[2881:5832] ensures Winter operation only
  a1_BAT3_EL_A = 1;
```

```
else

  a1_BAT3_EL_A=0;
end


str_WT_EL =10   ;                       %start and stop SOC WATER TANK
REQUIRED to supply ELEctrolyser
stp_WT_EL =10;
if SOC_H2O_WT_A>str_WT_EL
  a2_EL_FT_A=1;
else
  a2_EL_FT_A=0;
end

e_avail_EL_FT_A = a1_BAT3_EL_A && a2_EL_FT_A ;% || r_EL_FT;
%e_EL_FT_A = e_req_EL_FT_A && (A_g_EL_FT1(k-1+c)&& A_g_EL_FT2(k-1+c)) ;

%ACTIVATION FOR BATTERY TO ELECTROLYSER
e_BAT3_EL_A = e_EL_FT_A;

%ACTIVATION FOR WATER TANK TO ELECTROLYSER
e_WT_EL_A=e_EL_FT_A;

%ACTIVATION FOR FLOW TANK TO FUEL CELL
e_FT_FC_A=e_FC_BAT3_A   ;                               %The Logic for SOC to
CONVERTER is the same as CONVERTER TO SOC

%ACTIVATION FOR FUEL CELL TO WATER TANK
e_FC_WT=e_FC_BAT3;

A_e_BAT3_LD3_A(k)=e_BAT3_LD3_A;
A_e_PV3_BAT3_A(k)= e_PV3_BAT3_A;
A_e_WG2_BAT3_A(k)=e_WG2_BAT3_A;
A_e_BAT3_EL_A(k)=e_BAT3_EL_A ;
A_e_WT_EL_A(k)= e_WT_EL_A ;
A_e_EL_FT_A(k)=e_EL_FT_A  ;
A_e_FT_FC_A(k)=e_FT_FC_A;
A_e_FC_WT_A(k)=e_FC_WT_A;
%A_e_FC_BAT3_A(k)=e_FC_BAT3_A;
A_e_DSL3_BAT3_A(k)=e_DSL3_BAT3_A;
% % %

%%%%%%%%%%%%%%%%%%%%%%%%%%%%%%%%%% FEEDBACK THE STATES OF SOC AND LOGIC
%%%%%%%%%%%%%%%%%%%%%%%%%%%%%%%%%% TO PINCH SECTION

% e_BAT3_LD3=e_BAT3_LD3_A;
% e_PV3_BAT3= e_PV3_BAT3_A;
% e_WG2_BAT3=e_WG2_BAT3_A;
% e_BAT3_EL=e_BAT3_EL_A ;
% e_WT_EL= e_WT_EL_A;
% e_EL_FT=e_EL_FT_A;
% e_FT_FC=e_FT_FC_A;
% e_FC_WT=e_FC_WT_A;
% e_FC_BAT3=e_FC_BAT3_A;
```

```
% e_DSL3_BAT3=e_DSL3_BAT3_A;
%
% SOC_H2O_WT=SOC_H2O_WT_A;
%
% SOC_H2_FT=SOC_H2_FT_A;
%
% SOC_BAT3=SOC_BAT3_A;


% %%%%%%%%%%%%%%%%%%%% END OF ACTUAL SYSTEM
%%%%%%%%%%%%%%%%%%%%%%%%%%%%%%%%

%%%%%%%%%%%%%%%%%%%%%%%%COUNTER INCREMENTAL LOOP%%%%%%%%%%
  if k==stop
  startt=stop+1;
  stop=stop+24;

 end

%  Counter=Counter+1;
%  if Counter ==25
%      Counter=1;
%  end
%%%%%%%%%%%%%%%%%%%%%%%%%%%%%%%%%%%%%%%%%%%%%%%%
ii(k)=k;

sstart(k)=start;









%%%%%%%%%%%%%%%% IAE CALC %%%%%%%%%%%%%%
SOC_ref=Pinch_Data(k);
if Pinch_Data(k)<30||SOC_BAT3_A<30
    SOC_ref=30;
end
if Pinch_Data(k)>90||SOC_BAT3_A>90
    SOC_ref=90;
end

A_SOC_ref(k)=SOC_ref;
IAE=abs(SOC_ref-SOC_BAT3_A)/SOC_ref;% change between system and model
A_IAE(k)=IAE;

if SOC_BAT3_A>90&&e_avail_EL_FT_A*A_g_EL_FT(k-1+e)*P_BAT3_EL(k-1+e)<1
    EPL(k)=(SOC_BAT3_A-90)*BAT3_Cap/100;
end

%%%%%%%%%%%%%%%%%%%%%%%%%%%%%%%%%%%%%%%%%%%%%%%%%%%%%%%%%%%%%%%%%%%%% ERROR
REGRESSION
%%%%%%%%%%%%%%%%%%%%%%%%%%%%%%%%%%%%%%%%%%%%%%%%%%%%%%%%%%%%%%%%%%%%% PLOT
```

```
% XxY1=XxY1
+((SOC_BAT3_A*((Lower_b(l,k)+Upper_b(l,k))/2)/((Lower_b(l,k)+Upper_b(l,k))/2)
^2)-XxY1)/24;%stop-Start;% Average
%    XxY1=1;
% A_XxY(k)=XxY1;

%%%%%%%AX+B Linear regression
if stop-startt<22
   mdl = fitlm(mean([A_Upper_b(1:k);A_Lower_b(1:k)]),A_SOC_BAT3_A(1:k));
   A=mdl.Coefficients{1,1};% coefficient for multiplying vairable
   B=mdl.Coefficients{2,1};%intercept
else
    A=1;
    B=0;
end
   A_A(k)=A;
   A_B(k)=B;
%%%%%%%%%%%%%%%%%%%%%%%%%%%%%%%% %%%%%%%%%% %%%%%%%%%%%%% %%%%%%%%%%%%%%%%


set(groot,'defaultFigureVisible','off')



end
tt=1:k;
plot(tt,A_SOC_ref(1:k),tt,A_SOC_BAT3_A) %

IAE_a=sum(A_IAE)/k
LOLP=(sum(DEFICIT_A)/sum(LOAD_D_A))/number_count

end
```

References

[1] A. Q. Jakhrani, A.-K. Othman, A. R. H. Rigit, S. R. Samo, and S. A. Kamboh, "A novel analytical model for optimal sizing of standalone photovoltaic systems," *Energy*, vol. 46, no. 1, pp. 675–682, 2012.

[2] M. S. Adaramola, S. S. Paul, and O. M. Oyewola, "Assessment of decentralized hybrid pv solar-diesel power system for applications in northern part of nigeria," *Energy for Sustainable Development*, vol. 19, pp. 72–82, 2014.

[3] M. G. Barade and A. Roy, "Design and optimization of photovoltaic-diesel generator-battery hybrid system for off-grid areas," *International Journal of Current Engineering and Technology*, vol. issue 5, pp. 344–353, 2016.

[4] A. Colmenar-Santos, M.-Á. Pérez, D. Borge-Diez, and C. Pérez-Molina, "Reliability and management of isolated smart-grid with dual mode in remote places: Application in the scope of great energetic needs," *International Journal of Electrical Power & Energy Systems*, vol. 73, pp. 805–818, 2015.

[5] A. O. Haruni, M. Negnevitsky, M. E. Haque, and A. Gargoom, "A novel operation and control strategy for a standalone hybrid renewable power system," *IEEE transactions on sustainable energy*, vol. 4, no. 2, pp. 402–413, 2013.

[6] D. Arcos-Aviles, J. Pascual, L. Marroyo, P. Sanchis, and F. Guinjoan, "Fuzzy logic-based energy management system design for residential grid-connected microgrids," *IEEE Transactions on Smart Grid*, vol. 9, no. 2, pp. 530–543, 2018.

[7] W. Kellogg, M. Nehrir, G. Venkataramanan, and V. Gerez, "Generation unit sizing and cost analysis for stand-alone wind, photovoltaic, and hybrid wind/pv systems," *IEEE Transactions on energy conversion*, vol. 13, no. 1, pp. 70–75, 1998.

[8] D. Giaouris, A. I. Papadopoulos, S. Voutetakis, S. Papadopoulou, and P. Seferlis, "A power grand composite curves approach for analysis and adaptive operation of renewable energy smart grids," *Clean Technologies and Environmental Policy*, vol. 17, no. 5, pp. 1171–1193, 2015.

[9] D. Abbes, A. Martinez, and G. Champenois, "Eco-design optimisation of an autonomous hybrid wind–photovoltaic system with battery storage," *IET Renewable Power Generation*, vol. 6, no. 5, pp. 358–371, 2012.

[10] A. Hirsch, Y. Parag, and J. Guerrero, "Microgrids: A review of technologies, key drivers, and outstanding issues," *Renewable and Sustainable Energy Reviews*, vol. 90, pp. 402–411, 2018.

[11] S. Hajiaghasi, A. Salemnia, and M. Hamzeh, "Hybrid energy storage system for microgrids applications: A review," *Journal of Energy Storage*, vol. 21, pp. 543–570, 2019.

[12] E. E. C. Alves, A. Steiner, M. de Almeida Medeiros, and M. E. A. da Silva, "From a breeze to the four winds: A panel analysis of the international diffusion of renewable energy incentive policies (2005–2015)," *Energy Policy*, vol. 125, pp. 317–329, 2019.

[13] D. T. Ton and M. A. Smith, "The us department of energy's microgrid initiative," *The Electricity Journal*, vol. 25, no. 8, pp. 84–94, 2012.

[14] P. Nema, R. Nema, and S. Rangnekar, "A current and future state of art development of hybrid energy system using wind and pv-solar: A review," *Renewable and Sustainable Energy Reviews*, vol. 13, no. 8, pp. 2096–2103, 2009.

[15] K. Ajao, O. Oladosu, and O. Popoola, "Using homer power optimization software for cost benefit analysis of hybrid-solar power generation relative to utility cost in nigeria," *International Journal of Research and Reviews in Applied Sciences*, vol. 7, no. 1, p. 14, 2011.

[16] T. Bocklisch, "Hybrid energy storage systems for renewable energy applications," *Energy Procedia*, vol. 73, pp. 103–111, 2015.

[17] D. Giaouris, A. I. Papadopoulos, C. Ziogou, D. Ipsakis, S. Voutetakis, S. Papadopoulou, P. Seferlis, F. Stergiopoulos, and C. Elmasides, "Performance investigation of a hybrid renewable power generation and storage system using systemic power management models," *Energy*, vol. 61, pp. 621–635, 2013.

[18] X. Feng, H. Gooi, and S. Chen, "Hybrid energy storage with multimode fuzzy power allocator for pv systems," *IEEE Transactions on Sustainable Energy*, vol. 5, no. 2, pp. 389–397, 2014.

[19] L. W. Chong, Y. W. Wong, R. K. Rajkumar, and D. Isa, "An optimal control strategy for standalone pv system with battery-supercapacitor hybrid energy storage system," *Journal of Power Sources*, vol. 331, pp. 553–565, 2016.

[20] A. Maleki and F. Pourfayaz, "Sizing of stand-alone photovoltaic/wind/diesel system with battery and fuel cell storage devices by harmony search algorithm," *Journal of Energy Storage*, vol. 2, pp. 30–42, 2015.

[21] V. Dash and P. Bajpai, "Power management control strategy for a stand-alone solar photovoltaic-fuel cell–battery hybrid system," *Sustainable Energy Technologies and Assessments*, vol. 9, pp. 68–80, 2015.

[22] S. Nasri, B. S. Sami, and A. Cherif, "Power management strategy for hybrid autonomous power system using hydrogen storage," *International Journal of Hydrogen Energy*, vol. 41, no. 2, pp. 857–865, 2016.

[23] T. Alnejaili, S. Drid, D. Mehdi, L. Chrifi-Alaoui, R. Belarbi, and A. Hamdouni, "Dynamic control and advanced load management of a stand-alone hybrid renewable power system for remote housing," *Energy Conversion and Management*, vol. 105, pp. 377–392, 2015.

[24] S. Sikkabut, P. Mungporn, C. Ekkaravarodome, N. Bizon, P. Tricoli, B. Nahid-Mobarakeh, S. Pierfederici, B. Davat, and P. Thounthong, "Control of high-energy high-power densities storage devices by li-ion battery and supercapacitor for fuel cell/photovoltaic hybrid power plant for autonomous system applications," *IEEE Transactions on Industry Applications*, vol. 52, no. 5, pp. 4395–4407, 2016.

[25] M. Minutillo, A. L. Lavadera, and E. Jannelli, "Assessment of design and operating parameters for a small compressed air energy storage system integrated with a stand-alone renewable power plant," *Journal of Energy Storage*, vol. 4, pp. 135–144, 2015.

[26] Z. Nie, X. Xiao, Q. Kang, R. Aggarwal, H. Zhang, and W. Yuan, "Smes-battery energy storage system for conditioning outputs from direct drive linear wave energy converters," *IEEE Transactions on Applied Superconductivity*, vol. 23, no. 3, pp. 5000705–5000705, 2013.

[27] D. Ipsakis, S. Voutetakis, P. Seferlis, F. Stergiopoulos, and C. Elmasides, "Power management strategies for a stand-alone power system using renewable energy sources and hydrogen storage," *International journal of hydrogen energy*, vol. 34, no. 16, pp. 7081–7095, 2009.

[28] H. Mahmood, D. Michaelson, and J. Jiang, "A power management strategy for pv/battery hybrid systems in islanded microgrids," *IEEE Journal of Emerging and Selected topics in Power electronics*, vol. 2, no. 4, pp. 870–882, 2014.

[29] H. Zhao, Q. Wu, S. Hu, H. Xu, and C. N. Rasmussen, "Review of energy storage system for wind power integration support," *Applied energy*, vol. 137, pp. 545–553, 2015.

[30] L. K. Gan, J. K. Shek, and M. A. Mueller, "Hybrid wind–photovoltaic–diesel–battery system sizing tool development using empirical approach, life-cycle cost and performance analysis: A case study in scotland," *Energy Conversion and Management*, vol. 106, pp. 479–494, 2015.

[31] L. Qiao, "A summary of optimal methods for the planning of stand-alone microgrid system," *Energy and Power Engineering*, vol. 5, no. 04, p. 992, 2013.

[32] E. Muljadi, C. Wang, and M. H. Nehrir, "Parallel operation of wind turbine, fuel cell, and diesel generation sources," in *IEEE Power Engineering Society General Meeting, 2004.*, pp. 1927–1932, IEEE, 2004.

[33] T. Dorji, T. Urmee, and P. Jennings, "Options for off-grid electrification in the kingdom of bhutan," *Renewable Energy*, vol. 45, pp. 51–58, 2012.

[34] F. Delfino, G. Ferro, M. Robba, and M. Rossi, "An architecture for the optimal control of tertiary and secondary levels in small-size islanded microgrids," *International Journal of Electrical Power & Energy Systems*, vol. 103, pp. 75–88, 2018.

[35] J. Bernard, S. Delprat, F. Buechi, and T. M. Guerra, "Global optimisation in the power management of a fuel cell hybrid vehicle (fchv)," in *2006 IEEE Vehicle Power and Propulsion Conference*, pp. 1–6, IEEE, 2006.

[36] Y. Kim, D. Shin, M. Petricca, S. Park, M. Poncino, and N. Chang, "Computer-aided design of electrical energy systems," in *Proceedings of the International Conference on Computer-Aided Design*, pp. 194–201, IEEE Press, 2013.

[37] E. Eriksson and E. M. Gray, "Optimization and integration of hybrid renewable energy hydrogen fuel cell energy systems–a critical review," *Applied energy*, vol. 202, pp. 348–364, 2017.

[38] S. Hadayeghparast, A. S. Farsangi, and H. Shayanfar, "Day-ahead stochastic multi-objective economic/emission operational scheduling of a large scale virtual power plant," *Energy*, vol. 172, pp. 630–646, 2019.

[39] M.-C. Hu, S.-Y. Lu, and Y.-H. Chen, "Stochastic programming and market equilibrium analysis of microgrids energy management systems," *Energy*, vol. 113, pp. 662–670, 2016.

[40] V. S. Tabar, M. A. Jirdehi, and R. Hemmati, "Energy management in microgrid based on the multi objective stochastic programming incorporating portable renewable energy resource as demand response option," *Energy*, vol. 118, pp. 827–839, 2017.

[41] D. Giaouris, A. I. Papadopoulos, C. Patsios, S. Walker, C. Ziogou, P. Taylor, S. Voutetakis, S. Papadopoulou, and P. Seferlis, "A systems approach for management of microgrids considering multiple energy carriers, stochastic loads, forecasting and demand side response," *Applied energy*, vol. 226, pp. 546–559, 2018.

[42] S. R. W. Alwi, N. E. M. Rozali, Z. Abdul-Manan, and J. J. Klemeš, "A process integration targeting method for hybrid power systems," *Energy*, vol. 44, no. 1, pp. 6–10, 2012.

[43] S. Bandyopadhyay, "Design and optimization of isolated energy systems through pinch analysis," *Asia-Pacific Journal of Chemical Engineering*, vol. 6, no. 3, pp. 518–526, 2011.

[44] D. Giaouris, A. I. Papadopoulos, P. Seferlis, S. Voutetakis, and S. Papadopoulou, "Power grand composite curves shaping for adaptive energy management of hybrid microgrids," *Renewable energy*, vol. 95, pp. 433–448, 2016.

[45] S. Norbu and S. Bandyopadhyay, "Power pinch analysis for optimal sizing of renewable-based isolated system with uncertainties," *Energy*, vol. 135, pp. 466–475, 2017.

[46] N.-B. B. Etim, D. Giaouris, A. I. Papadopoulos, H. Patsios, S. Papadopoulou, S. Voutetakis, P. Seferlis, S. Walker, P. Taylor, and S. Gadoue, "Adaptive power pinch analysis for energy management of hybrid energy storage systems," in *2018 IEEE International Symposium on Circuits and Systems (ISCAS)*, pp. 1–5, IEEE, 2018.

[47] N.-B. B. Etim, D. Giaouris, H. Patsios, S. Gadoue, A. I. Papadopoulos, P. Seferlis, S. Voutetakis, and S. Papadopoulou, "Probabilistic adaptive model predictive power pinch analysis (popa) energy management approach to uncertainty," *The Journal of Engineering*, 2019.

[48] M. Srinivasarao, K. R. Sudha, and C. Bhanu, "A simple and reliable method of design for standalone photovoltaic systems," *Journal of The Institution of Engineers (India): Series B*, vol. 98, no. 3, pp. 245–253, 2017.

[49] T. Khatib, I. A. Ibrahim, and A. Mohamed, "A review on sizing methodologies of photovoltaic array and storage battery in a standalone photovoltaic system," *Energy Conversion and Management*, vol. 120, pp. 430–448, 2016.

[50] A. Q. Jakhrani, A.-K. Othman, A. R. H. Rigit, S. R. Samo, and S. A. Kamboh, "A novel analytical model for optimal sizing of standalone photovoltaic systems," *Energy*, vol. 46, no. 1, pp. 675–682, 2012.

[51] M. Sidrach-de Cardona and L. M. Lopez, "A simple model for sizing stand alone photovoltaic systems," *Solar Energy Materials and Solar Cells*, vol. 55, no. 3, pp. 199–214, 1998.

[52] M. Collares-Pereira and A. Rabl, "The average distribution of solar radiation-correlations between diffuse and hemispherical and between daily and hourly insolation values," *Solar energy*, vol. 22, no. 2, pp. 155–164, 1979.

[53] J. E. Hay and D. C. McKAY, "Estimating solar irradiance on inclined surfaces: a review and assessment of methodologies," *International Journal of Solar Energy*, vol. 3, no. 4-5, pp. 203–240, 1985.

[54] M. Khan and M. Iqbal, "Pre-feasibility study of stand-alone hybrid energy systems for applications in newfoundland," *Renewable energy*, vol. 30, no. 6, pp. 835–854, 2005.

[55] J. Li, W. Wei, and J. Xiang, "A simple sizing algorithm for stand-alone pv/wind/battery hybrid microgrids," *energies*, vol. 5, no. 12, pp. 5307–5323, 2012.

[56] H. Suryoatmojo, A. Elbaset, F. Pamuji, D. Riawan, M. Abdillah, *et al.*, "Optimal sizing and control strategy of hybrid pv-diesel-battery systems for isolated island*," *no*, vol. 1, pp. 1–6, 2014.

[57] R. Siddaiah and R. Saini, "A review on planning, configurations, modeling and optimization techniques of hybrid renewable energy systems for off grid applications," *Renewable and Sustainable Energy Reviews*, vol. 58, pp. 376–396, 2016.

[58] D. P. Clarke, Y. M. Al-Abdeli, and G. Kothapalli, "Multi-objective optimisation of renewable hybrid energy systems with desalination," *Energy*, vol. 88, pp. 457–468, 2015.

[59] T. Khatib, A. Mohamed, K. Sopian, and M. Mahmoud, "Optimal sizing of building integrated hybrid pv/diesel generator system for zero load rejection for malaysia," *Energy and Buildings*, vol. 43, no. 12, pp. 3430–3435, 2011.

[60] M. Jamil Ahmad and G. N Tiwari, "Optimization of tilt angle for solar collector to receive maximum radiation," *The Open Renewable Energy Journal*, vol. 2, no. 1, 2009.

[61] V. Khare, S. Nema, and P. Baredar, "Optimisation of the hybrid renewable energy system by homer, pso and cpso for the study area," *International Journal of Sustainable Energy*, vol. 36, no. 4, pp. 326–343, 2017.

[62] S. B. Jeyaprabha and A. I. Selvakumar, "Optimal sizing of photovoltaic/battery/diesel based hybrid system and optimal tilting of solar array using the artificial intelligence for remote houses in india," *Energy and Buildings*, vol. 96, pp. 40–52, 2015.

[63] S. Sharma, S. Bhattacharjee, and A. Bhattacharya, "Grey wolf optimisation for optimal sizing of battery energy storage device to minimise operation cost of microgrid," *IET Generation, Transmission & Distribution*, vol. 10, no. 3, pp. 625–637, 2016.

[64] B. Khan and P. Singh, "Selecting a meta-heuristic technique for smart micro-grid optimization problem: A comprehensive analysis," *IEEE Access*, vol. 5, pp. 13951–13977, 2017.

[65] W. Peng, A. Maleki, M. A. Rosen, and P. Azarikhah, "Optimization of a hybrid system for solar-wind-based water desalination by reverse osmosis: Comparison of approaches," *Desalination*, vol. 442, pp. 16–31, 2018.

[66] T. Khatib, A. Mohamed, K. Sopian, and M. Mahmoud, "A new approach for optimal sizing of standalone photovoltaic systems," *International Journal of Photoenergy*, vol. 2012, 2012.

[67] T. Khatib and W. Elmenreich, "An improved method for sizing standalone photovoltaic systems using generalized regression neural network," *International Journal of Photoenergy*, vol. 2014, 2014.

[68] J.-Y. Lee, K. B. Aviso, and R. R. Tan, "Multi-objective optimisation of hybrid power systems under uncertainties," *Energy*, 2019.

[69] B. Linnhoff and J. R. Flower, "Synthesis of heat exchanger networks: I. systematic generation of energy optimal networks," *AIChE Journal*, vol. 24, no. 4, pp. 633–642, 1978.

[70] P. S. Varbanov, Z. Fodor, and J. J. Klemeš, "Total site targeting with process specific minimum temperature difference (δtmin)," *Energy*, vol. 44, no. 1, pp. 20–28, 2012.

[71] N. E. M. Rozali, S. R. W. Alwi, Z. A. Manan, J. J. Klemeš, and M. Y. Hassan, "Process integration techniques for optimal design of hybrid power systems," *Applied Thermal Engineering*, vol. 61, no. 1, pp. 26–35, 2013.

[72] I. J. Esfahani, S. Lee, and C. Yoo, "Extended-power pinch analysis (epopa) for integration of renewable energy systems with battery/hydrogen storages," *Renewable energy*, vol. 80, pp. 1–14, 2015.

[73] E. R. Stephens, D. B. Smith, and A. Mahanti, "Game theoretic model predictive control for distributed energy demand-side management," *IEEE Transactions on Smart Grid*, vol. 6, no. 3, pp. 1394–1402, 2015.

[74] H.-T. Yang, C.-M. Huang, Y.-C. Huang, and Y.-S. Pai, "A weather-based hybrid method for 1-day ahead hourly forecasting of pv power output," *IEEE transactions on sustainable energy*, vol. 5, no. 3, pp. 917–926, 2014.

[75] Y. Zhang, T. Zhang, R. Wang, Y. Liu, and B. Guo, "Optimal operation of a smart residential microgrid based on model predictive control by considering uncertainties and storage impacts," *Solar Energy*, vol. 122, pp. 1052–1065, 2015.

[76] Y. Zhang, R. Wang, T. Zhang, Y. Liu, and B. Guo, "Model predictive control-based operation management for a residential microgrid with considering forecast uncertainties and demand response strategies," *IET Generation, Transmission & Distribution*, vol. 10, no. 10, pp. 2367–2378, 2016.

[77] L. I. Minchala-Avila, L. E. Garza-Castañón, A. Vargas-Martínez, and Y. Zhang, "A review of optimal control techniques applied to the energy management and control of microgrids," *Procedia Computer Science*, vol. 52, pp. 780–787, 2015.

[78] R. Palma-Behnke, C. Benavides, F. Lanas, B. Severino, L. Reyes, J. Llanos, and D. Sáez, "A microgrid energy management system based on the rolling horizon strategy," *IEEE Transactions on smart grid*, vol. 4, no. 2, pp. 996–1006, 2013.

[79] L. I. Minchala-Avila, L. Garza-Castañón, Y. Zhang, and H. J. A. Ferrer, "Optimal energy management for stable operation of an islanded microgrid," *IEEE Transactions on Industrial Informatics*, vol. 12, no. 4, pp. 1361–1370, 2016.

[80] J. A. Martin and I. A. Hiskens, "Corrective model-predictive control in large electric power systems," *IEEE Transactions on Power Systems*, vol. 32, no. 2, pp. 1651–1662, 2017.

[81] K. Jia, Y. Chen, T. Bi, Y. Lin, D. Thomas, and M. Sumner, "Historical-data-based energy management in a microgrid with a hybrid energy storage system," *IEEE Transactions on Industrial Informatics*, vol. 13, no. 5, pp. 2597–2605, 2017.

[82] S. Vosen and J. Keller, "Hybrid energy storage systems for stand-alone electric power systems: optimization of system performance and cost through control strategies," *International journal of hydrogen energy*, vol. 24, no. 12, pp. 1139–1156, 1999.

[83] A. Aktas, K. Erhan, S. Özdemir, and E. Özdemir, "Dynamic energy management for photovoltaic power system including hybrid energy storage in smart grid applications," *Energy*, vol. 162, pp. 72–82, 2018.

[84] X. Li, L. Han, H. Liu, W. Wang, and C. Xiang, "Real-time optimal energy management strategy for a dual-mode power-split hybrid electric vehicle based on an explicit model predictive control algorithm," *Energy*, vol. 172, pp. 1161–1178, 2019.

[85] J. Xiao, P. Wang, and L. Setyawan, "Hierarchical control of hybrid energy storage system in dc microgrids," *IEEE Transactions on Industrial Electronics*, vol. 62, no. 8, pp. 4915–4924, 2015.

[86] S. Dimopoulou, A. Oppermann, E. Boggasch, and A. Rausch, "A markov decision process for managing a hybrid energy storage system," *Journal of Energy Storage*, vol. 19, pp. 160–169, 2018.

[87] A. Tabanjat, M. Becherif, D. Hissel, and H. Ramadan, "Energy management hypothesis for hybrid power system of h2/wt/pv/gmt via ai techniques," *International Journal of Hydrogen Energy*, vol. 43, no. 6, pp. 3527–3541, 2018.

[88] R. S. Sutton, "Learning to predict by the methods of temporal differences," *Machine learning*, vol. 3, no. 1, pp. 9–44, 1988.

[89] A. Geramifard, T. J. Walsh, S. Tellex, G. Chowdhary, N. Roy, J. P. How, *et al.*, "A tutorial on linear function approximators for dynamic programming and reinforcement learning," *Foundations and Trends® in Machine Learning*, vol. 6, no. 4, pp. 375–451, 2013.

[90] H. Al-Hamadi and S. Soliman, "Short-term electric load forecasting based on kalman filtering algorithm with moving window weather and load model," *Electric power systems research*, vol. 68, no. 1, pp. 47–59, 2004.

[91] C. J. Watkins and P. Dayan, "Q-learning," *Machine learning*, vol. 8, no. 3-4, pp. 279–292, 1992.

[92] N. ALTUNTAŞ, E. Imal, N. Emanet, and C. N. Öztürk, "Reinforcement learning-based mobile robot navigation," *Turkish Journal of Electrical Engineering & Computer Sciences*, vol. 24, no. 3, pp. 1747–1767, 2016.

[93] Q. Zhang, M. Li, X. Wang, and Y. Zhang, "Reinforcement learning in robot path optimization.," *JSW*, vol. 7, no. 3, pp. 657–662, 2012.

[94] R. S. Sutton, "Dyna, an integrated architecture for learning, planning, and reacting," *ACM SIGART Bulletin*, vol. 2, no. 4, pp. 160–163, 1991.

[95] D. Ernst, M. Glavic, F. Capitanescu, and L. Wehenkel, "Reinforcement learning versus model predictive control: a comparison on a power system problem," *IEEE Transactions on Systems, Man, and Cybernetics, Part B (Cybernetics)*, vol. 39, no. 2, pp. 517–529, 2008.

[96] K. S. Peng and C. T. Morrison, "Model predictive prior reinforcement learning for a heat pump thermostat," in *IEEE International Conference on Automatic Computing: Feedback Computing*, vol. 16, 2016.

[97] T. Liu, B. Wang, and C. Yang, "Online markov chain-based energy management for a hybrid tracked vehicle with speedy q-learning," *Energy*, vol. 160, pp. 544–555, 2018.

[98] T. Liu, X. Hu, W. Hu, and Y. Zou, "A heuristic planning reinforcement learning-based energy management for power-split plug-in hybrid electric vehicles," *IEEE Transactions on Industrial Informatics*, 2019.

[99] R. Xiong, J. Cao, and Q. Yu, "Reinforcement learning-based real-time power management for hybrid energy storage system in the plug-in hybrid electric vehicle," *Applied energy*, vol. 211, pp. 538–548, 2018.

[100] X. Lin, Y. Wang, P. Bogdan, N. Chang, and M. Pedram, "Reinforcement learning based power management for hybrid electric vehicles," in *Proceedings of the 2014 IEEE/ACM International Conference on Computer-Aided Design*, pp. 32–38, IEEE Press, 2014.

[101] V. François-Lavet, D. Taralla, D. Ernst, and R. Fonteneau, "Deep reinforcement learning solutions for energy microgrids management," in *European Workshop on Reinforcement Learning (EWRL 2016)*, 2016.

[102] A. Anvari-Moghaddam, A. Rahimi-Kian, M. S. Mirian, and J. M. Guerrero, "A multi-agent based energy management solution for integrated buildings and microgrid system," *Applied energy*, vol. 203, pp. 41–56, 2017.

[103] P. Kofinas, A. Dounis, and G. Vouros, "Fuzzy q-learning for multi-agent decentralized energy management in microgrids," *Applied energy*, vol. 219, pp. 53–67, 2018.

[104] E. Kuznetsova, Y.-F. Li, C. Ruiz, E. Zio, G. Ault, and K. Bell, "Reinforcement learning for microgrid energy management," *Energy*, vol. 59, pp. 133–146, 2013.

[105] F.-D. Li, M. Wu, Y. He, and X. Chen, "Optimal control in microgrid using multi-agent reinforcement learning," *ISA transactions*, vol. 51, no. 6, pp. 743–751, 2012.

[106] M. Glavic, R. Fonteneau, and D. Ernst, "Reinforcement learning for electric power system decision and control: Past considerations and perspectives," *IFAC-PapersOnLine*, vol. 50, no. 1, pp. 6918–6927, 2017.

[107] J. M. Buhmann, A. Gronskiy, M. Mihalák, T. Pröger, R. Šrámek, and P. Widmayer, "Robust optimization in the presence of uncertainty: A generic approach," *Journal of Computer and System Sciences*, vol. 94, pp. 135–166, 2018.

[108] M. Cai, G. Huang, J. Chen, Y. Li, and Y. Fan, "A generalized fuzzy chance-constrained energy systems planning model for guangzhou, china," *Energy*, vol. 165, pp. 191–204, 2018.

[109] Y. Huang, L. Wang, W. Guo, Q. Kang, and Q. Wu, "Chance constrained optimization in a home energy management system," *IEEE Transactions on Smart Grid*, vol. 9, no. 1, pp. 252–260, 2016.

[110] Y. Zhao, Y. Cao, J. Liu, Z. Zhan, X. Li, and W. Li, "Single-wall carbon nanotube-coated cotton yarn for electrocardiography transmission," *Micromachines*, vol. 9, no. 3, p. 132, 2018.

[111] Y. Li, Z. Yang, G. Li, D. Zhao, and W. Tian, "Optimal scheduling of an isolated microgrid with battery storage considering load and renewable generation uncertainties," *IEEE Transactions on Industrial Electronics*, vol. 66, no. 2, pp. 1565–1575, 2018.

[112] R. Rocchetta, L. Bellani, M. Compare, E. Zio, and E. Patelli, "A reinforcement learning framework for optimal operation and maintenance of power grids," *Applied Energy*, vol. 241, pp. 291–301, 2019.

[113] A. Dehghani-Sanij, E. Tharumalingam, M. Dusseault, and R. Fraser, "Study of energy storage systems and environmental challenges of batteries," *Renewable and Sustainable Energy Reviews*, vol. 104, pp. 192–208, 2019.

[114] S. Sadeghi and M. Ameri, "Comparison the combination of different power generators with photovoltaic panels and batteries," in *Computer Applications for Security, Control and System Engineering*, pp. 376–387, Springer, 2012.

[115] W.-Y. Chang, "The state of charge estimating methods for battery: A review," *ISRN Applied Mathematics*, vol. 2013, 2013.

[116] V. Ramdas, M. Pramod, P. Satyanarayana, K. Venkatesh, and M. Ravindra, "Prediction of li-ion battery discharge characteristics at different temperatures and discharge rates based on a hybrid soc estimation approach," *ISRN Applied Mathematics*, vol. 4, no. 11, pp. 327–333, 2015.

[117] A. Ogunjuyigbe, T. Ayodele, and O. Akinola, "Optimal allocation and sizing of pv/wind/split-diesel/battery hybrid energy system for minimizing life cycle cost, carbon emission and dump energy of remote residential building," *Applied Energy*, vol. 171, pp. 153–171, 2016.

[118] B. R. Prusty and D. Jena, "A critical review on probabilistic load flow studies in uncertainty constrained power systems with photovoltaic generation and a new approach," *Renewable and Sustainable Energy Reviews*, vol. 69, pp. 1286–1302, 2017.

[119] J. M. Morales and J. Perez-Ruiz, "Point estimate schemes to solve the probabilistic power flow," *IEEE Transactions on power systems*, vol. 22, no. 4, pp. 1594–1601, 2007.

[120] J. M. Morales, L. Baringo, A. J. Conejo, and R. Mínguez, "Probabilistic power flow with correlated wind sources," *IET generation, transmission & distribution*, vol. 4, no. 5, pp. 641–651, 2010.

[121] "Chalmers university of technology ,TMS150/MSG400, stochastic data processing and simulation 2018." http://www.math.chalmers.se/Stat/Grundutb/CTH/tms150/1516/MC_20151008.pdf. [Online; accessed 19-July-2019].

[122] "P. gremaud, Advanced numerics and modeling in science and engineering, north carolina state university, 2018, Advanced numerics and modeling in science and engineering", north carolina state university, 2018." http://www4.ncsu.edu/~gremaud/MA798C/mc.pdf. [Online; accessed 10-July-2018].

[123] G. Mavrotas, K. Florios, and D. Vlachou, "Energy planning of a hospital using mathematical programming and monte carlo simulation for dealing with uncertainty in the economic parameters," *Energy Conversion and Management*, vol. 51, no. 4, pp. 722–731, 2010.

[124] W. Du, "Model validation by statistical methods on a monte-carlo simulation of residential low voltage grid," in *Future Communication, Computing, Control and Management*, pp. 93–98, Springer, 2012.

[125] E. J. da Silva Pereira, J. T. Pinho, M. A. B. Galhardo, and W. N. Macêdo, "Methodology of risk analysis by monte carlo method applied to power generation with renewable energy," *Renewable Energy*, vol. 69, pp. 347–355, 2014.

[126] P. Beraldi, A. Violi, M. Bruni, and G. Carrozzino, "A probabilistically constrained approach for the energy procurement problem," *Energies*, vol. 10, no. 12, p. 2179, 2017.

[127] C. Battistelli, Y. P. Agalgaonkar, and B. C. Pal, "Probabilistic dispatch of remote hybrid microgrids including battery storage and load management," *IEEE Transactions on Smart Grid*, vol. 8, no. 3, pp. 1305–1317, 2016.

[128] P. Pflaum, M. Alamir, and M. Y. Lamoudi, "Probabilistic energy management strategy for ev charging stations using randomized algorithms," *IEEE Transactions on Control Systems Technology*, vol. 26, no. 3, pp. 1099–1106, 2017.

[129] M. Aien, M. G. Khajeh, M. Rashidinejad, and M. Fotuhi-Firuzabad, "Probabilistic power flow of correlated hybrid wind-photovoltaic power systems," *IET Renewable Power Generation*, vol. 8, no. 6, pp. 649–658, 2014.

[130] M. Rastegar, M. Fotuhi-Firuzabad, H. Zareipour, and M. Moeini-Aghtaieh, "A probabilistic energy management scheme for renewable-based residential energy hubs," *IEEE Transactions on Smart Grid*, vol. 8, no. 5, pp. 2217–2227, 2016.

[131] D. Gan, Y. Wang, N. Zhang, and W. Zhu, "Enhancing short-term probabilistic residential load forecasting with quantile long–short-term memory," *The Journal of Engineering*, vol. 2017, no. 14, pp. 2622–2627, 2017.

[132] "NREL." http://pvwatts.nrel.gov/pvwatts.php. [Online; accessed 19-July-2019].

[133] "ELEXON." http://data.ukedc.rl.ac.uk/simplebrowse/edc/efficiency/residential/LoadProfile/data. [Online; accessed 19-July-2019].

[134] V. A. Epanechnikov, "Non-parametric estimation of a multivariate probability density," *Theory of Probability & Its Applications*, vol. 14, no. 1, pp. 153–158, 1969.

[135] J. S. Galpin and D. M. Hawkins, "The use of recursive residuals in checking model fit in linear regression," *The American Statistician*, vol. 38, no. 2, pp. 94–105, 1984.

[136] F. Kianifard and W. H. Swallow, "A review of the development and application of recursive residuals in linear models," *Journal of the American Statistical Association*, vol. 91, no. 433, pp. 391–400, 1996.

[137] M. Y. Ata, "Determining the optimal sample size in the monte carlo experiments," *Selcuk Journal of Applied Mathematics*, vol. 7, no. 2, pp. 103–111, 2006.

[138] D. Ding, A. Gandy, and G. Hahn, "A simple method for implementing monte carlo tests," *arXiv preprint arXiv:1611.01675*, 2016.

[139] Z. Wan, H. Li, and H. He, "Residential energy management with deep reinforcement learning," in *2018 International Joint Conference on Neural Networks (IJCNN)*, pp. 1–7, IEEE, 2018.

[140] V. Mnih, K. Kavukcuoglu, D. Silver, A. Graves, I. Antonoglou, D. Wierstra, and M. Riedmiller, "Playing atari with deep reinforcement learning," *arXiv preprint arXiv:1312.5602*, 2013.

[141] D. Silver, A. Huang, C. J. Maddison, A. Guez, L. Sifre, G. Van Den Driessche, J. Schrittwieser, I. Antonoglou, V. Panneershelvam, M. Lanctot, *et al.*, "Mastering the game of go with deep neural networks and tree search," *nature*, vol. 529, no. 7587, p. 484, 2016.

[142] D. Silver, J. Schrittwieser, K. Simonyan, I. Antonoglou, A. Huang, A. Guez, T. Hubert, L. Baker, M. Lai, A. Bolton, *et al.*, "Mastering the game of go without human knowledge," *Nature*, vol. 550, no. 7676, p. 354, 2017.

[143] A. D. Tijsma, M. M. Drugan, and M. A. Wiering, "Comparing exploration strategies for q-learning in random stochastic mazes," in *2016 IEEE Symposium Series on Computational Intelligence (SSCI)*, pp. 1–8, IEEE, 2016.

[144] S. Carden, "Convergence of a reinforcement learning algorithm in continuous domains," 2014.

[145] J. S. Campbell, S. N. Givigi, and H. M. Schwartz, "Multiple model q-learning for stochastic asynchronous rewards," *Journal of Intelligent & Robotic Systems*, vol. 81, no. 3-4, pp. 407–422, 2016.

[146] M. Tokic, "Adaptive ε-greedy exploration in reinforcement learning based on value differences," in *Annual Conference on Artificial Intelligence*, pp. 203–210, Springer, 2010.

[147] R. Bellman, "Dynamic programming, courier corporation," *New York, NY*, vol. 707, 2013.

[148] F. Bach, "Breaking the curse of dimensionality with convex neural networks," *The Journal of Machine Learning Research*, vol. 18, no. 1, pp. 629–681, 2017.

[149] N. J. Pizzi and W. Pedrycz, "Classifying high-dimensional patterns using a fuzzy logic discriminant network," *Advances in Fuzzy Systems*, vol. 2012, p. 4, 2012.

[150] S. Har-Peled, P. Indyk, and R. Motwani, "Approximate nearest neighbor: Towards removing the curse of dimensionality," *Theory of computing*, vol. 8, no. 1, pp. 321–350, 2012.

[151] T. Poggio, H. Mhaskar, L. Rosasco, B. Miranda, and Q. Liao, "Why and when can deep-but not shallow-networks avoid the curse of dimensionality: a review," *International Journal of Automation and Computing*, vol. 14, no. 5, pp. 503–519, 2017.

[152] V. Mnih, K. Kavukcuoglu, D. Silver, A. A. Rusu, J. Veness, M. G. Bellemare, A. Graves, M. Riedmiller, A. K. Fidjeland, G. Ostrovski, *et al.*, "Human-level control through deep reinforcement learning," *Nature*, vol. 518, no. 7540, p. 529, 2015.

[153] J. Farebrother, M. C. Machado, and M. Bowling, "Generalization and regularization in dqn," *arXiv preprint arXiv:1810.00123*, 2018.

[154] L. Yu, X. Shao, Y. Wei, and K. Zhou, "Intelligent land-vehicle model transfer trajectory planning method based on deep reinforcement learning," *Sensors*, vol. 18, no. 9, p. 2905, 2018.

[155] E. Mocanu, D. C. Mocanu, P. H. Nguyen, A. Liotta, M. E. Webber, M. Gibescu, and J. G. Slootweg, "On-line building energy optimization using deep reinforcement learning," *IEEE Transactions on Smart Grid*, 2018.

[156] A. Gruslys, M. G. Azar, M. G. Bellemare, and R. Munos, "The reactor: A sample-efficient actor-critic architecture," *arXiv preprint arXiv:1704.04651*, vol. 5, 2017.

[157] J. Buitrago and S. Asfour, "Short-term forecasting of electric loads using nonlinear autoregressive artificial neural networks with exogenous vector inputs," *Energies*, vol. 10, no. 1, p. 40, 2017.

[158] R. DiPietro, C. Rupprecht, N. Navab, and G. D. Hager, "Analyzing and exploiting narx recurrent neural networks for long-term dependencies," *arXiv preprint arXiv:1702.07805*, 2017.

[159] H. Chen, T. N. Cong, W. Yang, C. Tan, Y. Li, and Y. Ding, "Progress in electrical energy storage system: A critical review," *Progress in natural science*, vol. 19, no. 3, pp. 291–312, 2009.

[160] S. Rehman, L. M. Al-Hadhrami, and M. M. Alam, "Pumped hydro energy storage system: A technological review," *Renewable and Sustainable Energy Reviews*, vol. 44, pp. 586–598, 2015.

[161] R. Madlener and J. Latz, "Economics of centralized and decentralized compressed air energy storage for enhanced grid integration of wind power," *Applied Energy*, vol. 101, pp. 299–309, 2013.

[162] D. Connolly, "An investigation into the energy storage technologies available, for the integration of alternative generation techniques," *University of Limerick*, 2007.

[163] A. H. Fathima and K. Palanisamy, "Integration and energy management of a hybrid li-vrb battery for renewable applications," *Renewable Energy Focus*, vol. 30, pp. 13–20, 2019.

[164] H. Sun, M. Yu, Q. Li, K. Zhuang, J. Li, S. Almheiri, and X. Zhang, "Characteristics of charge/discharge and alternating current impedance in all-vanadium redox flow batteries," *Energy*, vol. 168, pp. 693–701, 2019.

[165] D. P. Scamman, G. W. Reade, and E. P. Roberts, "Numerical modelling of a bromide–polysulphide redox flow battery: Part 1: Modelling approach and validation for a pilot-scale system," *Journal of Power Sources*, vol. 189, no. 2, pp. 1220–1230, 2009.

[166] C. Menictas, M. Skyllas-Kazacos, and T. M. Lim, *Advances in batteries for medium and large-scale energy storage: types and applications*. Elsevier, 2014.

[167] H. Zhou, H. Zhang, P. Zhao, and B. Yi, "A comparative study of carbon felt and activated carbon based electrodes for sodium polysulfide/bromine redox flow battery," *Electrochimica Acta*, vol. 51, no. 28, pp. 6304–6312, 2006.

[168] Q. Lai, H. Zhang, X. Li, L. Zhang, and Y. Cheng, "A novel single flow zinc–bromine battery with improved energy density," *Journal of Power Sources*, vol. 235, pp. 1–4, 2013.